Généralisation des précodeurs MIMO basés sur la distance euclidienne minimale

Quoc-Tuong Ngo

N° d'ordre : 2012REN1E001 ANNÉE 2012

UNIVERSITÉ DE RENNES 1

THÈSE / UNIVERSITÉ DE RENNES 1
sous le sceau de l'Université Européenne de Bretagne

pour le grade de

DOCTEUR DE L'UNIVERSITÉ DE RENNES 1

Mention : Traitement du Signal et Télécommunications

École doctorale MATISSE

présentée par

Quoc-Tuong NGO

préparée à l'unité de recherche UMR6074 IRISA
Institut de recherche en informatique et systèmes aléatoires - CAIRN
École Nationale Supérieure des Sciences Appliquées et de Technologie

---

Generalized minimum Euclidean distance based precoders for MIMO spatial multiplexing systems

Thèse soutenue à Lannion
le 17 janvier 2012

devant le jury composé de :

CANCES Jean-Pierre
Professeur à l'Université de Limoges / rapporteur

SLOCK Dirk
Professeur à EURECOM / rapporteur

BUREL Gilles
Professeur à l'Université de Bretagne Occidentale / examinateur

DIOURIS Jean-FranÐois
Professeur à l'Université de Nantes / examinateur

SCALART Pascal
Professeur à l'Université de Rennes 1 / directeur de thèse

BERDER Olivier
Maître de Conférences à l'Université de Rennes 1/ co-directeur de thèse

"The only way to do great work is to love what you do. If you haven't found it yet, keep looking. Don't settle. As with all matters of the heart, you'll know when you find it. And, like any great relationship, it just gets better and better as the years roll on."

— Steve Jobs

Acknowledgements

The three year graduate work in IRISA/CAIRN Lab is a most memorial period in my life, not only because I have been led to an exciting field, the MIMO precoding techniques which were totally new to me before, but also I have got the opportunity to study and work in a very dynamic laboratory .

Firstly, I would like to thank my supervisor Prof. Pascal Scalart and co-supervisor Olivier Berder for their consistent supervision and encouragement throughout my study and research, their patient guidance on direction of my work. All of their feedbacks, suggestions, and gentleness at various stages have been significantly improved my knowledges, scientific minds, and skills of writing and presentation.

I would also like to thank all the members of the jury for reading part of my thesis: Prof. Jean-Pierre CANCES at the University of Limoges, Prof. Dirk SLOCK at the EURECOM (Nice) , Prof. Gilles BUREL at the University of Bretagne Occidentale, and Prof. Jean-Françoisand DIOURIS at the University of Nantes. Their suggestions and comments are really appreciated.

I am most grateful to Prof. Oliver Sentieys, the head of CAIRN Lab, for his kind attitude and constant willingness to help makes my graduate study a very enjoyable experience.

I also want to thank all of my friends in Lannion who make my stay a memorial period.

My warmest thanks also go to my parents for their never ending support. They always assist me in implementing my desires.

Finally, I would like to say something special to my girlfriends. She is a powerful emotional support that I can share my burdens, fears and sadness. Thanks you for her understanding, her helps, and her endless love.

Contents

Abbreviations

$\simeq$		approximately equal to
$\mathbf{A}^*$		Hermitian (complex and conjugate) of matrix $\mathbf{A}$
$\mathbf{A}^T$		transpose of matrix $\mathbf{A}$
$\mathbf{A}^+$		pseudo inverse of matrix $\mathbf{A}$
$E\{x\}$		expectation of x
$\mathbf{I}_b$		Identity matrix of size $b \times b$
$\|x\|$		vector 2-norm
$\breve{\mathbf{x}}$		difference vector
$\hat{\mathbf{x}}$		detected symbol, or estimated value of $\mathbf{x}$
$\|\mathbf{F}\|$		Frobenius norm of matrix $\mathbf{F}$
$\text{diag}\{x_1, x_2, \cdots, x_n\}$		diagonal matrix with n diagonal elements $x_1, x_2, \cdots, x_n$
n_T		number of transmit antennas
n_R		number of receive antennas
$n_s = \|n_T - n_R\|$		asymmetric coefficient
E_s		average transmit power for n_T transmit antennas
b		number of datastreams
$\mathbf{H}$	$[n_R \times n_T]$	channel matrix
$\mathbf{F}$	$[n_T \times b]$	precoding matrix
$\mathbf{G}$	$[b \times n_R]$	decoding matrix
$\mathbf{s}$	$[b \times 1]$	transmitted symbol vector
η	$[b \times 1]$	additive noise vector
$\mathbf{H}_v$	$[b \times b]$	virtual channel matrix
$\mathbf{F}_v$	$[n_T \times b]$	diagonalization matrix at the transmitter
$\mathbf{G}_v$	$[b \times n_R]$	diagonalization matrix at the receiver
$\mathbf{F}_d$	$[b \times b]$	precoding matrix for virtual channel
$\mathbf{G}_d$	$[b \times b]$	decoding matrix for virtual channel
$\mathcal{C}$		channel capacity
SNR		Signal to Noise ratio
$d_{\min}$		minimum Euclidean distance of the received constellation
$\bar{d}_{\min}$		normalized minimum Euclidean distance

γ	angle of the virtual channel for two substreams
ρ	gain of the virtual channel for two substreams
$\mathcal{R}_{d_{\min}}$	ratio of the minimum distance gain

List of Figures

List of Tables

Introduction

In the early decade of this century, it is apparent that wireless communication technologies have an exponential growth. Various communication techniques have been employed to serve various demands of high-speed wireless links such as higher data rate, increased robustness, and greater user capacity. The next generation of wireless communications is based on an all-IP switched network and can provide a peak data rate up to hundreds of Mbits/s for high mobility, and to Gbits/s for low-mobility end-users. For instance, the Wi-Fi standard (IEEE 802.11n) can provide a data rate up to 600 Mbps in physical layer, and the Wi-Max standard (IEEE 802.16) can support a gross data rate up to 100 Mbps for mobile network.

One of the most well-known techniques for wireless communications is multiple-input multiple-output orthogonal frequency division multiplexing (MIMO-OFDM). This technique not only offers diversity and capacity gains but also achieves higher spectral efficiency and higher link reliability in comparison with single antenna or single carrier systems. The benefits of MIMO communication are generally ensured by both open-loop and closed-loop MIMO techniques. The open-loop techniques, such as space time coding (STC) and spatial multiplexing (SM), are used without the need for channel state information (CSI) at the transmitter. In order to overcome the multipath effect and improve the robustness of spatial multiplexing systems, linear precoding closed-loop techniques can be used at the transmitter. The principle of the precoding techniques is that, when the channel knowledge is available at the transmitter, the transmit signal is pre-multiplied by a precoding matrix such that the inter-symbol interference (ISI) in the receiver is greatly reduced.

The channel state information at the transmitter (CSIT) can be obtained through the feedback links, but it is difficult to achieve perfect CSIT in a MIMO system with a rapidly

changing channel. Therefore, the transmitters in many MIMO systems have no knowledge about the current channel. This motivates the use of limited feedback precoding methods such as channel quantization and codebook designs. The key of this method is that the optimal precoding matrix is constrained to a number of distinct matrices, which are referred to codebook entries, and known a priori to both the transmitter and receiver. Many precoding codebooks can be proposed in order to optimizing different criteria of the precoded system, and the receiver defines the optimal precoding matrix based on the current channel conditions. Since the codebook is also known at the transmitter, the receiver only needs to feedback a binary index of the optimal precoding matrix, rather than the entire precoding matrix itself. The limited feedback precoding technique is already used in Wi-Max standard (802.16e) with two codebooks: one with 8 entries and the other with 64 entries. These codebooks correspond respectively to 3-bit and 6-bit indices for each precoding matrix.

Considering the CSI from the receiver, antenna power allocation strategies can be performed thanks to the joint optimization of linear precoder (at the transmitter) and decoder (at the receiver) according to various criteria such as maximizing the output capacity, maximizing the received signal-to-noise ratio (SNR), minimizing the mean square error (MSE), minimizing the bit error rate (BER), or maximizing the minimum singular value of the channel matrix. These optimized precoding matrices are diagonal in the virtual channel representation and belong to an important set of linear precoding techniques named diagonal precoders. Another group of precoding techniques is obviously the non-diagonal linear structure. One of the most efficient non-diagonal precoder is based on the maximization of the minimum Euclidean distance (max-$d_{\min}$) between two received data vectors. The max-$d_{\min}$ precoder offers a significant improvement in terms of BER compared to other precoding strategies. Since the minimum distance based transceiver needs a Maximum-Likelihood (ML) detector, the complexity of max-$d_{\min}$ precoder is fairly complicated. Furthermore, it is difficult to define the closed-form of the optimized precoding matrix for large MIMO system with high-order modulations. In this thesis, we will study the performances, and propose some extensions of the max-$d_{\min}$ solution.

Following this introduction, this document is organized as follows:

Chapter 1

In this chapter, the propagation over wireless channels is firstly presented. The principles and different types of diversity techniques are then investigated. A brief introduction of the MIMO technologies with capacity and diversity gains are referred, and the space time coding technique is described. Finally, the precoding system structure which consists of an encoder, a precoder and a decoder is presented.

Chapter 2

A virtual transformation is used to diagonalize the channel matrix, and the principles of some existing precoders are presented in the chapter. The performance of the max-$d_{\min}$ precoder in terms of minimum distance and bit-error-rate is also considered in comparison with other precoders.

Chapter 3

The max-$d_{\min}$ solution was only available in closed-form for two independent data-streams with low-order modulations (BPSK and QPSK). That is due to the expression of the distance $d_{\min}$ that depends on the number of data-streams, the channel characteristics, and the modulation. Therefore, we present the optimized solution of the max-$d_{\min}$ precoder for two 16-QAM symbols. This new strategy selects the best precoding matrix among five different expressions which depend on the value of the channel angle γ. In order to reduce the complexity of the max-$d_{\min}$ precoder, we propose a general expression of minimum Euclidean distance based precoders for all rectangular QAM modulations. For a two independent data-streams transmission, the precoding matrix is obtained by optimizing the minimum distance on both virtual subchannels. Hence, the optimized expressions can be reduced to two simple forms: the precoder $\mathbf{F}_1$ pours power only on the strongest virtual subchannel, and the precoder $\mathbf{F}_2$ uses both virtual subchannels to transmit data symbols. These precoding matrices are designed to optimize the distance $d_{\min}$ whatever the dispersive characteristics of the channels are.

Chapter 4

This chapter proposes a heuristic solution which permits increasing the number of transmit symbols. Firstly, a suboptimal solution, denoted as Equal-$d_{\min}$(E-$d_{\min}$), is obtained by decomposing the propagation channel into 2×2 eigen-channel matrices, and applying the new max-$d_{\min}$ precoder for independent pairs of data-streams. It is noted that this sub-optimal solution can only achieve an even number of data-streams. Therefore, we

extend, herein, the design of max-$d_{\min}$ precoders for a three parallel data-stream scheme. Thanks to the three-dimensional scheme, an extension for an odd number of data-streams is obtained by decomposing the virtual channel into (2×2) and (3×3) eigen-channel matrices.

Chapter 5

Not only the minimum Euclidean distance but also the number of neighbors providing it has an important role in reducing the error probability when a Maximum Likelihood detection is considered at the receiver. Aiming at reducing the number of neighbors, a new precoder in which the rotation parameter has no influence is proposed for two independent datastreams transmitted. The expression of the new precoding strategy is less complex and the space of solution is, therefore, smaller. In addition, we also propose the general Neighbor-$d_{\min}$ precoder for three independent data-streams. The simulation results confirm a significant bit-error-rate reduction for the new precoder in comparison with other traditional precoding strategies.

Chapter 6

Still considering the maximization of the minimum Euclidean distance, we propose, in this chapter, a new linear precoder obtained by observing the SNR-like precoding matrix. An approximation of the minimum distance is derived, and its maximum value is obtained by maximizing the minimum diagonal element of the SNR-like matrix. The precoding matrix is first parameterized as the product of a diagonal power allocation matrix and an input-shaping matrix acting on rotation and scaling of the input symbols on each virtual subchannel. We demonstrate that the minimum diagonal entry of the SNR-like matrix is obtained when the input-shaping matrix is a DFT-matrix. In comparison with the traditional max-$d_{\min}$ solution, the new precoder provides a slight improvement in BER performance. But the major advantage of this design is that the solution can be available for all rectangular QAM-modulations and for any number of datastreams.

The conclusions and perspectives are given individually at the end of this thesis.

Chapter 1

Wireless communication and MIMO technology

The propagation over wireless channels is a complicated phenomenon characterized by various effects such as path loss, shadowing, and multipath fading. One of the most well-known techniques to combat the fading effects and exploit the multipath propagation in wireless communications is diversity. This technique uses different mediums like different time slots, different frequencies, different polarizations or different antennas to transmit multiple versions of the same signal [1].

Among different types of diversity techniques, the spatial diversity, which uses multiple transmit and receive antennas, not only increases efficiently the channel capacity and the transmission data rate but also provides a higher spectral efficiency and a higher link reliability in comparison with single antenna links. This technique is named as MIMO (multiple input multiple output) and can be divided into three main categories: spatial multiplexing (SM), diversity coding, and precoding. The diversity coding technique is used when there is no channel state information at the transmitter (CSIT) while the precoding technique exploits the CSIT by operating on the signal before transmission. For different forms of partial CSIT, the precoding technique can be considered as a multimode beamformer which splits the transmit signal into independent eigenbeams and assigns the powers on each beam based on the channel knowledge.

In this chapter, the propagation over wireless channels is firstly presented. The principles and different types of diversity techniques are then investigated. After that, a brief

introduction of the MIMO technologies with the capacity and diversity gain is referred. The space time coding technique is then described, and finally, the precoding system structure that consists of an encoder, a precoder and a decoder, is presented.

1.1 Transmission channel

1.1.1 Path loss

In wireless channel, the transmit signals are attenuated because of the propagation. It may be due to many effects, such as free-space loss, refraction, diffraction, reflection, and absorption [2]. The loss in signal strength of an electromagnetic wave from a line-of-sight path (LOS) through free space, known as free-space path loss (FSPL), is given by

$$\mathrm{L} = \left(\frac{\lambda}{4\pi d}\right)^2 = \left(\frac{c}{4\pi df}\right)^2, \tag{1.1}$$

where λ is the signal wavelength, d is the distance from the transmitter, f is the signal frequency, and c is the speed of light in vacuum. The path loss is, in reality, influenced by environment (urban or rural), the propagation medium, and the location of antennas. The loss of transmit signals is, therefore, exponentially proportional to the distance d.

$$\mathrm{L} = k\, d^{-n}, \tag{1.2}$$

where k is a constant and the exponent n generally varies from 2 to 5. This relation is often used in evaluating macrocellular systems. For microcells performances, the authors in [3] present another expression of FSPL

$$\mathrm{L} = d^{-n_1}\left(1 + \frac{d}{d_b}\right)^{-n_2}, \tag{1.3}$$

where n_1, n_2 are two separate constants and d_b is a measured breakpoint. Table below shows different values for n_1, n_2, and d_b fitted to measurements in three different cities.

TABLE 1.1: Empirical power drop-off values

City	n_1	n_2	d_b
London	1.7–2.1	2–7	200–300
Melbourne	1.5–2.5	3–5	150
Orlando	1.3	3.5	90

1.1.2 Fading

In wireless communications, fading is used to describe the deviation of the radio signal over different periods of time. It is a phenomenon in wireless channel which is caused by the interference of two or more transmit signals arriving to the receiver. A fading phenomenon may be due to the multipath propagation or due to shadowing from obstacles. The distinction between slow and fast fading is related to the coherence time T_c of the channel, which measures the period of time over which the fading process is correlated. Slow fading occurs when the coherence time of the channel is large relative to the delay constraint of the channel, while fast fading is opposite. In other words, the fading is said to be slow if the symbol time duration T_s is smaller than the channel coherence time T_c; otherwise, it is considered to be fast. In general, the coherence time is related to the channel Doppler spread by

$$T_c \approx \frac{1}{B_d}, \tag{1.4}$$

where B_d is the Doppler spread (or Doppler shift).

Doppler effect

When the transmitter and receiver have a relative motion, the frequency of the signal at the received size is changed relatively. This phenomenon is called as Doppler effect and named after Austrian physicist Christian Doppler. The Doppler spread (or frequency spread), noted as B_d, is the difference between the observed frequency and emitted frequency and given by

$$B_d = \Delta f = \frac{v}{\lambda}, \tag{1.5}$$

where v is the velocity of the source relative to the receiver, and λ is is the wavelength of the transmitted wave.

Multipath propagation

Multipath is used to describe the phenomenon in which the radio signals reach the received antenna by multiple paths. Causes of propagation path include the ground wave, ionospheric refraction and refraction, reflection from water bodies and terrestrial objects such as mountains and buildings. One should note that if frequency of signals

exceeds to 30 MHz, the electrical wave passes through the ionospheric layer, and there does not exist multipath from ionospheric refraction.The received signal is expressed by

$$r(t) = \sum_{n=0}^{N-1} \alpha_n s(t - \tau_n) + \eta(t), \tag{1.6}$$

where $s(t)$ is the transmit signal, $\eta(t)$ is additive noise, N is the total number of paths, α_n and τ_n are the attenuation and the delay of each path, in respectively. The maximum delay spread (or multipath time) is defined as the time delay existing between the first and the last signal

$$T_M = \max_i(\tau_i) - \min_i(\tau_i). \tag{1.7}$$

In addition, the coherence bandwidth B_c is related to the multipath time by

$$B_c \approx \frac{1}{T_M}. \tag{1.8}$$

Frequency selectivity is also an important characteristic of fading channels. The fading is said to be frequency nonselective or, equivalently, frequency flat if the transmitted signal bandwidth B_s is much smaller than the channel coherence bandwidth B_c.

The probability distribution of the attenuation α depends on the nature of the radio propagation environment. Therefore, there are different models describing the statistical behavior of the multipath fading. The Rayleigh distribution is frequently used to model multipath fading with no direct line-of-sight (LOS) path. In this case the probability density function (PDF) of the channel fading amplitude is defined by [4]

$$\begin{cases} p(\arg(\alpha)) = \frac{1}{2\pi}\ [0; 2\pi] \\ p(|\alpha|) = \frac{\alpha}{\Omega} e^{-\frac{\alpha^2}{2\Omega}} \end{cases} \tag{1.9}$$

where Ω is mean-square error of α.

The Rice (Nakagami-n) Model is often used to model propagation paths consisting of one strong direct LOS component and many random weaker components. Here the channel fading amplitude follows the distribution [5]

$$\begin{cases} p(\arg(\alpha)) = \frac{1}{2\pi}\ [0; 2\pi] \\ p(|\alpha|) = \frac{2\alpha(K+1)}{\Omega} e^{-\left(K + \frac{(K-1)\alpha^2}{\Omega}\right)} I_0\left(2\alpha\sqrt{\frac{K(K+1)}{\Omega}}\right) \end{cases} \tag{1.10}$$

where K is Rician factor which is related to the Nakagami-n fading parameter n by $K = n^2$, and $I_0(x)$ is the zero-order modified Bessel function of the first kind.

1.2 Diversity technique

Diversity refers to a technique for improving the reliability of the transmit signal by using different mediums like different time slots, different frequencies, different polarizations or different antennas. Multiple versions of the same signal are transmitted over different fading channels and, then, recombined at the receiver. This technique plays an important role in combating the fading effect, and exploiting the multipath propagation.

The diversity gain $\mathcal{G}$ in decibels (dB) is given by

$$\mathcal{G} = \lim_{\mathrm{SNR}\to\infty} \frac{\log P_e}{\log \mathrm{SNR}}, \tag{1.11}$$

where P_e is the error probability of the received signal and SNR is the received Signal to Noise Ratio.

1.2.1 Temporal diversity

When two or more copies of the same signal are transmitted at different time slots, it is called temporal diversity. It is noted that the time interval between two time slots must be higher or equal to the coherence time T_c of the channel to assure independent fades (see Fig. 1.1). The receiver will combine multiple versions of signal without interference to estimate the information.

1.2.2 Frequency diversity

In this technique, multiple copies of the same signal are transmitted through different carrier frequencies. These carrier frequencies should be separated by an interval larger than the coherence bandwidth B_c of the channel (see Fig. 1.1). Similarly to temporal diversity, the receiver needs to tune to different carrier frequencies for signal reception and, therefore, has no bandwidth efficiency.

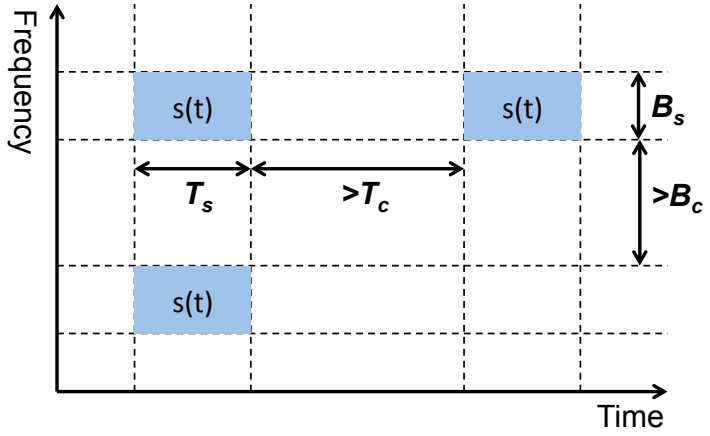

FIGURE 1.1: Principle of temporal diversity and frequency diversity

1.2.3 Spatial diversity

In this technique, the signal is transmitted over several different propagation paths. For a wireless transmission, it can be achieved by using multiple transmitter antennas (transmit diversity) and/or multiple receiving antennas (receive diversity).

- Receive diversity uses multiple antennas at the receive side. The received signals from the different antennas are then combined at the receiver to exploit the diversity gain. Receive diversity is characterized by the number of independent fading channels, and its diversity gain is proportional to the number of receive antennas.
- Transmit diversity uses multiple antennas at the transmit side. Information is processed at the transmitter and then spread across the multiple antennas for the simultaneous transmission. Transmit diversity was firstly introduced in [6] and becomes an active research area of space time coding techniques.

1.2.4 Antenna diversity

Antenna diversity is another technique using antennas for providing the diversity. There are two main techniques of antenna diversity:

- Angular diversity uses directional antennas to achieve diversity. Different copies of the same signal are received from different angles of the receive antenna. Unlike spatial diversity, angular diversity does not need a minimum separation distance between antennas. For this reason, angular diversity is helpful for small devices.

- Polarization diversity uses the difference of the vertical and horizontal polarized signals to achieve the diversity gain. In this technique, multiple versions of a signal are received via antennas with different polarizations. Like angular diversity, polarization diversity also does not require the minimum separation distance for the antennas and then suitable for small device.

1.3 Multiple-Input Multiple-Output techniques

In wireless communication, multiple-input multiple-output (MIMO) is the use of multiple antennas at both transmission and reception sides of a communication system. The idea of using multiple transceivers and receivers was first proposed by Bell Labs [7], and, then, has been worldwide utilized to adapt to various high-speed wireless transmissions. This technique not only offers diversity and capacity gains but also achieves higher spectral efficiency and higher link reliability in comparison with single antenna or single carrier systems [8]. Because of these properties, MIMO becomes one of the most important parts of modern wireless communication standards such as IEEE 802.11n (Wifi), 4G, 3GPP Long Term Evolution, WiMAX and HSPA+.

MIMO techniques can be divided into three main categories: spatial multiplexing (SM), diversity coding, and precoding.

- Spatial multiplexing is the technique in which a high rate signal is split into multiple independent data-streams and each stream is transmitted from a different transmit antenna. These signals are distinguished by different spatial signatures, and a good separability can be, therefore, assured. Spatial multiplexing offers a significant improvement in channel capacity at higher signal-to-noise ratios (SNR), but it is limited by the smaller number of transmitters or receivers [9]. This technique can be used without transmit channel knowledge, and can also be employed for simultaneous transmission to multiple receivers.

- Diversity Coding technique is used when there is no channel state information (CSI) at the transmitter. In this method, the signal is emitted from each of the transmit antennas using techniques called space-time coding. Diversity coding exploits the diversity gain to achieve a higher reliability, high spectral efficiency in comparison

with single antenna links. Space time codes can be split into two main types: Space–time block codes (STBCs) and Space–time trellis codes (STTCs).

- Precoding is a processing technique that exploits the channel state information at transmitter (CSIT) by operating on the signal before transmission. For different forms of partial CSIT, a linear precoder can be considered as a multimode beamformer which optimally matches the input signal on one side to the channel on the other side. It splits the transmit signal into independent eigenbeams and assigns the powers on each beam based on the channel knowledge. Precoding design depends on the types of CSIT and the performance criterion [10].

1.3.1 Basic system model

Let us consider a MIMO transmission with n_T transmit and n_R receive antennas. When $n_T = 1$, the MIMO channel reduces to a single-input multiple-output (SIMO) channel. Similarly, when $n_R = 1$, the MIMO channel reduces to a multiple-input single-output (MISO). When both $n_T = 1$ and $n_R = 1$, the MIMO channel simplifies to a simple scalar or single-input single-output (SISO) channel. The basic MIMO system model is illustrated in Fig 1.2. At a certain time t, the received signal at antenna j can be expressed as

$$y_{t,j} = \sum_{i=1}^{n_T} h_{j,i} s_{t,i} + \eta_{t,j}, \tag{1.12}$$

where $h_{j,i}$ is the channel gain of the path between the receive antenna j and the transmit antenna i, $s_{t,i}$ is the complex transmit signal at antenna i, and $\eta_{t,j}$ is the noise term at the receive antenna j. The MIMO channel can be similarly described as

$$\mathbf{y} = \mathbf{H}\mathbf{s} + \mathbf{n}, \tag{1.13}$$

where $\mathbf{y} = [y_{t,1}, y_{t,2}, ..., y_{t,n_R}]^T$ is the receive vector, $\mathbf{s} = [s_{t,1}, s_{t,2}, ..., s_{t,n_T}]^T$ is the transmit vector, $\mathbf{H}$ is the channel matrix, and $\mathbf{n}$ is the noise vector. The channel matrix $\mathbf{H}$ represents $n_R \times n_T$ paths between n_T transmitters and n_R receivers and is defined by

$$\mathbf{H} = \begin{pmatrix} h_{1,1} & \cdots & h_{1,n_T} \\ \vdots & \ddots & \vdots \\ h_{n_R,1} & \cdots & h_{n_R,n_T} \end{pmatrix} \tag{1.14}$$

The elements of channel matrix are random and chosen based on different statistical models like Rayleigh, Rice or Nakagami [5]. In the remainder of the study, we will consider the Rayleigh model, e.g. the path gains are modeled by independent complex Gaussian random variables. The noise is considered as an additive white Gaussian noise (AWGN) and its elements $\eta_{t,j}$ are independent from each other and have a complex Gaussian distribution.

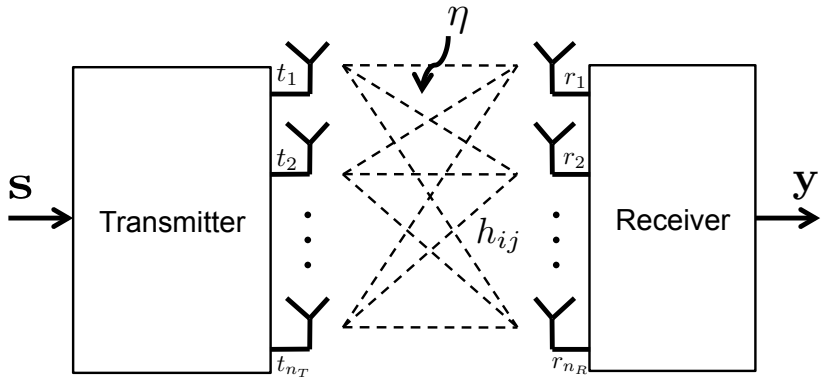

FIGURE 1.2: MIMO model with n_T transmit antennas and n_R receive antennas

1.3.2 MIMO channel capacity

It has been shown in [9] that MIMO systems provide a significant improvement in terms of capacity compared to SISO systems. The channel capacity is the maximum error-free data rate that a channel can transmit. It was first derived by Claude Shannon [11] for a SISO system

$$C = \log_2 (1 + \mathrm{SNR}) . \tag{1.15}$$

In contrast to single antenna links, multiple antenna channels combat fading and cover a spatial dimension. The capacity of a deterministic MIMO channel is given by [12]

$$C = E\left[\log_2 \left(\det(\mathbf{I}_{n_R} + \frac{\mathrm{SNR}}{n_T}\mathbf{H}\mathbf{H}^*)\right)\right], \tag{1.16}$$

where $E[x]$ denotes an expectation of random variable x, $\mathbf{I}_{n_R}$ is the identity matrix of size n_R, and $\mathbf{H}^*$ is conjugate transpose of matrix $\mathbf{H}$. At high SNR, the capacity of a Rayleigh fading channel can be approximated as

$$\mathcal{C} \approx \min(n_T, n_R) \log_2 \left(\frac{\mathrm{SNR}}{n_T}\right). \tag{1.17}$$

It is observed that improvement of the MIMO channel capacity is proportional to the value $\min(n_T, n_R)$ in comparison with SISO systems. The figure 1.3 illustrates the ergodic channel capacity as a function of average SNRs for Rayleigh fading channels.

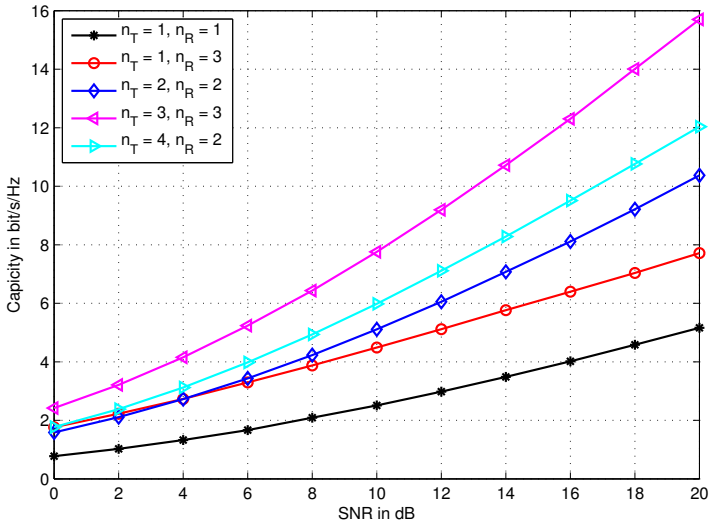

FIGURE 1.3: The ergodic capacity of MIMO channels.

1.4 Space Time Coding

Space Time Coding technique is used when there is no channel state information (CSI) at the transmitter. In general, space-time coding can be divided into two categories: space-time trellis codes (STTC) and space-time block codes (STBC). The first STBC scheme was proposed by Alamouti [13] with a full diversity and a full data rate transmission for two transmit antennas. This scheme was, then, generalized to an arbitrary number of transmit antennas by applying the orthogonal space-time codes [14, 15] and was named as space-time block codes. However, for more than two transmit antennas, there does not exist STBC with full diversity and full data rate. Therefore, many different code design methods were proposed for providing either full diversity or full data rate at the cost of a higher complexity, for example QOSTBC [16].

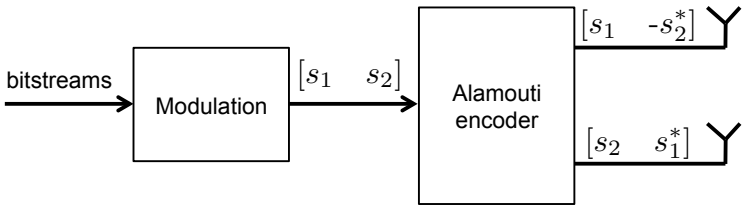

	t_1	t_2
antenna 1	s_1	$-s_2^*$
antenna 2	s_2	s_1^*

FIGURE 1.4: Alamouti encoding scheme.

1.4.1 Alamouti Code

Alamouti code can be considered as the first space time code which provides full diversity and full data rate for two transmit antennas. A block diagram of the Alamouti space-time encoder is illustrated in Fig. 1.4. We denote s_1 et s_2 as two transmit symbols entering the space time encoder, the Alamouti code is defined by

$$\mathbf{C_2} = \begin{pmatrix} s_1 & -s_2^* \\ s_2 & s_1^* \end{pmatrix} \tag{1.18}$$

In the first period, the symbols s_1 and s_2 are transmitted simultaneously from two antennas. In the second period, the symbol $-s_2^*$ and s_1^* are transmitted from antenna one and antenna two, in respectively. One should note that the matrix $\mathbf{C_2}$ is orthogonal

$$\mathbf{C_2}\mathbf{C_2}^* = \left(\|s_1\|^2 + \|s_2\|^2\right)\mathbf{I_2}, \tag{1.19}$$

where $\mathbf{I_2}$ is a 2×2 identity matrix. This property implies that the receiver can detect two symbols s_1 and s_2 independently by a simple linear signal processing operation.The received signals of the antenna j at two periods are denoted as r_j^1 et r_j^2 and defined by

$$\begin{aligned} r_j^1 &= h_{j,1}.s_1 + h_{j,2}.s_2 + \eta_j^1 \\ r_j^2 &= -h_{j,1}.s_2^* + h_{j,2}.s_1^* + \eta_j^2 \end{aligned} \tag{1.20}$$

where n_j^1 and n_j^2 are the additive white Gaussian noise at the receiver j. A maximum likelihood (ML) detector is consider with two simple linear combinations of the received signals

$$\begin{aligned} \tilde{s}_1 &= \sum_{j=1}^{n_R}\left\{h_{j,1}^*.r_j^1 + h_{j,2}.(r_j^2)^*\right\} = \sum_{i=1}^{2}\sum_{j=1}^{n_R}\|h_{j,i}\|^2.s_1 + \sum_{j=1}^{n_R}\left\{h_{j,1}^*.\eta_j^1 + h_{j,2}.(\eta_j^2)^*\right\} \\ \tilde{s}_2 &= \sum_{j=1}^{n_R}\left\{h_{j,2}^*.r_j^1 - h_{j,1}.(r_j^2)^*\right\} = \sum_{i=1}^{2}\sum_{j=1}^{n_R}\|h_{j,i}\|^2.s_2 + \sum_{j=1}^{n_R}\left\{h_{j,2}^*.\eta_j^1 - h_{j,1}.(\eta_j^2)^*\right\} \end{aligned} \tag{1.21}$$

The ML decoder, then, finds the closest symbol $\hat{s}_1$ and $\hat{s}_2$ for two estimated symbols $\tilde{s}_1$ and $\tilde{s}_1$ in the symbol constellation

$$\begin{aligned} \hat{s}_1 &= \underset{s_1 \epsilon S}{\operatorname{argmin}}\, d^2(\tilde{s}_1, s_1) \\ \tilde{s}_2 &= \underset{s_2 \epsilon S}{\operatorname{argmin}}\, d^2(\tilde{s}_2, s_2) \end{aligned} \tag{1.22}$$

1.4.2 Orthogonal Space-Time Block Codes

The space time code proposed by Alamouti is only available for MIMO systems with two transmit antennas. The author V.Tarokh presented in [14, 17] the orthogonal designs for an arbitrary number of transmitters. The generated code is a matrix with two dimensions of space and time, and satisfies the orthogonal property

$$\mathbf{C}\mathbf{C}^* = \sum_{i=1}^{n} \|s_i\|^2 \mathbf{I}_{n_T}. \tag{1.23}$$

The i^{th} column of $\mathbf{C}$ corresponds to the symbols transmitted by the i^{th} antenna, while the j^{th} row of $\mathbf{C}$ represents the symbols transmitted simultaneously at time j. It is noted that the columns of the transmission matrix $\mathbf{C}$ are orthogonal to another. In other words, the signal sequences from any two transmit antennas are orthogonal to each other. If the space time code can transmit n_s symbols in n_p periods, the transmission rate of STBC is defined by

$$\mathcal{R} = \frac{n_s}{n_p}. \tag{1.24}$$

For example, the following code matrices obtain the transmission rate 1/2 and 3/4 for the case of 3 transmit antennas. One should note that the OSTBC can not obtain a

transmission rate equals to one for complex transmit signals.

$$\mathbf{C}_{1/2} = \begin{pmatrix} s_1 & s_2 & s_3 \\ -s_2 & s_1 & -s_4 \\ -s_3 & s_4 & s_1 \\ -s_4 & -s_3 & s_2 \\ s_1^* & s_2^* & s_3^* \\ -s_2^* & s_1^* & -s_4^* \\ -s_3^* & s_4^* & s_1^* \\ -s_4^* & -s_3^* & s_2^* \end{pmatrix} \tag{1.25}$$

$$\mathbf{C}_{3/4} = \begin{pmatrix} s_1 & s_2 & \frac{s_3}{\sqrt{2}} \\ -s_2^* & s_1^* & \frac{s_3}{\sqrt{2}} \\ \frac{s_3}{\sqrt{2}} & \frac{s_3}{\sqrt{2}} & \frac{-s_1-s_1^*+s_2-s_2^*}{2} \\ \frac{s_3^*}{\sqrt{2}} & -\frac{s_3^*}{\sqrt{2}} & \frac{s_2+s_2^*+s_1-s_1^*}{2} \end{pmatrix} \tag{1.26}$$

1.4.3 Quasi-Orthogonal Space-Time Block Codes

The OSTBC design obtains a full diversity gain, but it can not provide the full transmission rate in the case of more than two transmit antennas. To design a full-rate space time codes, the author in [16] proposed a design which decodes independent pair of symbols. This code is called Quasi Orthogonal Space-Time Block Codes (QSTBC) and based on the full-diversity full-rate Alamouti schemes.

Let us consider the case of $n_s = n_p = 4$, the QOSTBC for four transmit antennas is then defined by

$$\mathbf{C}_{Jafar} = \begin{pmatrix} \mathbf{C_2}(s_1, s_2) & \mathbf{C_2}(s_3, s_4) \\ -\mathbf{C_2}(s_3, s_4)^* & \mathbf{C_2}(s_1, s_2)^* \end{pmatrix} = \begin{pmatrix} s_1 & s_2 & s_3 & s_4 \\ -s_2^* & s_1^* & -s_4^* & s_3^* \\ -s_3 & -s_4 & s_1 & s_2 \\ s_4^* & -s_3^* & -s_2^* & s_1^* \end{pmatrix} \tag{1.27}$$

where $\mathbf{C_2}(s_i, s_j)$ is the Alamouti code for two symbols s_i and s_j. Let us denote $\mathbf{v}_i$ as as the i^{th} column of the matrix $\mathbf{C}_{Jafar}$, we obtain

$$< \mathbf{v}_1, \mathbf{v}_2 >=< \mathbf{v}_1, \mathbf{v}_3 >=< \mathbf{v}_2, \mathbf{v}_4 >=< \mathbf{v}_3, \mathbf{v}_4 >= 0 \tag{1.28}$$

where $< \mathbf{v}_i, \mathbf{v}_j >$ is the inner product of vectors $\mathbf{v}_i$ and $\mathbf{v}_j$. For this reason, two pairs of transmitted symbols (s_1, s_4) and (s_2, s_3) can be decoded independently at the receiver. The encoding of QOSTBC is, then, similar to the encoding of orthogonal STBC.

1.4.4 Space Time Trellis Codes

The Space Time Trellis Codes (STTC) are first proposed by Tarokh et al. [16] and are the extension of the classic trellis code presented in [18] for MIMO systems. This goal of the STTC design is the achievement of full diversity and full transmission rate for any number of transmit antennas. STTCs code combine the modulation and channel coding to transmit information over multiple transmit antennas. The principle of STTCs are to create the relationship between the transmit signals in n_t antennas and in each packet of symbols.

Let us consider, for example, the coding trellis of the full rate 2 bits/ channel uses STTCs with two transmit antennas. Fig 1.5 illustrates the 4-states space time code using 4-PSK modulation. STTCs code is represented by a trellis and pairs of symbols that are transmitted from the two antennas for every paths in the trellis. The indices of the symbols are used to present the transmitted symbols for each path (see Fig. 1.5).

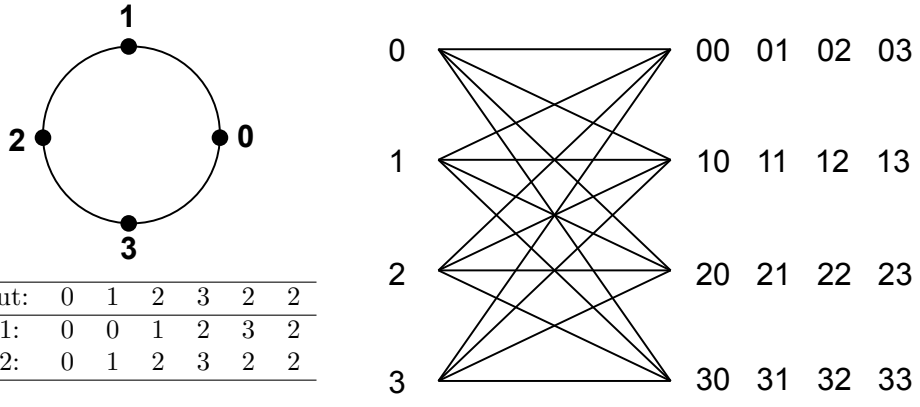

Input:	0	1	2	3	2	2
Tx 1:	0	0	1	2	3	2
Tx 2:	0	1	2	3	2	2

FIGURE 1.5: Four state STTC with two transmit antennas, using 4-PSK modulation.

1.5 Precoding technique

Precoding is a technique which exploits the channel state information at transmitter (CSIT) by processing signal before transmission. A basic precoding system structure which contains an encoder, a precoder and a decoder is shown in Fig 1.6. The encoder intakes data bits and performs necessary coding for error correction, and then maps the coded bits into vector symbols. The precoder processes these symbols before transmission according to different forms of channel state information. At the receive side, a decoder is considered to recover the bit streams.

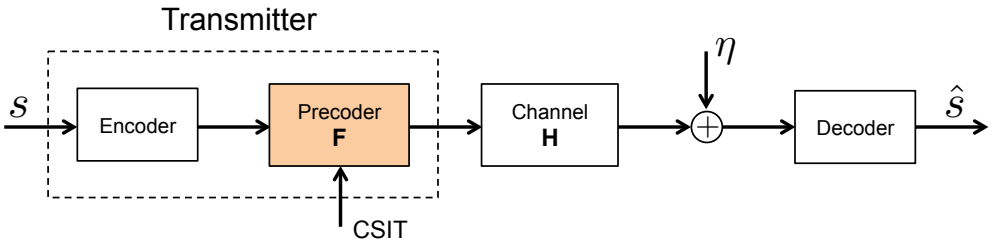

FIGURE 1.6: Precoding system structure.

1.5.1 Encoding structure

An encoder often consists of a channel coding and interleaving block and a symbol-mapping block. The encoding structure can be classified into two categories: spatial multiplexing and space time coding which are based on the symbol mapping block. The spatial multiplexing structure de-multiplexes the data bits to multiple independent bit streams. These bit streams are then mapped into vector symbols and are directly operated by a precoder, as shown in Fig 1.7. Since these streams are independent with individual signal to noise ratio (SNR), per-stream rate adaptation can be used for transmission.

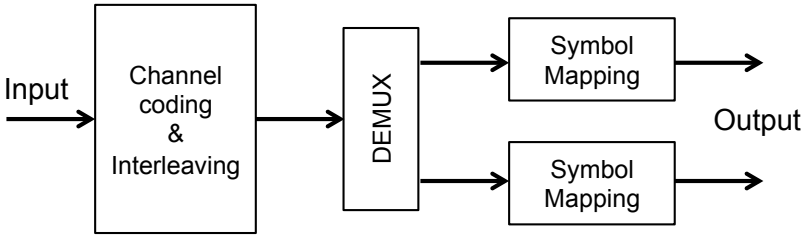

FIGURE 1.7: A multiplexing encoding structure.

For space-time coding structure, the output bits of the channel coding and interleaving block are directly mapped into symbols, and processed by a space-time encoder block (see Section 1.4). The vector symbols are then pre-multiplied by a precoding matrix, detailed in Fig 1.8.

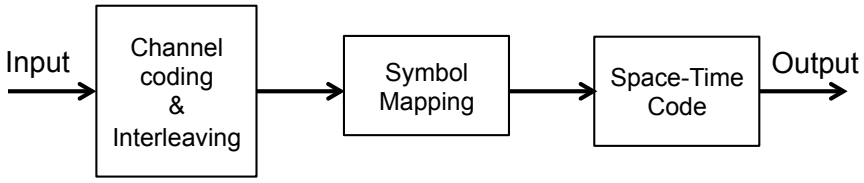

FIGURE 1.8: A space-time encoding structure.

1.5.2 Linear precoding structure

When the CSI is available at the transmitter, the precoder can optimize various criteria such as, for example, maximizing the output capacity [12], maximizing the mutual information [19], etc. However, it has also a general structure which is based on the singular value decomposition (SVD)

$$\mathbf{F} = \mathbf{U}\boldsymbol{\Sigma}\mathbf{V}. \tag{1.29}$$

In this structure, a linear precoder is considered as a combination of an input shaper and a multimode beamformer. The orthogonal beam directions are the left singular matrix $\mathbf{U}$, where each column represents a beam direction (pattern). One should note that the matrix $\mathbf{U}$ contains all eigenvectors of the matrix $\mathbf{F}\mathbf{F}^*$, thus it is often referred to as eigen-beamforming. The matrix $\boldsymbol{\Sigma}$ controls the power allocation on each beam. These powers correspond to the squared singular values of $\boldsymbol{\Sigma}^2$. The right singular matrix $\mathbf{V}$ concerns with the rotation and scaling of the input symbols on each beam and hence is referred to as the input shaping matrix. The linear precoding structure is illustrated in Figure 1.9. To conserve the total transmit power, the precoder must satisfy the condition

$$\text{trace}(\mathbf{F}\mathbf{F}^*) = E_s. \tag{1.30}$$

where E_s is the average transmit power. In other words, the sum of power over all beams must be a constant. The individual beam power is different to each other according to the design criterion, the signal to noise ratio, and the CSIT.

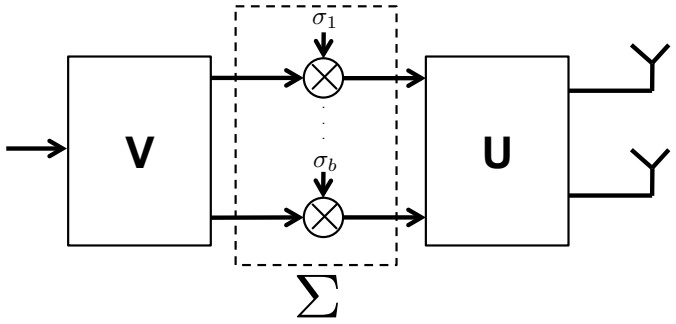

FIGURE 1.9: A linear precoding structure.

1.5.3 Receiver structure

Let us denote $\mathbf{s}$ as the symbol vectors entering the precoder $\mathbf{F}$ at the transmitter, the received signal is then defined by

$$\mathbf{y} = \mathbf{HFs} + \eta, \tag{1.31}$$

where η is a vector of additive white Gaussian noise. The received signal is then decoded to obtain an estimate of the transmitted codeword $\mathbf{s}$. There are many detection methods, depending on the performance of the system and the complexity of the detection. We present herein three representative methods: zero forcing (ZF), linear MMSE, and maximum-likelihood (ML).

Zero Forcing receiver

The zero-forcing receiver uses an inverse filter of the matrix $\mathbf{HF}$ to remove all of the interferences from other symbols. In the case of full rank square matrix $\mathbf{HF}$ (e.g. $n_T = n_R$), the inverse matrix $(\mathbf{HF})^{-1}$ exists and can be used to separate the received symbols. When the number of transmit and receive antennas are not the same, the Moore–Penrose pseudo-inverse $(\mathbf{HF})^{+}$ is proposed to achieve a zero-forcing equalizer [20]. The estimation of the transmit symbols is then

$$\hat{\mathbf{s}} = (\mathbf{HF})^{+}\mathbf{y} = \mathbf{s} + (\mathbf{HF})^{+}\eta, \tag{1.32}$$

where $(\mathbf{HF})^{+}$ denotes the pseudo-inverse matrix of $\mathbf{HF}$, and is defined by $(\mathbf{HF})^{+} = (\mathbf{F}^{*}\mathbf{H}^{*}\mathbf{HF})^{-1}\mathbf{F}^{*}\mathbf{H}^{*}$. We observe that the symbols are separated from each other, and

the power of the effective noise $(\mathbf{HF})^{+}\eta$ may be enhanced by the process of eliminating the symbol interference.

Minimum Mean-Squared Error receiver

In contrast to the ZF receiver, a linear minimum mean square error (MMSE) receiver is proposed to minimize the total effective noise. This receiver contains a weighting matrix $\mathbf{W}$ which is designed according to

$$\min_{\mathbf{W}} E\{\|\hat{\mathbf{s}} - \mathbf{s}\|^2\} = \min_{\mathbf{W}} E\{\|(\mathbf{WHF} - \mathbf{I})\mathbf{s} + \mathbf{W}\eta\|^2\}, \tag{1.33}$$

where the expectation is taken over the input signal and noise distributions. For zero-mean signals with covariance equal to one, the optimum MMSE receiver is given as

$$\mathbf{W} = (\mathbf{F}^{*}\mathbf{H}^{*}\mathbf{HF} + \frac{n_T}{\mathrm{SNR}}\mathbf{I})^{-1}\mathbf{F}^{*}\mathbf{H}^{*}, \tag{1.34}$$

where n_T is the number of transmit antennas, and SNR is the signal to noise ratio. Using the MMSE criterion, the linear least-mean-squares estimation of transmitted symbols is defined by

$$\hat{\mathbf{s}} = \mathbf{Wy}. \tag{1.35}$$

It is observed that when the ratio $\frac{n_T}{\mathrm{SNR}}$ approaches to zero at high SNR, the ZF and MMSE receivers are equivalent.

Maximum Likelihood receiver

The Maximum Likelihood (ML) detection provides a best performance in terms of bit-error-rate (BER) compared to other receivers. The estimation of the transmitted symbol $\mathbf{s}$ is defined by

$$\hat{\mathbf{s}} = \underset{\mathbf{s}}{\mathrm{argmin}} \|\mathbf{y} - \mathbf{HFs}\|^2 \tag{1.36}$$

The ML requires the receiver to consider all possible codewords $\mathbf{s}$ before making the decision and, therefore, can be computationally expensive. The complexity of the ML detection is exponentially proportional to the number of transmit antennas (proportion to M^{n_T}, where M is the size of the transmitted constellation). A new algorithm which

attains ML performances with significantly reduced complexity is presented in [21]. This scheme excludes unreliable candidate symbols in data streams and is based on the MMSE criterion to reduce the ML complexity. In order to decrease the computational complexity, the algorithm of sphere decoder can also be used to obtain an equivalent performance [22], [23].

Sphere Decoding Technique

The principle of sphere decoding technique is based on a bounded distance search among all possible points falling inside a sphere centered at the received point [24]. This concept is illustrated in Fig. 1.10, in which the received signal vector and the possible codewords are represented by a small and large circles, respectively. It is obvious that the overall complexity of the sphere decoding technique is lower than that of the original maximum-likelihood detection that implements a full search in all codewords space.

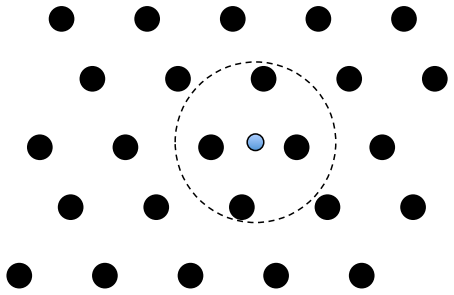

FIGURE 1.10: Principle of sphere decoding technique.

The search region in codewords space, i.e. the number of codewords close to the received signal, depends on the received signal-to-noise-ratio. Although worst case complexity is exponential, the expected complexity of the sphere decoding algorithms is polynomial [25, 26]. The fixed-complexity sphere decoder presented in [27] is one of the most promising approaches to not only enable quasi-ML decoding accuracy but also to reduce the computational complexity. Another efficient closest point search algorithm, based on the Schnorr–Euchner variation of the Pohst method, is also presented in [28].

1.6 Conclusion

The primary purpose of this chapter is to review briefly the principal characteristics of MIMO wireless communications. Firstly, we presented the propagation over wireless channels and different types of diversity techniques. After that, a brief introduction of some MIMO techniques is referred. These techniques can be divided into three main categories: spatial multiplexing, space-time coding, and precoding. The space-time coding technique is available when there is no channel state information at the transmitter while the precoding technique exploits the CSIT and processes signal before transmission. As the channel knowledge at the transmitter offers a high improvement in MIMO performance, the precoding technique becomes of great practical interest in wireless communications. In the rest of this thesis, we investigate the performance and some extensions of the precoding technique based on the maximization of the minimum Euclidean distance in the received constellation.

Chapter 2

MIMO linear precoding techniques

The previous chapter has introduced the basic MIMO system model expressed by a random matrix which represents the channel gains of the paths between the n_T transmit and n_R receive antennas. There exist many methods to estimate MIMO channel at the receiver [29, 30], and we assume, in this thesis, that channel estimation provides a perfect channel state information at the receiver (CSIR). Through a feedback channel, channel state information is returned to the transmitter (CSIT), and a linear precoder can be designed according to this channel knowledge. Precoding design depends not only on the type of CSIT but also on the optimization criteria such as, for example, maximizing the received signal-to-noise ratio (SNR) [31], minimizing the mean square error (MSE) [32], or maximizing the minimum singular value of the channel matrix [33]. These solutions are all based on the singular value decomposition (SVD), which decouples MIMO channels into independent and parallel data-streams. Furthermore, they all perform a power allocation strategy on the MIMO eigen-subchannels. In other words, the data-streams at the transmitter are premultiplied by an eigen-diagonal precoding matrix. Hence, these precoders belong to an important set of linear precoding techniques named as diagonal precoders.

An alternative set of linear precoders is obviously the non-diagonal strategies. One of the most well-known non-diagonal precoding structure was invented independently by Tomlinson [34] and Harashima [35]. To optimize the Schur-convex functions of MSE for all channel substreams, a specific precoding matrix, which also leads to the non-diagonal structure, was proposed in [36]. Another non-diagonal precoder based on an

interesting criterion: maximizing the minimum Euclidean distance (max-$d_{\min}$) between two received data vectors, was firstly presented in [37]. It will be shown, in this chapter, that the precoder max-$d_{\min}$ proposes many interesting improvements compared to other techniques. This precoder will be also investigated, in details, the performance in terms of bit error rate. Its extensions for high-order modulations will be shown in chapter 3, and for large MIMO systems in chapter 4.

2.1 Virtual transformation

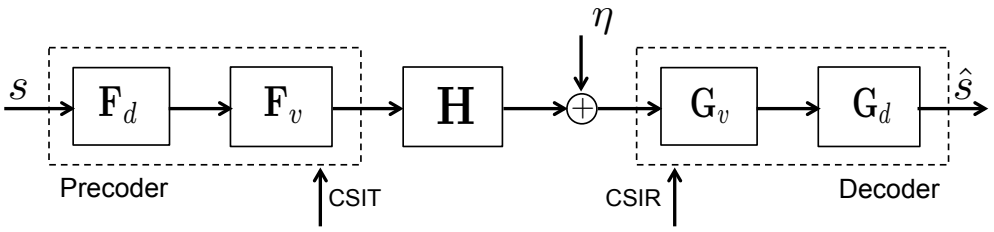

FIGURE 2.1: Virtual model of MIMO systems

Let us consider a MIMO channel with n_R receive, n_T transmit antennas over which we want to transmit b independent data streams. Suppose there are a precoding matrix $\mathbf{F}$ at the transmitter and a decoding matrix $\mathbf{G}$ at the receiver, the basic system model can be expressed as

$$\mathbf{y} = \mathbf{GHFs} + \mathbf{G}\eta, \tag{2.1}$$

where $\mathbf{H}$ is the $n_R \times n_T$ channel matrix, $\mathbf{F}$ is the $n_T \times b$ precoding matrix, $\mathbf{G}$ is the $b \times n_R$ decoding matrix, $\mathbf{s}$ is the $b \times 1$ transmitted vector symbol, and η is the $n_R \times 1$ additive noise vector. We should remark that $b \leq \text{rank}(\mathbf{H}) \leq \min(n_T, n_R)$, so n_T and n_R can be larger than b. In the following sections, we assume

$$E[\mathbf{ss}^*] = \mathbf{I}_b, E[\mathbf{s}\eta^*] = 0 \text{ and } E[\eta\eta^*] = \mathbf{R}_\eta, \tag{2.2}$$

where $\mathbf{I}_b$ is the identity matrix of size $b \times b$ and $\mathbf{R}_\eta$ is the noise covariance matrix. Let us define E_s as the average transmit power. Thereafter, the precoding matrix $\mathbf{F}$ must satisfy the power constraint

$$\text{trace}\{\mathbf{FF}^*\} = E_s. \tag{2.3}$$

Step	Method	$\mathbf{F}_i$	$\mathbf{G}_i$	$\mathbf{H}_{v_i}$	$\mathbf{R}_{v_i}$
Noise whitening	$\mathbf{R}_n{=}\mathbf{Q}\mathbf{\Lambda}\mathbf{Q}^*$	$\mathbf{F}_1{=}\mathbf{I}_{n_T}$	$\mathbf{G}_1{=}\mathbf{\Lambda}^{-\frac{1}{2}}\mathbf{Q}^*$	$\mathbf{H}_{v_1}{=}\mathbf{G}_1\mathbf{H}\mathbf{F}_1$	$\mathbf{R}_{v_1}{=}\mathbf{I}_{n_R}$
Channel diagonalization	$\mathbf{H}_{v_1}{=}\mathbf{A}\mathbf{\Sigma}\mathbf{B}^*$	$\mathbf{F}_2{=}\mathbf{B}$	$\mathbf{G}_2{=}\mathbf{A}^*$	$\mathbf{H}_{v_2}{=}\mathbf{\Sigma}$	$\mathbf{R}_{v_2}{=}\mathbf{I}_{n_R}$
Dimensionality reduction		$\mathbf{F}_3{=}\begin{pmatrix}\mathbf{I}_b\\0\end{pmatrix}$	$\mathbf{G}_3{=}(\mathbf{I}_b \quad 0)$	$\mathbf{H}_v{=}\mathbf{\Sigma}_b$	$\mathbf{R}_{n_\eta}{=}\mathbf{I}_b$

TABLE 2.1: Steps to obtain the diagonal MIMO system in the case of CSIT

If the channel state information (CSI) is perfectly known at both the transmitter and receiver, a diagonalized channel matrix and a whitened noise can be obtained. This operation is decomposed in three steps and is denoted as virtual transformation. The key of this method is illustrated in Fig. 2.1. Firstly, the precoding and decoding matrices are decomposed as $\mathbf{F} = \mathbf{F}_v\mathbf{F}_d$ and $\mathbf{G} = \mathbf{G}_d\mathbf{G}_v$. Then, the new decompositions of two matrices $\mathbf{F}_v$ and $\mathbf{G}_v$ into the product of three matrices are considered.

$$\mathbf{F}_v = \mathbf{F}_1\mathbf{F}_2\mathbf{F}_3 \qquad \text{and} \qquad \mathbf{G}_v = \mathbf{G}_1\mathbf{G}_2\mathbf{G}_3, \tag{2.4}$$

where $(\mathbf{F}_i, \mathbf{G}_i)$ perform the particular operations which are detailed in Tab. 2.1.

2.1.1 Noise whitening

Let us consider the eigenvalue decomposition of the noise covariance matrix

$$\mathbf{R}_\eta = E[\eta\eta^*] = \mathbf{Q}\mathbf{\Lambda}\mathbf{Q}^*, \tag{2.5}$$

where $\mathbf{Q}$ is a unitary matrix and $\mathbf{\Lambda}$ is a diagonal matrix. The goal of this step is to obtain the correlation matrix $\mathbf{R}_{v_1} = E[\mathbf{G_1}\eta\eta^*\mathbf{G_1}^*] = \mathbf{G_1}\mathbf{Q}\mathbf{\Lambda}\mathbf{Q}^*\mathbf{G_1}^*$ equal to an identity matrix. The matrix $\mathbf{G_1}$ is therefore defined by

$$\mathbf{G_1} = \mathbf{\Lambda}^{-1/2}\mathbf{Q}^*. \tag{2.6}$$

The intermediate channel of this operation is given by

$$\mathbf{H}_{v_1} = \mathbf{G}_1\mathbf{H}\mathbf{F}_1, \tag{2.7}$$

where $\mathbf{F}_1$ is considered as an identity matrix of size n_T.

2.1.2 Channel diagonalization

The singular value decomposition (SVD) of the intermediate matrix $\mathbf{H}_{v_1}$ is used to diagonalize the channel. Indeed, we have

$$\mathbf{H}_{v_1} = \mathbf{A}\mathbf{\Sigma}\mathbf{B}^*, \tag{2.8}$$

where $\mathbf{A}$ and $\mathbf{B}^*$ are unitary matrices, and $\mathbf{\Sigma}$ is a diagonal matrix whose elements represent the square roots of all eigenvalues of the matrix $\mathbf{H}_{v_1}\mathbf{H}_{v_1}^*$. One should note that these eigenvalues are real positive numbers and sorted in decreasing order. The number of non-null eigenvalues depends on the rank of the matrix $\mathbf{H}_{v_1}$

$$k = \text{rank}(\mathbf{H}_{v_1}) \leq \min(n_T, n_R). \tag{2.9}$$

The diagonal matrix Σ can be then expressed by these non-null eigenvalues

$$\Sigma = \begin{pmatrix} \mathbf{\Sigma}_k & 0 \\ 0 & 0 \end{pmatrix} \tag{2.10}$$

where the matrix Σ_k contains all of the non-null eigenvalues. To diagonalize the intermediate channel matrix $\mathbf{H_{v_1}}$, the proposed solution is

$$\mathbf{F}_2 = \mathbf{B} \quad \text{and} \quad \mathbf{G}_2 = \mathbf{A}^*. \tag{2.11}$$

The second intermediate channel matrix $\mathbf{H_{v_2}}$ is then diagonal and defined by

$$\mathbf{H}_{v_2} = \mathbf{G}_2\mathbf{H_{v_1}}\mathbf{F}_2 = \mathbf{\Sigma}. \tag{2.12}$$

In addition, the correlation matrix $\mathbf{R}_{v_2}$ is given by

$$\mathbf{R}_{v_2} = \mathbf{G}_2\mathbf{R}_{v_1}\mathbf{G}_2^* = \mathbf{G}_2\mathbf{G}_2^* = \mathbf{I}_{n_R}, \tag{2.13}$$

it is because $\mathbf{G}_2$ is a unitary matrix.

2.1.3 Dimensionality reduction

The diagonal form of the matrix $\mathbf{H_{v_2}}$ corresponds to the gains of each subchannels. It is noted that these diagonal elements are sorted in decreasing order. The goal of this operation is to obtain the dimension corresponding to the number of desired data-streams b. The matrices $\mathbf{F}_3$ and $\mathbf{G}_3$ are then defined by

$$\mathbf{F}_3 = \begin{pmatrix} \mathbf{I}_b \\ 0 \end{pmatrix} \quad \text{and} \quad \mathbf{G}_3 = (\mathbf{I}_b \quad 0). \tag{2.14}$$

These operations are only available if $b \leq k$, so we consider the channel matrix such that $b \leq k = \min(n_T, n_R)$. The resulting matrix is given by

$$\mathbf{H}_v = \mathbf{G}_3 \mathbf{H_{v_2}} \mathbf{F}_3 = \mathbf{\Sigma}_b, \tag{2.15}$$

where $\mathbf{\Sigma}_b$ represents the b largest singular values of $\mathbf{H}_{v_1}$. The correlation matrix of the noise is also identity but the dimension is different

$$\mathbf{R}_{\eta_v} = \mathbf{I}_b. \tag{2.16}$$

2.1.4 Virtual channel representaion

The received signal in (2.1) is now re-expressed as

$$\mathbf{y} = \mathbf{G}_d \mathbf{H}_v \mathbf{F}_d \mathbf{s} + \mathbf{G}_d \eta_v, \tag{2.17}$$

where $\mathbf{H}_v = \mathbf{G}_v \mathbf{H} \mathbf{F}_v$ is the $b \times b$ eigen-channel matrix, $\eta_v = \mathbf{G}_v \eta$ is the $b \times 1$ virtual noise vector. Thanks to virtual transformation, the eigen-channel matrix $\mathbf{H}_v$ is diagonal and defined by

$$\mathbf{H}_v = \text{diag}(\sigma_1, ..., \sigma_b), \tag{2.18}$$

where σ_i stands for every subchannel gain and is sorted by decreasing order. One should note that the virtual precoding matrix $\mathbf{F}_v$ is orthonormal (e.g. $\mathbf{F}_v^* \mathbf{F}_v = \mathbf{I}$), and the power constraint is then given by

$$\text{trace}\{\mathbf{F}\mathbf{F}^*\} = \text{trace}\{\mathbf{F}_d \mathbf{F}_d^*\} = E_s. \tag{2.19}$$

The basic and the equivalent diagonal transmission systems are shown by the block diagram in Fig. 2.2. In these models, the input bit streams are firstly modulated to symbol streams are then passed through a linear precoder. The linear precoding matrix **F** add redundancy to the input symbol streams to improve the system performance. The output of the precoder is then sent to the channel **H** with the additive gaussian noise η. The decoding matrix **G** is used to remove any redundancy that has been introduced by the precoder. For the diagonal transmission model, the decoding matrix $\mathbf{G}_d$ will have no influence on the performance and is consequently assumed to be an identity matrix if a maximum likelihood (ML) detection is considered at the receiver.

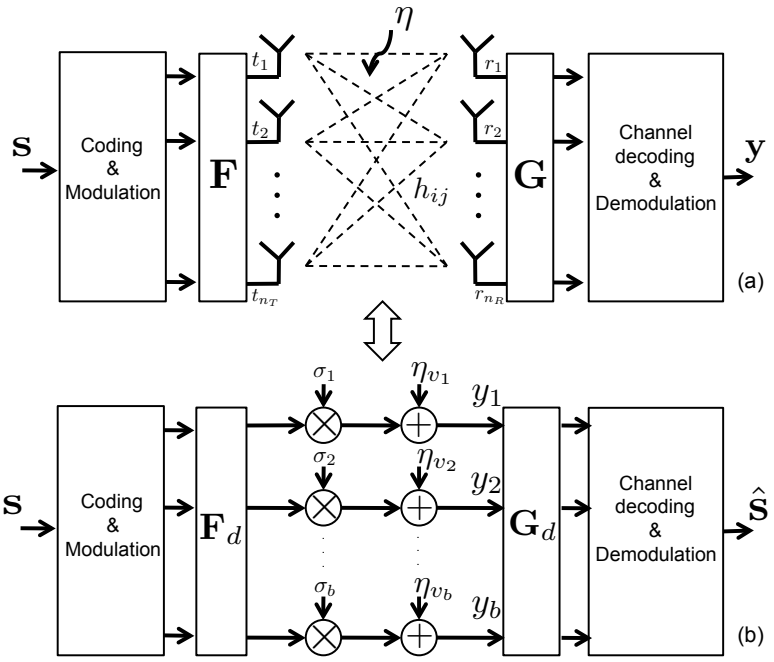

FIGURE 2.2: Block diagram of a MIMO system: basic model (a), diagonal transmission model (b).

The virtual precoding matrix $\mathbf{F}_d$ is used to optimize the criteria such as maximizing the output capacity [12], maximizing the received signal-to-noise ratio (SNR) [31], minimizing the mean square error (MSE) [32], maximizing the minimum singular value of the channel matrix [33]. These precoders belong to the diagonal group. In other words, the precoding matrix $\mathbf{F}_d$ is diagonal and leads to power allocation on b parallel independent data streams.

In the next sections, we present some of the traditional precoders and concentrate on a non-diagonal precoder which optimizes the minimum Euclidean distance between the received signals.

2.2 Existing precoders

Due to the form of the precoder $\mathbf{F}$, the precoding technique can be classified into two categories: diagonal and non-diagonal schemes. A precoder is called as diagonal if and only if the precoding and decoding matrices $(\mathbf{F}_d, \mathbf{G}_d)$ in (2.17) are diagonal. When the receiver is based on a maximum likelihood detection, the decoding matrix $\mathbf{G}_d$ has no influence on the performance and only the precoding matrix $\mathbf{F}_d = \text{diag}(f_1, f_2, ..., f_b)$ is considered in the optimization. The general principle of the diagonal precoder is illustrated in the Fig 2.3. The problem becomes finding the power distribution expressed by the coefficients f_i^2 to optimize a particular criterion. We present, herein, some diagonal precoders such as Beamforming, Water-Filling, Minimum Mean Square Error (MMSE), Quality of Service (QoS), and Equal Error (EE).

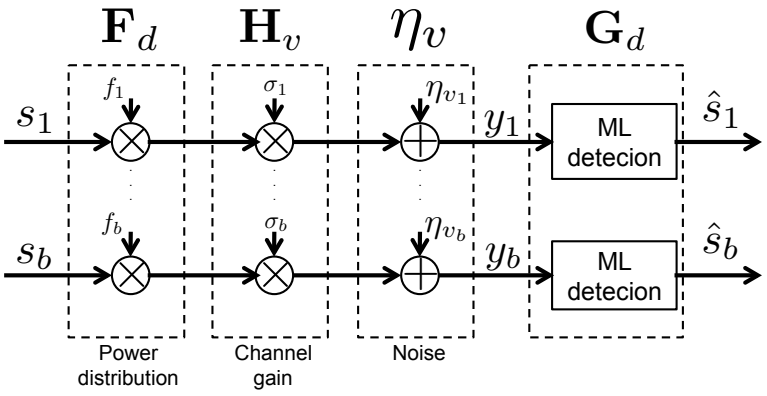

FIGURE 2.3: Diagonal precoding schema using maximum likelihood detection (ML) at the receiver.

2.2.1 Beamforming or max-SNR precoder

As its name implies, this precoder maximizes the signal to noise ratio (SNR) at the transmitter, and uses only the strongest virtual subchannel corresponding to the SNR σ_1^2 [38, 39]. It concentrates all of the transmit power on the most favorable direction represented by the singular vector associated with the maximum eigenvalue [31]. The expression of the received signal, in virtual representation, is then

$$\mathbf{y} = \sqrt{E_s}\sigma_1\mathbf{s} + \eta, \tag{2.20}$$

where $\mathbf{s}$ is the transmit signal, η is the additive white Gaussian noise of the channel. We see that the structure of this precoder is rather simple. However, only one symbol is transmitted in each time slot, and, therefore, the data rate is limited by the modulation used at the transmitter.

2.2.2 Water-Filling precoder

The goal of this precoder is maximizing the capacity of the MIMO system. By using (1.16), the capacity of a virtual channel can be simplified by

$$C = \sum_{i=1}^{b} \log_2(1 + f_i^2 \sigma_i^2), \quad \text{with} \quad \sum_{i=1}^{b} f_i^2 = E_s. \tag{2.21}$$

The optimized solution is given by

$$f_i^2 = \begin{cases} \Psi_{\text{WF}} - \frac{1}{\sigma_i^2} & \text{if } \Psi_{\text{WF}} > \frac{1}{\sigma_i^2} \\ 0 & \text{others} \end{cases} \quad \text{with} \quad i = 1, ..., b \tag{2.22}$$

where the threshold Ψ_{WF} depends on the virtual channel and is defined by

$$\Psi_{\text{WF}} = \frac{E_s + \gamma_{\text{WF}}}{b_{\text{WF}}} \quad \text{with} \quad \gamma_{\text{WF}} = \sum_{i=1}^{b_{\text{WF}}} \frac{1}{\sigma_i^2} \tag{2.23}$$

where b_{WF} is the number of the subchannels used by the water-filling precoder. The algorithm to determine the number of virtual channels b_{WF} is illustrated in Fig. 2.4.

2.2.3 Minimum Mean Square Error precoder

The minimum mean square error (MMSE) precoder is proposed to minimize the total effective noise where the optimized equation is given by

$$\min_{\mathbf{F}_d, \mathbf{G}_d} E[\|y - s\|^2] = \min_{\mathbf{F}_d, \mathbf{G}_d} \sum_{i=1}^{b} E\left[\|g_i \sigma_i f_i s_i + g_i \eta_{v_i} - s_i\|^2\right], \tag{2.24}$$

where the decoding matrix is defined by $\mathbf{G}_d = \text{diag}(g_1, g_2, ..., g_b)$. The power constraint is expressed by

$$\sum_{i=1}^{b} f_i^2 = E_s. \tag{2.25}$$

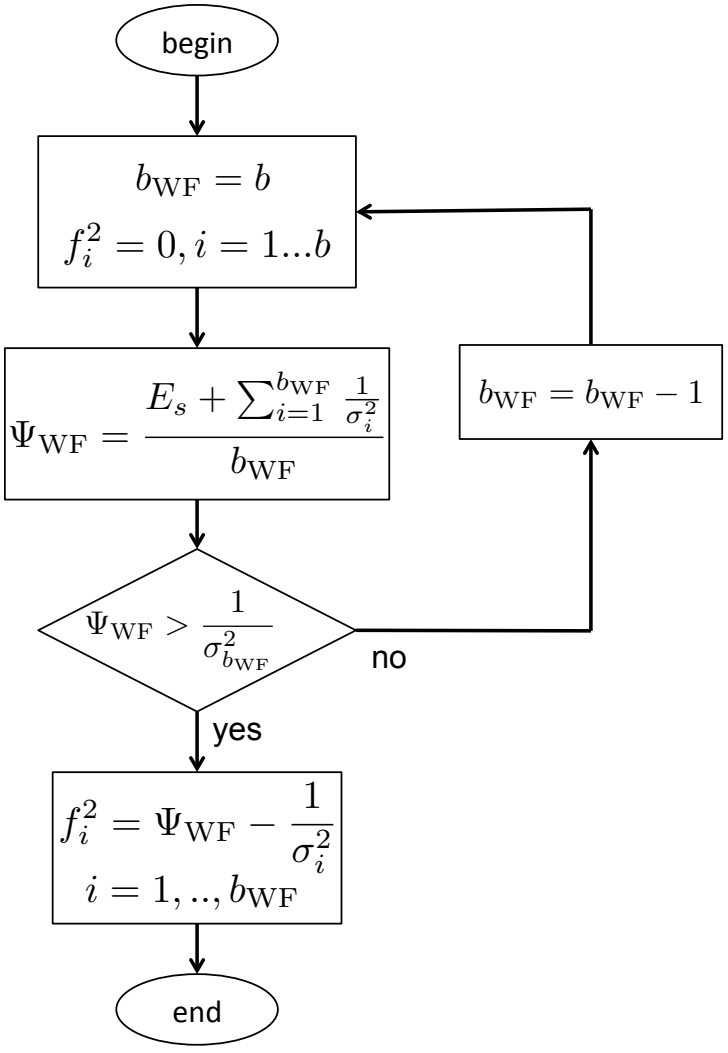

FIGURE 2.4: Algorithm of Water-Filling precoder.

As for the Water-Filling case, the optimized solution of MMSE precoder is defined by

$$f_i^2 = \begin{cases} \frac{1}{\sigma_i}\left(\Psi_{\mathrm{MSE}} - \frac{1}{\sigma_i}\right) & \text{if } \Psi_{\mathrm{MSE}} > \frac{1}{\sigma_i} \\ 0 & \text{others} \end{cases} \quad \text{with } i = 1, ..., b \tag{2.26}$$

where b_{MSE} is the number of virtual subchannels such that $\Psi_{\mathrm{MSE}} > 1/\sigma_i$, for $i = 1, ..., b$. The threshold Ψ_{MSE} is given by

$$\Psi_{\mathrm{MSE}} = \frac{E_s + \gamma_{\mathrm{MSE}}}{\sum_{i=1}^{b_{\mathrm{MSE}}} \frac{1}{\sigma_i}} \quad \text{with} \quad \gamma_{\mathrm{MSE}} = \sum_{i=1}^{b_{\mathrm{MSE}}} \frac{1}{\sigma_i^2}. \tag{2.27}$$

The MMSE and Water-Filling precoders have the same algorithm to determine the number of active virtual subchannels (as shown in Fig. 2.4). Both precoders remove some

subchannels and pour power on the others to optimize different criteria. The number of used subchannels depends on the characteristics of the channel and the optimized criterion.

2.2.4 Quality of Service precoder

The principle of this precoder is based on the different demands of Signal to Noise Ratio on each subchannel [32]. For example, a data-streams represents the video while another transfers the speech. The data-rate of the first channel is obviously higher than the second. Consequently, the first one needs a higher SNR than the second one. Indeed, the SNR of each subchannel is noted by

$$f_i^2 \sigma_i^2 = \omega_i f_b^2 \sigma_b^2 \quad \text{with } i = 1, ..., b \tag{2.28}$$

where ω_i represents the SNR of the subchannel i compared to the subchannel b. The gains of the subchannels are ordered and the first one corresponds to the most important signal to noise ratio, e.g. $\omega_1 \geq \omega_2 \geq \cdots \geq 1$. The coefficients of this precoder is then given by

$$f_i^2 = w_i \frac{E_s}{\sigma_i^2 \sum_{k=1}^{b} \frac{w_k}{\sigma_k^2}} \tag{2.29}$$

Unlike the WF and MMSE precoders, the QoS solution always uses a same number of virtual subchannels for all of the signal to noise ratios.

2.2.5 Equal Error precoder

This precoder is a special case of the QoS scheme when the SNR coefficients ω_i are all equal. It is also the solution which maximizes a lower bound of the minimum Euclidean distance. The diagonal entries of this precoder are defined by

$$f_i^2 = \frac{E_s}{\sigma_i^2 \sum_{k=1}^{b} \frac{1}{\sigma_k^2}} \tag{2.30}$$

In the precoder, the average error rate of each subchannel is identical and the number of used subchannels is constant. By maximizing the minimum eigenvalues $\lambda_{\min}(\mathrm{SNR}(\mathbf{F},\mathbf{G}))$, it optimizes a lower bound of the minimum distance between two received symbols for an ML detection [33].

2.2.6 Minimum BER diagonal precoder

The authors in [40] proposed a diagonal precoder in order to minimize the criteria: Bit Error Rate. For a square M-QAM constellation and white Gaussian noise with variance one, the probability of error on the subchannel i of the virtual channel $\mathbf{H}_v$ is defined by [41]

$$P_{e,i} = \alpha_M \mathrm{erfc}\left(\sqrt{\beta_M f_i^2 \sigma_i^2}\right), \tag{2.31}$$

where $\alpha_M = \frac{2}{\log_2 M}\left(1 - \frac{1}{\sqrt{M}}\right)$, and $\beta_M = \frac{3}{2(M-1)}$. Using Lagrange multiplier μ, the optimization criterion is given by

$$\mathcal{L} = \frac{\alpha_M}{b}\sum_{i=1}^{b} \mathrm{erfc}\left(\sqrt{\beta_M f_i^2 \sigma_i^2}\right) + \mu\left(\sum_{i=1}^{b} f_i^2 - E_s\right). \tag{2.32}$$

By canceling the partial derivative $\frac{\partial \mathcal{L}}{\partial f_i}$, we obtain

$$f_i^2 = \frac{1}{2\beta_M \sigma_i^2} W_0\left(\frac{2\sigma_i^4 \alpha_M^2 \beta_M^2}{\mu^2 \pi b^2}\right). \tag{2.33}$$

where W_0 stands for Lambert's W function of index 0 [42]. The function $W_0(x)$ is an increasing function, and is positive for $x > 0$. Hence, when μ^2 increases, the f_i^2 decrease. Therefore, the value of μ^2 can be easily determined by using the transmit power constraint. It is noted that the function $W_0(x)$ can be approximated by $W_0(x) \approx \log(x) - \log(\log(x))$, and the optimized solution is then defined by

$$f_i^2 = \frac{a_i(1 - \sum_k A_k) + A_i \sum_k a_k}{\sum_k a_k}, \tag{2.34}$$

where $a_i = \frac{1}{\beta_M \sigma_i^2}$, $b_i = \frac{2\sigma_i^4 \alpha_M^2 \beta_M^2}{\mu^2 \pi b^2}$, and $A_i = a_i\left(\log(b_i) - \log(\log(b_i))\right)$.One should note that the approximated solution is not available for the low SNRs. It is because that the value $\log(b_i)$ can be negative and the term A_i, then, can not be determined.

2.2.7 X- and Y-codes precoder

In order to improve the low diversity order, the authors in [43] have proposed X- and Y-Codes to pair subchannels having different diversity orders. The idea is that the information bits are first mapped to the information symbol vector $\mathbf{u} = (u_1, ..., u_b)^T \in \mathbb{C}_b$, and then mapped to the coded symbols $\mathbf{z} = (z_1, ..., z_b)^T \in \mathbb{C}_b$ using a $b \times b$ matrix $\mathbf{F}_c$, i.e., $\mathbf{z} = \mathbf{F}_c\mathbf{u} + \mathbf{u}_0$, where $\mathbf{u}_0 \in \mathbb{C}_b$ is a displacement vector used to reduce the average transmitted power. By using a channel diagonalization, the signal at the receiver is defined by [44]

$$y = \mathbf{H}_v\mathbf{F}_c\mathbf{u} + \mathbf{n} \tag{2.35}$$

where $\mathbf{F}_c$ is fully characterized by the list of pairings and the 2×2 encoder matrices for each pair. The information symbols the k-th pair u_{ik} and u_{jk} are jointly coded using a real 2×2 matrix $\mathbf{A}_k \triangleq \{a_{k,i,j}\}, i, j \in [1, 2]$. Each $\mathbf{A}_k$ is a submatrix of the code matrix $\mathbf{F}_c \triangleq \{f_{i,j}\}$, i.e.,

$$\begin{cases} f_{i_k,i_k} = a_{k,1,1} & f_{i_k,j_k} = a_{k,1,2} \\ f_{j_k,i_k} = a_{k,2,1} & f_{j_k,j_k} = a_{k,2,2} \end{cases} \tag{2.36}$$

In the case of $b = 6$, for example, the X-Code structure is given by

$$\mathbf{F}_c = \begin{pmatrix} a_{1,1,1} & & & & & a_{1,1,2} \\ & a_{2,1,1} & & & a_{2,1,2} & \\ & & a_{1,1,1} & a_{1,1,2} & & \\ & & a_{1,1,1} & a_{1,1,2} & & \\ & a_{2,1,1} & & & a_{2,1,2} & \\ a_{1,1,1} & & & & & a_{1,1,2} \end{pmatrix} \tag{2.37}$$

and the Y-Code structure is given by

$$\mathbf{F}_c = \begin{pmatrix} a_{1,1,1} & & & & & a_{1,1,2} \\ & a_{2,1,1} & & & a_{2,1,2} & \\ & & a_{1,1,1} & a_{1,1,2} & & \\ & & a_{1,1,1} & & & \\ & a_{2,1,1} & & & & \\ a_{1,1,1} & & & & & \end{pmatrix} \tag{2.38}$$

Let us define $\mathbf{u}_k \triangleq [u_{i_k}, u_{j_k}]^T$. Due to the transmit power constraint, and uniform transmit power allocation between $b/2$ pairs, the encoder matrices $\mathbf{A}_k$ must satisfy the condition

$$\mathbb{E}\left[\|\mathbf{A}_k\mathbf{u}_k + \mathbf{u}_k^0\|^2\right] = \frac{2E_s}{b}, \quad k = 1, 2, \ldots, b/2. \tag{2.39}$$

For X-Codes, the encoder matrices are 2×2 real orthogonal matrices parameterized by a single angle, and are given by

$$\mathbf{A}_k = \begin{pmatrix} \cos\theta_k & \sin\theta_k \\ -\sin\theta_k & \cos\theta_k \end{pmatrix} \tag{2.40}$$

For Y-Codes, the encoder matrices are considered by the form

$$\mathbf{A}_k = \begin{pmatrix} a_k & 2a_k \\ 2b_k & 0 \end{pmatrix} \tag{2.41}$$

The optimized design of X,Y-Code/Precoders are respectively detailed in [44]. It can be demonstrated that these designs achieve high rate and high diversity at low complexity by paring the virtual subchannels into the SVD precoding.

2.2.8 Tomlinson-Harashima precoder

In this section, we explore a different precoding technique for MIMO spatial systems. The structure of these precoders are no longer diagonal. A MIMO transceiver using the Tomlinson-Harashima precoder (THP) is shown in Fig. 2.5. Here, $\mathbf{H}$ is a $n_R \times n_T$ channel matrix, and $\mathbf{F}$ is a linear precoder. The received signal $\mathbf{y}$ is then defined by

$$\mathbf{y} = \mathbf{HFs} + \eta, \tag{2.42}$$

where $\mathbf{s}$ is transmitted vectors, and η is $n_R \times 1$ additive Gaussian noise vector. At the receiver, a Decision Feedback Equalizer (DFE) is considered. The DFE equalizer consists of a feedforward part $\mathbf{G}$ and a feedback part $\mathbf{B}$. The feedforward matrix $\mathbf{G}$ whitens noise and guarantees causality. Therefore, the decision feedback is ensured by restricting $\mathbf{B}$ to be lower triangular. The feedback matrix cancels the interference caused by already detected symbols.

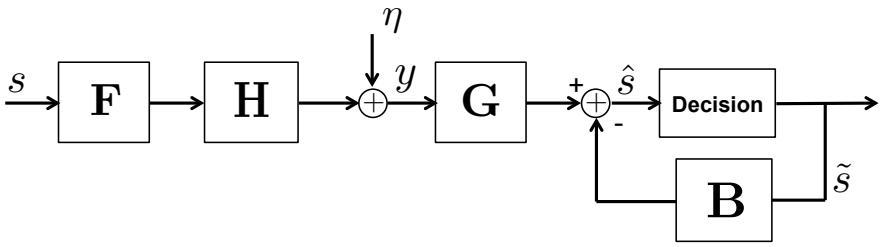

FIGURE 2.5: Block diagram of linear precoder and matrix DFE.

Let us denote $\tilde{\mathbf{s}}$ as the signal vector after the decision device, the input $\hat{\mathbf{s}}$ to the decision block is given by $\hat{\mathbf{s}} = \mathbf{GHFs} - \mathbf{B}\tilde{\mathbf{s}} + \mathbf{G}\eta$. Under the assumption of correct past decisions, i.e. $\tilde{\mathbf{s}} = \mathbf{s}$, we have

$$\hat{\mathbf{s}} = (\mathbf{GHF} - \mathbf{B})\mathbf{s} + \mathbf{G}\eta. \tag{2.43}$$

The feedback section of the DFE can separate the signal by the feedback matrix $\mathbf{B} = \mathbf{GHF} - \mathbf{I}$. This is DFE decision subject to a zero-forcing (ZF) constraint [45, 46]. An optimal linear transceiver of this design was presented in [47]. It is shown that the generalized triangular decomposition (GTD) offers an optimal family of solutions, and DFE transceiver using the geometric mean decomposition (GMD) is another member of the optimal family.

Other designs for DFE based schemes use a minimum mean square error (MMSE) criterion at the receiver [48, 49]. Defining the error signal $\mathbf{e} = \mathbf{s} - \hat{\mathbf{s}}$, the mean square error matrix can be written as

$$E\{\mathbf{ee}^*\} = \mathbf{CC}^* - \mathbf{CF}^*\mathbf{H}^*\mathbf{G}^* - \mathbf{GHFC}^* + \mathbf{GHFF}^*\mathbf{H}^*\mathbf{G}^* + \mathbf{GR}_\eta\mathbf{G}^*, \tag{2.44}$$

where $\mathbf{C} = \mathbf{I} + \mathbf{B}$ is a unit diagonal lower triangular matrix, and $\mathbf{R}_\eta$ is the covariance matrix of the Gaussian noise η. The object becomes to design $\mathbf{G}$, $\mathbf{C}$, and $\mathbf{F}$ for different criteria, subject to the power constraint. The authors in [50] propose a broad range of design criteria which can be expressed as Schur-convex or Schur-concave functions of the MSE, and provide optimal transceivers designs for these two classes.

2.3 Minimum Euclidean distance based precoder

This precoder is based on the maximization of the minimum Euclidean distance (max-$d_{\min}$) between signal points at the receiver side. The criterion provides a significant enhancement in terms of bit-error rate, especially when an ML receiver is used [51]. However, the optimization of max-$d_{\min}$ precoder is difficult for two reasons. Firstly, the space of solution is large and exponentially proportional to the number of data-streams b. Secondly, the exact expression of max-$d_{\min}$ precoder depends on many parameters such as the modulation used at the transmitter, and the characteristic of the virtual channel $\mathbf{H}_v$. For this reason, the optimized solution is limited for a small number of data streams ($b = 2$) and for low-order QAM modulations [37].

In this section, we present the simple solution of $d_{\min}$ criterion for two data-streams and QPSK modulation. After that, its performance will be shown in comparison with other traditional precoders.

2.3.1 Minimum Euclidean distance

When a symmetric constellation is considered at the transmitter, the minimum Euclidean distance between two symbols at the receiver is defined by

$$d^2_{\min} = \min_{\mathbf{s}_k,\mathbf{s}_l \in S, \mathbf{s}_k \neq \mathbf{s}_l} \|\mathbf{H}_v \mathbf{F}_d (\mathbf{s}_k - \mathbf{s}_l)\|^2, \tag{2.45}$$

where $\mathbf{x}_k$ and $\mathbf{x}_l$ are two transmit signals, and S is the set of all these possible transmit vectors. Let us define $\breve{\mathbf{x}}$ a difference vector as $\breve{\mathbf{x}} = \mathbf{s}_k - \mathbf{s}_l$, with $\mathbf{s}_k \neq \mathbf{s}_l$. Because there exist many collinear difference vectors, we introduce the reduced set $\breve{X}$ of S which does not contain the redundant difference vectors. The $d_{\min}$ criterion is now expressed as

$$d^2_{\min} = \min_{\breve{\mathbf{x}} \in \breve{X}} \|\mathbf{H}_v \mathbf{F}_d \breve{\mathbf{x}}\|^2. \tag{2.46}$$

This criterion is particularly well adapted for the ML receiver because the symbol error probability depends on the Euclidean distance between received vectors [52], [53]. Then,

the precoding matrix $\mathbf{F}_d$ is obtained by maximizing the minimum Euclidean distance

$$\mathbf{F}_{d_{min}} = \arg\max_{\mathbf{F}_d} \; d_{\min}, \tag{2.47}$$

under the power constraint $\text{trace}\{\mathbf{F}_d\mathbf{F}_d^*\} = E_s$.

2.3.2 Parameterized form for 2-D virtual subchannels

The optimization for 2-D virtual subchannels is obtained by the change of variables for two eigenvalues of the channel. These two new variables are defined by

$$\begin{cases} \sigma_1 = \rho\cos\gamma \\ \sigma_2 = \rho\sin\gamma \end{cases} \Leftrightarrow \begin{cases} \rho = \sqrt{\sigma_1^2 + \sigma_2^2} \\ \gamma = \arctan\frac{\sigma_1}{\sigma_2} \end{cases} \tag{2.48}$$

where ρ and γ represent the channel gain and channel angle, respectively. The virtual channel is then given by

$$\mathbf{H}_v = \begin{pmatrix} \sigma_1 & 0 \\ 0 & \sigma_2 \end{pmatrix} = \rho \begin{pmatrix} \cos\gamma & 0 \\ 0 & \sin\gamma \end{pmatrix} \tag{2.49}$$

Note that $\sigma_1 \geq \sigma_2 > 0$, so we have $0 < \gamma \leq \pi/4$. By using a singular value decomposition, it can be demonstrated that max-$d_{\min}$ precoding structure can be expressed by the product of the power allocation, the rotation and scaling matrices [37]

$$\mathbf{F}_d = \sqrt{E_s} \begin{pmatrix} \cos\psi & 0 \\ 0 & \sin\psi \end{pmatrix} \begin{pmatrix} \cos\theta & \sin\theta \\ -\sin\theta & \cos\theta \end{pmatrix} \begin{pmatrix} 1 & 0 \\ 0 & e^{i\varphi} \end{pmatrix}, \tag{2.50}$$

where ψ is linked to the power allocation on the eigen-subchannels, and θ and φ correspond to scaling and rotation of the received constellation. If θ and φ are both equal to zero, the matrix $\mathbf{F}_d$ is diagonal and leads to the power allocation case.

2.3.3 Optimal solution for QPSK modulation

For a QPSK modulation with $b = 2$ data-streams, the transmitted symbols belong to the set

$$S = \left\{ \frac{1}{\sqrt{2}}(1+i), \frac{1}{\sqrt{2}}(1-i), \frac{1}{\sqrt{2}}(-1+i), \frac{1}{\sqrt{2}}(-1-i) \right\}. \tag{2.51}$$

It was shown in [37] that the optimal solution is rather simple with only two precoder expressions

- if $0 \leq \gamma \leq \gamma_0$

$$\mathbf{F}_d = \mathbf{F}_{r_1} = \sqrt{E_s} \begin{pmatrix} \sqrt{\frac{3+\sqrt{3}}{6}} & \sqrt{\frac{3-\sqrt{3}}{6}} e^{i\frac{\pi}{12}} \\ 0 & 0 \end{pmatrix} \tag{2.52}$$

- if $\gamma_0 \leq \gamma \leq \pi/4$

$$\mathbf{F}_d = \mathbf{F}_{octa} = \sqrt{\frac{E_s}{2}} \begin{pmatrix} \cos\psi & 0 \\ 0 & \sin\psi \end{pmatrix} \begin{pmatrix} 1 & e^{i\frac{\pi}{4}} \\ -1 & e^{i\frac{\pi}{4}} \end{pmatrix} \tag{2.53}$$

$$\text{where} \begin{cases} \psi = \arctan \frac{\sqrt{2}-1}{\tan\gamma} \\ \gamma_0 = \arctan \sqrt{\frac{3\sqrt{3}-2\sqrt{6}+2\sqrt{2}-3}{3\sqrt{3}-2\sqrt{6}+1}} \approx 17,28^0 \end{cases}$$

The parameter ψ is linked to the power allocation on each sub-channel, and the constant threshold γ_0 allows the precoder to use one or two sub-channels. The value of γ_0 is obtained when considering that the two precoders give the same minimum Euclidean distance $d_{\min}$. This one depends on ρ and γ and is expressed as

$$d_{\min} = \begin{cases} \sqrt{E_s}\rho\sqrt{1-\frac{1}{\sqrt{3}}}\cos\gamma & \text{if } 0 < \gamma \leq \gamma_0 \\ \sqrt{E_s}\rho\sqrt{\frac{(4-2\sqrt{2})\cos^2\gamma\sin^2\gamma}{1+(2-2\sqrt{2})\cos^2\gamma}} & \text{if } \gamma_0 < \gamma \leq \pi/4 \end{cases} \tag{2.54}$$

Received constellation

One should note that $\mathbf{F}_{r_1}$ pours power only on the first virtual subchannel, while $\mathbf{F}_{octa}$ transmits symbols on both subchannels. The received constellation of the precoders $\mathbf{F}_{r_1}$ is illustrated in Fig. 2.6. This constellation looks like a rotation of 16-QAM modulation. The solution provides a slightly improvement in terms of $d_{\min}$ compared to the beamforming design that uses a 16-QAM modulation. However, the average number of nearest neighbors provided by max-$d_{\min}$ precoder is higher that that by max-SNR (detailed in the next chapter).

The received constellation found by the precoder $\mathbf{F}_{octa}$ is illustrated for both virtual subchannels in Fig. 2.7 and 2.8. It is observed that whenever two received vectors are close on one virtual subchannels (e.g., the points 3 and 10 in the first subchannel) they are distant on the second one.

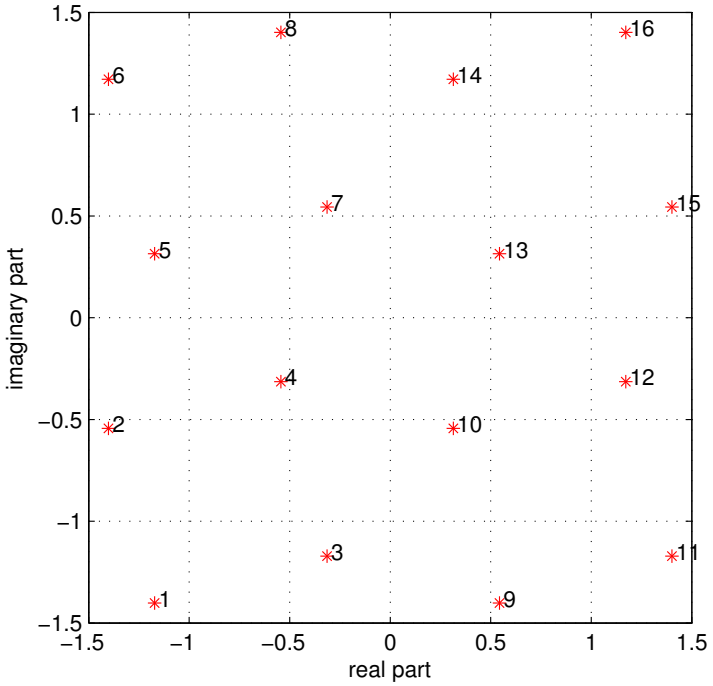

FIGURE 2.6: Received constellation on the first subchannel for the precoder $\mathbf{F}_{r_1}$.

The complexity of ML detection

The max-$d_{\min}$ precoder optimizes the minimum Euclidean distance between two pairs of symbols at the reception when considering a maximum-likelihood (ML) detection. One should note that the decoding matrix $\mathbf{G}_d$ has no effect on the ML detection, and then can be assumed to be an indentity matrix. For a MIMO system using M-QAM modulation, the number of ML tests for max-$d_{\min}$ solution is M^2 instead of $2M$ for diagonal precoders or the Alamouti code.

2.4 Comparison of linear precoders

2.4.1 Comparison of minimum Euclidean distance

Firstly, we indicate the improvement of the new precoder in terms of minimum Euclidean distance. Fig. 2.9 illustrates the normalized distance for each precoders in the case of QPSK modulation. It is observed that the difference between the max-$d_{\min}$ precoder remains constant for small channel angle γ. For MMSE and Waterfilling case, if the average transmit power is not large enough, these precoders allocate power on only the

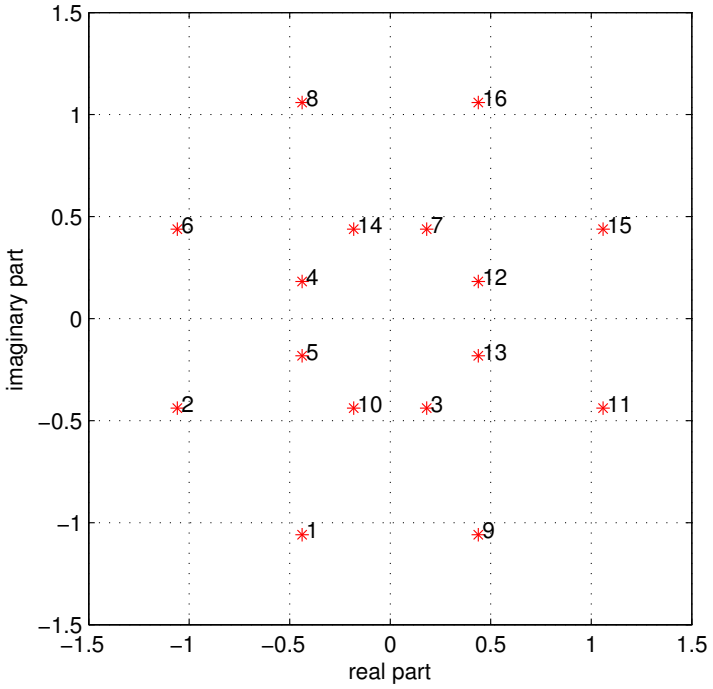

FIGURE 2.7: Received constellation on the first subchannel for the precoder $\mathbf{F}_{octa}$.

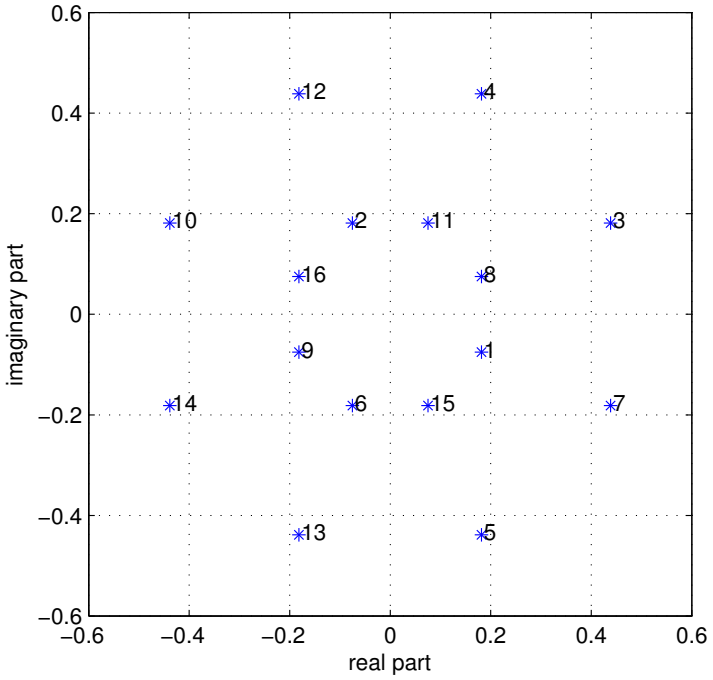

FIGURE 2.8: Received constellation on the second subchannel for the precoder $\mathbf{F}_{octa}$.

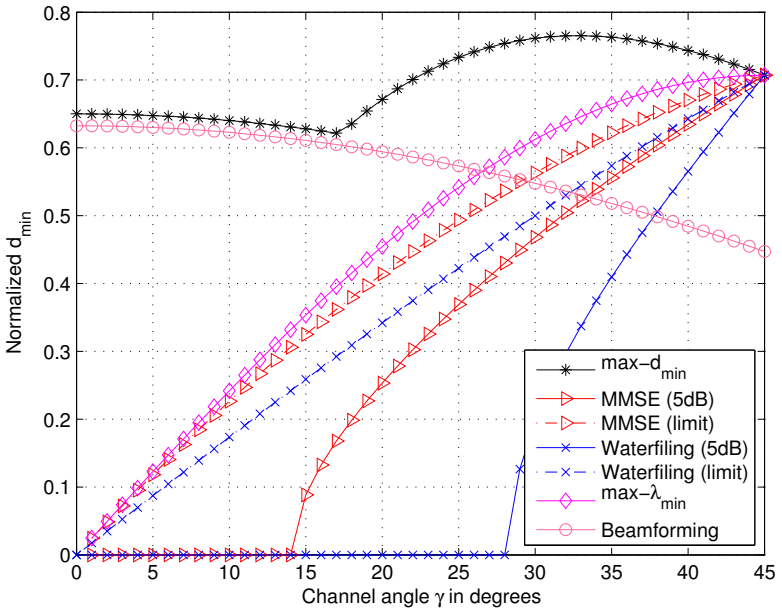

FIGURE 2.9: Normalized minimum Euclidean distance for QPSK modulation.

first virtual subchannel (in other words, the minimum distance is equal to zero). The max-$\lambda_{\min}$ precoder is better than the MMSE and Waterfilling solution in terms of $d_{\min}$ but is still outperformed by the max-$d_{\min}$ precoder.

Let us define the different ratio of $d_{\min}$ by

$$\mathcal{R}_{d_{\min}} = \frac{d_{\min}(precoder)}{d_{\min}(\max - d_{\min})} \tag{2.55}$$

This ratio corresponds to the minimum distance gain of a precoder compared to the max-$d_{\min}$ solution. Since the max-$d_{\min}$ precoder provides the optimal minimum distance, we have $\mathcal{R}_{d_{\min}} \leq 1$. Fig 2.10 shows the $\mathcal{R}_{d_{\min}}$ for the precoders max-SNR, MMSE, and max-$\lambda_{\min}$. In addition, the probability density functions of the angles γ are also illustrated for the systems (2,2), (4,2) and (6,2). A discontinuity can be observed at the channel angle $\gamma = \gamma_0 \simeq 17.28^o$.

If the channel angle γ is less than the threshold γ_0, the minimum distance of max-SNR and max-$d_{\min}$ precoder are very near: $\mathcal{R}_{d_{\min}} \simeq 0.97$. The ratios of $d_{\min}$ for MMSE and max-$\lambda_{\min}$ precoders vanish for $\gamma = 0$, and increase when the channel angle raises. If $\gamma \geq \gamma_0$, the max-$d_{\min}$ precoder augments its minimum distance in opposite to the max-SNR design, and the ratio $\mathcal{R}_{d_{\min}}$(max-SNR) is, then, decreased. The others ratios of $d_{\min}$

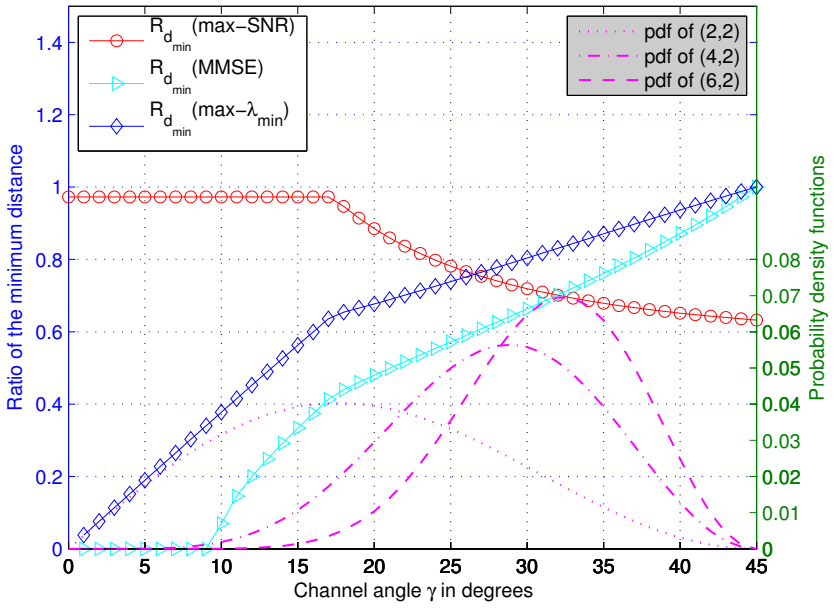

FIGURE 2.10: Comparison of the minimum Euclidean distance.

for MMSE and max-$\lambda_{\min}$ continue increasing and become higher than that of max-SNR design when the channel angle grows near $\pi/4$.

It is clear that the improvement in terms of $d_{\min}$ comes from both precoding matrices $\mathbf{F}_{r_1}$ and $\mathbf{F}_{octa}$. However, the distribution of these precoders depends on the channel characteristics (the angle γ_0) and the number of antennas used at the transmitter and the receiver. It can be observed, in Fig. 2.10, that the less dispersive the virtual subchannels are (more antennas are used, for example), the less we need the precoder $\mathbf{F}_{r_1}$, and the enhancement of $d_{\min}$ is therefore more significant in comparison with the max-SNR solution. Thanks to the $d_{\min}$ enhancement, we can expect a large performance improvement in terms of BER compared to the diagonal precoders.

2.4.2 Bit-Error-Rate performance

We consider a MIMO system using QPSK modulation with $n_T = 3$ transmit and $n_R = 2$ receive antennas over which we want to transmit $b = 2$ independent datastreams. Fig 2.11 plots the BER performance for QPSK modulation. These results clearly demonstrate that the max-$d_{\min}$ criterion is particularly suited for BER minimization when an ML detection is considered at the transmitter. The performance of diagonal solutions, such as max-$\lambda_{\min}$, MMSE and Waterfilling, is really outperformed by the max-$d_{\min}$ precoder.

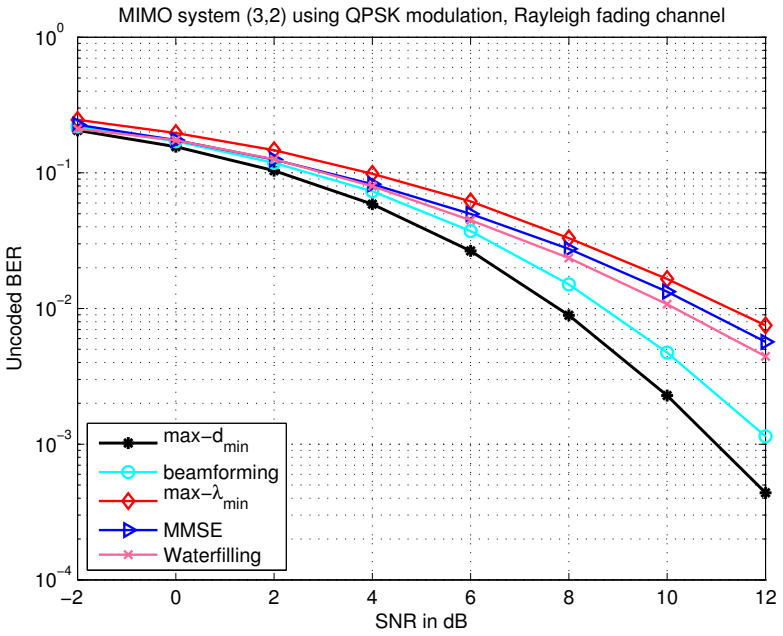

FIGURE 2.11: Uncoded BER performance for QPSK modulation.

Furthermore, we can observe a performance improvement of about 1dB, in comparison with max-SNR at BER is equal to 10^{-3}. This gain can be explained by the selection of $\mathbf{F}_{octa}$ to transmit signal when there is a small dispersion of the subchannels SNRs.

2.5 Conclusion

Through a feedback link, the channel state information is available at the transmitter and linear precoders can be designed to optimize various criteria such as maximizing the received signal-to-noise ratio (SNR), minimizing the mean square error (MSE), or maximizing the minimum singular value of the channel matrix. Those solutions lead to power allocation with diagonal solutions based on the singular value decomposition (SVD). In the first section of this chapter, we introduced the virtual channel transformation, which decouples MIMO channels into independent and parallel data-streams. Thanks to this transformation, we presented in the next section the diagonal precoders: Beamforming, Water-Filling, Minimum Mean Square Error (MMSE), Quality of Service (QoS), and Equal Error (EE). A MIMO transceiver using the Tomlinson-Harashima precoder (THP) is also shown in the chapter. This precoder belongs to an alternative set of linear precoders: the non-diagonal precoding schemes. We, then, proposed a different

non-diagonal precoder, named as X- and Y-Codes, for MIMO systems with a pair number of subchannels. In this thesis, the non-diagonal linear precoder which maximizes the minimum Euclidean distance between two received data vectors is studied. We presented, herein, the simple solution of $d_{\min}$ criterion for two data-streams and QPSK modulation. The simulation results show that the max-$d_{\min}$ precoder provides a large performance improvement in terms of BER compared to diagonal precoders.

Chapter 3

Extension of max-$d_{\min}$ precoder for high-order QAM modulations

Various criteria can be used for designing a precoding matrix. An efficient non-diagonal precoder, which minimizes the upper bound of pairwise error probability (PEP) when using arbitrary STBC over correlated Ricean fading channels, is illustrated in [54]. As presented in the chapter 2, the non-diagonal max-$d_{\min}$ precoder obtains a large performance improvement in terms of BER compared to diagonal precoders. Unfortunately, the max-$d_{\min}$ solution is only available for two independent data-streams with a low-order QAM modulation (BPSK and QPSK). That is due to the expression of the distance $d_{\min}$ that depends on the number of data-streams, the channel characteristics, and the modulation.

In this chapter, we firstly present the optimized solution of the max-$d_{\min}$ precoder for two 16-QAM symbols. This new strategy selects the best precoding matrix among five different expressions, depending on the value of the channel angle γ. In order to reduce the complexity of the max-$d_{\min}$ precoder, we propose a general expression of minimum Euclidean distance based precoders for all rectangular QAM modulations. For a two independent data-streams transmission, the precoding matrix is obtained by optimizing the minimum distance on both virtual subchannels. Hence, the optimized expressions can be reduced into two simple forms: the precoder $\mathbf{F}_1$ pours power only on the strongest virtual subchannel, and the precoder $\mathbf{F}_2$ uses both virtual subchannels to transmit data symbols. These precoding matrices are designed to optimize the distance $d_{\min}$ whatever

the dispersive characteristics of the channels are. The expression of $\mathbf{F}_1$ depends on the order of the rectangular QAM modulation, while that of $\mathbf{F}_2$ does not change for all QAM modulations.

Assuming that the channel state information is available at the transmitter, a MIMO system with n_T transmit, n_R receive antennas and b independent data-streams over Rayleigh fading channel can be modeled as

$$\mathbf{y} = \mathbf{H}_v \mathbf{F}_d \mathbf{s} + \eta_v, \tag{3.1}$$

where $\mathbf{H}_v = \mathbf{G}_v \mathbf{H} \mathbf{F}_v$ is the $b \times b$ virtual channel matrix, $\eta_v = \mathbf{G}_v \nu$ is the $b \times 1$ transformed additive Gaussian noise vector.

As presented in Chapter 2, the virtual channel matrix for two independent data-streams can be parameterized as

$$\mathbf{H}_v = \begin{pmatrix} \sigma_1 & 0 \\ 0 & \sigma_2 \end{pmatrix} = \rho \begin{pmatrix} \cos\gamma & 0 \\ 0 & \sin\gamma \end{pmatrix}, \tag{3.2}$$

where $\rho = \sqrt{\sigma_1^2 + \sigma_2^2}$ is the channel gain, and $\gamma = \arctan \frac{\sigma_2}{\sigma_1}$ is the channel angle ($0 \leq \gamma \leq \pi/4$). Due to the symmetries of rectangular QAM modulation, the precoding matrix $\mathbf{F}_d$ can be represented as

$$\mathbf{F}_d = \sqrt{E_s} \begin{pmatrix} \cos\psi & 0 \\ 0 & \sin\psi \end{pmatrix} \begin{pmatrix} \cos\theta & \sin\theta \\ -\sin\theta & \cos\theta \end{pmatrix} \begin{pmatrix} 1 & 0 \\ 0 & e^{i\varphi} \end{pmatrix}, \tag{3.3}$$

with $0 \leq \psi, \varphi \leq \pi/2$ and $0 \leq \theta \leq \pi/4$. The parameter ψ controls the power allocation while θ and φ correspond to scaling and rotation of the received constellation, respectively.

3.1 Optimized max-$d_{\min}$ precoder for 16-QAM modulation

In the case of a 16-QAM modulation, the symbols belong to the following set

$$S_{16\text{–}QAM} = \left\{ \frac{1}{\sqrt{10}}(\pm 1 \pm i), \frac{1}{\sqrt{10}}(\pm 1 \pm 3i), \frac{1}{\sqrt{10}}(\pm 3 \pm i), \frac{1}{\sqrt{10}}(\pm 3 \pm 3i) \right\}. \tag{3.4}$$

A numerical search on ψ, θ et φ to maximize the Euclidean distance for every angle γ leads to five different expressions. If γ stays under γ_0, then only the best subchannel is used as in the max-SNR strategy and the precoder will be denoted $\mathbf{F}_{r1}$. On the other hand, if $\gamma_i < \gamma \leq \gamma_{i+1}$, the precoder leads to a 256-points constellation on both receivers, and it will be denoted as $\mathbf{F}_{T_i}$, $i = 1 \cdots 4$, respectively.

3.1.1 Expression of the max-$d_{\min}$ precoder

Precoder $\mathbf{F}_{r_1}$

For every $\gamma \leq \gamma_0$, the numerical maximization of $d_{\min}$ gives an angle $\psi = 0$, meaning that only the best virtual subchannel is used (i.e. the first one, since $\sigma_1 \geq \sigma_2$). A received constellation on this subchannel is represented on Fig. 3.1 (for $\psi = 0$ and arbitrary θ and φ). It is observed that there are 256 points corresponding to the 256 received symbols. One should note that the distance $d_{\min}$ is optimized when nearest neighbors

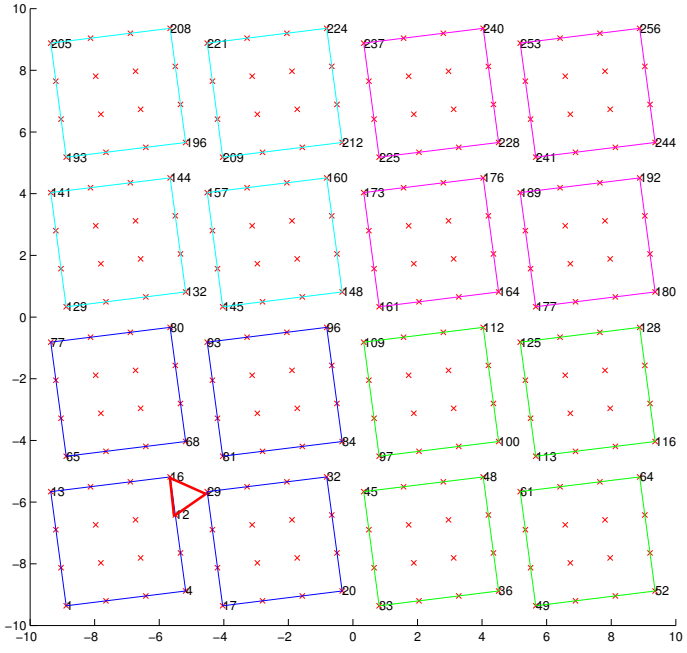

FIGURE 3.1: The received constellation on the first virtual subchannel for $\psi = 0$.

have the same distance. We observe, in Fig. 3.1, that the optimized solution is obtained when $d_{12,16} = d_{16,29} = d_{29,12}$. In other words, the different distances provided by three

corresponding vector below are equal

$$\breve{x}_1 = \frac{1}{\sqrt{10}}\begin{pmatrix}0\\2\end{pmatrix} \quad , \quad \breve{x}_2 = \frac{1}{\sqrt{10}}\begin{pmatrix}2\\-6\end{pmatrix} \quad \text{and} \quad \breve{x}_3 = \frac{1}{\sqrt{10}}\begin{pmatrix}2\\-6+2i\end{pmatrix}. \tag{3.5}$$

The corresponding distances lead to the system

$$\begin{cases} d^2_{\breve{x}_1} = \frac{\cos^2\gamma}{10} \times (4 - 4\cos^2\theta) \\ d^2_{\breve{x}_2} = \frac{\cos^2\gamma}{10} \times (-32\cos^2\theta - 24\cos\theta.\sin\theta.\cos\varphi + 36) \\ d^2_{\breve{x}_3} = \frac{\cos^2\gamma}{10} \times (-8\cos\theta.\sin\theta.\sin\varphi - 36\cos^2\theta + 40 - 24\cos\theta.\sin\theta.\cos\varphi) \end{cases} \tag{3.6}$$

whose resolution gives

$$\begin{cases} \varphi = \arctan\frac{1}{6+\sqrt{3}} \approx 7.3693^o \\ \theta = \arctan(2\sin\varphi) \approx 14.3877^o \end{cases} \tag{3.7}$$

The received constellation then looks like a 256-QAM constellation rotated by 7.3693^o. This solution is close to the max-SNR strategy, but leads to a little higher $d_{\min}$. It is observed that the optimization of $d_{\min}$ is obtained by the difference vector $\frac{1}{\sqrt{10}}(0\ 2)^T$. Therefore, the minimum distance provided by the precoder $\mathbf{F}_{r1}$ is given by

$$d^2_{\mathbf{F}_{r_1}} = E_s\rho^2\frac{2}{5(11+3\sqrt{3})}\cos^2\gamma. \tag{3.8}$$

Precoder $\mathbf{F}_{T_1}$

A numerical approach shows that, for every $\gamma_0 < \gamma \leq \gamma_1$, the angles θ and φ are fixed. Furthermore, the angle ψ that controls the power allocation over the two virtual sub-channels, depends on the channel angle γ. The minimum Euclidean distance of $\mathbf{F}_{T_1}$ is obtained when $\theta = 45^0$ and $\varphi = 45^0$. Then, the max-$d_{\min}$ precoder can be expressed as a function of ψ

$$\mathbf{F}_{T_1} = \frac{\sqrt{E_s}}{2}\begin{pmatrix}\cos\psi & 0\\ 0 & \sin\psi\end{pmatrix}\begin{pmatrix}\sqrt{2} & 1+i\\ -\sqrt{2} & 1+i\end{pmatrix}. \tag{3.9}$$

When γ is explored from 0^0 to 45^0, the value of ψ that maximizes the minimum distance is obtained with the two difference vectors

$$\breve{x}_{a_1} = \frac{1}{\sqrt{10}}\begin{pmatrix}2\\-2+2i\end{pmatrix} \quad \text{and} \quad \breve{x}_{b_1} = \frac{1}{\sqrt{10}}\begin{pmatrix}4+4i\\-6\end{pmatrix}. \tag{3.10}$$

If we denote $d_{\breve{a}_1}$ and $d_{\breve{b}_1}$ as the normalized minimum distance linked respectively to the difference vectors $\breve{x}_{a_1}$ and $\breve{x}_{b_1}$, the optimum precoder is obtained when these distances are equal

$$\begin{cases} d^2_{\breve{a}_1} = 6 + 4\sqrt{2} + 12\cos^2\gamma\cos^2\psi - 6\cos^2\psi - 6\cos^2\gamma - 4\sqrt{2}\cos^2\psi - 4\sqrt{2}\cos^2\gamma \\ d^2_{\breve{b}_1} = 34 + 24\sqrt{2} - 68\cos^2\gamma\cos^2\psi - 34\cos^2\psi - 34\cos^2\gamma - 24\sqrt{2}\cos^2\psi - 24\sqrt{2}\cos^2\gamma \end{cases}$$

By considering $d_{\breve{a}_1} = d_{\breve{b}_1}$, we get ψ as a function of γ

$$\psi = \arctan\frac{5\sqrt{2}-7}{\tan\gamma}. \tag{3.11}$$

The corresponding distance provided by $\mathbf{F}_{T_1}$ is

$$d^2_{T_1} = E_s\rho^2\frac{20-14\sqrt{2}}{5}\frac{\sin^2\gamma}{\tan^2\gamma + (5\sqrt{2}-7)^2}. \tag{3.12}$$

Precoder $\mathbf{F}_{T_2}$

For γ such that $\gamma_1 < \gamma \leq \gamma_2$, it is observed that the angles θ and φ are fixed, and ψ depends on γ for the precoder maximizing the minimum distance. Furthermore, the numerical research shows that the distance $d_{\min}$ is obtained when $\theta = 45^0$. Then, the precoder $\mathbf{F}_{T_2}$ can be expressed as a function of φ and ψ

$$\mathbf{F}_{T_2} = \sqrt{E_s}/\sqrt{2}\begin{pmatrix} \cos\psi & \cos\psi(\cos\varphi + i\sin\varphi) \\ -\sin\psi & \sin\psi(\cos\varphi + i\sin\varphi) \end{pmatrix}. \tag{3.13}$$

When the channel angle γ varies, the difference vectors that provide the minimum distance are

$$\breve{x}_{a_2} = \frac{1}{\sqrt{10}}\begin{pmatrix} 2 \\ -2 \end{pmatrix}, \quad \breve{x}_{b_2} = \frac{1}{\sqrt{10}}\begin{pmatrix} 2+2i \\ -2 \end{pmatrix}, \quad \text{and} \quad \breve{x}_{c_2} = \frac{1}{\sqrt{10}}\begin{pmatrix} 2+4i \\ -4-2i \end{pmatrix}.$$

Let us denote $d_{\breve{a}_2}$, $d_{\breve{b}_2}$ and $d_{\breve{c}_2}$ as the Euclidean distance corresponding to $\breve{x}_{a_2}$,$\breve{x}_{b_2}$ and $\breve{x}_{c_2}$, respectively, the optimized precoder is obtained when $d_{\breve{a}_2} = d_{\breve{b}_2} = d_{\breve{c}_2}$

$$\begin{cases} d^2_{\breve{a}_3} = 1/10 \times \left(8\cos^2\gamma\cos^2\psi + (1-\cos^2\gamma-\cos^2\psi)\times(4+4\cos\varphi)\right) \\ d^2_{\breve{b}_3} = 1/10 \times \left(12\cos^2\gamma\cos^2\psi + (1-\cos^2\gamma-\cos^2\psi)\times(6+4\cos\varphi+4\sin\varphi)\right) \\ d^2_{\breve{c}_3} = 1/10 \times \left(40\cos^2\gamma\cos^2\psi + (1-\cos^2\gamma-\cos^2\psi)\times(20+16\cos\varphi+12\sin\varphi)\right) \end{cases}$$

Solving the equations $d_{\breve{a}_2} = d_{\breve{b}_2} = d_{\breve{c}_2}$, we get

$$\begin{cases} \varphi = \arctan\frac{3}{5} \\ \psi = \arccos\frac{\alpha-\alpha.\cos^2\gamma}{\alpha-2\cos^2\gamma} \end{cases} \tag{3.14}$$

where $\alpha = 1+\frac{6}{\sqrt{34}}$. The distance $d_{\min}$ provided by $\mathbf{F}_{T_2}$ is then

$$d^2_{T_2} = \frac{E_s\rho^2}{10}\frac{8}{6+\sqrt{34}}\cos^2\gamma\frac{\alpha-\alpha\cos^2\gamma}{\alpha-2\cos^2\gamma}. \tag{3.15}$$

Precoder $\mathbf{F}_{T_3}$

For γ such that $\gamma_2 < \gamma \leq \gamma_3$, a numerical approach shows that the minimum distance is provided by four difference vectors

$$\breve{x}_{a_3} = \frac{1}{\sqrt{10}}\begin{pmatrix}0\\2\end{pmatrix},\ \breve{x}_{b_3} = \frac{1}{\sqrt{10}}\begin{pmatrix}2\\-2\end{pmatrix},\ \breve{x}_{c_3} = \frac{1}{\sqrt{10}}\begin{pmatrix}2\\-2+2i\end{pmatrix},\ \text{and}\ \breve{x}_{d_3} = \frac{1}{\sqrt{10}}\begin{pmatrix}2\\-4\end{pmatrix}.$$

The corresponding Euclidean distances of these vectors are

$$\begin{cases} d^2_{\breve{a}_3} = 1/10 \times \left[4N_T\cos^2\theta + 4\cos^2\gamma\cos^2\psi\right] \\ d^2_{\breve{b}_3} = 1/10 \times \left[4N_T(1+\sin 2\theta\cos\varphi) + 8\cos^2\gamma\cos^2\psi\right] \\ d^2_{\breve{c}_3} = 1/10 \times \left[4N_T(1+2\sin 2\theta\cos\varphi+3\cos^2\theta) + 20\cos^2\gamma\cos^2\psi\right] \\ d^2_{\breve{d}_3} = 1/10 \times \left[4N_T(1+\sin 2\theta\cos\varphi+\cos^2\theta+\sin 2\theta\sin\varphi) + 12\cos^2\gamma\cos^2\psi\right] \end{cases} \tag{3.16}$$

where $N_T = 1-\cos^2\psi-\cos^2\gamma$. By considering $d_{\breve{a}_3} = d_{\breve{b}_3} = d_{\breve{c}_3} = d_{\breve{d}_3}$, we obtain

$$\begin{cases} \varphi = \arctan\frac{1}{3} \\ \theta = \frac{1}{2}\arctan\frac{\sqrt{10}}{2} \\ \psi = \arctan\frac{\sqrt{10/\sqrt{14}-1}}{\tan\gamma\sqrt{10/\sqrt{14}+1}} \end{cases} \tag{3.17}$$

By substituting the values of the angles φ, θ and ψ into the expression of max-$d_{\min}$ precoder, we have

$$d^2_{T_3} = E_s\rho^2 \frac{2N_T \cos^2\theta + 2\cos^2\psi\cos^2\gamma}{5}. \tag{3.18}$$

Precoder $\mathbf{F}_{T_4}$

Like the precoder $\mathbf{F}_{T_1}$, the minimum distance of this precoder is obtained when $\theta = 45^0$, $\varphi = 45^0$, and ψ depends on the channel angle γ.

$$\mathbf{F}_{T_4} = \frac{\sqrt{E_s}}{2}\begin{pmatrix}\cos\psi & 0\\ 0 & \sin\psi\end{pmatrix}\begin{pmatrix}\sqrt{2} & 1+i\\ -\sqrt{2} & 1+i\end{pmatrix}. \tag{3.19}$$

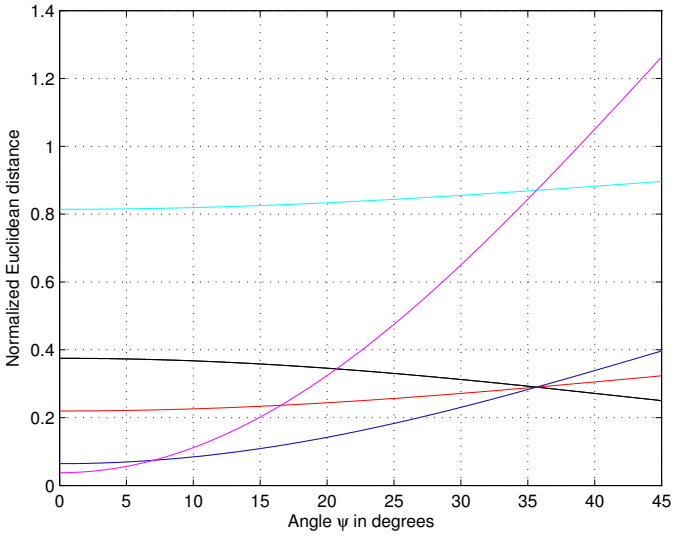

FIGURE 3.2: Euclidean distance with $\varphi = 45^o$ and $\theta = 45^o$ for some difference vectors with respect to ψ in degrees for channel angle $\gamma = 30^o$.

Fig 3.2 illustrates the Euclidean distance for each difference vector with respect to ψ for a given channel in the interval from γ_3 to 45^0 (i.e. $\gamma = 30^o$). It is observed that the value of ψ that maximizes the distance $d_{\min}$ is given at the intersection of the two curves which corresponds to

$$\breve{x}_{a_4} = \frac{1}{\sqrt{10}}\begin{pmatrix}0\\ 2\end{pmatrix}, \quad \breve{x}_{b_4} = \frac{1}{\sqrt{10}}\begin{pmatrix}2\\ -2+2i\end{pmatrix}.$$

If we denote $d_{\breve{a}_4}$ et $d_{\breve{b}_4}$ as the Euclidean distance corresponding to the vectors $\breve{x}_{a_4}$ et $\breve{x}_{b_4}$, respectively, the optimal precoder is obtained when $d_{\breve{a}_4} = d_{\breve{b}_4}$

$$\begin{cases} d^2_{\breve{a}_4} = 1/10 \times \left((6+4\sqrt{2})N_T + 12\cos^2\gamma\cos^2\psi\right) \\ d^2_{\breve{b}_4} = 1/10 \times \left(2N_T + 4\cos^2\gamma\cos^2\psi\right) \end{cases} \tag{3.20}$$

where $N_T = 1 - \cos^2\psi - \cos^2\gamma$. By considering $d_{\breve{a}_4} = d_{\breve{b}_4}$, we get ψ with respect to γ

$$\psi = \arctan\frac{\sqrt{2}-1}{\tan\gamma}. \tag{3.21}$$

The precoder $\mathbf{F}_{T_4}$ is then computed by substituting ψ into (3.19), which finally gives the optimal $d_{\min}$ ruled only on the channel angle

$$d^2_{T_4} = \frac{E_s\rho^2}{10}\left(2\sin^2\gamma + \frac{4\sin^2\gamma - 2\tan^2\gamma}{\tan^2\gamma + 3 - 2\sqrt{2}}\right). \tag{3.22}$$

3.1.2 Received constellation of the max-$d_{\min}$ precoder

Fig 3.4 illustrates the received constellation provided by the precoder $\mathbf{F}_{r1}$. Only the first virtual receiver is considered because the second one is not used. It is observed that the constellation looks like a 7.37^o rotation of 256-QAM modulation. The minimum distance provided by this precoder is therefore close to the max-SNR design using 256-QAM modulation, but it provides a slight improvement in $d_{\min}$.

On the other hand, the received constellations of the precoders $\mathbf{F}_{T_i}$ $(i = 1\cdots4)$, are available on both subchannels. Fig 3.3 shows the constellation obtained by $\mathbf{F}_{T_4}$. It is noted that two received vectors, which are close on one virtual subchannel, are distant on the other subchannel.

3.1.3 Evolution of the minimum Euclidean distance

Fig 3.5 shows the distance $d_{\min}$ provided by the precoders $\mathbf{F}_{r_1}$ and $\mathbf{F}_{T_i}$ $(i = 1\cdots4)$. The optimal distances are only governed by the channel angle γ. To choose between $\mathbf{F}_{r_1}$ and $\mathbf{F}_{T_i}$, and get the corresponding threshold we have to look values such that these distances are equal.

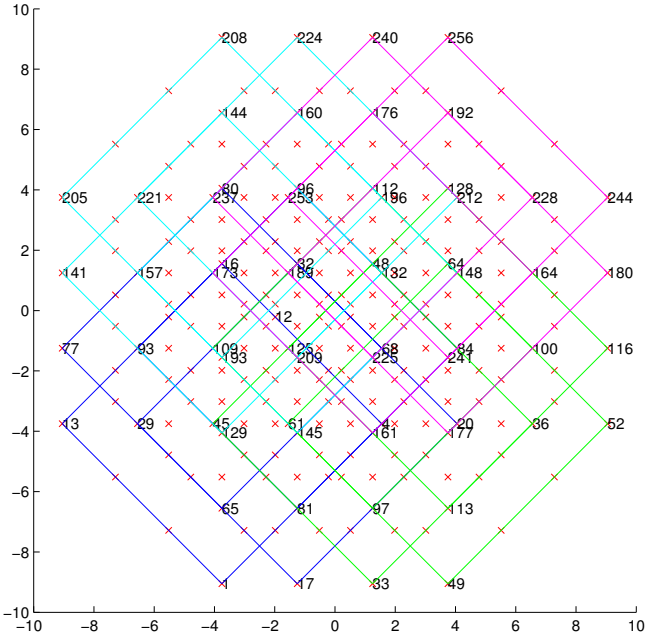

(a) first virtual subchannel

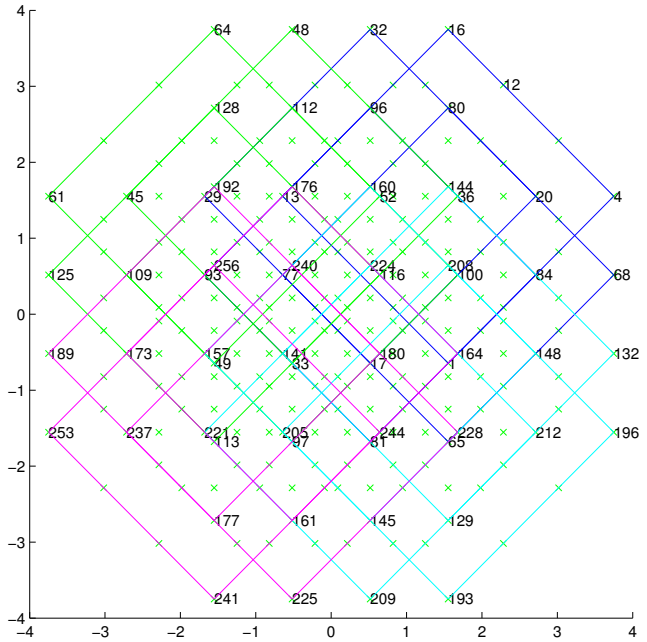

(b) second virtual subchannel

FIGURE 3.3: Received constellation for the precoder $\mathbf{F}_{T_4}$

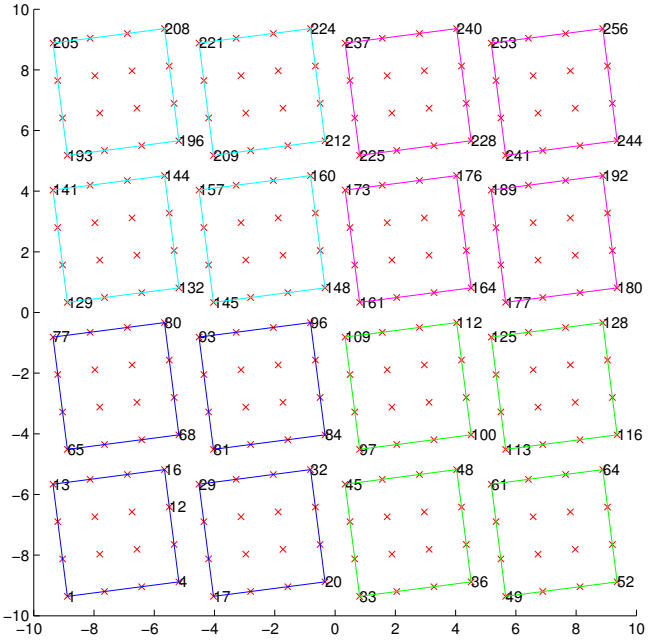

FIGURE 3.4: The received constellation obtained by the precoder $\mathbf{F}_{r_1}$

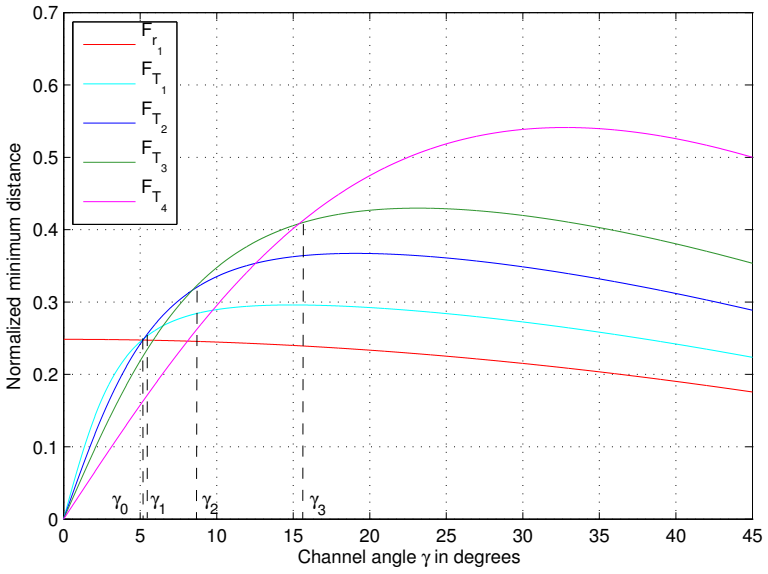

FIGURE 3.5: Evolution of $d_{\min}$ with respect to γ for a 16-QAM modulation

For example, let us solve the equation $d_{r_1} = d_{T_1}$ to obtain γ_0. The corresponding distances are given by

$$\begin{cases} d^2_{r_1} = E_s\rho^2 \frac{2}{5(11+3\sqrt{3})} \cos^2\gamma \\ d^2_{T_1} = E_s\rho^2 \frac{20-14\sqrt{2}}{5} \frac{\sin^2\gamma}{\tan^2\gamma+(5\sqrt{2}-7)^2} \end{cases} \tag{3.23}$$

By considering $d_{r1} = d_{T_1}$, we obtain

$$\gamma_0 = \arctan\sqrt{\frac{M_0}{1-M_0}(5\sqrt{2}-7)^2} \approx 5.128^0, \tag{3.24}$$

where $M_0 = \frac{1}{(10-7\sqrt{2})(11+3\sqrt{3})}$. The other thresholds γ_i are obtained by using the same process

$$\begin{cases} \gamma_1 \approx 5.26^o \\ \gamma_2 \approx 8.40^o \\ \gamma_3 \approx 15.38^o \end{cases} \tag{3.25}$$

3.1.4 Performance of the max-$d_{\min}$ precoder for 16-QAM modulation

Minimum Euclidean distances for minimum distance based precoder in comparison with diagonal precoders are shown in Fig. 3.6 in the case of a 16-QAM modulation. The black curve represents the upper bound of max-$d_{\min}$ precoder depending on the value of γ. It means that its expression is selected among $\mathbf{F}_{r_1}$ and $\mathbf{F}_{T_i}$ $(i = 1\cdots4)$.

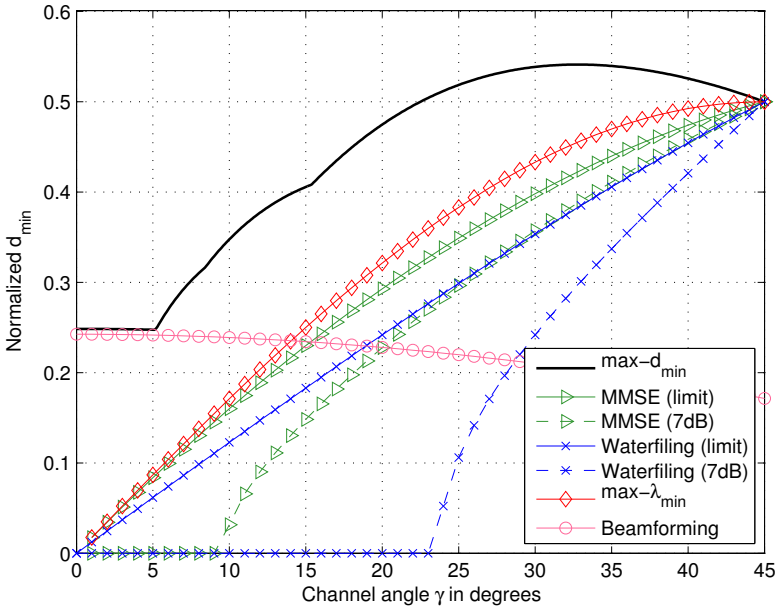

FIGURE 3.6: Comparison in terms of the minimum Euclidean distance.

For $\gamma \leq \gamma_0$, the performances of max-$d_{\min}$ and beamforming are very close with the same difference. The light advantage of the proposed precoder is due to the rotation of 7.36^0 in the 256-QAM constellation. These precoders are both different to zero when the value

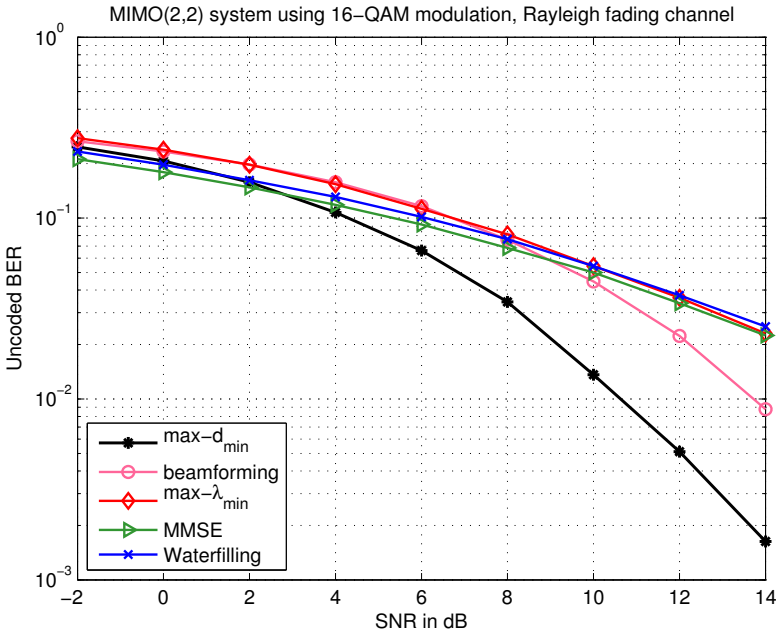

(a) BER performance for MIMO(2,2) system

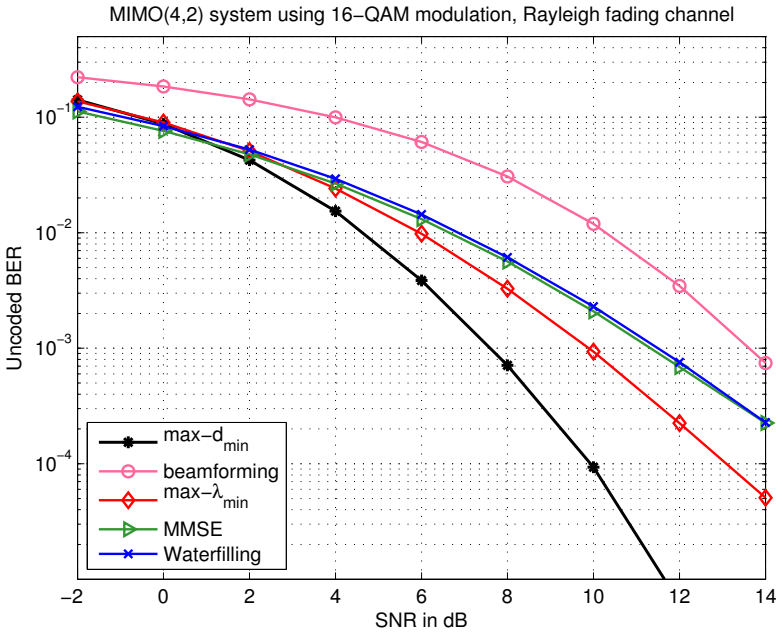

(b) BER performance for MIMO(4,2) system

FIGURE 3.7: Comparison the performance in terms of BER for 16-QAM modulation.

of the channel angle γ is small. When γ increases, the max-$\lambda_{\min}$ solution is better than MMSE, WF, QoS 3dB, and WF solutions in terms of $d_{\min}$, but it is really outperformed by the max-$d_{\min}$ precoder.

Due to the considerable improvement of $d_{\min}$, a significant increase of BER is expected

in comparison with diagonal precoders. Fig. 3.7 represents the BER performance with respect to the SNR for a MIMO system using a 16-QAM modulation. For MIMO(2,2) system, we observed that the proposed precoder provides a gain of 3 dB compared to beamforming design for a BER = 10^{-2}. It clearly confirms the max-$d_{\min}$ interest when an ML receiver is used. This gain will even be higher if the number of antennas increases. For MIMO(4,2) system, the max-$d_{\min}$ precoder provides a gain of about 6 dB in comparison with beamforming at BER = 10^{-3}.

3.2 General expression of max-$d_{\min}$ precoder for high-order QAM modulations

The max-$d_{\min}$ solution is only available for two independent data-streams with a low-order QAM modulation. That is due to the expression of the distance $d_{\min}$ that depends on the number of data-streams, the channel characteristics, and the modulation. The authors in [55] presented a design of a max-$d_{\min}$ precoder which allows transmitting more than two independent data-streams, and increasing the 4-QAM alphabet to 16-QAM or 64-QAM modulations. However, this precoding technique is only suitable to quasi-stationary MIMO channels where a suboptimal solution is proposed by considering a block-Toeplitz form.

We present, herein, an idea not only to reduce the complexity of the max-$d_{\min}$ precoder but also to provide a significant enhancement of the minimum distance with respect to existing precoding strategies for all rectangular QAM modulations. For a two independent data-streams transmission, the MIMO channel is diagonalized by using a virtual transformation and the precoding matrix is obtained by optimizing the minimum distance on both virtual subchannels. Then, the optimized expressions can be reduced to two simple forms: the precoder $\mathbf{F}_1$ pours power only on the strongest virtual subchannel, and the precoder $\mathbf{F}_2$ uses both virtual subchannels to transmit data symbols. These precoding matrices are designed to optimize the distance $d_{\min}$ whatever the dispersive characteristics of the channels are.

For a rectangular 4^k-QAM modulation, the transmitted symbols belong to the set

$$S = \frac{1}{\sqrt{M}} \{a + b\,i\ ;\ a - b\,i\ ;\ -a + b\,i\ ;\ -a - b\,i\} \tag{3.26}$$

where $M = \frac{2}{3}(4^k - 1)$ and $a, b \in (1, 3, \ldots, 2^k - 1)$.

3.2.1 Precoder $\mathbf{F}_1$

When the max-$d_{\min}$ precoder pours power only on the first virtual subchannel, it means that the angles $\psi = 0$. The precoding matrix in (3.3) is, then, simplified as

$$\mathbf{F}_1 = \sqrt{E_s}\begin{pmatrix} \cos\theta & \sin\theta\, e^{i\varphi} \\ 0 & 0 \end{pmatrix}. \tag{3.27}$$

Fig 3.8 illustrates the received constellation on the first virtual subchannel provided by a form of the precoder $\mathbf{F}_1$. We observe that it can be divided into four regions with four corner points named as A,B,C, and D. When the angles θ and φ in (3.27) vary, these four regions are scaled and rotated, respectively. The distance $d_{\min}$ is optimized such that the nearest neighbors have the same distance. In other words, the triangle (C,D,E) which is created by three transmitted vectors $(\frac{1-i}{\sqrt{M}}, \frac{-N+Ni}{\sqrt{M}})^T$, $(\frac{-1-i}{\sqrt{M}}, \frac{N+Ni}{\sqrt{M}})^T$, and $(\frac{-1-i}{\sqrt{M}}, \frac{N+(N-2)i}{\sqrt{M}})^T$, where $N = 2^k - 1$, is equilateral. The corresponding difference vectors are defined by

$$\breve{x}_1 = \frac{2}{\sqrt{M}}\begin{pmatrix} 0 \\ i \end{pmatrix}, \breve{x}_2 = \frac{2}{\sqrt{M}}\begin{pmatrix} 1 \\ -N \end{pmatrix}, \breve{x}_3 = \frac{2}{\sqrt{M}}\begin{pmatrix} 1 \\ -N+i \end{pmatrix}.$$

The corresponding normalized distances $\left(d^2/(E_s\rho^2\frac{4}{M})\right)$, are then given by

$$\begin{cases} \bar{d}^2_{\breve{x}_1} = \cos^2\gamma \sin^2\theta \\ \bar{d}^2_{\breve{x}_2} = \cos^2\gamma[\cos^2\theta - 2\cos\theta.\sin\theta.N\cos\varphi + N^2\sin^2\theta] \\ \bar{d}^2_{\breve{x}_3} = \cos^2\gamma[\cos^2\theta - 2\cos\theta.\sin\theta.(N\cos\varphi + \sin\varphi) + (N^2+1)\sin^2\theta] \end{cases}$$

By considering $\bar{d}^2_{\breve{x}_1} = \bar{d}^2_{\breve{x}_2} = \bar{d}^2_{\breve{x}_3}$, we get

$$\begin{cases} \varphi_{F_1} = \arctan\frac{1}{2N+\sqrt{3}} \\ \theta_{F_1} = \arctan(2\sin\varphi_{F_1}). \end{cases} \tag{3.28}$$

The minimum Euclidean distance obtained by the precoder $\mathbf{F}_1$ is then

$$d^2_{F_1} = E_s\rho^2 \frac{4}{M} \frac{\cos^2\gamma}{N^2+\sqrt{3}N+2}. \tag{3.29}$$

For the beamforming precoder which has the same bit rate, i.e. $M' = \frac{2}{3}(4^{2k}-1)$, the distance $d_{\min}$ is given by

$$d^2_{F_{beam}} = E_s\rho^2 \frac{4}{M'} \cos^2\gamma = E_s\rho^2 \frac{4}{M} \frac{\cos^2\gamma}{N^2+2N+2}. \tag{3.30}$$

It is observed that the precoder $\mathbf{F}_1$ provides a slight improvement in terms of $d_{\min}$ in comparison with the beamforming design. The normalized distance of the new precoder is plotted in the Fig. 3.10 and its performance will be discussed in Section 3.3.

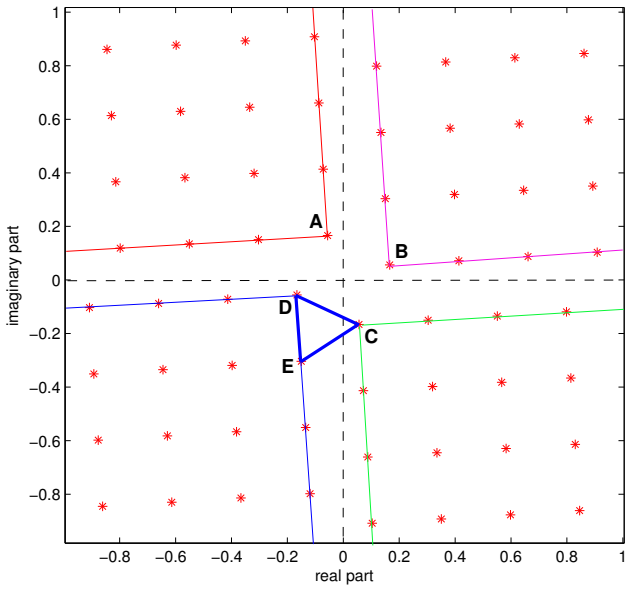

FIGURE 3.8: Received constellation of the precoder $\mathbf{F}_1$.

3.2.2 Precoder $\mathbf{F}_2$

We presented, in the previous section, the optimized max-$d_{\min}$ solution for a 16-QAM modulation. It has many expressions, and each expression corresponds to different interval of the channel angle γ. Let us consider the last expression, i.e., the precoder $\mathbf{F}_{T_4}$. The optimized expression is obtained with $\theta = \pi/4$, $\varphi = \pi/4$, and ψ depending on γ. This

precoder is denoted as $\mathbf{F}_2$, and is expressed as

$$\mathbf{F}_2 = \frac{\sqrt{E_s}}{2}\begin{pmatrix}\cos\psi & 0\\ 0 & \sin\psi\end{pmatrix}\begin{pmatrix}\sqrt{2} & 1+i\\ -\sqrt{2} & 1+i\end{pmatrix}. \tag{3.31}$$

The optimized $d_{\min}$ of the precoder $\mathbf{F}_2$ is always provided by the two difference vectors

$$\breve{x}_4 = \frac{2}{\sqrt{M}}\begin{pmatrix}1\\ 0\end{pmatrix}, \breve{x}_5 = \frac{2}{\sqrt{M}}\begin{pmatrix}1\\ -1+i\end{pmatrix}.$$

The corresponding normalized distances are defined by

$$\begin{cases}\bar{d}^2_{\breve{x}_4} = \frac{1}{2}\cos^2\gamma\cos^2\psi + \frac{1}{2}\sin^2\gamma\sin^2\psi\\ \bar{d}^2_{\breve{x}_5} = \frac{2-\sqrt{2}}{2}\cos^2\gamma\cos^2\psi + \frac{2+\sqrt{2}}{2}\sin^2\gamma\sin^2\psi\end{cases}$$

By solving equation $\bar{d}^2_{\breve{x}_4} = \bar{d}^2_{\breve{x}_4}$, we obtain

$$\psi_{F_2} = \arctan\frac{\sqrt{2}-1}{\tan\gamma}. \tag{3.32}$$

It can be realized that the form of $\mathbf{F}_2$ is rather simple. Therefore, for small dispersive channels, only precoding matrix $\mathbf{F}_2$ in (3.31) is used to transmit signals on both virtual subchannels. The minimum distance obtained by $\mathbf{F}_2$ is

$$d^2_{F_2} = E_s\rho^2\frac{4}{M}\frac{(2-\sqrt{2})\cos^2\gamma\sin^2\gamma}{1+(2-2\sqrt{2})\cos^2\gamma}. \tag{3.33}$$

Firstly, we demonstrate that the precoder $\mathbf{F}_2$ optimizes the distance $d_{\min}$ when there is no dispersion between both virtual subchannels. Indeed, the minimum Euclidean distance of $\mathbf{F}_2$ at the channel angle $\gamma = \pi/4$ is given by

$$d^2_{\pi/4} = E_s\rho^2\frac{4}{M}\frac{1}{4} = E_s\rho^2/M. \tag{3.34}$$

Proposition 3.1. *When the channel angle $\gamma = \pi/4$, the maximum value of $d_{\min}$ is given by $\sqrt{E_s\rho^2/M}$, and obtained if and only if $\psi = \pi/4$ or $\theta = \pi/4$.*

Proof: see Appendix A.

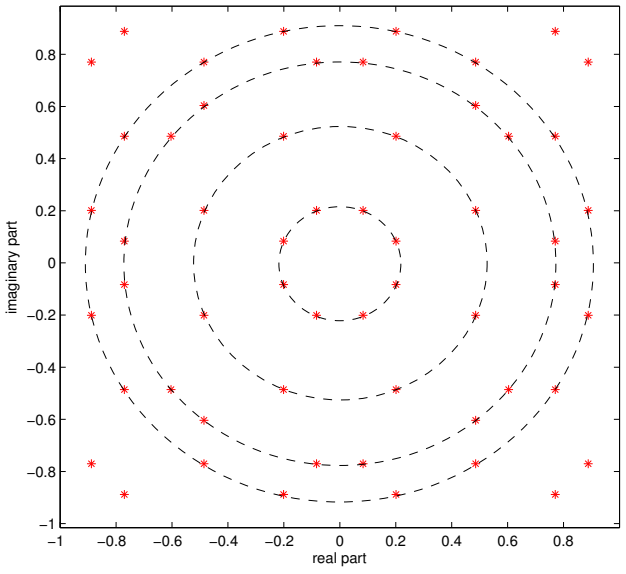

(a) First virtual subchannel

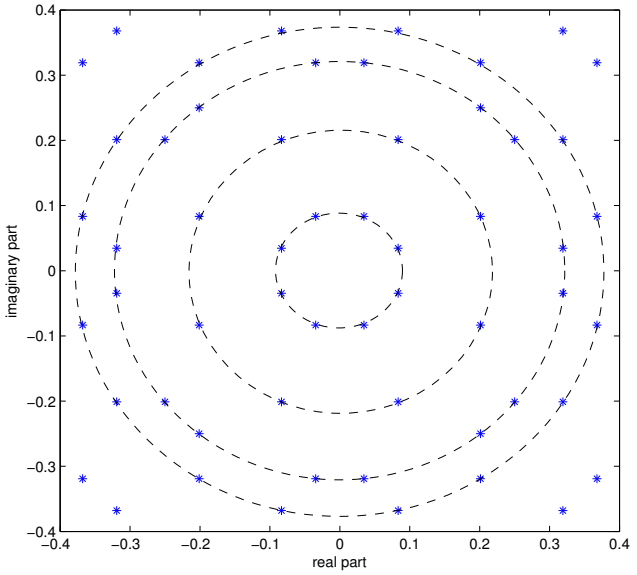

(b) Second virtual subchannel

FIGURE 3.9: Received constellation of the precoder $\mathbf{F}_2$.

The normalized distance $d_{\min}/\sqrt{4E_s\rho^2/M}$ of precoder $\mathbf{F}_2$ is shown on the Fig. 3.10. It is observed that the maximum value of d_{F_2} occurs when $\gamma = \gamma_{\max} \simeq 32.7^o$. The exact

value of $\gamma_{\max}$ can be determined by using the calculus below

$$\frac{\partial}{\partial\gamma} d_{F_2}^2 = 0, \quad \text{and} \quad \frac{\partial^2}{\partial\gamma^2} d_{F_2}^2 < 0. \tag{3.35}$$

By solving the equation of the first derivative and verifying the second derivative test, we obtain

$$\cos^2\gamma_{\max} = \frac{1}{\sqrt{2}}, \text{or } \gamma_{\max} = \arccos\frac{1}{\sqrt[4]{2}}\,. \tag{3.36}$$

The minimum Euclidean distance at $\gamma_{\max}$ is then

$$d_{F_2|\gamma=\gamma_{\max}}^2 = E_s\rho^2\frac{4}{M}\sin^2\gamma_{\max} = E_s\rho^2\frac{4}{M}\frac{\sqrt{2}-1}{\sqrt{2}}\,. \tag{3.37}$$

Proposition 3.2. *For every channel angle $\gamma \geq \gamma_{\max}$, the distance $d_{\min}$ obtained by a precoding matrix $\mathbf{F}_d$ cannot exceed the distance d_{F_2} in (3.33).*

Proof: see Appendix B.

In other words, the optimized minimum distance, for every channel angle $\gamma \geq \gamma_{\max}$, is only provided by the precoder $\mathbf{F}_2$. Furthermore, the distance defined in (3.37) is the maximum value that a linear precoder can obtain (see Appendix C). These properties reaffirm that the proposed precoding matrix $\mathbf{F}_2$ is suitable to optimize the distance $d_{\min}$ on both virtual subchannels, especially when the channels SNRs are small dispersive.

The received constellation of the precoder $\mathbf{F}_2$ is shown in the Fig. 3.9. It is observed that the received symbols on both virtual subchannels are arranged on concentric circles. The arrangement of received vectors on both subchannels are quite similar. One should note that any two received vectors, which are close on one subchannel, are distant on the other subchannel.

3.2.3 Channel threshold γ_0

Fig. 3.10 illustrates the normalized distance $d_{\min}$ obtained by two new precoding matrix $\mathbf{F}_1$ and $\mathbf{F}_2$. It is observed that the optimal distance is only governed by the channel angle γ. The precoder $\mathbf{F}_1$ is just available for small γ, while precoder $\mathbf{F}_2$ is valid for high value of the channel angle.

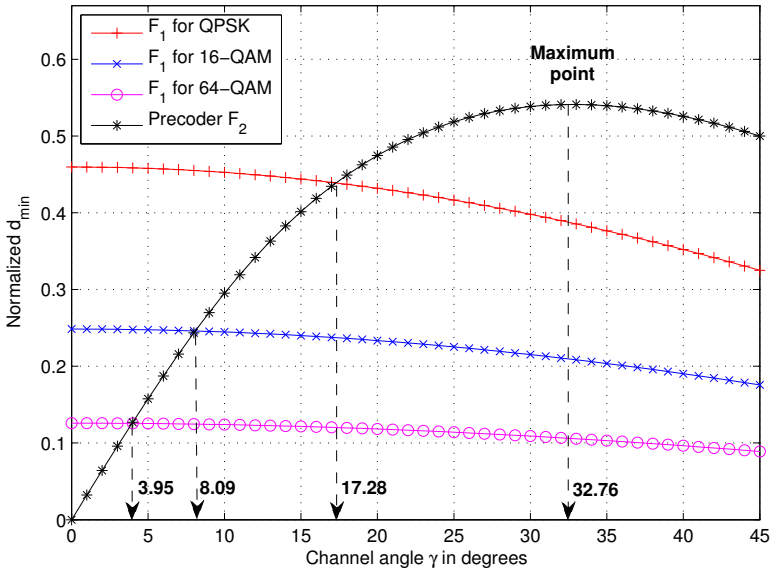

FIGURE 3.10: Normalized minimum Euclidean distance.

For a given modulation, by considering $d^2_{F_1} = d^2_{F_2}$ in (3.29) and (3.33), we obtain the value of channel optimal threshold γ_o such that

$$\tan^2 \gamma_0 = \frac{\sqrt{2}-1}{\sqrt{2}N^2 + \sqrt{6}N + \sqrt{2}-1} \tag{3.38}$$

When $\gamma < \gamma_0$, the precoder $\mathbf{F}_1$ is used and the signal is transmitted over the strongest virtual subchannel. On the contrary, when $\gamma \geq \gamma_0$, the precoder $\mathbf{F}_2$ is chosen and both virtual subchannels are used to transmit signal. It is obvious that the higher order of the modulation (N increases), the less we use the precoder $\mathbf{F}_1$, in other words, the smaller γ_0 is (eg: $\gamma_0 \simeq 17.28^o$ for QPSK, $\gamma_0 \simeq 8.09^o$ for 16-QAM, and $\gamma_0 \simeq 3.95^o$ for 64-QAM modulation).

3.3 Performance for high-order QAM modulations

3.3.1 Comparison of minimum Euclidean distance

Firstly, we indicate the improvement of our new precoder in terms of minimum Euclidean distance. For diagonal precoders, the minimum Euclidean distance between two transmit

vectors $\mathbf{s}$ and $\mathbf{r}$ can be simplified as

$$\begin{aligned} d^2_{\min} &= \min_{\mathbf{s},\mathbf{r}\in S,\mathbf{s}\neq\mathbf{r}} \|\mathbf{H}_v\mathbf{F}_d(\mathbf{s}-\mathbf{r})\|^2 \\ &= \min_{\mathbf{s},\mathbf{r}\in S,\mathbf{s}\neq\mathbf{r}} E_s \sum_i^b \lambda_i f_i^2 |s_i - r_i|^2 \end{aligned} \tag{3.39}$$

where $\mathbf{s} = [s_1, s_2, .., s_b]^T$, $\mathbf{r} = [r_1, r_2, .., r_b]^T$, $\mathbf{F}_d = \text{diag}(f_1, .., f_b)$, and $\lambda_1 \geq \lambda_2 \geq .. \lambda_b$ are the ordered eigenvalues of $\mathbf{HH}^*$. It is obvious that the minimum Euclidean distance is obtained when the vectors $\mathbf{s}$ and $\mathbf{r}$ are different from only one symbol. The minimum Euclidean distance of diagonal precoders is then defined by

$$\begin{aligned} d^2_{\min} &= E_s \min_{\mathbf{s},\mathbf{r}\in S,\mathbf{s}\neq\mathbf{r}} \min_{i=1..b} \lambda_i f_i^2 |s_i - r_i|^2 \\ &= E_s \min_{i=1..b} \lambda_i f_i^2 \min_{\mathbf{s},\mathbf{r}\in S,\mathbf{s}\neq\mathbf{r}} |s_i - r_i|^2 \\ &= 4\beta_M E_s \min_{i=1..b} \lambda_i f_i^2 \end{aligned} \tag{3.40}$$

where $4\beta_M = 4/M = 6/(4^k - 1)$ is the minimum Euclidean distance squared of the constellation for a rectangular 4^k-QAM modulation.

Precoder	Minimum squared distance $d^2_{\min}$
Beamforming	$E_s\rho^2 \frac{4}{M} \frac{\cos^2\gamma}{N^2+2N+2}$ (see Eq. (3.30))
max-$\lambda_{\min}$	$E_s\rho^2 \frac{4}{M} \cos^2\gamma \sin^2\gamma$
MMSE	$E_s\rho^2 \frac{4}{M} \frac{\sin^2\gamma}{1+\tan\gamma}$
Water-filling	$E_s\rho^2 \frac{2}{M} \sin^2\gamma$
max-$d_{\min}$	$\begin{cases} E_s\rho^2 \frac{4}{M} \frac{\cos^2\gamma}{N^2+\sqrt{3}N+2} & \text{if } \gamma \leq \gamma_0 \\ E_s\rho^2 \frac{4}{M} \frac{(2-\sqrt{2})\cos^2\gamma\sin^2\gamma}{1+(2-2\sqrt{2})\cos^2\gamma} & \text{other} \end{cases}$

TABLE 3.1: Comparison of the minimum Euclidean distances.

Thanks to the equation (3.40), the minimum distance corresponding to each precoder can now be determined. Tab. 3.1 shows the distance $d_{\min}$ obtained by diagonal precoders in comparison with our max-$d_{\min}$ precoder. The normalized distances $d_{\min}/\sqrt{4E_s\rho^2/M}$ for each precoder in the case of 64-QAM modulation are illustrated in Fig. 3.11. We note that, for diagonal precoders (eg. WaterFiling [12], MMSE [32], max-$\lambda_{\min}$ [33]), the average transmit power is chosen large enough such that the power is allocated on both virtual subchannels. It is observed that when $\gamma \leq \gamma_0$, the max-$d_{\min}$ precoder performs

a slight enhancement compared to beamforming designs. This improvement remains in constant for every channel angle γ and and reduces for higher-order modulations. The performance of the max-$\lambda_{\min}$ solution is better than the Water-filling and MMSE ones, but it is really outperformed by the proposed precoder.

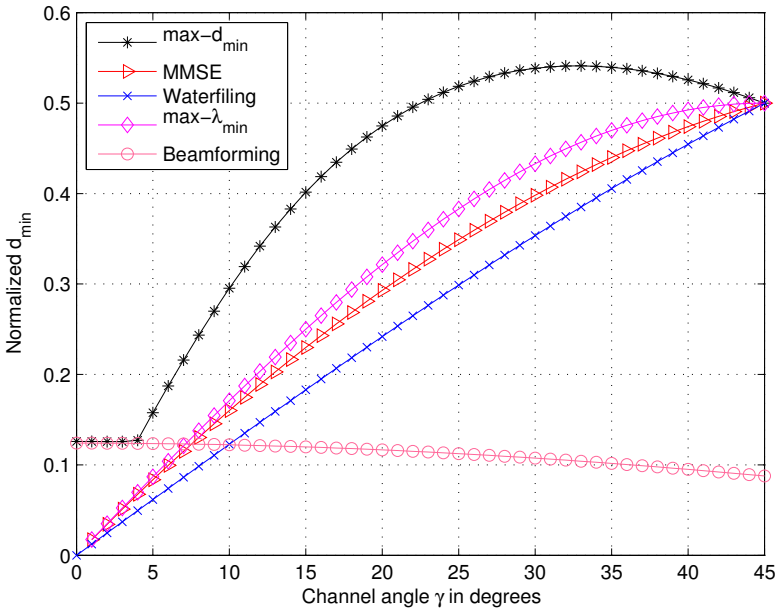

FIGURE 3.11: Normalized minimum Euclidean distance for 64-QAM.

3.3.2 Diversity order of max-$d_{\min}$ precoder

This section demonstrates that our new precoder obtains the diversity order $n_T \times n_R$ with the rectangular 4^k-QAM modulation. For a Rayleigh fading channel, we consider the approximation of error probability associated with constellations at the minimum distance $d_{\min}$ multiplied by the number of neighbors at this distance [56]

$$P_e \approx \frac{N_{d_{\min}}}{2} \operatorname{erfc}\left(\sqrt{\frac{d_{\min}^2}{4N_0}}\right), \tag{3.41}$$

where $N_{d_{\min}}$ is the average number of all nearest neighbors by each vector symbol, and N_0 is the variance of the white gaussian noise ν.

The expressions of $d_{\min}$ obtained by $\mathbf{F}_1$ and $\mathbf{F}_2$ allow us to regulate the minimum distance with two bounds depending only on λ_1. Firstly, we recognized that the minimum distance of max-$d_{\min}$ precoder is bounded below by that of $\mathbf{F}_1$. By considering the following

inequality, we can find the upper bound of the minimum distance

$$\frac{(2-\sqrt{2})\cos^2\gamma\sin^2\gamma}{1+(2-2\sqrt{2})\cos^2\gamma} \leq \frac{\cos^2\gamma}{2}. \tag{3.42}$$

Therefore, the minimum distance obtained by the max-$d_{\min}$ precoder satisfies the condition below

$$E_s\rho^2\frac{4}{M}\frac{\cos^2\gamma}{N^2+\sqrt{3}N+2} \leq d^2_{\min} \leq E_s\rho^2\frac{2}{M}\cos^2\gamma, \tag{3.43}$$

and for $\lambda_1 = \rho^2\cos^2\gamma$

$$E_s\xi_1\lambda_1 \leq d^2_{\min}(\text{max-}d_{\min}) \leq E_s\xi_2\lambda_1, \tag{3.44}$$

where $\xi_1 = \frac{4}{M(N^2+\sqrt{3}N+2)}$, and $\xi_2 = \frac{2}{M}$. By using, then, the condition of the largest eigenvalue [57] in function of $\|\mathbf{H}\|^2$

$$\frac{\|\mathbf{H}\|^2}{m} \leq \lambda_1 \leq \|\mathbf{H}\|^2 \tag{3.45}$$

where $m = \min(n_T, n_R)$, we have

$$\frac{E_s\xi_1\|\mathbf{H}\|^2}{m} \leq d^2_{\min}(\text{max-}d_{\min}) \leq E_s\xi_2\|\mathbf{H}\|^2 \tag{3.46}$$

The error probability in (3.41) is now bounded by

$$\frac{N_{d_{\min}}}{2}\operatorname{erfc}\left(\frac{E_s\xi_2\|\mathbf{H}\|^2}{4N_0}\right) \leq P_e \leq \frac{N_{d_{\min}}}{2}\operatorname{erfc}\left(\frac{E_s\xi_1\|\mathbf{H}\|^2}{4mN_0}\right)$$

One should note that $\operatorname{erfc}(x) \simeq e^{-x^2}$ for $x \gg 1$, so the inequality above can be rewritten as

$$\frac{N_{d_{\min}}}{2}e^{-\frac{E_s\xi_2\|\mathbf{H}\|^2}{4N_0}} \leq P_e \leq \frac{N_{d_{\min}}}{2}e^{-\frac{E_s\xi_1\|\mathbf{H}\|^2}{4mN_0}}$$

The average error probability can now be determined by using the Rayleigh characteristic of the transmit channel $\mathbf{H}$, i.e: $E[e^{-x\|\mathbf{H}\|^2}] = (1+x)^{-n_T n_R}$. The upper and lower bounds are then

$$\frac{N_{d_{\min}}}{2}\left(\frac{\text{SNR}.\xi_2}{4}\right)^{-n_T n_R} \leq \bar{P}_e \leq \frac{N_{d_{\min}}}{2}\left(\frac{\text{SNR}.\xi_1}{4mN_0}\right)^{-n_T n_R}$$

It is obvious that the error probability is bounded by two terms which vary as the exponential function of $\mathrm{SNR}^{-n_T n_R}$. Consequently, the proposed precoder obtains a full diversity order, i.e., $n_T n_R$.

3.3.3 Distribution of the channel angle and max-$d_{\min}$ precoder

When the channel varies, the max-$d_{\min}$ precoder uses $\mathbf{F}_1$ or $\mathbf{F}_2$ to optimize the minimum Euclidean distance. Hence, the $d_{\min}$ enhancement depends on the channel angle γ. The authors in [58] provided the joint probability distribution of two nonzero eigenvalues of the matrix $\mathbf{W} = \mathbf{H}\mathbf{H}^*$

$$f^{(2)}_{\lambda_1,\lambda_2}(\lambda_1,\lambda_2) = \frac{1}{n_s!(n_s+1)!}(\lambda_1\lambda_2)^{n_s} e^{-(\lambda_1+\lambda_2)}(\lambda_1-\lambda_2)^2$$

where $n_s = |n_T - n_R|$. By applying the change of variables $\lambda_1 = \rho^2\cos^2\gamma$ and $\lambda_2 = \rho^2\sin^2\gamma$, the joint probability distribution of the channel gain ρ and channel angle γ are given by

$$f^{(2)}_{\rho,\gamma}(\rho,\gamma) = f^{(2)}_{\lambda_1,\lambda_2}(\rho^2\cos^2\gamma, \rho^2\sin^2\gamma)|\mathbf{J}| \tag{3.47}$$

with the Jacobian of the transformation is defined by

$$|\mathbf{J}| = 4\rho^3\sin\gamma\cos\gamma(\cos^2\gamma+\sin^2\gamma) = 2\rho^3\sin 2\gamma$$

The joint distribution in (3.47) can be now simplified as

$$f^{(2)}_{\rho,\gamma}(\rho,\gamma) = \frac{2^{-2n_s+1}}{n_s!(n_s+1)!}\cos^2 2\gamma(\sin 2\gamma)^{2n_s+1}\rho^{7+4n_s}e^{-\rho^2}$$

One should note that

$$\Gamma(k) = \int_0^\infty \rho^{2k+1}e^{-\rho^2}\,d\rho = \frac{1}{2}\int_0^\infty t^k e^{-t}\,dt = \Gamma(k+1) = \frac{k!}{2}$$

The probability distribution of the channel angle γ is then obtained by

$$\begin{aligned} f^{(2)}_{\rho}(\rho) &= \int_0^\infty f^{(2)}_{\rho,\gamma}(\rho,\gamma)\,d\rho \\ &= \frac{2^{-2n_s}(2n_s+3)!}{n_s!(n_s+1)!}\cos^2 2\gamma(\sin 2\gamma)^{2n_s+1} \end{aligned} \tag{3.48}$$

Figure 3.12 illustrates the distribution of the channel angle γ with different values of n_s. It is observed that the curve moves to the right when the number of antennas increases. In other words, the more antennas we use, the less we need the precoder $\mathbf{F}_1$. The distribution of the expression $\mathbf{F}_1$ for QPSK, 16-QAM and 64-QAM are illustrated in the Tab. 4.2. It can be seen that the precoder $\mathbf{F}_1$ is also used less for higher orders of the rectangular modulation. This property can be explained by the change of the channel threshold γ_0 in (3.38).

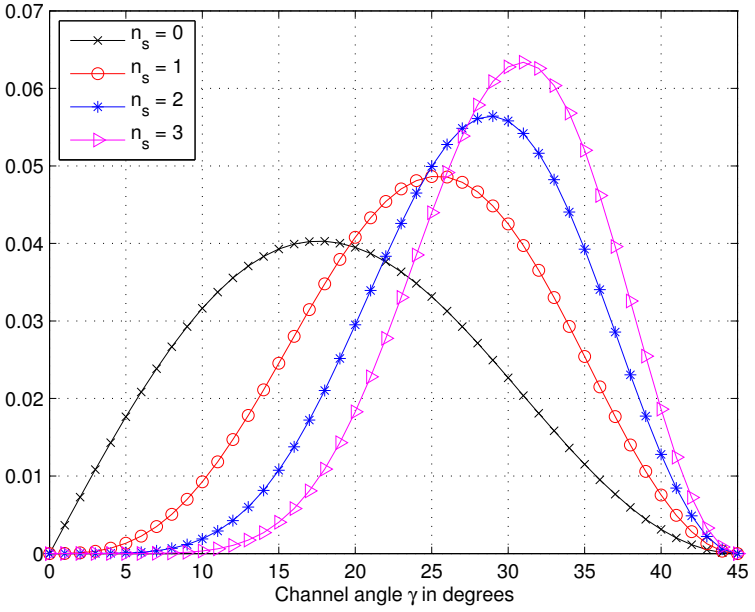

FIGURE 3.12: Probability density functions of the angles γ.

Expressions	MIMO (2,2)	MIMO (3,2)	MIMO (4,2)
QPSK	44.166 %	17.202 %	6.352 %
16-QAM	11.424 %	1.102 %	0.099 %
64-QAM	2.821 %	0.066 %	$\simeq 0\%$

TABLE 3.2: Percentage of use $\mathbf{F}_1$ for uncorrelated Rayleigh fading channels.

3.3.4 Bit-Error-Rate performance

This section illustrates the BER improvement of the new max-$d_{\min}$ precoder in comparison with other traditional precoding strategies. Let us consider a MIMO system with $n_T = 3$ transmit and $n_R = 2$ receive antennas. In this system, the symbols are separated into 2 independent data-streams. The channel matrix $\mathbf{H}$ is i.i.d zero-mean complex Gaussian, while ν is zero-mean additive white Gaussian noise.

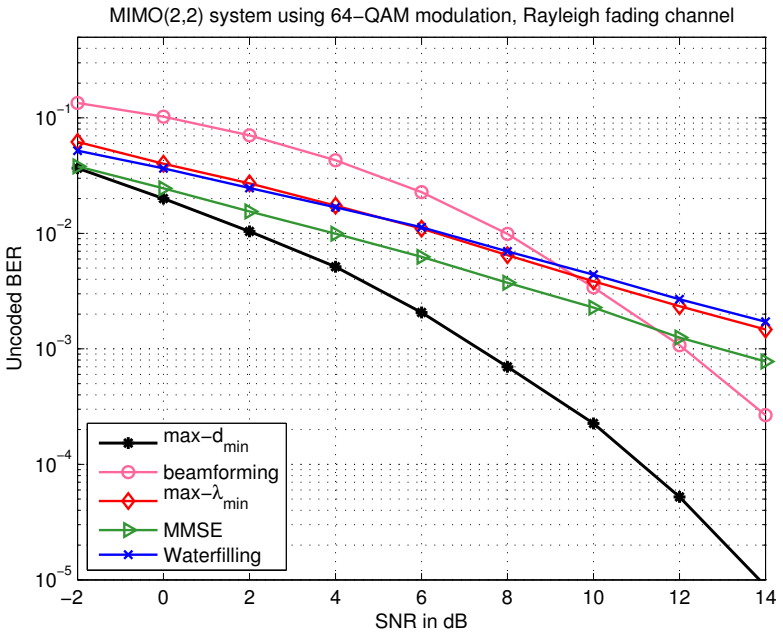

(a) BER performance for MIMO(2,2) system

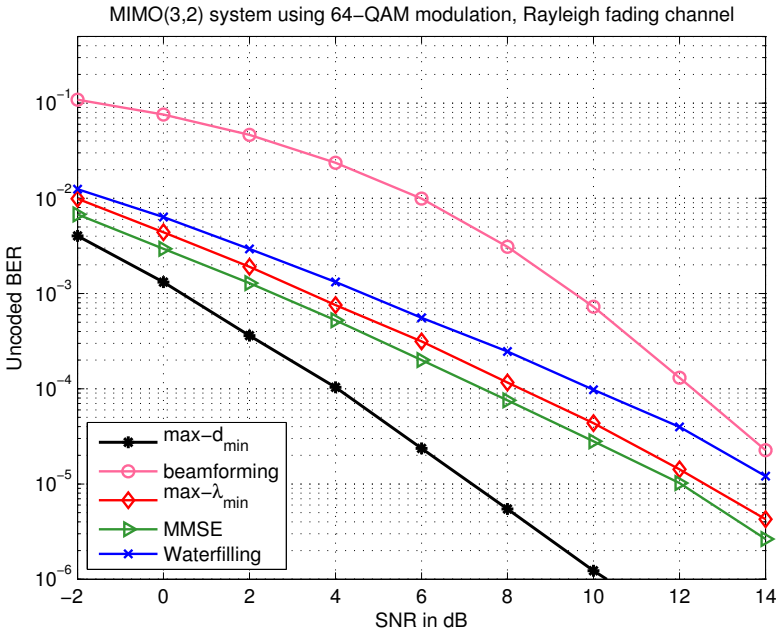

(b) BER performance for MIMO(3,2) system

FIGURE 3.13: Comparison the performance in terms of BER for 64-QAM modulation.

Given the enhancement of the minimum Euclidean distance, we can expect a gain of our max-$d_{\min}$ precoder in terms of BER compared to diagonal precoding strategies. Fig. 3.13 illustrates the BER performance with respect to SNR for a 64-QAM modulation. It is obvious that the max-$d_{\min}$ precoder obtains a large BER improvement compared to

diagonal precoders. This result clearly demonstrates that our new precoder is particular suited for reducing BER when an ML detection rule is considered at the receiver. When the virtual channels are less dispersive (more antennas are used, for example), the BER enhancement is more significant. A gain of about 8 dB can be observed at BER = 10^{-3} for MIMO(3,2) in comparison with 6 dB gain of SNR for MIMO(2,2).

3.4 Conclusion

We firstly introduced, in this chapter, the optimized solution of the max-$d_{\min}$ precoder for two 16-QAM symbols. This optimal precoder selects the best precoding matrix among five different expressions. In order to reduce the complexity of the max-$d_{\min}$ precoder for high-order QAM modulations, a general expression of the minimum Euclidean distance based precoder is also presented. For two independent data-streams, the proposed max-$d_{\min}$ precoder has two expressions: $\mathbf{F}_1$ pours power only on the first virtual subchannel, and $\mathbf{F}_2$ uses both virtual subchannels. It is demonstrated that our general form obtains the optimized minimum distance for small and large dispersive channels.

As presented in the simulation results, the new precoder offers a significant improvement on BER performance in comparison with traditional precoding strategies such as beamforming, water-filling, minimizing the mean square error, and max-$\lambda_{\min}$. Furthermore, the distribution of both precoding matrices depends on the channel characteristics and the number of antennas used at the transmitter and receiver. The more dispersive the virtual subchannels are (more antennas are used, for example), the less we need the precoder $\mathbf{F}_1$.

Appendices of chapter 3

A Proof of Proposition 3.1

Let us consider two difference vectors below

$$\breve{x}_a = \frac{2}{\sqrt{M}}\begin{pmatrix}1\\0\end{pmatrix}, \breve{x}_b = \frac{2}{\sqrt{M}}\begin{pmatrix}0\\1\end{pmatrix}$$

We assume that there exist a precoding matrix $\mathbf{F}_d$ such that the minimum Euclidean distance is larger or equal to $\sqrt{E_s\rho^2/M}$. At that time, two corresponding normalized distances must satisfy the condition

$$\begin{cases} \bar{d}_a^2 = \frac{1}{2}\cos^2\psi\cos^2\theta + \frac{1}{2}\sin^2\psi\sin^2\theta \geq \frac{1}{4} \\ \bar{d}_b^2 = \frac{1}{2}\cos^2\psi\sin^2\theta + \frac{1}{2}\sin^2\psi\cos^2\theta \geq \frac{1}{4} \end{cases}$$

One should note that $\bar{d}_a^2 + \bar{d}_b^2 = \frac{1}{2}\cos^2\psi + \frac{1}{2}\sin^2\psi = \frac{1}{2}$, so the distance $\bar{d}_a^2$ and $\bar{d}_b^2$ can not both greater than $\frac{1}{4}$. The minimum Euclidean distance $d_{\min}$, therefore, can not be larger than $\sqrt{E_s\rho^2/M}$. By considering $\bar{d}_a^2 = \bar{d}_b^2 = \frac{1}{4}$, it can be concluded that the optimized $d_{\min}$ can be obtained with $\theta = 45^o$ or $\psi = 45^o$.

B Proof of Proposition 3.2

Let us consider two more difference vectors

$$\breve{x}_c = \frac{2}{\sqrt{M}}\begin{pmatrix}1\\-1\end{pmatrix}, \breve{x}_d = \frac{2}{\sqrt{M}}\begin{pmatrix}1\\i\end{pmatrix}$$

where corresponding normalized distances are given by

$$\begin{cases} \bar{d}_a^2 = \cos^2\gamma\cos^2\psi\cos^2\theta + \sin^2\gamma\sin^2\psi\sin^2\theta \\ \bar{d}_b^2 = \cos^2\gamma\cos^2\psi\sin^2\theta + \sin^2\gamma\sin^2\psi\cos^2\theta \\ \bar{d}_c^2 = \cos^2\gamma\cos^2\psi(1-2\sin\theta\cos\theta\cos\varphi) + \sin^2\gamma\sin^2\psi(1+2\sin\theta\cos\theta\cos\varphi) \\ \bar{d}_d^2 = \cos^2\gamma\cos^2\psi(1-2\sin\theta\cos\theta\sin\varphi) + \sin^2\gamma\sin^2\psi(1+2\sin\theta\cos\theta\sin\varphi) \end{cases} \tag{3.49}$$

We assume that there exist a precoding matrix $\mathbf{F}_d$ at a channel angle $\gamma \geq \gamma_m$ such that the minimum Euclidean distance is greater or equal to d_{F_2}. In other words, four corresponding distances $\bar{d}_a^2$, $\bar{d}_b^2$, $\bar{d}_c^2$ and $\bar{d}_d^2$ are all greater or equal to the normalized distance $\bar{d}_{F_2}^2$. We have

$$\bar{d}_a^2 + \bar{d}_b^2 = \cos^2\gamma\cos^2\psi + \sin^2\gamma\sin^2\psi \tag{3.50}$$

Firstly, we demonstrate that

$$\cos^2\gamma\cos^2\psi \geq \sin^2\gamma\sin^2\psi \tag{3.51}$$

Indeed, it is obvious that $\bar{d}_a^2 + \bar{d}_b^2 \geq 2.\bar{d}_{F_2}^2 \geq 1/2$, for $\gamma \geq \gamma_m$. Therefore, if $\tan^2\psi > 1/\tan^2\gamma$ and $\gamma \leq \pi/4$ (i.e. $\cos^2\gamma \geq \sin^2\gamma$), we can obtain the contradiction below

$$\bar{d}_a^2 + \bar{d}_b^2 < \cos^2\gamma\sin^2\gamma + \sin^2\gamma\cos^2\gamma \leq 1/2$$

Furthermore, $\bar{d}_b^2$ can be rewritten as

$$\bar{d}_b^2 = (\cos^2\gamma\cos^2\psi - \sin^2\gamma\sin^2\psi)\sin^2\theta + \sin^2\gamma\sin^2\psi$$

Since $\bar{d}_b^2 \geq \bar{d}_{F_2}^2$, we get

$$(\cos^2\gamma\cos^2\psi - \sin^2\gamma\sin^2\psi)\sin^2\theta \geq \bar{d}_{F_2}^2 - \sin^2\gamma\sin^2\psi$$

Please note that $\cos^2\gamma\cos^2\psi - \sin^2\gamma\sin^2\psi \geq 0$ (3.51) and $\sin\theta\cos\theta \geq \sin^2\theta$, so we have

$$(\cos^2\gamma\cos^2\psi - \sin^2\gamma\sin^2\psi)\sin\theta\cos\theta \geq \bar{d}_{F_2}^2 - \sin^2\gamma\sin^2\psi \tag{3.52}$$

In addition, the difference vectors which are provided by $\breve{x}_c$ and $\breve{x}_d$ depend on the rotation angle φ:

- For $\varphi \leq \pi/4$, or $\cos\varphi \geq 1/\sqrt{2}$

The normalized distance d_c^2 can be now represented as

$$\begin{aligned} d_c^2 = &\left[\cos^2\gamma\cos^2\psi + \sin^2\gamma\sin^2\psi\right] \\ &- \left[\cos^2\gamma\cos^2\psi - \sin^2\gamma\sin^2\psi\right] 2\sin\theta\cos\theta\cos\varphi \end{aligned}$$

From (3.52), we have

$$\begin{aligned} d_c^2 &\leq \left[\cos^2\gamma\cos^2\psi + \sin^2\gamma\sin^2\psi\right] - \sqrt{2}(\bar{d}_{F_2}^2 - \sin^2\gamma\sin^2\psi) \\ &\leq \cos^2\gamma\cos^2\psi + (\sqrt{2}+1)\sin^2\gamma\sin^2\psi - \sqrt{2}.\bar{d}_{F_2}^2 \end{aligned} \tag{3.53}$$

One should note that

$$\begin{cases} \cos^2\gamma\cos^2\psi_2 + \sin^2\gamma\sin^2\psi_2 = 2.\bar{d}_{F_2}^2 \\ \cos^2\gamma\cos^2\psi_2 + (\sqrt{2}+1)\sin^2\gamma\sin^2\psi_2 = (\sqrt{2}+1).\bar{d}_{F_2}^2 \end{cases}$$

where $\psi_2 = \arctan\frac{\sqrt{2}-1}{\tan\gamma}$ is the power allocation parameter of the precoding matrix $\mathbf{F}_2$. Moreover, it is obvious that

$$(\sqrt{2}+1)\sin^2\gamma \geq \cos^2\gamma \geq \sin^2\gamma$$

for all value of γ in the range of $\pi/4 \geq \gamma \geq \gamma_m$. For this reason, we obtain

i) if $\psi > \psi_2$

$$\cos^2\gamma\cos^2\psi + \sin^2\gamma\sin^2\psi < 2.\bar{d}_{F_2}^2$$

ii) if $\psi < \psi_2$

$$\cos^2\gamma\cos^2\psi + (\sqrt{2}+1)\sin^2\gamma\sin^2\psi < (\sqrt{2}+1).\bar{d}^2_{F_2}$$

From (3.50), (3.53), and the above property, it can be concluded that the distances $\bar{d}^2_a$, $\bar{d}^2_b$, and $\bar{d}^2_c$ can not be all greater than the normalized distance $\bar{d}^2_{F_2}$.

- For $\pi/2 \geq \varphi \geq \pi/4$, or $\sin\varphi \geq 1/\sqrt{2}$

Hence, the normalized distance d^2_d which is defined by

$$\begin{aligned} d^2_d = &\left[\cos^2\gamma\cos^2\psi + \sin^2\gamma\sin^2\psi\right] \\ &- \left[\cos^2\gamma\cos^2\psi - \sin^2\gamma\sin^2\psi\right] 2\sin\theta\cos\theta\sin\varphi \end{aligned}$$

can be superior limited by

$$d^2_d \leq \cos^2\gamma\cos^2\psi + (\sqrt{2}+1)\sin^2\gamma\sin^2\psi - \sqrt{2}.\bar{d}^2_{F_2} \tag{3.54}$$

By using the same method as the case $\varphi \leq \pi/4$, we can concluded that $\bar{d}^2_a$, $\bar{d}^2_b$, and $\bar{d}^2_d$ can not be all greater than $\bar{d}^2_{F_2}$.

C Maximum value of the distance $d_{\min}$

We consider two more difference vectors

$$\breve{x}_e = \frac{2}{\sqrt{M}}\begin{pmatrix} 1 \\ -1+i \end{pmatrix}, \breve{x}_f = \frac{2}{\sqrt{M}}\begin{pmatrix} 1+i \\ -1 \end{pmatrix}$$

The corresponding normalized distances are given by

$$\begin{cases} \bar{d}^2_e = \cos^2\gamma\cos^2\psi(\cos^2\theta + 2\sin^2\theta - 2\Phi\sin\theta\cos\theta) \\ \qquad + \sin^2\gamma\sin^2\psi(\sin^2\theta + 2\cos^2\theta + 2\Phi\sin\theta\cos\theta) \\ \bar{d}^2_f = \cos^2\gamma\cos^2\psi(2\cos^2\theta + \sin^2\theta - 2\Phi\sin\theta\cos\theta) \\ \qquad + \sin^2\gamma\sin^2\psi(2\sin^2\theta + \cos^2\theta + 2\Phi\sin\theta\cos\theta) \end{cases}$$

where $\Phi = \sin\varphi + \cos\varphi$. If we assume that there exist a precoding matrix $\mathbf{F}_d$ such that the minimum Euclidean distance is greater or equal to d_{γ_m}, it means that $\bar{d}_a^2$, $\bar{d}_b^2$, $\bar{d}_c^2$, $\bar{d}_d^2$, $\bar{d}_e^2$, and $\bar{d}_f^2$ are all greater or equal to $(\sqrt{2}-1)/\sqrt{2}$.

Like Appendix 3.2, we can demonstrate that ψ satisfies the inequality (3.51) and the optimized minimum Euclidean distance in $\bar{d}_a^2$, $\bar{d}_b^2$,..., $\bar{d}_f^2$ is obtained by $\sin\theta\cos\theta = \sin^2\theta$ ($\theta = \pi/4$). The normalized distances above can be now simplified as

$$\begin{cases} \bar{d}_c^2 = \cos^2\gamma\cos^2\psi(1-\cos\varphi) + \sin^2\gamma\sin^2\psi(1+\cos\varphi) \\ \bar{d}_d^2 = \cos^2\gamma\cos^2\psi(1-\sin\varphi) + \sin^2\gamma\sin^2\psi(1+\sin\varphi) \\ \bar{d}_e^2 = \bar{d}_f^2 = \cos^2\gamma\cos^2\psi(3/2-\cos\varphi-\sin\varphi) \\ \quad + \sin^2\gamma\sin^2\psi(3/2+\cos\varphi+\sin\varphi) \end{cases}$$

In the end of this appendix, we show that $\bar{d}_c^2$, $\bar{d}_d^2$ and $\bar{d}_e^2$ can not be all greater than $(\sqrt{2}-1)/\sqrt{2}$.

- For $\varphi \le \pi/4$, we have $\bar{d}_c^2 \le \bar{d}_d^2$

By using the same method as the Appendix 3.2, we find that the optimized $d_{\min}$ of two distances $\bar{d}_c^2$ and $\bar{d}_e^2$ is obtained when $\bar{d}_c^2 = \bar{d}_e^2$ or

$$\tan^2\psi_{opt} = \frac{2\sin\varphi - 1}{2\sin\varphi + 1}\frac{1}{\tan^2\gamma} \tag{3.55}$$

By substituting ψ_{opt} into the $\bar{d}_c^2$, we get

$$\begin{aligned} \bar{d}_c^2 &= \Psi(2\sin\varphi+1)(1-\cos\varphi) + \Psi(2\sin\varphi-1)(1+\cos\varphi) \\ &= 2\Psi(2\sin\varphi-\cos\varphi) \le 2\Psi(2\frac{1}{\sqrt{2}} - \frac{1}{\sqrt{2}}) \end{aligned}$$

where $\Psi = \frac{\sin^2\gamma\sin^2\psi}{2\sin\varphi-1} = \frac{\cos^2\gamma\cos^2\psi}{2\sin\varphi+1}$. The optimized $d_{\min}$ is, therefore, provided by $\varphi = \pi/4$ and $\psi_{opt} = \psi_2$. In other words, the maximum value of the distance $d_{\min}$ is d_{γ_m}.

- For $\varphi \ge \pi/4$, we can implement a similar way by considering the optimal parameter

$$\tan^2\psi_{opt} = \frac{2\cos\varphi - 1}{2\cos\varphi + 1}\frac{1}{\tan^2\gamma} \tag{3.56}$$

Chapter 4

Extension of max-$d_{\min}$ precoder for large MIMO systems

In the previous chapter, we presented a non-diagonal linear precoder which maximizes the minimum Euclidean distance (max-$d_{\min}$) for rectangular QAM modulations. This max-$d_{\min}$ precoder obtains a large performance improvement in terms of BER compared to diagonal precoders. However, the max-$d_{\min}$ solution is only available for two independent data-streams. That is due to the expression of the distance $d_{\min}$ that depends on the number of data-streams, the channel characteristics, and the modulation.

This chapter proposes a heuristic solution which permits increasing the number of transmit symbols. Firstly, by decomposing the propagation channel into 2×2 eigen-channel matrices, and applying the new max-$d_{\min}$ precoder (presented in Chapter 3) for independent pairs of data-streams, a suboptimal solution for large MIMO systems can be obtained [59]. The precoder is denoted as Equal-$d_{\min}$(E-$d_{\min}$), and is presented in section 4.1. One should note that this sub-optimal solution can only achieve an even number of data-streams. Therefore, we extend, in section 4.2, the design of max-$d_{\min}$ precoders for a three parallel data-stream schemes. Thanks to the three-dimensional (3-D) scheme, an extension for an odd number of data-streams is obtained by decomposing the virtual channel into (2×2) and (3×3) eigen-channel matrices. The simulation results with perfect and imperfect CSI estimation confirm a significant improvement in terms of BER for the proposed solution.

4.1 Cross-form precoding matrix for large MIMO systems

4.1.1 Principle of E-$d_{\min}$ precoder

Let us consider a large MIMO system over which an even number of datastreams ($b \geq 4$) are transmitted. As known, by using the virtual transformation, the input-output relation can be expressed as

$$\mathbf{y} = \mathbf{H}_v \mathbf{F}_d \mathbf{s} + \eta_v, \tag{4.1}$$

where $\mathbf{H}_v = \mathbf{G}_v \mathbf{H} \mathbf{F}_v$ is the $b \times b$ virtual channel matrix, $\eta_v = \mathbf{G}_v \nu$ is the $b \times 1$ transformed additive Gaussian noise vector. The eigen-channel matrix is diagonal and denoted as $\mathbf{H}_v = \text{diag}\{\sigma_1, \sigma_2, \cdots, \sigma_b\}$.

As presented in chapter 3, for a M-QAM ($M = 4^k$) modulation with $b = 2$ data-streams, the optimal precoding matrix has two expressions

- if $0 \leq \gamma \leq \gamma_0$

$$\mathbf{F}_d = \mathbf{F}_1 = \sqrt{E_s} \begin{pmatrix} \cos\theta_1 & \sin\theta_1 \, e^{i\varphi_1} \\ 0 & 0 \end{pmatrix} \tag{4.2}$$

  where $\begin{cases} \varphi_1 = \arctan \frac{1}{2(2^k-1)+\sqrt{3}} \\ \theta_1 = \arctan(2\sin\varphi_1). \end{cases}$

- if $\gamma_0 \leq \gamma \leq \pi/4$

$$\mathbf{F}_d = \mathbf{F}_2 = \frac{\sqrt{E_s}}{2} \begin{pmatrix} \cos\psi_2 & 0 \\ 0 & \sin\psi_2 \end{pmatrix} \begin{pmatrix} \sqrt{2} & 1+i \\ -\sqrt{2} & 1+i \end{pmatrix} \tag{4.3}$$

  where $\psi_2 = \arctan \frac{\sqrt{2}-1}{\tan\gamma}$.

The value of the optimal channel threshold γ_0 is defined by

$$\tan^2 \gamma_0 = \frac{\sqrt{2}-1}{\sqrt{2}N^2 + \sqrt{6}N + \sqrt{2} - 1}, \tag{4.4}$$

where $N = 2^k - 1$.

In the case of large MIMO channels ($b > 2$), we can extend this solution by decomposing the ($b \times b$) eigen-channel matrix into 2×2 eigen-channel matrices and optimize the distance

$d_{\min}$ for each pair of data-streams. The extension is denoted as E-$d_{\min}$, and consists of four main steps [59]:

1. Obtain the virtual diagonal matrix $\mathbf{H_v}$ by using a virtual transformation.
2. Associate $b/2$ couples of singular values following the combination (σ_1, σ_b), (σ_2, σ_{b-1}), ..., $(\sigma_{b/2}, \sigma_{b/2+1})$ to obtain $b/2$ 2-D virtual sub-systems.
3. Apply the optimal 2D max-$d_{\min}$ solution on each subsystem with the power constraint equals to 1.
4. Allocate the power of each subsystem by the coefficient Υ_i such that

$$\Upsilon_i^2 = E_s \left(\delta_i^2 \sum_{k=1}^{b/2} \frac{1}{\delta_k^2} \right)^{-1} \quad \text{for } i = 1, ..., b/2 \tag{4.5}$$

where δ_i is the minimum Euclidean distance of the subsystem $\#i$ given in the step 3.

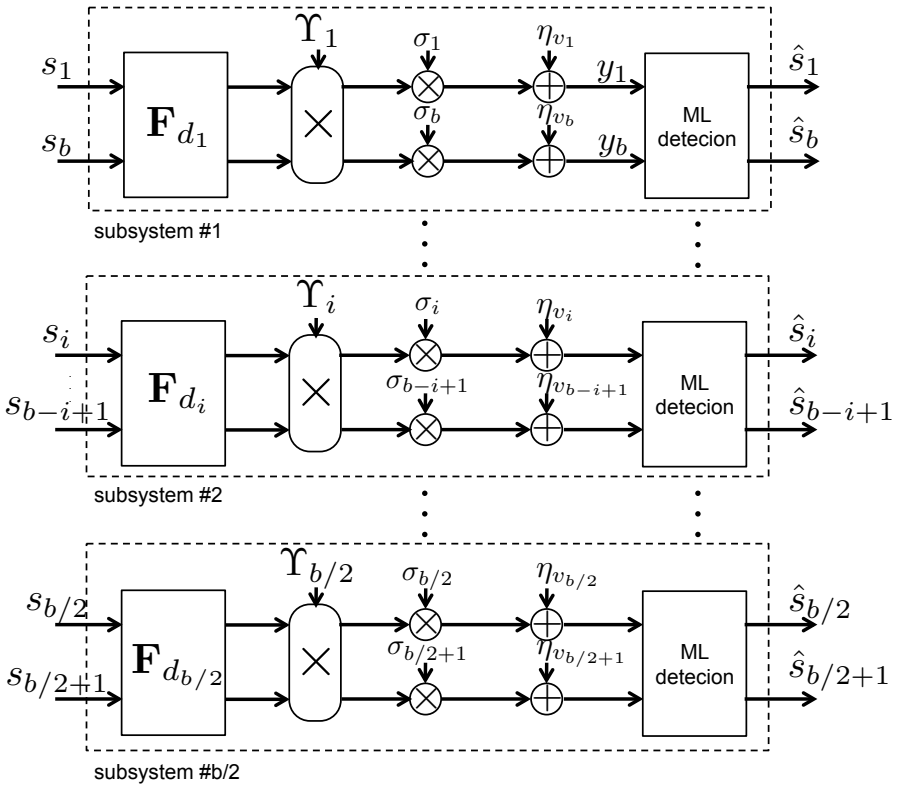

FIGURE 4.1: System model E-$d_{\min}$ solution.

On this scheme, the precoding matrix $\mathbf{F}_d$ in (4.1) is expressed as

$$\mathbf{F}_d = \begin{pmatrix} \Upsilon_1 f_1^{(1)} & & & & & & \Upsilon_1 f_2^{(1)} \\ & \Upsilon_2 f_1^{(2)} & & & & \Upsilon_2 f_2^{(2)} & \\ & & \ddots & & \iddots & & \\ & & & \Upsilon_{b/2} f_1^{(b/2)} & \Upsilon_{b/2} f_2^{(b/2)} & & \\ & & & \Upsilon_{b/2} f_3^{(b/2)} & \Upsilon_{b/2} f_4^{(b/2)} & & \\ & & \iddots & & \ddots & & \\ & \Upsilon_2 f_3^{(2)} & & & & \Upsilon_2 f_4^{(2)} & \\ \Upsilon_1 f_3^{(1)} & & & & & & \Upsilon_1 f_4^{(1)} \end{pmatrix} \tag{4.6}$$

where the sub-precoder $\mathbf{F}_d = \begin{pmatrix} f_1^{(i)} & f_2^{(i)} \\ f_3^{(i)} & f_4^{(i)} \end{pmatrix}$ is the 2-D max-$d_{\min}$ solution (presented in 4.2) for the eigen-channel matrix $\mathbf{H}_{v_i} = \text{diag}\{\sigma_i, \sigma_{b-i+1}\}$, with $i = 1, \cdots, b/2$. The precoder $\mathbf{F}_d$ can also be expressed as

$$\begin{aligned} \mathbf{F}_d = \text{diag}\left\{\Upsilon_1 f_1^{(1)}, \cdots, \Upsilon_{b/2} f_1^{(b/2)}, \Upsilon_{b/2} f_4^{(b/2)}, \cdots, \Upsilon_1 f_4^{(1)}\right\} \\ + \text{antidiag}\left\{\Upsilon_1 f_2^{(1)}, \cdots, \Upsilon_{b/2} f_2^{(b/2)}, \Upsilon_{b/2} f_3^{(b/2)}, \cdots, \Upsilon_1 f_3^{(1)}\right\} \end{aligned} \tag{4.7}$$

This expression is the association of a diagonal precoder and a new anti-diagonal form in order to enhance the performance of the system (i.e. improve the $d_{\min}$ criterion). Fig. 4.1 illustrates the synoptic of E-$d_{\min}$ solution with $b/2$ subsystem. At the receiver, several ML detections are used to optimize the minimum distance for $b/2$ pairs of datastreams. The number of distances to be compared is therefore equal to $b/2 \times M^2$ for a M-QAM modulation. In comparison with diagonal precoders, where the complexity of this quantizer is bM, the complexity of the proposed precoder is higher, but it is really less than the general non-diagonal solution (i.e. M^b for full ML detections).

4.1.2 Performance for large MIMO systems

In this section, we compare the performance of the proposed precoder with other sophisticated transceivers such as the linear precoder using Decision Feedback Equalization

(DFE) transceiver [60], the linear transceiver with bit allocation [61], the vector perturbation precoding scheme [62], and the minimum BER block design for ZF equalization [63].

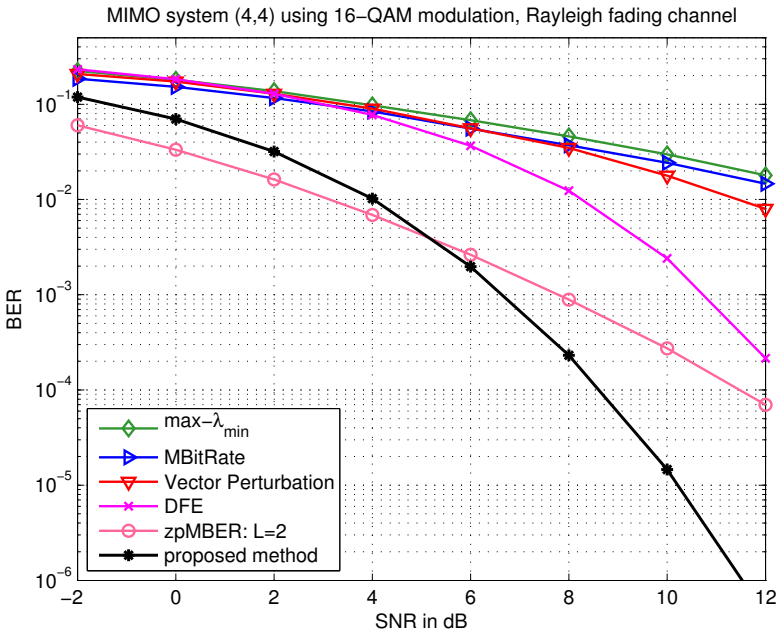

FIGURE 4.2: BER performance for large MIMO systems.

Since the extension for large MIMO channel is obtained by decomposing the channel into 2×2 eigen-channel matrices and optimize the distance $d_{\min}$ for each pair of data-streams, $\frac{b}{2}M^2$ ML tests are implemented to optimize the minimum distances of $b/2$ sub-systems. In comparison with the sophisticated transceivers above, the ML complexity of our proposed precoder is higher (i.e. $\frac{b}{2}M^2$ compared to bM). However, the extension of the 2D-max-$d_{\min}$ precoder exhibits a higher diversity order than the other precoding strategies. Fig. 4.2 illustrates the BER performance for MIMO (4,4) systems using 16-QAM modulation. The comparison of our proposed precoder and other schemes shows that the BER performance is significantly enhanced at high SNR. A gain of about 4 dB is observed at high SNR in comparison with other precoding schemes.

Then, we consider the impact of imperfect CSI estimation on the BER improvement of max-dmin precoder. Fig. 4.3 illustrates the BER performance with respect to SNR in the case of perfect CSI and imperfect CSI estimation. The estimated channel matrix of imperfect CSI system can be modeled as $\mathbf{H}_{est} = \mathbf{H} + \mathbf{H}_{err}$, where $\mathbf{H}_{err}$ represents the channel estimation error. The optimal training signals for the MIMO-OFDM channel estimation can be found in [64]. In this simulation, we assume that the entries of $\mathbf{H}_{err}$

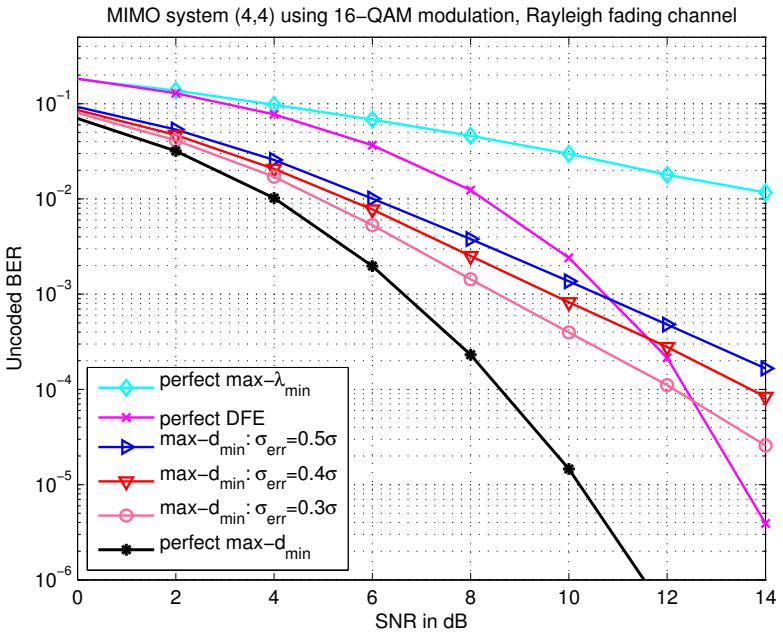

FIGURE 4.3: BER performance for perfect CSI and imperfect CSI estimations.

are complex Gaussian i.i.d random with mean zero and variance $\sigma_{err} = 0.5\sigma$, $\sigma_{err} = 0.4\sigma$, and $\sigma_{err} = 0.3\sigma$, where σ^2 is the variance of the complex Gaussian entries of $\mathbf{H}$. It is observed that the BER performance of the max-dmin precoder decreases at high SNR, but the BER improvement of our new precoder remains significant in comparison with other precoders.

4.2 Three-Dimensional max-$d_{\min}$ precoder

We propose, in this section, a new design of max-$d_{\min}$ precoders for a three parallel data-stream scheme. This precoder is the optimal solution of the three-dimensional $d_{\min}$ scheme presented in [65]. The proposed precoder not only allocates power on the three subchannels but also optimizes the minimum Euclidean distance between symbol points at the receiver. Therefore, when a maximum likelihood (ML) detection is considered at the receiver [51], the performance of the MIMO system in terms of BER is significantly enhanced. For large MIMO systems with odd number of data-streams, we can extend the new 3-D max-$d_{\min}$ solution by decomposing the $(b \times b)$ eigen-channel matrix into 2×2 and 3×3 eigen-channel matrices, and optimize the minimum Euclidean distance for each sub-systems.

4.2.1 Parameterized form of the three-dimensional max-$d_{\min}$ precoder

In the case of three independent datastreams, the virtual channel matrix can be parameterized as

$$\mathbf{H}_v = \rho \begin{pmatrix} \cos\gamma_1 & 0 & 0 \\ 0 & \sin\gamma_1 \cos\gamma_2 & 0 \\ 0 & 0 & \sin\gamma_1 \sin\gamma_2 \end{pmatrix}, \tag{4.8}$$

where ρ, γ_1 and γ_2 represent respectively the channel gain and the channel angles. As the diagonal elements of $\mathbf{H}_v$ are sorted in decreasing order, we have $0 \leq \gamma_2 \leq \pi/4$ and $\cos\gamma_2 \leq \operatorname{cotan}\gamma_1$.

Our objective is to find the precoding matrix $\mathbf{F}_d$ in 4.1 satisfying the power constraint $\text{trace}\{\mathbf{F}_d\mathbf{F}_d^*\} = E_s$. By using a singular value decomposition (SVD), we can reduce the complexity of the precoding matrix $\mathbf{F}_d$. This matrix is then represented as

$$\mathbf{F}_d = \mathbf{A}\mathbf{\Sigma}\mathbf{B}^*, \tag{4.9}$$

where $\mathbf{A}$ and $\mathbf{B}^*$ are 3×3 unitary matrices, and $\mathbf{\Sigma}$ is a 3×3 diagonal matrix with real positive values in decreasing order. It is noted that

$$\text{trace}\{\mathbf{F}_d\mathbf{F}_d^*\} = \text{trace}\{\mathbf{\Sigma}\mathbf{\Sigma}^*\} = E_s. \tag{4.10}$$

Hence, the power constraint across all transmit antennas can be replaced by the following decomposition of the diagonal matrix $\mathbf{\Sigma}$

$$\mathbf{\Sigma} = \sqrt{E_s} \begin{pmatrix} \cos\psi_1 & 0 & 0 \\ 0 & \sin\psi_1 \cos\psi_2 & 0 \\ 0 & 0 & \sin\psi_1 \sin\psi_2 \end{pmatrix}. \tag{4.11}$$

In order to simplify the constrained optimization problem, we consider a lower bound on the minimum Euclidean distance presented in [33]

$$d_{\min}^2 \geq \lambda_{\min}(SNR(\mathbf{F}_d)) \min_{x_k, x_l \in S, x_k \neq x_l} \|(\mathbf{x}_k - \mathbf{x}_l)\|^2 \tag{4.12}$$

where $\lambda_{min}(SNR(\mathbf{F}_d))$ is the minimum eigenvalue of the SNR-like matrix given by $SNR(\mathbf{F}_d) = \mathbf{H}_v\mathbf{F}_d\mathbf{F}_d^*\mathbf{H}_v$.

It is obvious that the higher the minimum eigenvalue of $SNR(\mathbf{F}_d)$, the greater the minimum Euclidean distance. Therefore, we can reduce the complexity of the optimization problem by maximizing the smallest eigenvalue of $SNR(\mathbf{F}_d)$.

The unitary matrix $\mathbf{B}$ has no effect on the eigenvalue of $SNR(\mathbf{F}_d)$. In other words, the singular values of the global channel $\mathbf{H}_v\mathbf{F}_d$ are not dependent on matrix $\mathbf{B}$.

Proposition 4.1. *The optimized singular values of the matrix* $\mathbf{H}_v\mathbf{F}_d$ *are given by* $\mathbf{A} = \mathbf{I}_3$.

Proof: see Appendix A.

By proposing only a diagonal matrix $\mathbf{\Sigma}$ to maximize the minimum singular value of $\mathbf{H}_v\mathbf{F}_d$, we could find the $\max -\lambda_{\min}$ solution presented in [33]. In this paper, the criterion that optimizes the minimum Euclidean distance is concerned. Therefore, not only the matrix $\mathbf{\Sigma}$ but also the matrix $\mathbf{B}^*$ are considered to maximize $d_{\min}$.

The 3×3 unitary matrix $\mathbf{B}^*$ can be parameterized as [66]

$$\mathbf{B}^* = \mathbf{B}_\beta \mathbf{B}_\theta \mathbf{B}_\varphi \tag{4.13}$$

with $\mathbf{B}_\beta = \begin{pmatrix} e^{i\beta_1} & 0 & 0 \\ 0 & e^{i\beta_2} & 0 \\ 0 & 0 & e^{i\beta_3} \end{pmatrix}$, $\mathbf{B}_\varphi = \begin{pmatrix} 1 & 0 & 0 \\ 0 & e^{i\varphi_2} & 0 \\ 0 & 0 & e^{i\varphi_3} \end{pmatrix}$

and $\mathbf{B}_\theta = \begin{pmatrix} c_1 & s_1c_2 & s_1s_2 \\ s_1c_3 & -c_1c_2c_3 - e^{i\varphi_1}s_2s_3 & -c_1s_2c_3 + e^{i\varphi_1}c_2s_3 \\ s_1s_3 & -c_1c_2s_3 + e^{i\varphi_1}s_2c_3 & -c_1s_2s_3 - e^{i\varphi_1}c_2c_3 \end{pmatrix}$

where $c_i = \cos\theta_i$ and $s_i = \sin\theta_i$ for $i = 1, .., 3$ with $0 \leq \theta_i \leq \pi/2$, $0 \leq \beta_i$ and $\varphi_i \leq 2\pi$.

Proposition 4.2. *The matrix* $\mathbf{B}_\beta$ *has no influence on* $d_{\min}$ *and the range of the angles in* $\mathbf{B}_\theta$ *and* $\mathbf{B}_\varphi$ *can be bounded by* $0 \leq \theta_1, \theta_3 \leq \pi/2$, $0 \leq \theta_2 \leq \pi/4$ *and* $0 \leq \varphi_1, \varphi_2, \varphi_3 \leq \pi$.

Proof: see Appendix B.

Consequently, the parameterized form of the three-dimensional max-$d_{\min}$ precoder can be simplified as

$$\mathbf{F}_d = \mathbf{\Sigma}\mathbf{B}_\theta\mathbf{B}_\varphi. \tag{4.14}$$

Our objective becomes searching for the different angles ψ_i, θ_i and φ_i to maximize the minimum Euclidean distance. As in the two-dimensional case, the angles ψ_i control the

power allocation on virtual subchannels, while θ_i and φ_i correspond to the scaling and the rotation of the received constellation, respectively.

The main difference between our precoder and diagonal precoders is the dependence of the optimized solution on the constellation of transmitted signals. It is observed that the more symbols the constellation has, the more complex the expression of the precoder is. In fact, the max-$d_{\min}$ precoder transforms a M-QAM transmitted signal into M^3 symbols on each subchannel. Therefore, it is difficult to determine which distances are minimum and how to optimize these distances. In the next sections, we point out the max-$d_{\min}$ solutions for three dimensional MIMO spatial multiplexing systems.

4.2.2 Optimal max-$d_{\min}$ precoder for a BPSK modulation

If a BPSK modulation is considered at the transmitter, the symbols on each data stream belong to the set $\{1,-1\}$. Let us define $\breve{\mathbf{x}}$ as the difference between the possible transmitted vectors, i.e., $\breve{\mathbf{x}} = \mathbf{x}_k - \mathbf{x}_l$ with $\mathbf{x}_k \neq \mathbf{x}_l$. Then, the difference vectors are combinations of three elements in the set $\{0,2,-2\}$. In the case of $b = 3$ data streams, the set of difference vectors denoted as $\breve{\mathbf{X}}_{BPSK}$ has $3^b - 1 = 80$ elements. By eliminating the collinear vectors, we can reduce $\breve{\mathbf{X}}_{BPSK}$ to only 13 elements.

A numerical search on precoder angles which maximize the minimum Euclidean distance for all channel angles γ_1 and γ_2, shows that the max-$d_{\min}$ precoder has two main different expressions. The first one uses only the strongest virtual subchannel, and it will be denoted as $\mathbf{F}_{bc_1}$. The other precoder allows power allocation on all subchannels, and it will be denoted as $\mathbf{F}_{bc_2}$. Appendix 4.3 demonstrates that the third virtual subchannel is not used for BPSK modulation, but all antennas are used physically at both the transmit and receive sides.

Precoder $\mathbf{F}_{bc_1}$

Only the first virtual subchannel is used for this precoder, meaning that the matrix $\mathbf{\Sigma} = \mathrm{diag}(1,0,0)$. Then, the angles θ_3 and φ_1 have no influence on the matrix precoder $\mathbf{F}_{bc_1}$ and can be assumed to be 0. A numerical maximization of the Euclidean distance shows that $\theta_2 = \pi/4$. The exact values of the other angles θ_2, φ_2 and φ_3 are shown in

our works [65]. By replacing the values into the expression (4.14), the precoder $\mathbf{F}_{bc_1}$ is then simplified as

$$\mathbf{F}_{bc_1} = \frac{\sqrt{E_s}}{\sqrt{5}} \begin{pmatrix} \sqrt{3}\, e^{i\pi/2} & e^{i\pi/6} \\ 0 & 0 & 0 \\ 0 & 0 & 0 \end{pmatrix} \tag{4.15}$$

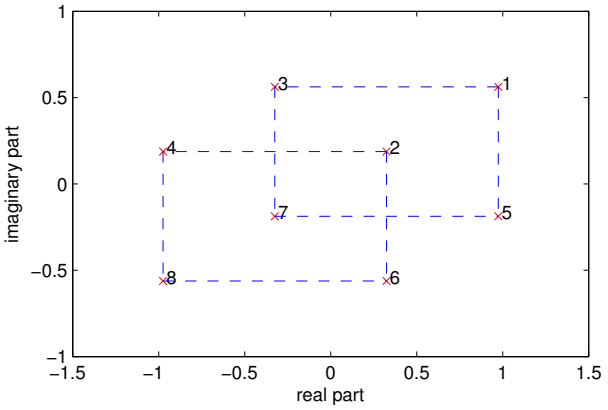

FIGURE 4.4: Received constellation for the precoder $\mathbf{F}_{bc_1}$.

A received constellation obtained by the optimal precoder $\mathbf{F}_{bc_1}$ is represented on Fig. 4.4. In the figure, the points denoted from 1 to 8 correspond to the 8 possible received symbols. We observe that the optimized $d_{\min}$ is obtained when point 7 is the center of the rectangular created by the points (2,4,6,8). The minimum distance is defined by

$$d^2_{bc_1} = \frac{4}{5} E_s \rho^2 \cos^2 \gamma_1 \tag{4.16}$$

Precoder $\mathbf{F}_{bc_2}$

If the difference between the first and second virtual subchannels is small, the precoder $\mathbf{F}_{bc_2}$ is considered at the transmitter. In Appendix C, we demonstrate that the optimized $d_{\min}$ is obtained for the angle $\psi_2 = 0$. In other words, only two virtual subchannels are used for the precoder. Fig. 4.5 illustrates the received constellations on the two subchannels with the points numbered from 1 to 8 like the case of precoder $\mathbf{F}_{bc_1}$. One should note that the received vectors on the second virtual subchannel stay on the horizontal axes. This remark can be explained by the symmetric properties of difference vectors, the form of $\mathbf{F}_{bc_2}$, and the rotation angles such that $\varphi_2 = \pi - \varphi_3$.

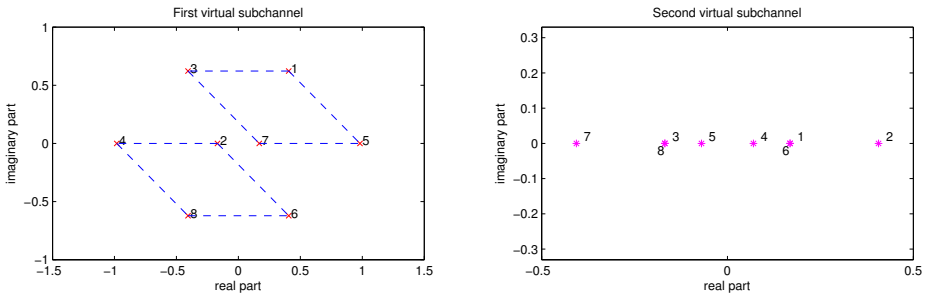

FIGURE 4.5: Received constellation for the precoder $\mathbf{F}_{bc_2}$.

We can also find, in Appendix C, the analytical angles for precoder $\mathbf{F}_{bc_2}$. The angle ψ_1 depends on the channel angles, while the others are constants:

$$\begin{cases} \psi_1 = \arctan\sqrt{\dfrac{\operatorname{cotan}^2\gamma_1/\cos^2\gamma_2}{R_{max}}} \\ \theta_1 \simeq 55.838^o, \theta_2 = 45^o, \theta_3 \simeq 31.306^o, \varphi_1 = 90^o, \varphi_3 \simeq 47.266^o \end{cases} \tag{4.17}$$

where R_{max} is the maximum value of $R_{12} = \Psi_1/\Psi_2$ and defined in Appendix C. The optimal $d_{\min}$ for the precoder $\mathbf{F}_{bc_2}$ is therefore expressed as a function of the channel parameters

$$d^2_{bc_2} = \frac{4}{3}E_s\rho^2\cos^2\gamma_1\frac{R_{max}+1}{R_{max}+\sigma_1^2/\sigma_2^2} \tag{4.18}$$

where $\sigma_1/\sigma_2 = \operatorname{cotan}\gamma_1/\cos\gamma_2$ corresponds to a ratio between the first and the second virtual subchannels.

Range of definition for precoders $\mathbf{F}_{bc_1}$ and $\mathbf{F}_{bc_2}$

Range of definition for $\mathbf{F}_{bc_1}$ and $\mathbf{F}_{bc_2}$ is obtained by comparing two quantities $d^2_{bc_1}$ and $d^2_{bc_2}$, defined respectively in (4.16) and (4.18). It is noted that both distances are only governed by the channel angles γ_1 and γ_2. Fig. 4.6 illustrates the normalized Euclidean distances $d_{\min}$ with respect to channel parameters (in degrees) for $\mathbf{F}_{bc_1}$ and $\mathbf{F}_{bc_2}$ precoders. We see that the distance d_{bc_1} depends on γ_1 only, while d_{bc_2} depends on both channel angles γ_1 and γ_2. By considering $d^2_{bc_1} = d^2_{bc_2}$, the threshold for the precoder can be defined by

$$\sigma_1^2/\sigma_2^2 = \frac{2R_{max}+5}{3} \tag{4.19}$$

Consequently, the ratio between the first and the second virtual subchannels determines the optimal precoder: $\mathbf{F}_{bc_1}$ for $\sigma_1/\sigma_2 \geq \sqrt{(2R_{max}+5)/3} \simeq 2.79$ and $\mathbf{F}_{bc_2}$ for $\sigma_1/\sigma_2 \leq 2.79$.

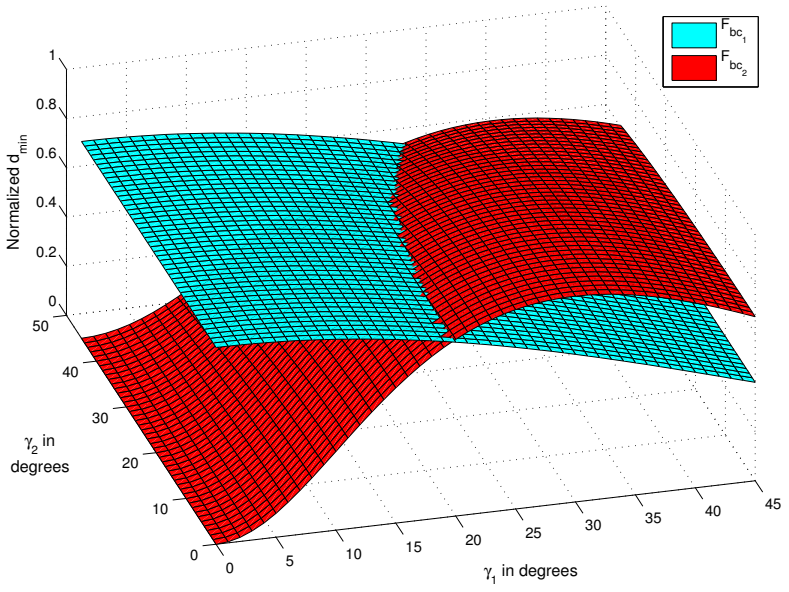

FIGURE 4.6: Range of definition for precoders $\mathbf{F}_{bc_1}$ and $\mathbf{F}_{bc_2}$.

4.2.3 Optimal max-$d_{\min}$ precoder for a QPSK modulation

The transmitted symbols belong to $S = \frac{1}{\sqrt{2}}\{1+i, 1-i, -1+i, -1-i\}$ for a QPSK modulation. By eliminating the collinear vectors, the set of difference vectors, denoted as $\breve{\mathbf{X}}_{QPSK}$, has up to 151 elements. Therefore, the expression of max-$d_{\min}$ precoder for a QPSK modulation is more complex than for the case of BPSK. The expressions of this precoder can be classified into three categories which enable power on one, two and three virtual subchannels, in respectively.

Precoder $\mathbf{F}_{qc_1}$

The received constellation on the first virtual subchannel of $\mathbf{F}_{qc_1}$ is shown in Fig. 4.7. It is observed that the constellation looks like a rotation of the 64-QAM modulation. Because the second and the third virtual subchannels are not available, the angles φ_1 and θ_3 have no influence on the performance of $d_{\min}$ and are consequently assumed to be zero. It was shown in [65] that the other angles of $\mathbf{F}_{qc_1}$ are constant and defined by

$$\begin{cases} \theta_1 = \arctan\frac{\sqrt{5}(\sqrt{3}+1)}{\sqrt{2}}, \theta_2 = \arctan\frac{1}{2} \\ \varphi_2 = \varphi_3 = \pi/12 \end{cases} \tag{4.20}$$

The minimum distance obtained by $\mathbf{F}_{qc_1}$ is then

$$d^2_{qc_1} = 2E_s\rho^2\cos^2\gamma_1\frac{1}{11+5\sqrt{3}} \tag{4.21}$$

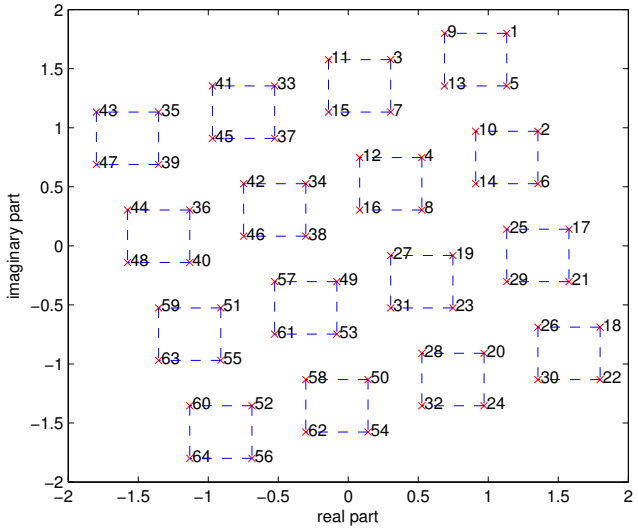

FIGURE 4.7: Received constellation for the precoder $\mathbf{F}_{qc_1}$.

Precoder $\mathbf{F}_{qc_2}$ and precoder $\mathbf{F}_{qc_3}$

These precoders enable power on two and three virtual subchannels, respectively. The complexity of the $d_{\min}$ optimization problem is exponentially proportional to the order of the modulation and to the number of the virtual subchannels used for transmitting signal.

Proposition 4.3. *When channel varies from (γ_1,γ_2) to (γ_1',γ_2'), the Euclidean distances provided by any two difference vectors can be kept equal by changing only the angles ψ_1, ψ_2 but retaining values of the angles θ_i and φ_i ($i = 1..3$).*

Proof: see Appendix D.

One should note that the optimized $d_{\min}$ is always provided by a limited number of difference vectors. By equalizing the Euclidean distances created by these vectors, we can obtain the exact expressions of the max-$d_{\min}$ precoder. Thanks to the Proposition 4.3, it can be concluded that the precoders $\mathbf{F}_{qc_2}$ and $\mathbf{F}_{qc_3}$ are provided by different sets of the constant angles θ_i and φ_i (i.e. the matrix $\mathbf{B}^\star$ is not changed).

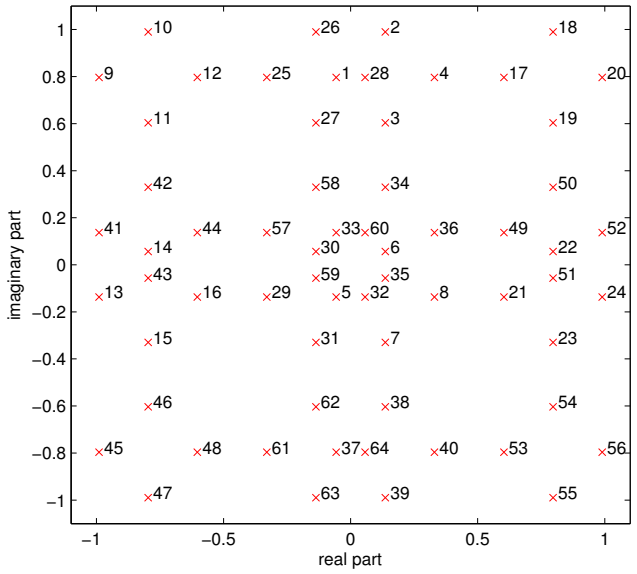

(a) First virtual subchannel

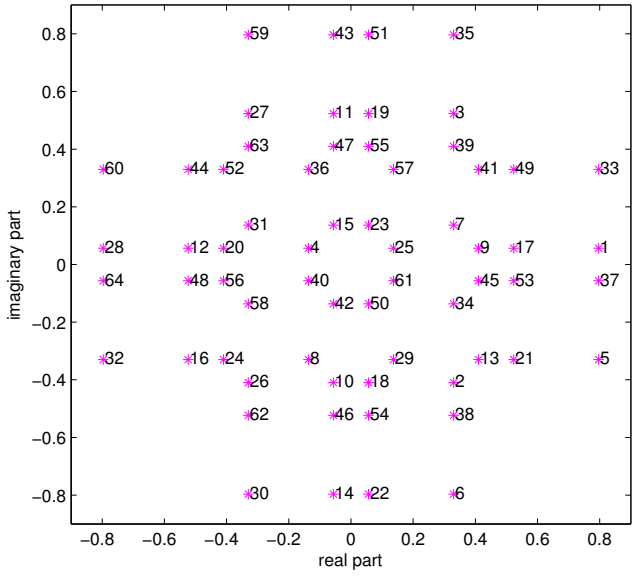

(b) Second virtual subchannel

FIGURE 4.8: Received constellation for the fourth expression of the precoder $\mathbf{F}_{qc_2}$.

a) Expressions of $\mathbf{F}_{qc_2}$: A numerical search, which maximizes the minimum Euclidean distance, shows that the precoder $\mathbf{F}_{qc_2}$ can have four different expressions. The received constellation of the fourth form is illustrated on the Fig. 4.8. We observe that whenever two received vectors are close on one virtual subchannel, they are distant on the other. The optimized solution is obtained when the minimum Euclidean distance is provided by several difference vectors. By solving the system of trigonometric equations, the

analytical values of all angles in the max-$d_{\min}$ precoder are determined (see Appendix D). These optimized angles are described in the Tab. 4.1. It is noted that θ_i and φ_i are constant while ψ_i varies and is defined by using standard sets (γ_i^s,ψ_i^s). Because the precoder $\mathbf{F}_{qc_2}$ uses only two first virtual subchannels, the angle ψ_2 then has no impact on the performance and can be assumed to be 0. The optimized angle ψ_1 for a channel (γ_1, γ_2) is given by

$$\psi_1 = \operatorname{atan}\sqrt{\frac{\tan^2\gamma_1^s\,\cos^2\gamma_2^s}{\tan^2\gamma_1\,\cos^2\gamma_2}\tan^2\psi_1^s} \tag{4.22}$$

where ψ_1^s is the optimized angle for the standard channel (γ_1^s,γ_2^s).

b) Expressions of $\mathbf{F}_{qc_3}$: The analytical values of all angles in $\mathbf{F}_{qc_3}$ are solved by using the process presented in Appendix D. There are three exact expressions of the precoder $\mathbf{F}_{qc_3}$ (see in Tab. 4.1). Like the case of $\mathbf{F}_{qc_2}$, the optimized angles θ_i and φ_i (i = 1..3) are constant, while the optimized angles ψ_1 and ψ_2 for a channel (γ_1, γ_2) are defined by

$$\psi_2 = \operatorname{atan}\sqrt{\frac{C_2}{\tan^2\gamma_2}}, \psi_1 = \operatorname{atan}\sqrt{\frac{C_1}{\tan^2\gamma_1\,\cos^2\gamma_2\,\cos^2\psi_2}} \tag{4.23}$$

where $C_1 = \tan^2\gamma_1^s\,\cos^2\gamma_2^s\,\cos^2\psi_2^s\,\tan^2\psi_1^s$, and $C_2 = \tan^2\gamma_2^s\,\tan^2\psi_2^s$ with (ψ_1^s,ψ_2^s) are the optimized angles for the standard channel (γ_1^s,γ_2^s).

$\mathbf{F}_{qc_2}$	θ_1	θ_2	θ_3	φ_1	φ_2	φ_3	(γ_1^s,γ_2^s) → ψ_1^s
(a)	44.49197	30.59366	39.65316	0	161.56505	0	(15,15) → 38.52143
(b)	32.34322	37.85164	56.71270	180	0	45	(20,20) → 39.79551
(c)	62.52239	22.59606	66.97236	85.31834	21.52669	118.15496	(30,15) → 35.82249
(d)	37.42924	22.5	38.45324	180	90	135	(40,10) → 39.90584
$\mathbf{F}_{qc_3}$	θ_1	θ_2	θ_3	φ_1	φ_2	φ_3	(γ_1^s,γ_2^s) → (ψ_1^s,ψ_2^s)
(a)	42.33339	45	50.63553	90	155.25922	24.74077	(25,40) → (50.50301, 42.03657)
(b)	52.86439	40.77576	53.32112	115.27892	145.43734	72.71867	(40,30) → (46.29106, 39.24208)
(c)	52.01812	45	90	0	45	135	(45,45) → (38.45504, 33.51067)

TABLE 4.1: Optimized angles in degree for the precoders $\mathbf{F}_{qc_2}$ and $\mathbf{F}_{qc_3}$

4.2.4 Range of definition for precoders $\mathbf{F}_{qc_1}$, $\mathbf{F}_{qc_2}$ and $\mathbf{F}_{qc_3}$

Our objective is to select among the eight expressions of $\mathbf{F}_{qc_1}$, $\mathbf{F}_{qc_2}$ and $\mathbf{F}_{qc_3}$ the precoder which provides the highest minimum Euclidean distance. By substituting the angles in Tab. 4.1 into (4.14), the $d_{\min}$ distances obtained by these precoders are determined.

Please note that the minimum distances for the precoder $\mathbf{F}_{qc_2}$ and $\mathbf{F}_{qc_3}$ are always provided by the difference vector $[0, 0, \sqrt{2}]^T$, and, therefore, defined by

$$d^2_{\min} = \|\mathbf{H}_v \mathbf{\Sigma} \mathbf{B}_\theta \mathbf{B}_\varphi \times [0, 0, \sqrt{2}]^T)\|^2. \tag{4.24}$$

Fig. 4.9 plots the range of definition for the eight expressions of our max-$d_{\min}$ precoder as a function of the channel angles γ_1 and γ_2 in degrees. It is observed that the precoder $\mathbf{F}_{qc_1}$ is available for a small channel angle γ_1 (e.g., less than $\pi/18$) and the distance $d^2_{qc_1}$ depends only on γ_1. For $\mathbf{F}_{qc_2}$, the first expression is available for all values of the channel angle γ_2. The others expressions of $\mathbf{F}_{qc_2}$ are presented for small values of γ_2, while three expressions of the precoder $\mathbf{F}_{qc_3}$ are available for higher γ_2. However, the minimum Euclidean distances obtained by $\mathbf{F}_{qc_2}$ and $\mathbf{F}_{qc_3}$ both depend on the two channel angles.

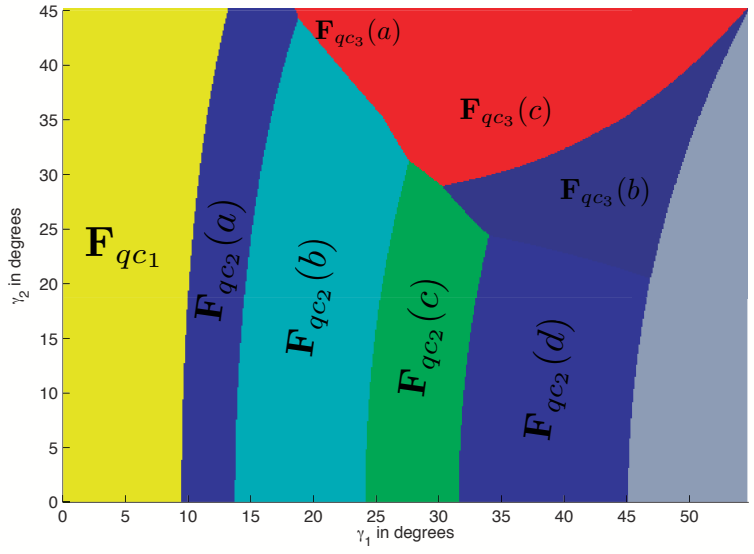

FIGURE 4.9: Range of definition for QPSK modulation.

4.2.5 Simulation results

Comparison of the minimum Euclidean distance

The normalized minimum Euclidean distance for max-$d_{\min}$ and diagonal precoders in the case of BPSK and QPSK modulations are plotted in Fig. 4.10 and Fig. 4.11, respectively. For diagonal precoders, the average transmit power E_s is chosen large

enough such that the precoders always allocate power on all eigen-subchannels (i.e. the minimum Euclidean distance is greater than 0).

In the case of BPSK modulation, three diagonal precoders are compared with our precoder: max-$\lambda_{\min}$ [33], MMSE [32] and WaterFilling [12]. It is observed that the $\mathbf{F}_{bc_1}$ solution is better than the diagonal precoders in terms of $d_{\min}$ for most of different channel angles. When the three eigen-subchannels are close ($\sigma_1 \simeq \sigma_2 \simeq \sigma_3$), the diagonal precoders are better than $\mathbf{F}_{bc_1}$ but are really outperformed by the max-$d_{\min}$ precoder.

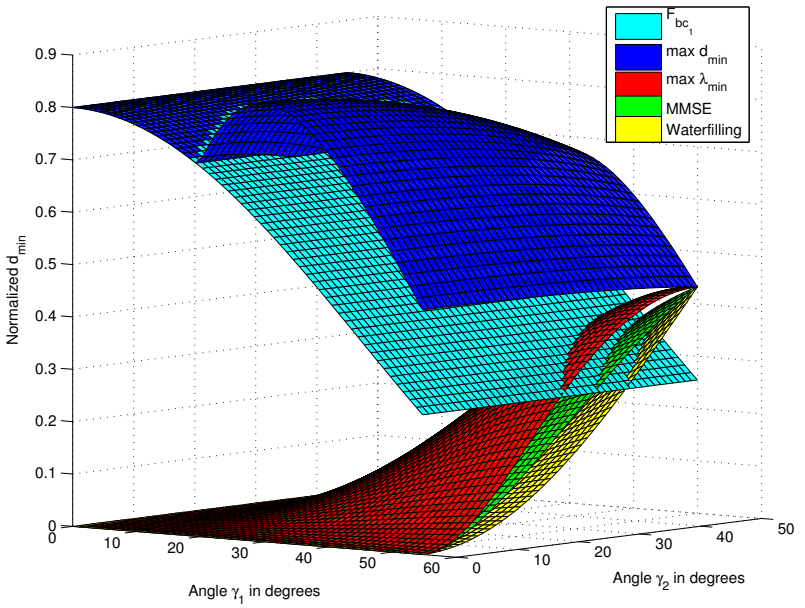

FIGURE 4.10: Normalized Euclidean distance $d_{\min}$ for BPSK.

To examine the performance of the minimum Euclidean distance for QPSK modulation, we consider, for example, a specific channel in which the SNRs of the second and third virtual subchannels are equal (i.e. $\rho_2 = \rho_3$ or $\gamma_2 = \pi/4$). The normalized minimum Euclidean distances (i.e. $d^2_{\min}/E_s/\rho^2$) for the proposed precoder and several diagonal precoders are plotted in Fig. 4.11. The optimized distance of our max-$d_{\min}$ precoder is then provided by $\mathbf{F}_{qc_1}$, $\mathbf{F}_{qc_2}(a)$, $\mathbf{F}_{qc_3}(a)$ and $\mathbf{F}_{qc_3}(c)$. It is observed that the precoder $\mathbf{F}_{qc_1}$ has a small improvement in terms of $d_{\min}$ compared with the beamforming 64-QAM precoder. This gain remains constant for every channel and comes from the rotation of the 64-QAM constellation. One should note that both precoders are much larger than zero for small channel angles γ_1. When γ_1 increases, the minimum Euclidean distance of max-$\lambda_{\min}$, MMSE and WF are better than that of beamforming but can not be compared

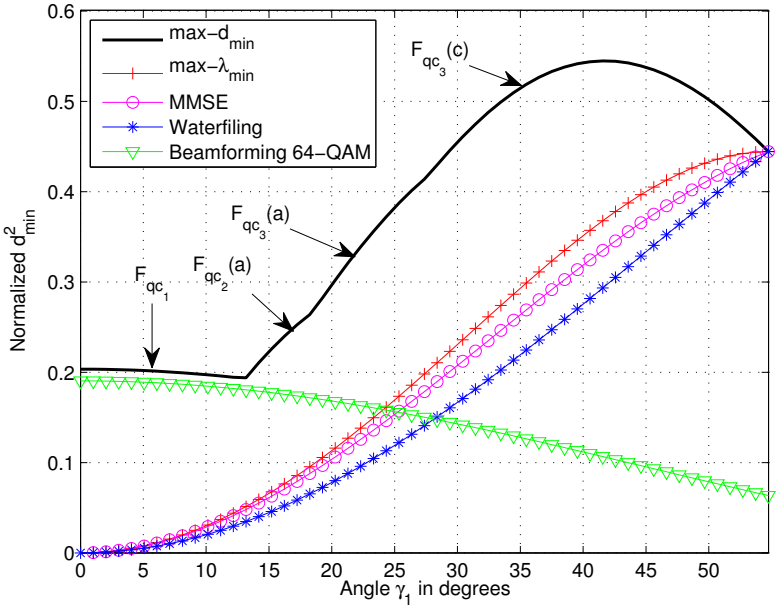

FIGURE 4.11: Normalized Euclidean distance $d_{\min}$ for QPSK modulation with $\gamma_2 = 45^o$.

to our max-$d_{\min}$ precoder. Due to the raise of the minimum Euclidean distance, the proposed precoder, therefore, is expected to provide a large improvement in terms of BER compared to diagonal precoders.

BER performance of the precoder max-$d_{\min}$

A MIMO-OFDM system with $n_T = 3$ transmit antennas and $n_R = 3$ receive antennas is considered in this section, meaning that we can send $b = 3$ independent data streams. The transmission channel is a Rayleigh fading channel and the noise vector elements are zero-mean complex Gaussian. For each SNR, 60 000 random complex Gaussian matrices $\mathbf{H}$ are generated and the precoder is optimized for each of them. Four diagonal precoders are selected to compare with our max-$d_{\min}$ precoder: WaterFilling [12], Beamforming [31], MMSE [32] and max-$\lambda_{\min}$ [33].

Fig. 4.12 and Fig. 4.13 illustrate the BER performance with respect to the SNR for BPSK and QPSK modulations, respectively. In the case of a BPSK modulation, the precoder max-$d_{\min}$ obtains a large performance improvement in terms of BER in comparison with diagonal precoders. A gain of about 2.5 dB can be observed in comparison with the precoder $\mathbf{F}_{bc_1}$ (see Fig. 4.12).

For QPSK modulation, the BER enhancement is more significant when using the precoder max-$d_{\min}$ in comparison with diagonal precoders. We observe that the precoder max-$\lambda_{\min}$ is better than MMSE and WaterFilling in terms of BER. Because the max-SNR precoder uses only the strongest virtual-subchannel, it has to transmit $4^3 = 64$ information bits on the eigenmode. Furthermore, the max-SNR solution is the diagonal precoder that has the best performance of BER. However, the precoder is really outperformed by our new precoder max-$d_{\min}$.

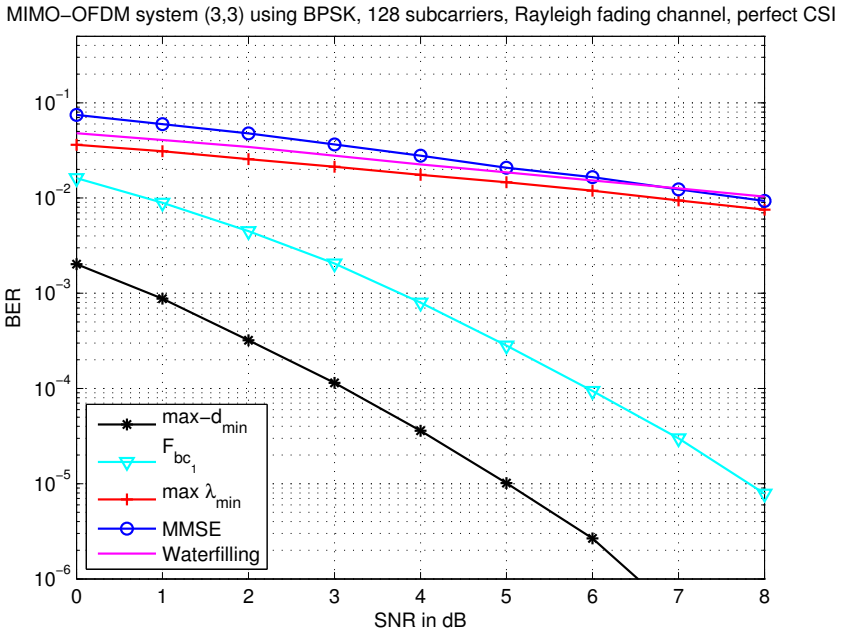

FIGURE 4.12: Comparison of precoders in terms of BER for BPSK modulation with a MIMO (3,3) uncorrelated Rayleigh fading channel.

Distribution of the channel angles and precoders

When the channel varies, the max-$d_{\min}$ precoder uses different expressions to optimize the minimum Euclidean distance. For this reason, the $d_{\min}$ improvement depends on the channel characteristics. In other words, the BER enhancement depends on the channel angles γ_1 and γ_2. Fig. 4.14 plots the probability density function (pdf) of γ_1 and γ_2 for MIMO (3,3) and MIMO (4,3) systems with uncorrelated Rayleigh fading channels. We observe that the pdf of small γ_1, e.g., less than $\pi/18$, is very small ($\Pr[\gamma_1 < \pi/18]_{MIMO(3,3)} \simeq 0.03\%$). As a consequence, the precoders which direct power only to the most favored virtual-subchannel is not often used to optimize the channel (e.g.,

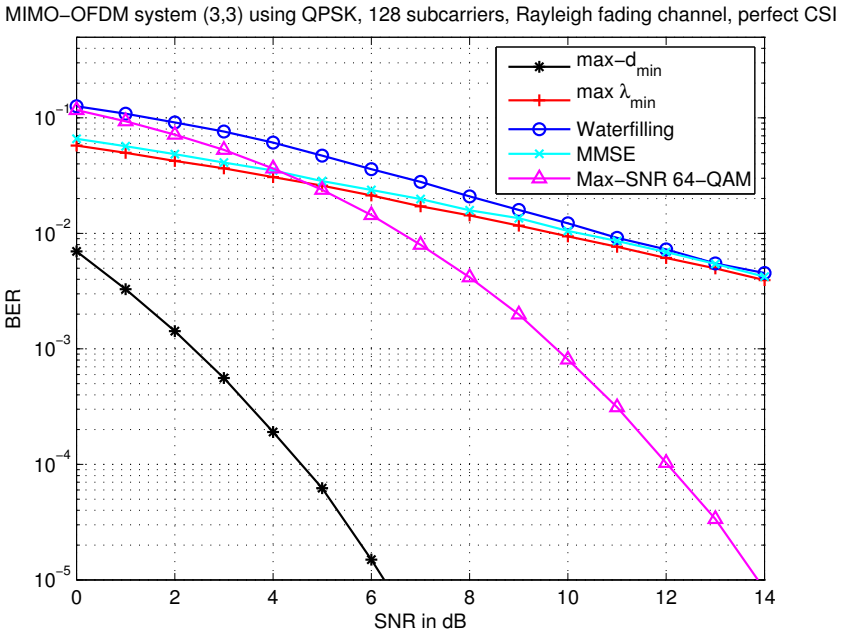

FIGURE 4.13: Comparison of precoders in terms of BER for QPSK modulation with a MIMO (3,3) uncorrelated Rayleigh fading channel.

$\Pr[\mathbf{F}_d = \mathbf{F}_{qc_1}]_{QPSK(3,3)} \simeq 0.03\%)$. The distributions of all max-$d_{\min}$ expressions for QPSK modulations are illustrated in the Tab. 4.2.

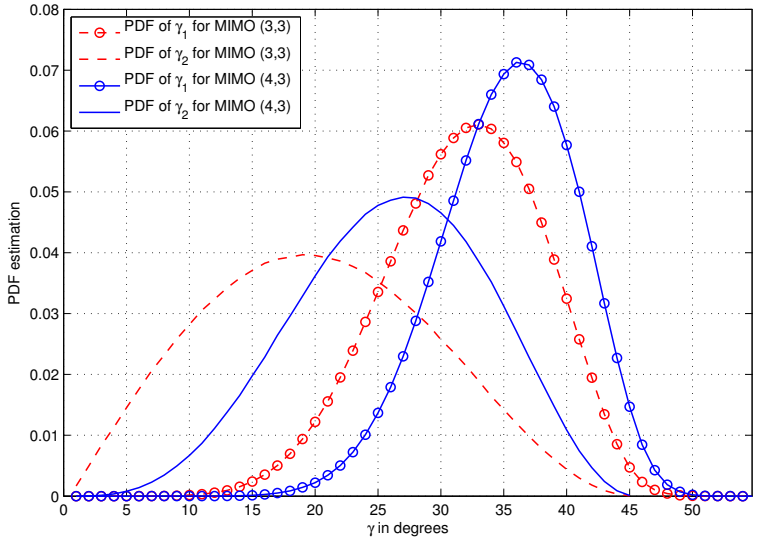

FIGURE 4.14: Probability density functions of the angles γ_1 and γ_2 for a MIMO system with uncorrelated Rayleigh fading channel (estimation with 10^6 random matrices).

The distributions of the max-$d_{\min}$ expressions for BPSK and QPSK modulations are illustrated in the Tab. 4.2. For BPSK modulation, it can be seen that the expression

$\mathbf{F}_{bc_2}$ is used more often than $\mathbf{F}_{bc_1}$ ($\Pr[\mathbf{F}_d = \mathbf{F}_{bc_1}]_{BPSK(3,3)} \simeq 6\%$). Furthermore, the probability depends on the number of antennas in use. The more antennas we use, the less we need $\mathbf{F}_{bc_1}$. In the case of QPSK modulation, we observe that the expressions $\mathbf{F}_{qc_1}$, $\mathbf{F}_{qc_2}(a)$ and $\mathbf{F}_{qc_3}(a)$ are available in a very small probability, especially $\mathbf{F}_{qc_1}$. The precoder $\mathbf{F}_{qc_1}$ uses only the strongest virtual subchannel to transform the signals, like the beamforming precoder. Therefore, we can see, in the Fig. 4.13, a large improvement in terms of BER for the precoder max-$d_{\min}$ in comparison with 64-QAM beamforming. Moreover, the improvement is more significant if the number of transmit or receive antennas increases.

Expressions	No	MIMO (3,3)	MIMO (4,3)
$\mathbf{F}_{bc_1}$		6.23 %	1.41 %
$\mathbf{F}_{bc_2}$		93.77 %	98.59 %
$\mathbf{F}_{qc_1}$		0.03 %	$\simeq 0\%$
$\mathbf{F}_{qc_2}$	(a)	0.44 %	0.03 %
	(b)	17.03 %	5.85 %
	(c)	31.99 %	19.39 %
	(d)	28.44 %	23.71 %
$\mathbf{F}_{qc_3}$	(a)	0.35 %	0.27 %
	(b)	11.39 %	27.39 %
	(c)	10.33 %	23.36 %

TABLE 4.2: Percentage of use for precoder max-$d_{\min}$ with uncorrelated Rayleigh fadding channels.

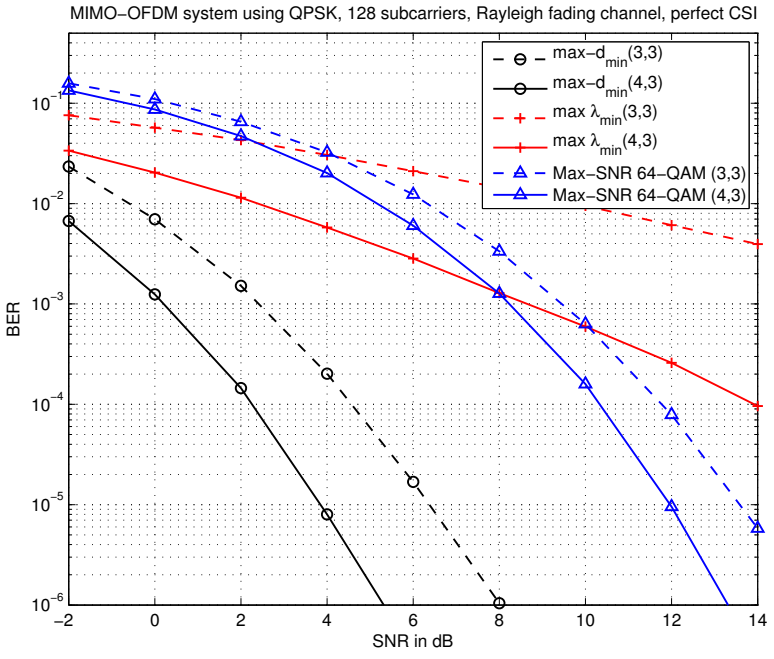

FIGURE 4.15: BER simulation of the precoder max-$d_{\min}$ compared to the max-$\lambda_{\min}$ and max-SNR with MIMO uncorrelated Rayleigh fading channels.

To demonstrate the influence of the channel characteristics, in general, and the number of antennas, in particular, on the BER performance, the MIMO (3,3) and MIMO (4,3) systems are considered in simulation. Fig. 4.15 illustrates the BER performances of three precoders: max-$d_{\min}$, max-$\lambda_{\min}$ and beamforming. It clearly shows a large BER enhancement of the max-$d_{\min}$ precoder compared to the beamforming strategy - a gain about 7 dB at BER equal to 10^{-5}. This gain is more significant if the number of transmit or receive antennas increases - about 8 dB at BER equal to 10^{-6} for MIMO (4,3) system.

BER performance for imperfect CSI estimation

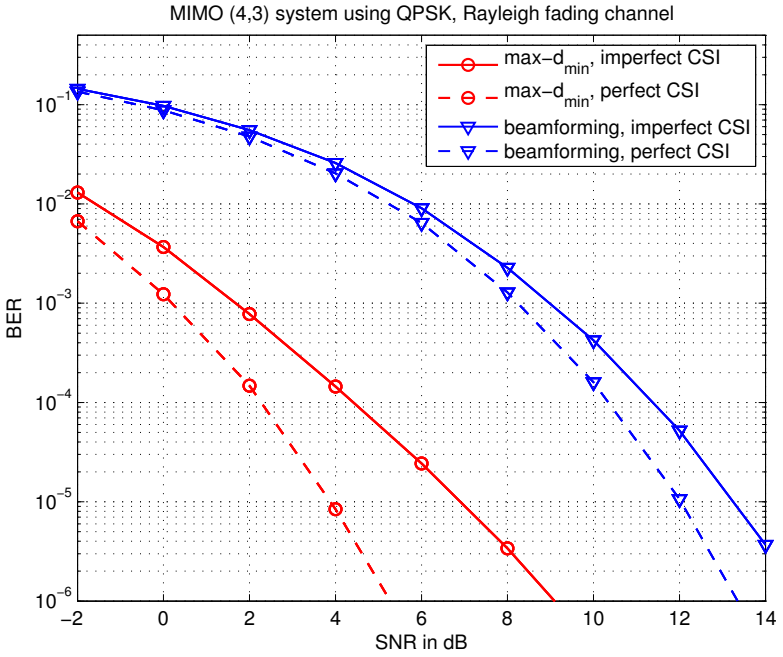

FIGURE 4.16: Comparison of precoders in terms of BER for perfect CSI and imperfect CSI estimation.

Let us consider the impact of imperfect CSI estimation at the transmitter on the BER enhancement of max-$d_{\min}$ precoder. Fig. 4.16 illustrates the BER performance with respect to SNR in the case of perfect CSI and imperfect CSI estimation. The estimated channel matrix of imperfect CSI system can be modeled as $\mathbf{H}_{est} = \mathbf{H} + \mathbf{H}_{err}$, where $\mathbf{H}_{err}$ represents the channel estimation error. The training signals for the MIMO-OFDM channel estimation can be found in [64]. In this simulation, we assume that the entries of $\mathbf{H}_{est}$ are complex Gaussian i.i.d random with mean zero and variance $\sigma^2_{err} = 0.25\,\sigma^2$, where σ^2 is the variance of the complex Gaussian entries of $\mathbf{H}$. It is observed that the BER performance of the max-$d_{\min}$ precoder decreases at high SNR, but the BER

improvement of our new precoder remains significant (gain about 6 dB at 10^{-5} BER in comparison with 64-QAM beamforming precoder).

4.3 Extension of max-$d_{\min}$ precoder for large MIMO system with an odd number of datastreams

4.3.1 General form of 3-D max-$d_{\min}$ precoder for QAM modulations

In the case of the rectangular 4^k-QAM modulation, the transmitted symbols belong to the set

$$S = \frac{1}{\sqrt{\beta_k}} \{a + b\,i\ ;\ a - b\,i\ ;\ -a + b\,i\ ;\ -a - b\,i\} \tag{4.25}$$

where $\beta_k = \frac{2}{3}(4^k - 1)$ and $a, b \in (1, 3, \ldots, 2^k - 1)$.

We first note that if $\frac{1}{\sqrt{\beta_k}}\breve{\mathbf{x}}$ is a difference vector of 4^k-QAM modulation, then $\frac{1}{\sqrt{\beta_{k'}}}\breve{\mathbf{x}}$ is also a difference vector of $4^{k'}$-QAM (with $k' \geq k$). Furthermore, the minimum distance is always provided by a limited number of different vectors. Therefore, the max-$d_{\min}$ precoder, which enables power on all three virtual subchannels, can provide the minimum Euclidean distance for not only QPSK but also all rectangular QAM modulations.

The number of optimal expressions for 3-D max-$d_{\min}$ precoder will increase when a high-order QAM modulation is considered at the transmitter. In Fig. 4.11, we observe that the less dispersive the channel is, the more we use the precoder $\mathbf{F}_{qc_3}(c)$. For this reason, we can simplify the form of the max-$d_{\min}$ precoder by choosing $\mathbf{F}_{qc_3}(c)$ to optimize the distance $d_{\min}$ for all rectangular QAM-modulations, especially when the channel is small dispersive. This precoder is, then, re-named as $\mathbf{F}_{\text{rec}}$ and defined by

$$\mathbf{F}_{\text{rec}} = \sqrt{E_s} \begin{pmatrix} \cos\psi_1 & 0 & 0 \\ 0 & \sin\psi_1 \cos\psi_2 & 0 \\ 0 & 0 & \sin\psi_1 \sin\psi_2 \end{pmatrix} \begin{pmatrix} \cos\theta_1 & \frac{\sin\theta_1}{\sqrt{2}} & \frac{\sin\theta_1}{\sqrt{2}} \\ 0 & \frac{-1}{\sqrt{2}} & \frac{1}{\sqrt{2}} \\ \sin\theta_1 & \frac{-\cos\theta_1}{\sqrt{2}} & \frac{-\cos\theta_1}{\sqrt{2}} \end{pmatrix} \begin{pmatrix} 1 & 0 & 0 \\ 0 & \frac{i+1}{\sqrt{2}} & 0 \\ 0 & 0 & \frac{i-1}{\sqrt{2}} \end{pmatrix} \tag{4.26}$$

where $\theta_1 = \frac{1}{2}\arctan(-4)$, $\psi_2 = \arctan\frac{\sqrt{5-\sqrt{17}}}{\sqrt{2}\tan\gamma_2}$, and $\psi_1 = \arctan\frac{\sqrt{2}}{\sqrt{5+\sqrt{17}}\tan\gamma_1\cos\gamma_2\cos\psi_2}$.

The minimum Euclidean distance obtained by $\mathbf{F}_{\text{rec}}$ is then

$$d^2_{\mathbf{F}_{\text{rec}}} = \frac{4}{\beta_k} E_s \rho^2 \frac{4\sin^2\gamma_1 \sin^2\gamma_2}{2\tan^2\gamma_2 + (5+\sqrt{17})\tan^2\gamma_1 \sin^2\gamma_2 + 5 - \sqrt{17}}\,. \tag{4.27}$$

Proposition 4.4. *When there is no dispersion of the subchannel SNRs, i.e.* $\mathbf{H}_v = \frac{\rho}{\sqrt{3}}\mathbf{I}_3$, *the distance* $d_{\min}$ *provided by* $\mathbf{F}_{rec}$ *is optimized for every rectangular QAM modulation.*

Proof: see Appendix F.

It is observed that if the power is enabled almost only on the strongest virtual subchannel ($\gamma_1 \to 0$), the minimum Euclidean distance provided by $\mathbf{F}_{\text{rec}}$ approaches to zero (see Fig. 4.11). We propose, herein, another precoder which optimizes the minimum distance for dispersive channels. Let us denote the precoder as $\mathbf{F}_{\text{snr}}$. When the channel is large dispersive, a numerical research shows that the optimized $d_{\min}$ is provided by five difference vectors:

$$\breve{x}_1 = \frac{2}{\sqrt{\beta_k}}\begin{pmatrix}1\\0\\0\end{pmatrix}, \breve{x}_2 = \frac{2}{\sqrt{\beta_k}}\begin{pmatrix}N\\-1\\N\end{pmatrix}, \breve{x}_3 = \frac{2}{\sqrt{\beta_k}}\begin{pmatrix}N\\0\\-1\end{pmatrix}, \breve{x}_4 = \frac{2}{\sqrt{\beta_k}}\begin{pmatrix}N+i\\0\\-1\end{pmatrix}, \breve{x}_5 = \frac{2}{\sqrt{\beta_k}}\begin{pmatrix}N+i\\-1\\N\end{pmatrix}$$

where $N = 2^k - 1$. This precoder pours power only on the first virtual subchannel, in other words, the angle $\psi_1 = 0$. The rotation angle φ_1 and the scaling angles θ_3, then, have no influence on the performance and are consequently assumed to be zero. By considering the corresponding distances of these vector, i.e. $d^2_{\breve{a}_1} = d^2_{\breve{a}_2} = d^2_{\breve{a}_3} = d^2_{\breve{a}_4} = d^2_{\breve{a}_5}$, we obtain

$$\mathbf{F}_{\text{snr}} = \sqrt{E_s}\begin{pmatrix}\cos\theta_1 & \sin\theta_1\cos\theta_2\, e^{i\varphi} & \sin\theta_1\sin\theta_2\, e^{i\varphi}\\ 0 & 0 & 0\\ 0 & 0 & 0\end{pmatrix} \tag{4.28}$$

where $\theta_1 = \operatorname{atan}\sqrt{(N^2+2N+2)(N^2+N\sqrt{3}+1)}$, $\theta_2 = \operatorname{atan}\frac{1}{N+1}$, and $\varphi = \operatorname{atan}\frac{1}{2N+\sqrt{3}}$.

The minimum Euclidean distance obtained by $\mathbf{F}_{\text{snr}}$ is defined by

$$d^2_{\mathbf{F}_{\text{snr}}} = \frac{4}{\beta_k}E_s\rho^2\frac{\cos^2\gamma_1}{1+(N^2+2N+2)(N^2+N\sqrt{3}+1)}\,. \tag{4.29}$$

It can be observed that this distance is different from zero when there is a large dispersion of the subchannel SNRs. Consequently, we can use two simple precoders $\mathbf{F}_{\text{rec}}$ and $\mathbf{F}_{\text{snr}}$ to optimize the minimum Euclidean distance for all rectangular QAM modulations.

4.3.2 Extension of 3-D max-$d_{\min}$ precoder for large MIMO systems

The authors in [59] presented an extension of max-$d_{\min}$ precoder for large MIMO systems, over which an even number of data-streams is transmitted. The main idea of this extension is to decompose the virtual channel matrix into (2×2) eigen-channel matrices and apply the 2-D max-$d_{\min}$ precoder for each pair of data-streams. We propose, herein, an extension for the odd number of data-streams ($b \geq 5$) by decomposing the virtual channel into (2×2) and (3×3) eigen-channel matrices. On each subsystem $\#i$, an optimal 2-D or 3-D max-$d_{\min}$ precoder $\tilde{\mathbf{F}}_{d_i}$ is applied. The power is, then, allocated to each subsystem under the power constraint

$$\sum_{i=1}^{n_b} \Upsilon_i^2 = E_s. \tag{4.30}$$

where n_b represents the number of virtual subsystems.

Let us define δ_i as the minimum distance provided by $\tilde{\mathbf{F}}_{d_i}$, i.e. $\delta_i = d_{\min}(\tilde{\mathbf{F}}_{d_i})$ with $\|\tilde{\mathbf{F}}_{d_i}\|_F^2 = 1$. The optimized solution for power allocation consists in equalizing the minimum distance, i.e. $d_{\min} = \Upsilon_i\delta_i$ for all subsystem $\#i$. The power allocation is then defined by

$$\Upsilon_i^2 = E_s\left(\delta_i^2 \sum_{j=1}^{n_b} \frac{1}{\delta_j^2}\right)^{-1} \quad \text{for } \forall i = 1,..,n_b \tag{4.31}$$

The minimum distance depends on the inverse of the minimum squared distance of each subsystem and defined by

$$d_{\min}^2 = \Upsilon_i^2\delta_i^2 = E_s\left(\sum_{j=1}^{n_b} \frac{1}{\delta_j^2}\right)^{-1} \tag{4.32}$$

Our objective becomes to find the combination of the subchannel SNRs to maximize the global minimum distance in (4.32). The optimization for $b \geq 5$ is rather complex, because it depends on the channel characteristics and the modulation used at the transmitter. One should note that when the virtual subchannels are small dispersive (more antennas are used for example), the minimum distance provided by 2-D max-$d_{\min}$ precoder is higher than that by 3-D max-$d_{\min}$. Therefore, we present herein a sub-optimal solution for an odd number of data-streams, in which a 3-D max-$d_{\min}$ subsystem is having priority. This solution is split into four steps

1. Obtain the virtual diagonal matrix $\mathbf{H_v}$ by using a virtual transformation.

2. Associate the $2b+1$ singular values by the following combination $(\rho_1, \rho_{b+1}, \rho_{2b+1})$, (ρ_2, ρ_{2b}), (ρ_3, ρ_{2b-1}), $\cdots$, (ρ_b, ρ_{b+2}) to obtain a 3-D virtual subsystem and $(b-1)$ 2-D virtual subsystems.

3. Apply the optimal 3-D max-$d_{\min}$ and 2-D max-$d_{\min}$ precoder on each subsystem under a unity power-constraint.

4. Allocate the power to each subsystem $\#i$ by computing the coefficient Υ_i such that

$$\Upsilon_i^2 = E_s \left(\delta_i^2 \sum_{j=1}^{b} \frac{1}{\delta_j^2} \right)^{-1} \qquad \forall i = 1..b$$

It is observed that, at the receiver side, b ML detectors are considered to optimize the minimum distances for $(b-1)$ pairs of datastreams and a group of three datastreams. Therefore, we need $(b-1)M^2 + M^3$ ML tests for a M-QAM rectangular modulation. The complexity of our proposed precoder is, then, given by $(M+b-1)M^2$. In comparison with diagonal precoders, where the complexity of this quantizer is $(2b+1)M$, the complexity of our proposed precoder is higher, but its performance is significantly improved.

4.3.3 BER performance for large MIMO systems

A numerical survey with 60000 uncorrelated Rayleigh fading channels using QPSK and 16-QAM modulations, confirms the BER enhancement of the sub-optimal solution for large MIMO systems. For MIMO(5,5) system using QPSK, more than 65% of optimal combinations corresponds to our solution. In the case of MIMO(6,5) with 16-QAM modulation, this proportion is even higher with about 78% of optimal combinations. The BER performance of the proposed precoder in comparison with those of another combination and diagonal precoders is shown in Fig. 4.17. It is clear that our new precoder obtains a significant improvement in terms of BER compared to other precoders.

4.4 Conclusion

We presented, in this chapter, a general parameterized form of the linear precoder that maximizes the minimum Euclidean distance between two received symbols. According to

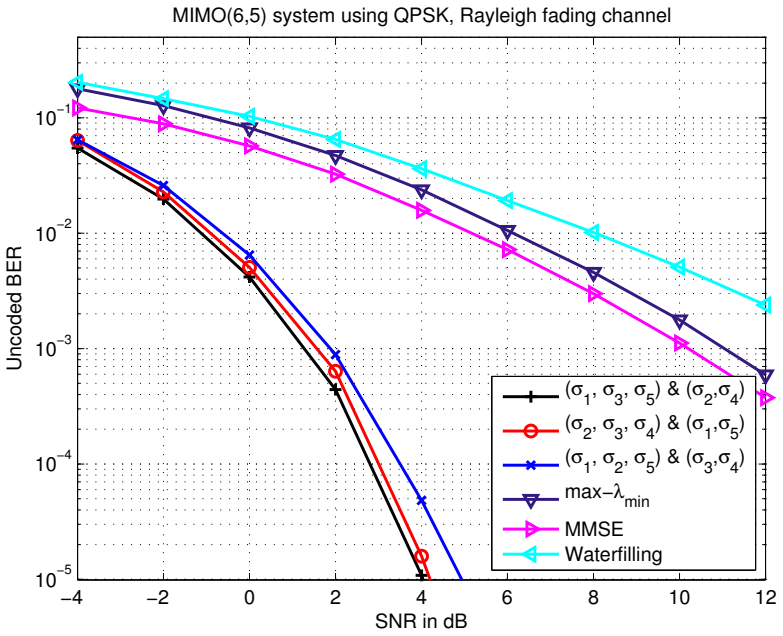

FIGURE 4.17: Comparison of precoders in terms of BER for MIMO(5,5) system.

this form, the optimal solution of the three-dimensional max-$d_{\min}$ criterion is proposed for all rectangular QAM modulations. The 3-D max-$d_{\min}$ precoder shows a significant improvement in BER performance compared to other precoding strategies such as beamforming, water-filling and minimizing the mean square error. The BER improvement of the proposed precoder depends on the channel characteristics. When the virtual subchannels are small dispersive (more antennas are used, for example), the improvement is more significant.

By using the new precoder, a suboptimal solution for large MIMO systems, which transmit not only an even but also an odd number of data-streams, is proposed. It can be demonstrated that, for a given number of data-streams, this extension exhibits a higher diversity order compared to diagonal solutions. Furthermore, the robustness of our proposed precoder is also confirmed when an imperfect CSI estimation is considered at the transmitter.

Appendices of chapter 4

A Proof of Proposition 4.1

The SNR-like matrix of the precoder $\mathbf{F}_d$ can be simplified as

$$SNR(\mathbf{F}_d) = \mathbf{H}_v\mathbf{F}_d\mathbf{F}_d^*\mathbf{H}_v = \mathbf{H}_v\mathbf{A}\boldsymbol{\Sigma}(\mathbf{B}^*\mathbf{B})\boldsymbol{\Sigma}^*\mathbf{A}^*\mathbf{H}_v = \mathbf{H}_v\mathbf{A}\boldsymbol{\Sigma}\boldsymbol{\Sigma}^*\mathbf{A}^*\mathbf{H}_v.$$

It is obvious that the unitary matrix $\mathbf{B}$ has no effect on the eigenvalue of $SNR(\mathbf{F}_d)$. In other words, the singular values of the global channel $\mathbf{H}_v\mathbf{F}_d$ are not dependent on matrix $\mathbf{B}$. Let us denote the singular values (SVs) of $\mathbf{H}_v\mathbf{A}\boldsymbol{\Sigma}$ as λ_k. One should note that the SVs are real, positive and sorted in decreasing order. Therefore, our objective is to find the matrix $\mathbf{A}$ that maximizes the singular value λ_3. The unitary matrix $\mathbf{A}$ has the general form like (4.13) and can be defined by

$$\mathbf{A} = \mathbf{A}_1\mathbf{A}_\alpha\mathbf{A}_2 \tag{4.33}$$

with $\mathbf{A}_1 = \begin{pmatrix} e^{i\eta_1} & 0 & 0 \\ 0 & e^{i\eta_2} & 0 \\ 0 & 0 & e^{i\eta_3} \end{pmatrix}$, $\mathbf{A}_2 = \begin{pmatrix} 1 & 0 & 0 \\ 0 & e^{i\kappa_2} & 0 \\ 0 & 0 & e^{i\kappa_3} \end{pmatrix}$

and $\mathbf{A}_\alpha = \begin{pmatrix} c_1 & s_1c_2 & s_1s_2 \\ s_1c_3 & -c_1c_2c_3 - e^{i\kappa_1}s_2s_3 & -c_1s_2c_3 + e^{i\kappa_1}c_2s_3 \\ s_1s_3 & -c_1c_2s_3 + e^{i\kappa_1}s_2c_3 & -c_1s_2s_3 - e^{i\kappa_1}c_2c_3 \end{pmatrix}$

where $c_i = \cos\alpha_i$ and $s_i = \sin\alpha_i$ for $i = 1..3$ with $0 \le \alpha_i \le \pi/2$ and $0 \le \eta_i, \kappa_i \le 2\pi$.

One should be reminded that the sum of the SVs square does not depend on $\mathbf{A}_1$ and $\mathbf{A}_2$. Indeed, we can write[1]:

$$\lambda_1^2 + \lambda_2^2 + \lambda_3^2 = \|\mathbf{H}_v\mathbf{A}_1\mathbf{A}_\alpha\mathbf{A}_2\mathbf{\Sigma}\|_\mathbf{F}^2 = \|\mathbf{A}_1\mathbf{H}_v\mathbf{A}_\alpha\mathbf{\Sigma}\mathbf{A}_2\|_\mathbf{F}^2 = \|\mathbf{H}_v\mathbf{A}_\alpha\mathbf{\Sigma}\|_\mathbf{F}^2. \tag{4.34}$$

Let us denote T as the sum of the SVs square. By substituting the angles ψ_i, θ_i, and φ_i into $\mathbf{H}_v$, $\mathbf{A}_\alpha$ and $\mathbf{\Sigma}$, we obtain:

$$\begin{aligned} T = {} & \sigma_1 c_1^2 \cos^2\psi_1 + \sigma_1 s_1^2 \sin^2\psi_1 . M \\ & + \sigma_2 s_1^2 c_3^2 \cos^2\psi_1 + \sigma_2 c_1^2 c_3^2 \sin^2\psi_1 . M + \sigma_2 s_3^2 \sin^2\psi_1 . N \\ & + \sigma_3 s_1^2 s_3^2 \cos^2\psi_1 + \sigma_3 c_1^2 s_3^2 \sin^2\psi_1 . M + \sigma_3 c_3^2 \sin^2\psi_1 . N \\ & + \frac{\sigma_2 - \sigma_3}{2} \cos\kappa_1 . c_1 \sin^2\psi_1 . \sin(2\alpha_2) . \sin(2\alpha_3) . \cos(2\psi_2) \end{aligned} \tag{4.35}$$

For every λ_1 and λ_2, the maximum value of λ_3 is obtained if the sum of SVs square is maximum. We first demonstrate that the maximum value of T is found when $c_1 = 1$. Indeed, we can rewrite the sum of SVs square as

$$\begin{aligned} T = {} & (\sigma_2 s_3^2 + \sigma_3 c_3^2)\sin^2\psi_1 N + c_1^2(\sigma_1 - \sigma_2 c_3^2 - \sigma_3 s_3^2)(\cos^2\psi_1 - M\sin^2\psi_1) \\ & + \frac{\sigma_2 - \sigma_3}{2} \cos\kappa_1 \, c_1 \sin^2\psi_1 \, \sin(2\alpha_2) \, \sin(2\alpha_3) \, \cos(2\psi_2). \end{aligned}$$

One should be noted that

$$\begin{cases} \cos^2\psi_1 \geq \sin^2\psi_1 . \cos^2\psi_2 = \sin^2\psi_1 . \cos^2\psi_2 . (c_2^2 + s_2^2) \\ \qquad\qquad \geq \sin^2\psi_1 . (\cos^2\psi_2 . c_2^2 + \sin^2\psi_2 . s_2^2) = \sin^2\psi_1 . M \\ \sigma_1 \geq \sigma_2 = \sigma_2(c_3^2 + s_3^2) \geq \sigma_2 . c_3^2 + \sigma_3 . s_3^2 \\ \sin(2\alpha_2), \sin(2\alpha_3), \cos(2\psi_2) \geq 0 \end{cases}$$

Therefore, the upper bound of T can be defined by

$$\begin{aligned} T \leq {} & (\sigma_2 s_3^2 + \sigma_3 c_3^2)\sin^2\psi_1 \, N + (\sigma_1 - \sigma_2 \, c_3^2 - \sigma_3 \, s_3^2)(\cos^2\psi_1 - M \, \sin^2\psi_1) \\ & + \frac{\sigma_2 - \sigma_3}{2} \sin^2\psi_1 \, \sin(2\alpha_2) \, \sin(2\alpha_3) \, \cos(2\psi_2). \end{aligned}$$

[1]The squared Frobenius norm of a matrix $\mathbf{M}$ is given by $\|\mathbf{M}\|_\mathbf{F}^2 = \text{trace}(\mathbf{M}\mathbf{M}^*)$.

The equality sign happens if and only if $\cos\kappa_1 = 1$ and c_1=1. By replacing $\cos\kappa_1$ and c_1 into (4.35), we can rewrite the expression of T as

$$\begin{aligned} T_{\max} &= \sigma_1 \cos^2\psi_1 + \frac{\sigma_2-\sigma_3}{2}\sin^2\psi_1.\sin(2\alpha_3).P \\ &\quad + \sigma_2 c_3^2 \sin^2\psi_1.M + \sigma_2 s_3^2 \sin^2\psi_1.N \\ &\quad + \sigma_3 s_3^2 \sin^2\psi_1.M + \sigma_3 c_3^2 \sin^2\psi_1.N \\ &= \sigma_1 \cos^2\psi_1 + \frac{M+N}{2}(\sigma_2+\sigma_3).\sin^2\psi_1 \\ &\quad + \frac{\sigma_2-\sigma_3}{2}\sin^2\psi_1\left[(M-N)\cos(2\alpha_3) + P\sin(2\alpha_3)\right] \end{aligned}$$

with $P = \sin(2\alpha_2)\cos(2\psi_2)$. We should note that $M - N = \cos(2\alpha_2)\cos(2\psi_2)$ and $M + N = 1$. Hence, the sum of the SVs square can be rewritten as

$$T_{\max} = \sigma_1 \cos^2\psi_1 + \frac{\sigma_2+\sigma_3}{2}\sin^2\psi_1 + \frac{\sigma_2-\sigma_3}{2}\sin^2\psi_1\cos(2\psi_2)\cos(2\alpha_2-2\alpha_3)$$

it is obvious that the maximum value of T is obtained if $\cos(2\alpha_2 - 2\alpha_3) = 1$ or $\alpha_2 = \alpha_3$. By substituting values of α_i and κ_1 into (4.33), we get $\mathbf{A}_\alpha = \mathrm{diag}(1,-1,-1)$.

Finally, if we choose $\mathbf{A}_1 = \mathbf{I}_3$ and $\mathbf{A}_2 = \mathrm{diag}(1,-1,-1)$, we can conclude that the highest singular values of $\mathbf{H}_v\mathbf{F}_d$ are obtained when $\mathbf{A}$ is an identity matrix.

B Proof of Proposition 4.2

Let us define a difference vector as $\breve{\mathbf{x}} = \mathbf{x}_k - \mathbf{x}_l$ with $\mathbf{x}_k \neq \mathbf{x}_l$. In this Appendix, we first demonstrate that the matrix $\mathbf{B}_\beta$ has no influence on the the minimum Euclidean distance, after that we reduce the range of the angles θ_i and φ_i. Indeed, the the Euclidean distance provided by a difference vector $\breve{\mathbf{x}}$ is given by

$$d_{\breve{\mathbf{x}}} = \|\mathbf{H}_v\mathbf{\Sigma}\mathbf{B}^*\breve{\mathbf{x}}\| = \|\mathbf{H}_v\mathbf{\Sigma}\mathbf{B}_\beta\mathbf{B}_\theta\mathbf{B}_\varphi\breve{\mathbf{x}}\| = \|\mathbf{B}_\beta\mathbf{H}_v\mathbf{\Sigma}\mathbf{B}_\theta\mathbf{B}_\varphi\breve{\mathbf{x}}\| = \|\mathbf{H}_v\mathbf{\Sigma}\mathbf{B}_\theta\mathbf{B}_\varphi\breve{\mathbf{x}}\|.$$

the equality is verified thanks to the diagonality and the unitarity of the matrix $\mathbf{B}_\beta$. Therefore, it can be concluded that $\mathbf{B}_\beta$ has no influence on the minimum Euclidean distance.

For symmetric constellations (e.g., centered square constellations), if $\breve{\mathbf{x}} = [x_1, x_2, x_3]^T$ is a difference vector, we have the following properties:

$$\begin{aligned} &i)\ \breve{\mathbf{x}}^c = [x_1^*, x_2^*, x_3^*]^T \text{is a difference vector} \\ &ii)\ \breve{\mathbf{x}}^{d_2} = [x_1, x_2, -x_3]^T \text{is a difference vector} \\ &iii)\ \breve{\mathbf{x}}^{d_3} = [x_1, -x_2, x_3]^T \text{is a difference vector} \\ &iv)\ \breve{\mathbf{x}}^e = [x_1, x_3, x_2]^T \text{is a difference vector} \end{aligned} \tag{4.36}$$

Basing on the property i), we can reduce the search range by $0 \leq \varphi_1 \leq \pi$. Indeed, if we replace φ_1 with $-\varphi_1$, the difference vector distance becomes[2]

$$\begin{aligned} d_{\breve{\mathbf{x}}} &= \|\mathbf{H}_v \boldsymbol{\Sigma} \mathbf{B}_\theta(\theta_i, -\varphi_1)\, \mathbf{B}_\varphi(\varphi_2, \varphi_3)\, \breve{\mathbf{x}}\| = \|(\mathbf{H}_v \boldsymbol{\Sigma} \mathbf{B}_\theta(\theta_i, -\varphi_1)\, \mathbf{B}_\varphi(\varphi_2, \varphi_3)\, \breve{\mathbf{x}})^c\| \\ &= \|\mathbf{H}_v \boldsymbol{\Sigma} \mathbf{B}_\theta(\theta_i, \varphi_1)\, \mathbf{B}_\varphi(-\varphi_2, -\varphi_3)\, \breve{\mathbf{x}}^c\| \end{aligned}$$

it is obvious that it is useless to test $-\varphi_1$ if φ_1 was already tested.

For the angles φ_2 and φ_3, we can also limit the search to $0 \leq \varphi_2, \varphi_3 \leq \pi$ by applying the remark below

$$d_{\breve{\mathbf{x}}} = \|\mathbf{H}_v \boldsymbol{\Sigma} \mathbf{B}_\theta\, \mathbf{B}_\varphi(\varphi_2, \varphi_3)\, \breve{\mathbf{x}}\| = \|\mathbf{H}_v \boldsymbol{\Sigma} \mathbf{B}_\theta\, \mathbf{B}_\varphi(\varphi_2 + \pi, \varphi_3)\, \breve{\mathbf{x}}^{d_2}\| = \|\mathbf{H}_v \boldsymbol{\Sigma} \mathbf{B}_\theta\, \mathbf{B}_\varphi(\varphi_2, \varphi_3 + \pi)\, \breve{\mathbf{x}}^{d_3}\|.$$

From properties ii) and iii), it is clear that it is useless to test $\varphi_k + \pi$ when φ_k (with $k = 2, 3$) was already tested. Finally, the search domain of θ_2 can be limited to $0 \leq \theta_2 \leq \pi/4$. Indeed, if θ_2 is replaced with $\pi/2 - \theta_2$, we have

$$\|\mathbf{B}_\theta(\theta_1, \pi/2 - \theta_2, \theta_3, \varphi_1)\, \mathbf{B}_\varphi(\varphi_2, \varphi_3)\, \breve{\mathbf{x}}\| = \|\mathbf{B}_\theta(\theta_1, \theta_2, \theta_3, \varphi_1 + \pi)\, \mathbf{B}_\varphi(\varphi_3, \varphi_2)\, \breve{\mathbf{x}}^e\| \tag{4.37}$$

By replacing (4.37) into the difference vector distance in (4.36) and applying the property iv), we can conclude that the influence of the angles can be studied only $0 \leq \theta_2 \leq \pi/4$.

[2] The conjugate and non-transposed matrix of $\mathbf{M}$ is denoted by $(\mathbf{M})^c$

C Exact values of the $\mathbf{F}_{bc_2}$ angles

A numerical search which maximizes $d_{\min}$ for precoder $\mathbf{F}_{bc_2}$ shows that $\theta_2 = \pi/4$. By analyzing the local maximum of $d_{\min}$, we realize that the optimal solution is always obtained from the three difference vectors $\breve{\mathbf{a}}_1 = [0,0,2]^T$, $\breve{\mathbf{a}}_2 = [0,2,0]^T$ and $\breve{\mathbf{a}}_3 = [2,0,0]^T$. The angle φ_1 is therefore equal to $\pi/2$ to satisfy the condition $d^2_{\breve{a}_1} = d^2_{\breve{a}_2}$. Then, the normalized distances of the difference vectors $\breve{a}_1$, $\breve{a}_2$ and $\breve{a}_3$ are defined by

$$\begin{cases} d^2_{\breve{a}_3} = 2(\Psi_1 \cos^2\theta_1 + \Psi_2 \cos^2\theta_3 \sin^2\theta_1 + \Psi_3 \sin^2\theta_3 \sin^2\theta_1) \\ d^2_{\breve{a}_1} = d^2_{\breve{a}_2} = \Psi_1 \sin^2\theta_1 + \Psi_2(\sin^2\theta_3 + \cos^2\theta_3 \cos^2\theta_1) + \Psi_3(\cos^2\theta_3 + \sin^2\theta_3 \cos^2\theta_1) \end{cases}$$

where

$$\begin{cases} \Psi_1 = 2\cos^2\gamma_1 \cos^2\psi_1 \\ \Psi_2 = 2\sin^2\gamma_1 \cos^2\gamma_2 \sin^2\psi_1 \cos^2\psi_2 \\ \Psi_3 = 2\sin^2\gamma_1 \sin^2\gamma_2 \sin^2\psi_1 \sin^2\psi_2 \end{cases} \tag{4.38}$$

One should note that $d^2_{\breve{a}_1} + \frac{d^2_{\breve{a}_3}}{2} = \Psi_1 + \Psi_2 + \Psi_3$, so the normalized distance $d_{\min}$ can be expressed as a function of the channel angles, ψ_1 and ψ_2

$$d^2_{\min} = d^2_{\breve{a}_1} = d^2_{\breve{a}_3} = \frac{2}{3}(\Psi_1 + \Psi_2 + \Psi_3) \tag{4.39}$$

Beside the three difference vectors $\breve{\mathbf{a}}_1$ $\breve{\mathbf{a}}_2$ and $\breve{\mathbf{a}}_3$, the minimum distance $d_{\min}$ is optimized such that three more vectors below have the same distances: $\breve{\mathbf{a}}_4 = [2,2,0]^T$, $\breve{\mathbf{a}}_5 = [2,0,\text{-}2]^T$ and $\breve{\mathbf{a}}_6 = [2,2,\text{-}2]^T$. We remark that the degree of freedom is greater than the number of the equations (7 compared with 5). Furthermore, the channel angles in (4.38) are ruled by $\cos^2\gamma_1 \geq \sin^2\gamma_1 \cos^2\gamma_2 \geq \sin^2\gamma_1 \sin^2\gamma_2$, so the optimal $d_{\min}$ in (4.39) is obtained if $\psi_2 = 0$ and ψ_1 minimum such that the system of equations $d^2_{\breve{a}_1} = d^2_{\breve{a}_2} = d^2_{\breve{a}_3} = d^2_{\breve{a}_4} = d^2_{\breve{a}_5} = d^2_{\breve{a}_6}$ has a root.

The normalized distance $d_{\min}$ for the precoder $\mathbf{F}_{bc_2}$ can be now rewritten as

$$d^2_{\min} = \frac{2}{3}(\Psi_1 + \Psi_2) \tag{4.40}$$

where Ψ_1 and Ψ_2 are simplified as $\begin{cases} \Psi_1 = 2\cos^2\gamma_1 \cos^2\psi_1 \\ \Psi_2 = 2\sin^2\gamma_1 \cos^2\gamma_2 \sin^2\psi_1 \end{cases}$

By solving $d^2_{\breve{a}_4} = d^2_{\breve{a}_5}$ and comparing with the numerical search, we obtain $\varphi_2 = \pi - \varphi_3$. In order to simplify the optimization problem, we substitute φ_2 into the equation $d^2_{\breve{a}_3} = d^2_{\breve{a}_6}$ to get the expression of φ_3

$$\tan(2\varphi_3) = -\frac{R_{12} + 1 - 3\sin^2\theta_3}{3\cos\theta_1\cos\theta_3\sin\theta_3} \tag{4.41}$$

where $R_{12} = \Psi_1/\Psi_2 = \sigma_1^2/\sigma_2^2.\,\mathrm{cotan}^2\,\psi_1$.

A similar way is proposed for the equation $d^2_{\breve{a}_1} = d^2_{\breve{a}_3} = d^2_{\breve{a}_4}$ and we get

$$3R_{12}\cos^2\theta_1 + 3\sin^2\theta_1.\cos^2\theta_3 = R_{12} + 1 \tag{4.42}$$

$$\cos\varphi_3.\tan\theta_1 + \frac{1}{\cos\varphi_3.\tan(2\theta_1)} = \frac{R_{12}+1}{\sqrt{2}(2R_{12}-1)} \tag{4.43}$$

Therefore, the problem becomes finding the minimum value of ψ_1 such that there is existence of root for the system of nonlinear equations created by (4.41), (4.42) and (4.43). Please note that the smaller ψ_1, the bigger the value of R_{12}. Furthermore, a numerical experiment confirms that the maximum value of R_{12} is determined at

$$R_{max} = 9.2426 \tag{4.44}$$

By substituting (4.44) into the system of equations (4.41), (4.42) and (4.43), we obtain $\theta_1 \simeq 55.8380^o$, $\theta_3 \simeq 31.3064^o$ and $\varphi_3 \simeq 47.2667^o$.

D Proof of Proposition 4.3

Let us denote $\breve{\mathbf{a}}_1$, $\breve{\mathbf{a}}_2$, as two difference vectors which have the same Euclidean distances. The two corresponding Euclidean distances are defined by

$$\begin{cases} d^2_{\breve{\mathbf{a}}_1} = \cos^2\gamma_1\,\cos^2\psi_1\,f_1(\theta_i,\varphi_i) + \sin^2\gamma_1\,\cos^2\gamma_2\,\sin^2\psi_1\,\cos^2\psi_2\,g_1(\theta_i,\varphi_i) \\ \qquad + \sin^2\gamma_1\,\sin^2\gamma_2\,\sin^2\psi_1\,\sin^2\psi_2\,h_1(\theta_i,\varphi_i) \\ d^2_{\breve{\mathbf{a}}_2} = \cos^2\gamma_1\,\cos^2\psi_1\,f_2(\theta_i,\varphi_i) + \sin^2\gamma_1\,\cos^2\gamma_2\,\sin^2\psi_1\,\cos^2\psi_2\,g_2(\theta_i,\varphi_i) \\ \qquad + \sin^2\gamma_1\,\sin^2\gamma_2\,\sin^2\psi_1\,\sin^2\psi_2\,h_2(\theta_i,\varphi_i) \end{cases}$$

where $f(\theta_i, \varphi_i)$, $g(\theta_i, \varphi_i)$ and $h(\theta_i, \varphi_i)$ are functions of six variables, θ_i and φ_i. It is observed that $d^2_{\breve{\mathbf{a}}_1}$ and $d^2_{\breve{\mathbf{a}}_2}$ have the same factors of γ_i and ψ_i. For this reason, when channels angles vary from (γ_1,γ_2) to (γ'_1,γ'_2), we can keep two distances equal by changing only the angles ψ_1 and ψ_2. Indeed, we define ψ'_1 and ψ'_2 satisfying

$$\frac{\cos^2\gamma'_1\cos^2\psi'_1}{\cos^2\gamma_1\cos^2\psi_1} = \frac{\sin^2\gamma'_1\cos^2\gamma'_2\sin^2\psi'_1\cos^2\psi'_2}{\sin^2\gamma_1\cos^2\gamma_2\sin^2\psi_1\cos^2\psi_2} = \frac{\sin^2\gamma'_1\sin^2\gamma'_2\sin^2\psi'_1\sin^2\psi'_2}{\sin^2\gamma_1\sin^2\gamma_2\sin^2\psi_1\sin^2\psi_2} = k$$

where k is a constant. The Euclidean distances of the two vectors then become

$$\begin{cases} d^2_{\breve{\mathbf{a}}'_1} = k \times d^2_{\breve{\mathbf{a}}_1} \\ d^2_{\breve{\mathbf{a}}'_2} = k \times d^2_{\breve{\mathbf{a}}_2} \end{cases}$$

Because $d^2_{\breve{\mathbf{a}}_1} = d^2_{\breve{\mathbf{a}}_2}$, we can conclude that $d^2_{\breve{\mathbf{a}}'_1} = d^2_{\breve{\mathbf{a}}'_2}$ and the angles ψ'_1 and ψ'_2 can be rewritten as

$$\psi'_2 = \text{atan}\sqrt{\frac{\tan^2\gamma_2}{\tan^2\gamma'_2}\times\tan^2\psi_2}, \text{ and } \psi'_1 = \text{atan}\sqrt{\frac{\tan^2\gamma_1\cos^2\gamma_2}{\tan^2\gamma'_1\cos^2\gamma'_2}\times\frac{\cos^2\psi_2}{\cos^2\psi'_2}\times\tan^2\psi_1} \tag{4.45}$$

E Expressions of the precoder $\mathbf{F}_{qc_2}$ & $\mathbf{F}_{qc_3}$

In the case of QPSK modulation, it is observed that there are more than eleven difference vectors which reach the minimum Euclidean distance. One should note that the degrees of freedom for all expression do not exceed the number of equations created by the difference vectors. Consequently, it is possible to define the analytical values of all angles by solving the system of trigonometric equations.

When the eigen-channels are close ($\sigma_1 \simeq \sigma_2 \simeq \sigma_3$), for example, a numerical search shows that the optimized solution for the precoder is obtained with $\theta_2 = \pi/4$, $\theta_3 = \pi/2$, $\varphi_1 = 0$, $\varphi_2 = \pi/4$ and $\varphi_3 = 3\pi/4$. This is the third expression of $\mathbf{F}_{qc_3}$ which is illustrated in the table below. To define the analytical values of other angles, we consider the four difference vectors following $\breve{\mathbf{a}}_1 = [0, 0, \sqrt{2}]^T$, $\breve{\mathbf{a}}_2 = [\sqrt{2}, 0, 0]^T$, $\breve{\mathbf{a}}_3 = [0, \sqrt{2}, i\sqrt{2}]^T$ and $\breve{\mathbf{a}}_4 = [\sqrt{2}, 0, \sqrt{2} + i\sqrt{2}]^T$. Figure below plots the normalized Euclidean distance of the four difference vectors with respect to the angle θ_1 for a given channel (γ_1,γ_2)=(π/4,π/4). The values of other angles that maximize the minimum Euclidean distance such that

the four curves, respectively, converge at one point. By substituting the angles of the precoder into the expression of the precoding matrix $\mathbf{F}_d$, the normalized distances can be simplified as

$$\begin{cases} d^2_{\breve{\mathbf{a}}_1} = \Phi_1.\sin^2\theta_1 + \Phi_2 + \Phi_3.\cos^2\theta_1 \\ d^2_{\breve{\mathbf{a}}_2} = 2\Phi_1.\cos^2\theta_1 + 2\Phi_3.\sin^2\theta_1 \\ d^2_{\breve{\mathbf{a}}_3} = 4\Phi_2 \\ d^2_{\breve{\mathbf{a}}_4} = 2\left[\Phi_1(\cos\theta_1 - \sin\theta_1)^2 + \Phi_2 + \Phi_3(\sin\theta_1 - \cos\theta_1)^2\right] \\ \qquad = 2\left[d^2_{\breve{\mathbf{a}}_1} + d^2_{\breve{\mathbf{a}}_2}/2 - 2\sin\theta_1.\cos\theta_1(\Phi_1 - \Phi_3)\right] \end{cases}$$

where $\begin{cases} \Phi_1 = \cos^2\gamma_1.\cos^2\psi_1 \\ \Phi_2 = \sin^2\gamma_1.\cos^2\gamma_2.\sin^2\psi_1.\cos^2\psi_2 \\ \Phi_3 = \sin^2\gamma_1.\sin^2\gamma_2.\sin^2\psi_1.\sin^2\psi_2 \end{cases}$

By solving $d^2_{\breve{\mathbf{a}}_1} = d^2_{\breve{\mathbf{a}}_2} = d^2_{\breve{\mathbf{a}}_3} = d^2_{\breve{\mathbf{a}}_4}$, it is possible to obtain the angles

$$\begin{cases} \theta_1 = \frac{1}{2}\arctan(-4) \simeq 52.01812^o \\ \psi_2 = \arctan\frac{\sqrt{5-\sqrt{17}}}{\sqrt{2}\tan\gamma_2} \\ \psi_1 = \arctan\frac{\sqrt{2}}{\sqrt{5+\sqrt{17}}\tan\gamma_1\cos\gamma_2\cos\psi_2} \end{cases}$$

for $(\gamma_1, \gamma_2) = (\pi/4, \pi/4)$, the optimized angles $(\psi_1, \psi_2) \simeq (38.45504^o, 33.51067^o)$.

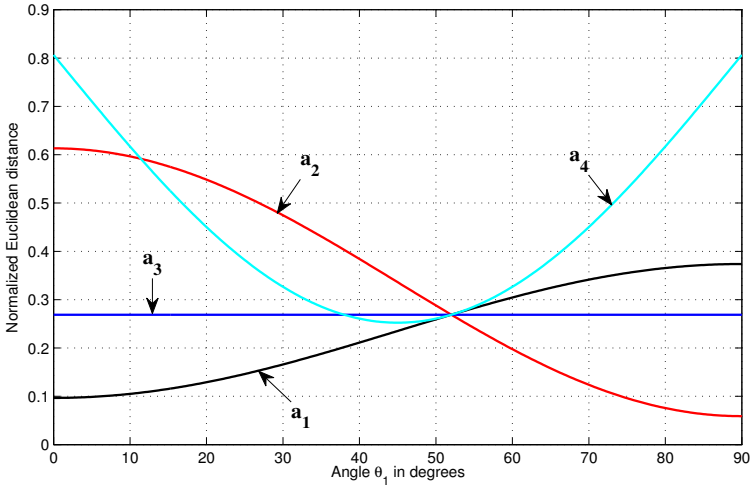

Figure: Euclidean distance with $\theta_2 = 45^o$, $\theta_3 = 90^o$, $\varphi_1 = 0^o$, $\varphi_2 = 45^o$ and $\varphi_3 = 135^o$ with respect to θ_1 at the channel angles $(\gamma_1, \gamma_2) = (45^o, 45^o)$.

The other expression can be determined by using a same process: solve the systems of trigonometric equations created by numbers of non-colinear difference vectors.

Expressions	No	Number of vectors
$\mathbf{F}_{qc_2}$	(a)	11
	(b)	11
	(c)	13
	(d)	13
$\mathbf{F}_{qc_3}$	(a)	15
	(b)	15
	(c)	15

Table: Number of non-colinear difference vectors used to solve the expressions of precoder max-$d_{\min}$.

F Proof of Proposition 4.4

When there is no dispersion of the subchannel SNRs, the minimum Euclidean distance obtained by $\mathbf{F}_{\text{rec}}$ equals $\frac{4}{9}E_s\rho^2/\beta_k$. We assume that there exists a precoder $\mathbf{F}_d$ such that the minimum Euclidean distance is larger than $d_{\min}$ obtained by $\mathbf{F}_{\text{rec}}$. Let us consider three difference vectors $\breve{x}_a = \frac{2}{\sqrt{\beta_k}}(1,0,0)^T$, $\breve{x}_b = \frac{2}{\sqrt{\beta_k}}(0,1,0)^T$, and $\breve{x}_c = \frac{2}{\sqrt{\beta_k}}(0,0,1)^T$. Then, the corresponding normalized distances have to satisfy the conditions below

$$\begin{cases} d^2_{\breve{\mathbf{x}}_a} = \frac{4}{3}(\sigma_1^2\mathfrak{b}_{11}^2 + \sigma_2^2\mathfrak{b}_{21}^2 + \sigma_3^2\mathfrak{b}_{31}^2) > \frac{4}{9} \\ d^2_{\breve{\mathbf{x}}_b} = \frac{4}{3}(\sigma_1^2\mathfrak{b}_{12}^2 + \sigma_2^2\mathfrak{b}_{22}^2 + \sigma_3^2\mathfrak{b}_{32}^2) > \frac{4}{9} \\ d^2_{\breve{\mathbf{x}}_c} = \frac{4}{3}(\sigma_1^2\mathfrak{b}_{13}^2 + \sigma_2^2\mathfrak{b}_{23}^2 + \sigma_3^2\mathfrak{b}_{33}^2) > \frac{4}{9} \end{cases} \tag{4.46}$$

where $\mathbf{\Sigma} = \text{diag}\{\sigma_1, \sigma_2, \sigma_3\}$, and $\mathbf{B}^* = (\mathfrak{b}_{ij})$. It is noted that $\mathbf{B}^*$ is a unitary matrix: $\mathbf{B}^*\mathbf{B} = \mathbf{I}_3$, or $\sum_{j=1}^3 \mathfrak{b}_{ij}^2 = 1$, for all $i = 1\cdots3$. Then, we have

$$d^2_{\breve{\mathbf{x}}_a} + d^2_{\breve{\mathbf{x}}_b} + d^2_{\breve{\mathbf{x}}_c} = \frac{4}{3}(\sigma_1^2 + \sigma_2^2 + \sigma_3^2) = \frac{4}{3} \tag{4.47}$$

From (4.46) and (4.47), it can be concluded that three normalized distances can not be all greater than 4/9. In other words, the distance $d_{\min}$ provided by $\mathbf{F}_{\text{rec}}$ is optimized.

Chapter 5

Reducing the number of neighbors for max-$d_{\min}$ precoder

As presented in the previous chapters, a non-diagonal precoder, which is based on the maximization of the minimum Euclidean distance between two received symbols, achieves a significant bit-error-rate (BER) improvement in comparison with diagonal precoders, especially when an ML detection is considered at the receiver. In the chapter, we propose a new version of maximum $d_{\min}$ based precoder. This precoding strategy considers not only the minimum Euclidean distance but also the number of neighbors providing it. The number of neighbors is statistically more important due to the maximization of the minimum distance. Aiming at reducing this number of neighbors, the rotation parameters of the new precoder are assumed to be zero. The expression of this precoding strategy is then less complex and the space of solution is smaller.

This chapter is organized as follows. Section 5.1 introduces the impact of the minimum Euclidean distance on the BER performance, and the principle of the new precoding strategy. The parameterization of the Neighbor-$d_{\min}$ precoder is described in Section 5.2. In Section 5.3, the optimization of the $d_{\min}$ criterion which reduces the number of neighbors for two datastreams is detailed. We propose, in Section 5.4, the Neighbor-$d_{\min}$ precoding matrices for three-dimensional virtual systems using rectangular QAM-modulations. Finally, the conclusions are given in Section 5.6.

5.1 Error probability of the linear precoding strategy

Let us define a vector $\mathbf{x} = \mathbf{H}_v\mathbf{F}_d\mathbf{s}$, and denote by A_{ij} the event that $\|\mathbf{y} - \mathbf{x}_j\| < \|\mathbf{y} - \mathbf{x}_i\|$ when the symbol $\mathbf{s}_i$ was sent at the transmitter. If the event A_{ij} happens, there will be error detections. The received constellation is decoded correctly if $\|\mathbf{y} - \mathbf{x}_i\| < \|\mathbf{y} - \mathbf{x}_j\|$ with $\forall j \neq i$ when $\mathbf{s}_i$ was sent. Then the average error probability can be defined by

$$P_e = \frac{1}{M_s}\sum_{i=1}^{M_s} P_{e_i}\{\mathbf{s}_i \text{ sent}\} = \frac{1}{M_s}\sum_{i=1}^{M_s} \text{Prob}\{\bigcup_{\substack{j=1 \\ j\neq i}}^{M_s} A_{ij}\} \tag{5.1}$$

where M_s is the number of all possible transmitted vectors $\mathbf{s}$. The average error probability can be approximated by

$$P_e \simeq \frac{1}{M_s}\sum_{i=1}^{M_s}\sum_{\substack{j=1 \\ j\neq i}}^{M_s} \text{Prob}\{A_{ij}\} \tag{5.2}$$

where

$$\begin{aligned}\text{Prob}\{A_{ij}\} &= \text{Prob}\{\|\mathbf{y} - \mathbf{x}_j\| < \|\mathbf{y} - \mathbf{x}_i\| \mid \mathbf{s}_i \text{ sent}\} \\ &= \text{Prob}\{\|\mathbf{x}_i + \nu_v - \mathbf{x}_j\| < \|\mathbf{x}_i + \nu_v - \mathbf{x}_i\|\} \\ &= \text{Prob}\{\|\nu_v - (\mathbf{x}_j - \mathbf{x}_i)\| < \|\nu_v\|\}\end{aligned}$$

Let us define $d_{ij} = \|\mathbf{x}_j - \mathbf{x}_i\|$ and n_v the projection of vector ν_v onto the vector $(\mathbf{x}_j - \mathbf{x}_i)$, we have

$$\begin{aligned}&\text{Prob}\{\|\nu_v - (\mathbf{x}_j - \mathbf{x}_i)\| < \|\nu_v\|\} = \text{Prob}\{n_v > \frac{d_{ij}}{2}\} \\ &= Q\left(\frac{d_{ij}}{2\sqrt{N_0}}\right) = Q\left(\frac{\bar{d}_{ij}}{2\sqrt{N_0}} \times \sqrt{E_s}\right)\end{aligned}$$

where N_0 is the variance of the white Gaussian noise ν_v, and $\bar{d}_{ij}$ is the normalized distance of vector $(\mathbf{x}_j - \mathbf{x}_i)$.

Therefore, the error probability can be simplified as

$$P_e \simeq \frac{1}{M_s}\sum_{i=1}^{M_s}\sum_{\substack{j=1 \\ j\neq i}}^{M_s} Q\left(\frac{\bar{d}_{ij}}{2\sqrt{N_0}} \times \sqrt{E_s}\right) \tag{5.3}$$

According to (5.3), we can appreciate the impact of the Euclidean distances on the BER performance of a MIMO system. Let us first consider the simplest case: there are only two Euclidean distances.

Lemma 5.1. *For every $d_\alpha < d_\beta < d_\chi < d_\delta$, we can find the value of R high enough satisfying the condition*

$$Q(d_\alpha.R) + Q(d_\delta.R) > Q(d_\beta.R) + Q(d_\chi.R) \tag{5.4}$$

Proof: see Appendix A.

It is obvious that we can improve the BER performance by increasing the minimum Euclidean distance of the received constellation. One should note that $Q(d_\beta.R) > Q(d_\chi.R)$, so $\forall d_\chi$ such that $d_\alpha < d_\chi < d_\delta$, we can obtain

$$Q(d_\alpha.R) + Q(d_\delta.R) > 2.Q(d_\chi.R) \tag{5.5}$$

This is an actual evidence that the optimized detection, in reality, is obtained when the minimum distance is reached by many Euclidean distances.

Lemma 5.2. *With two arrays d_{α_i} and d_{β_i} which are sorted by increasing order, if $d_{\alpha_1} < d_{\beta_1}$ and $k \geq 2$, we can find the value of R high enough such that*

$$\sum_{i=1}^{k} Q(d_{\alpha_i}.R) > \sum_{i=1}^{k} Q(d_{\beta_i}.R) \tag{5.6}$$

Proof: see Appendix B.

From the form of error probability in (5.3) and the remark in the *Lemma 5.2*, it can be concluded that the minimum Euclidean distance has a very important role in the BER improvement of the precoding strategies system. We can predict that the optimized precoder can be obtained when the minimum Euclidean distance on the received constellation is provided by many difference vectors.

Let us note N_i is the number of distances $\bar{d}_{ij}$ such that $\bar{d}_{ij} = d_{\min}$ where the minimum Euclidean distance $d_{\min}$ is defined by

$$d^2_{\min} = \min_{s_k, s_l \in S, s_k \neq s_l} \|\mathbf{H}_v \mathbf{F}_d (\mathbf{s}_k - \mathbf{s}_l)\|^2 \tag{5.7}$$

A numerical search over $\mathbf{F}_d$, which maximizes the minimum Euclidean distance obtained by many difference vectors, shows that the values of other Euclidean distances are much higher than the minimum distance when $d_{\min}$ is optimized. In that case, the other distances have no much impact on the bit-error-rate performance. The error probability in (5.3) can be then simplified as

$$\begin{aligned} P_e &\approx \frac{1}{M_s}\sum_{i=1}^{M_s} \mathrm{N}_i.Q\left(\frac{\bar{d}_{\min}}{2\sqrt{N_0}} \times \sqrt{E_s}\right) \\ &\approx \mathrm{N}_{d_{\min}}.Q\left(\frac{\bar{d}_{\min}}{2\sqrt{N_0}} \times \sqrt{E_s}\right) \end{aligned} \tag{5.8}$$

where $\mathrm{N}_{d_{\min}} = \frac{1}{M_s}\sum_{i=1}^{M_s} \mathrm{N}_i$. It is observed that to improve the BER performance of the precoding strategies system, we have to not only maximize the minimum Euclidean distance but also minimize the number of neighbors providing it. The new precoding strategy is, therefore, called as Neighbor-$d_{\min}$ precoder.

5.2 Parameterization of the Neighbor-$d_{\min}$ precoding matrix

Our objective is to parameterize the precoding matrix $\mathbf{F}_d$ which satisfies the power constraint. By using a singular value decomposition (SVD), the matrix $\mathbf{F}_d$ can be factorized as

$$\mathbf{F}_d = \mathbf{A}\mathbf{\Sigma}\mathbf{B}^*, \tag{5.9}$$

where $\mathbf{A}$ and $\mathbf{B}^*$ are $b \times b$ unitary matrices, and $\mathbf{\Sigma}$ is a $b \times b$ diagonal matrix with nonnegative real numbers on the diagonal. $\mathbf{\Sigma}$ can be regarded as a scaling matrix, whereas $\mathbf{A}$ and $\mathbf{B}^*$ can be viewed as rotation matrices.

It is noted that the form of the precoding matrix $\mathbf{F}_d$ depends on the channel characteristics. The authors in [67] showed that we can find a precoder $\mathbf{F}_d$ which do not contain the rotation matrix $\mathbf{A}$ such that performance function is not changed.

Proposition 5.3. *If* $\mathbf{A}$ *is assumed to be an identity matrix, the Euclidean distances provided by two any difference vectors are kept equal by changing only the scaling matrix* $\mathbf{\Sigma}$ *and retaining the rotation matrix* $\mathbf{B}^*$.

Proof: see Appendix C.

The numerical approach shows that the optimized constellation at the receiver is always obtained when some difference vectors provide the minimum Euclidean distances. According to the proposition above, we can conclude that not only the complexity of the optimization but also the number of precoding expressions is reduced if the matrix $\mathbf{A}$ has no influence on the precoding matrix. The parameterized form of the Neighbor-$d_{\min}$ precoder is then

$$\mathbf{F}_d = \mathbf{\Sigma}\mathbf{B}^*. \tag{5.10}$$

The power constraint can be rewritten as

$$\text{trace}\{\mathbf{F}_d\mathbf{F}_d^*\} = \text{trace}\{\mathbf{\Sigma}\mathbf{\Sigma}^*\} = E_s. \tag{5.11}$$

This power constraint is then replaced by the following decomposition

$$\mathbf{\Sigma} = \sqrt{E_s}\,\text{diag}\{\cos\psi_1, \sin\psi_1\cos\psi_2, .., \sin\psi_1\sin\psi_2\sin\psi_{b-1}\}. \tag{5.12}$$

Theorem: Any matrix $\mathbf{B}^*$, which belongs to the b-dimensional unitary matrix group $U(b)$, can be factorized into an ordered product of $2b-1$ matrices of the following form [68]

$$\mathbf{B}^* = \mathcal{D}_1^{b-1}\,\mathcal{O}_2^{b-2}\,\mathcal{D}_2^{b-2}\ldots\mathcal{O}_{b-1}^1\mathcal{D}_{b-1}^1\,\mathcal{O}_b\mathcal{D}_b, \tag{5.13}$$

where $\mathcal{D}_b$ is a diagonal matrix of the form $\mathcal{D}_b = \text{diag}\{e^{i\varphi_1},\ldots,e^{i\varphi_b}\}$ with $\varphi_i \in [0, 2\pi], i = 1,\ldots,b$ arbitrary phases, $\mathcal{D}_{b-k}^k$ is the same diagonal matrix with first $b-k$ entries equal to unity, i.e. $\mathcal{D}_{b-k}^k = \text{diag}\{1_{b-k}, e^{i\varphi_1'},\ldots,e^{i\varphi_k'}\}$.

The orthogonal matrices $\mathcal{O}_b$ ($\mathcal{O}_{b-k}^k$) is a product of $b-1$ ($b-k-1$) matrices of the form

$$\mathcal{O}_b = J_{1,2}\,J_{2,3}\ldots J_{b-2,b-1}\,J_{b-1,b} \tag{5.14}$$

where $J_{i,i+1}$ are $b\times b$ rotation matrices given by

$$J_{i,i+1} = \begin{pmatrix} \mathbf{I}_{i-1} & 0 & 0 & 0 \\ 0 & \cos\theta_i & \sin\theta_i & 0 \\ 0 & -\sin\theta_i & \cos\theta_i & 0 \\ 0 & 0 & 0 & \mathbf{I}_{b-i-1} \end{pmatrix}, \tag{5.15}$$

where I_i is an identity matrix of size i.

Remark 5.4. The angles that parameterize $\mathcal{O}_b$ are denoted as $\theta_1, \ldots, \theta_{b-1}$, then the angles of $\mathcal{O}_{b-1}^1$ are $\theta_b, \ldots, \theta_{2b-3}$, etc. and the last angle entering $\mathcal{O}_2^{b-1}$ will be $\theta_{b(b-1)/2}$. The matrix $\mathcal{O}_{b-k}^k$ has the same structure as $\mathcal{O}_b$

$$\mathcal{O}_{b-k}^k = \begin{pmatrix} \mathbf{I}_k & 0 \\ 0 & \mathcal{O}_{b-k} \end{pmatrix}. \tag{5.16}$$

It is realized that if all the phases entering $\mathbf{B}^*$ are zero, i.e. $\varphi_i = 0$, $i = 1, \ldots, b(b+1)/2$, the received constellation will have less distances providing the minimum distance. The property is explained by the non-rotated received constellation when a rectangular Quadrature Amplitude Modulation is used at the transmitter. Therefore, the unitary matrix $\mathbf{B}^*$ can be parameterized as

$$\mathbf{B}^* = \mathcal{O}_2^{b-2}\, \mathcal{O}_3^{b-3} \ldots \mathcal{O}_{b-1}^1\, \mathcal{O}_b. \tag{5.17}$$

Thanks to this representation, we are now able to find $(b-1)$ angles ψ_i and $b(b-1)/2$ angles θ_i which give the optimal precoder according to the minimum distance criterion.

5.3 Expression of Neighbor-$d_{\min}$ precoder for 2 sub-streams

To illustrate the method of optimization, let us consider a simple case: $b = 2$. By using a singular value decomposition, the authors in [37] and [69] simplified the virtual channel and precoding matrices as

$$\mathbf{H}_v = \begin{pmatrix} \sigma_1 & 0 \\ 0 & \sigma_2 \end{pmatrix} = \rho \begin{pmatrix} \cos\gamma & 0 \\ 0 & \sin\gamma \end{pmatrix} \tag{5.18}$$

where $\rho = \sqrt{\sigma_1^2 + \sigma_2^2}$ and $\gamma = \arctan \frac{\sigma_2}{\sigma_1}$ are the channel gain and channel angle, respectively.

$$\mathbf{F}_d = \sqrt{E_s} \begin{pmatrix} \cos\psi & 0 \\ 0 & \sin\psi \end{pmatrix} \begin{pmatrix} \cos\theta & \sin\theta \\ -\sin\theta & \cos\theta \end{pmatrix} \begin{pmatrix} 1 & 0 \\ 0 & e^{i\varphi} \end{pmatrix} \tag{5.19}$$

with $0 \le \theta \le \pi/4$ and $0 \le \psi, \varphi \le \pi/2$. The parameter ψ controls the power allocation on the virtual subchannels, θ and φ correspond to scaling and rotation of the received

constellation, respectively. When θ and φ are equal to 0, the precoding matrix is diagonal and equivalent to the power allocation strategies.

We present, herein, an original idea not only considering $d_{\min}$ and $\mathrm{N}_{d_{\min}}$, simultaneously, but also reducing the complexity of the solution. It is realized that if the coefficients of the precoding matrix $\mathbf{F}_D$ do not depend on the rotation parameter ($\varphi = 0$ or $\varphi = \pi/2$), the received constellation will have less distances which can reach the minimum Euclidean distance. The property could be explained by the non-rotated received constellation (or perpendicular rotated constellation) when a Quadrature Amplitude Modulation (QAM) is used at the transmitter.

For this reason, we propose a new precoding strategy in which we assume that the rotation parameter has no employ ($\varphi = 0$ or $\varphi = \pi/2$). By using the parameterized form of the precoder in (5.19), we are now looking for the angles ψ and θ which optimize the $d_{\min}$ criterion for each channel angle γ. A numerical approach for MIMO system using BPSK and QPSK modulation, which is considered in the following of this section, confirms a bit-error-rate improvement of our new precoder.

5.3.1 For BPSK modulation

It is observed that the difference vector as given by the difference between the two transmitted vectors ($\breve{\mathbf{s}} = \mathbf{s}_k - \mathbf{s}_l$ with $\mathbf{s}_k \neq \mathbf{s}_l$) is a vector created by the elements of the set $\{0, 2, -2\}$. A numerical search over ψ and θ which optimize the minimum Euclidean distance for two independent datastreams shows that the Neighbor-$d_{\min}$ precoder has the same form as the max-$d_{\min}$ precoder presented in [37]

$$\mathbf{F}_d = \sqrt{\frac{E_s}{2}} \begin{pmatrix} 1 & i \\ 0 & 0 \end{pmatrix} \tag{5.20}$$

One should note that the Neighbor-$d_{\min}$ solution pours power only on the strongest virtual sub-channels. The minimum Euclidean distance is then defined by

$$d^2_{BPSK} = 4E_s\rho^2 \cos^2\gamma \tag{5.21}$$

5.3.2 For QPSK modulation

The transmitted symbols belong to the following set $S = \frac{1}{\sqrt{2}}\{1+i, 1-i, -1+i, -1-i\}$. For QPSK modulation with two datastreams, the set of all difference vectors denoted as $\check{\mathbf{S}}_{QPSK}$ contains $16 \times 15 = 240$ elements. By eliminating the collinear vectors, we can reduce the size of $\check{\mathbf{S}}_{QPSK}$ to 14 elements.

A numerical search over ψ and θ which optimize the minimum Euclidean distance for each channel angle, shows that our precoder has two different expressions. The first one, denoted as $\mathbf{F}_{snr}$ pours power only on the strongest virtual subchannel. The other, obviously, uses all two virtual subchannels to transmit symbols, and is denoted as $\mathbf{F}_{rec}$.

The first expression

The power is concentrated only on the first virtual subchannel and the rotation parameter φ is not considered at the precoder. The form of the precoder $\mathbf{F}_{snr}$ can be expressed as

$$\mathbf{F}_{snr} = \sqrt{\frac{E_s}{5}} \begin{pmatrix} 2 & 1 \\ 0 & 0 \end{pmatrix} \tag{5.22}$$

The optimized $d_{\min}$ is provided by the difference vector $\frac{1}{\sqrt{2}}[0\,2]^T$, and defined by

$$d_{snr}^2 = \frac{2}{5} E_s \rho^2 \cos^2 \gamma \tag{5.23}$$

The received constellation obtained by $\mathbf{F}_{snr}$ looks like the 16-QAM constellation. Hence, the average number of neighbors providing $d_{\min}$ is given by $\mathrm{N}_{d_{\min}} = \frac{1}{16}(4\times2+8\times3+4\times4) = 3$. This value is less than the number of the minimum Euclidean distances obtained by the precoder $\mathbf{F}_{r1}$ presented in [37] ($\mathrm{N}_{d_{\min}} = \frac{1}{16}(4\times2+4\times3+4\times4+4\times5) = 3.5$). However, the distances $d_{\min}$ provided by two precoders remain very close. This explains why the new precoder has a slight improvement of BER in comparison with the max-$d_{\min}$ precoder (see section 5.4.4).

The second expression

The difference between two virtual subchannels is smaller than the case of $\mathbf{F}_{snr}$. A numerical search shows that the optimized solution is found when the angle $\theta = 45^o$ is fixed and ψ depends on the channel angle γ. Indeed, the optimization is obtained by three difference vectors $\breve{\mathbf{s}}_1 = \frac{1}{\sqrt{2}}[0\,2]^T$, $\breve{\mathbf{s}}_2 = \frac{1}{\sqrt{2}}[2\,0]^T$ and $\breve{\mathbf{s}}_3 = \frac{1}{\sqrt{2}}[2\text{-}2]^T$. The three corresponding normalized distances can be expressed as

$$\begin{cases} \bar{d}^2_{\breve{x}_1} = A.\sin^2\theta + B.\cos^2\theta \\ \bar{d}^2_{\breve{x}_2} = A.\cos^2\theta + B.\sin^2\theta \\ \bar{d}^2_{\breve{x}_3} = A.(\cos\theta - \sin\theta)^2 + B.(\cos\theta + \sin\theta)^2 \end{cases}$$

where $A = 4\cos^2\gamma\cos^2\psi$ and $B = 4\sin^2\gamma\sin^2\psi$. By considering $\bar{d}^2_{\breve{x}_1} = \bar{d}^2_{\breve{x}_2} = \bar{d}^2_{\breve{x}_3}$ in the interval value of θ and ψ, we obtain

$$\begin{cases} \theta = \pi/4 \\ \psi = \arctan\frac{1}{\sqrt{3}.\tan\gamma} \end{cases} \tag{5.24}$$

By substituting (5.31) into (5.19), the precoder $\mathbf{F}_{rec}$ is given by

$$\mathbf{F}_{rec} = \sqrt{\frac{E_s}{2}} \begin{pmatrix} \cos\psi & 0 \\ 0 & \sin\psi \end{pmatrix} \begin{pmatrix} 1 & 1 \\ \text{-}1 & 1 \end{pmatrix} \tag{5.25}$$

The minimum Euclidean distance provided by $\mathbf{F}_{rec}$ is then

$$d^2_{rec} = E_s\rho^2\frac{4\sin^2\gamma}{3\tan^2\gamma + 1} \tag{5.26}$$

Fig. 5.1 illustrates the received constellation of the precoder for QPSK modulation. It is observed that the average number of $d_{\min}$ is defined by $\mathrm{N}_{d_{\min}} = \frac{1}{16}(4\times4 + 8\times5 + 4\times6) = 5$. In comparison with the precoder in [37] where $\mathrm{N}_{d_{\min}} = \frac{1}{16}(8\times5 + 8\times9) = 7$, our new precoder has a good improvement.

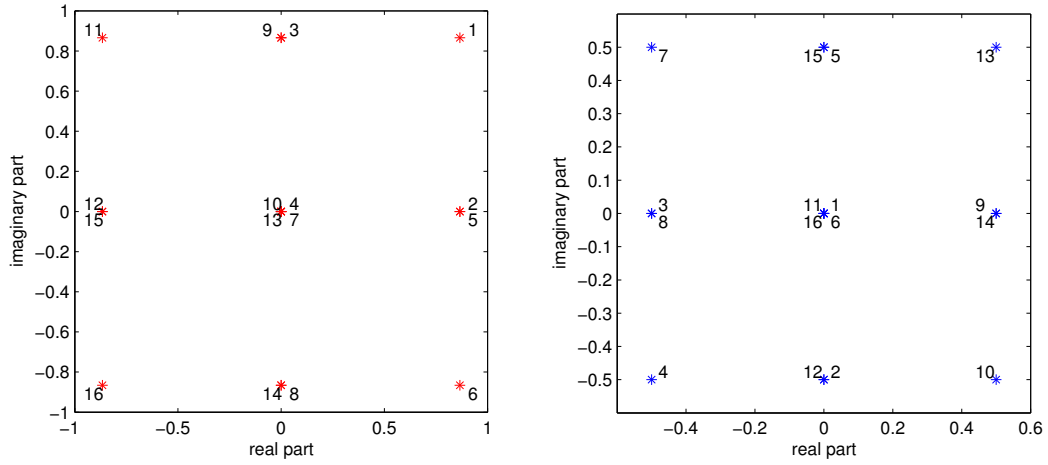

(a) First virtual subchannel (b) Second virtual subchannel

FIGURE 5.1: Received constellation of the precoder $\mathbf{F}_{rec}$ for QPSK.

The threshold γ_0

To choose between $\mathbf{F}_{snr}$ and $\mathbf{F}_{rec}$, we have to compare the error probabilities in (5.3) which are obtained by both precoders. It is observed that when the channel angle γ varies from 0 to $\pi/2$, the ratios of other distances to the distance $d_{\min}$ are fixed. Furthermore, we realize that the minimum Euclidean distance d_{snr} and d_{rec} in (5.23, 5.26) is proportional to E_s. For this reason, the threshold γ_0 is not constant and depends on the signal-to-noise ratio $\sqrt{E_s/N_0}$. The angle γ_0 increases to γ_c if the average transmit power E_s augments. The critical angle γ_c is given by

$$\begin{aligned} & d_{snr}^2 = d_{rec}^2 \\ \Leftrightarrow\ & \frac{2}{5}\cos^2\gamma_c = 4\frac{\sin^2\gamma_c}{3\tan^2\gamma_c + 1} \\ \Leftrightarrow\ & \gamma_c = \arctan\sqrt{1/7} \simeq 20.7048^o \end{aligned} \tag{5.27}$$

5.3.3 General expression for high-order QAM modulations

In the case of a 4^k-QAM modulation, the transmit symbols belong to the set

$$S = \sqrt{\beta_M}\,\{a + b\,i\ ;\ a - b\,i\ ;\ -a + b\,i\ ;\ -a - b\,i\} \tag{5.28}$$

where $\beta_M = \frac{3}{2(4^k-1)}$, and $a, b \in (1, 3, \ldots, 2^k - 1)$.

The expressions of the Neighbor-$d_{\min}$ precoder for two data streams can be classified into two types: the first one allocates power only on the highest virtual channel, and the other uses two virtual subchannels to transmit signals. These precoders are denoted as $\mathbf{F}_1$ and $\mathbf{F}_2$, in respectively.

Expression of the precoder $\mathbf{F}_1$

The first general expression is defined by

$$\mathbf{F}_1 = \sqrt{\frac{E_s}{4^k+1}} \begin{pmatrix} 2^k & 1 \\ 0 & 0 \end{pmatrix}. \tag{5.29}$$

A numerical research shows that the distance $d_{\min}$ provided by $\mathbf{F}_1$ is obtained by two difference vectors $\sqrt{\beta_M}[0\,2]^T$, and given by

$$d_{F_1}^2 = \frac{4}{4^k+1} E_s \rho^2 \beta_M \cos^2\gamma. \tag{5.30}$$

The constellation at the reception obtained by $\mathbf{F}_1$ is similar to that of a M^2-QAM modulation. As shown in the previous section, the proposed precoder gets fewer neighbor points, which have the same minimum distance, than those of the optimal max-$d_{\min}$ precoder [37].

Expression of the precoder $\mathbf{F}_2$

For every rectangular QAM modulation, a numerical approach shows that the optimal solution is obtained by the three difference vectors: $\breve{\mathbf{s}}_1 = \frac{1}{\sqrt{2}}[0\,2]^T$, $\breve{\mathbf{s}}_2 = \frac{1}{\sqrt{2}}[2\,0]^T$, and $\breve{\mathbf{s}}_3 = \frac{1}{\sqrt{2}}[2\text{-}2]^T$. Three corresponding distances are defined by

$$\begin{cases} \bar{d}_{\breve{x}_1}^2 = A\sin^2\theta + B\cos^2\theta \\ \bar{d}_{\breve{x}_2}^2 = A\cos^2\theta + B\sin^2\theta \\ \bar{d}_{\breve{x}_3}^2 = A(\cos\theta - \sin\theta)^2 + B(\cos\theta + \sin\theta)^2 \end{cases}$$

where $A = 4\cos^2\gamma\cos^2\psi$ and $B = 4\sin^2\gamma\sin^2\psi$. By considering $\bar{d}^2_{\check{x}_1} = \bar{d}^2_{\check{x}_2} = \bar{d}^2_{\check{x}_3}$, we obtain

$$\begin{cases} \theta = \pi/4 \\ \psi = \text{atan}\,\frac{1}{\sqrt{3}.\tan\gamma} \end{cases} \tag{5.31}$$

The second general expression $\mathbf{F}_2$ is given by

$$\mathbf{F}_2 = \sqrt{\frac{E_s}{2}} \begin{pmatrix} \cos\psi & 0 \\ 0 & \sin\psi \end{pmatrix} \begin{pmatrix} 1 & 1 \\ -1 & 1 \end{pmatrix} \tag{5.32}$$

where $\psi = \text{atan}\,\frac{1}{\sqrt{3}.\tan\gamma}$. The minimum distance provided by $\mathbf{F}_2$ is then

$$d^2_{F_2} = 4E_s\rho^2\beta_M \frac{2\sin^2\gamma}{3\tan^2\gamma + 1}\,. \tag{5.33}$$

The constellation obtained at the receiver by precoding matrix $\mathbf{F}_2$ is shown in Fig. 5.9. It should be noted that two received vectors, which are close on one subchannel , can be distant on the second one (for example: points A and B).

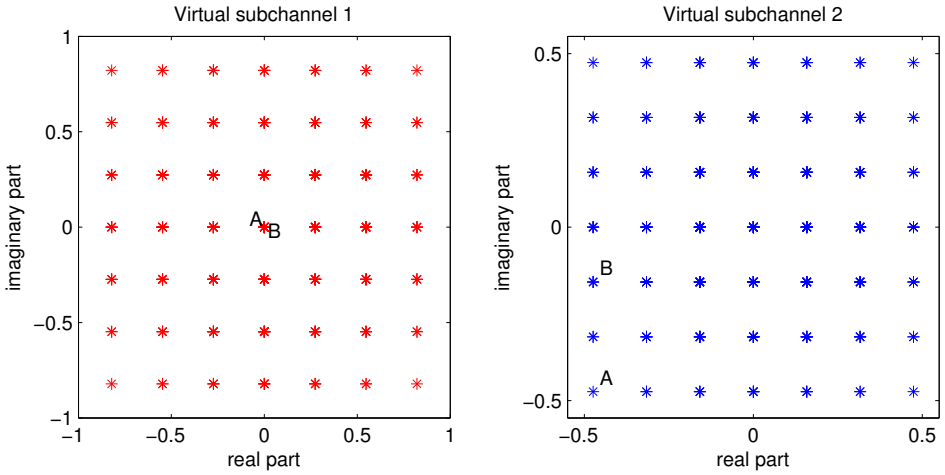

FIGURE 5.2: Received constellation provided by the precoder $\mathbf{F}_2$.

The threshold γ_0

Fig 5.3 illustrates the evolution of the normalized minimum distance with respect to the channel angle γ for two general expressions of the Neighbor-$d_{\min}$precoder. The precoder $\mathbf{F}_1$ provides the optimized distance $d_{\min}$ for small values of γ, while the precoder $\mathbf{F}_2$ is valid for large values of γ. In order to choose between $\mathbf{F}_1$ and $\mathbf{F}_2$, and obtain the

corresponding threshold, we have to find γ such that $d^2_{F_1} = d^2_{F_2}$ in (5.30) and (5.33). The threshold γ_0 is then defined by

$$\frac{\cos^2\gamma_0}{4^k+1} = \frac{2\sin^2\gamma_0}{3\tan^2\gamma_0+1}$$
$$\Leftrightarrow \gamma_0 = \operatorname{atan}\sqrt{\frac{1}{2.4^k-1}}. \tag{5.34}$$

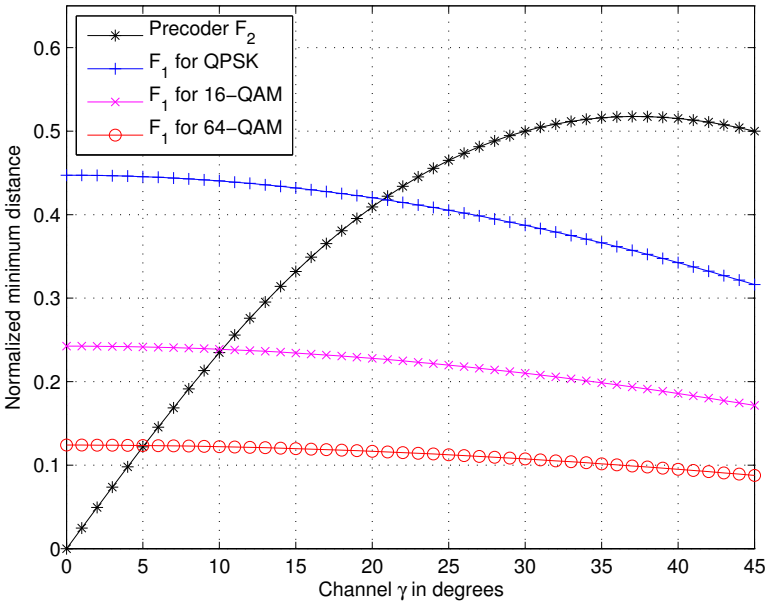

FIGURE 5.3: Normalized minimum distance for the precoder Neighbor-$d_{\min}$.

5.3.4 Performance of Neighbor-$d_{\min}$ precoder

For QPSK modulation

Fig. 5.4 shows the normalized minimum Euclidean distance $d_{\min}$ of the new precoder Neighbor-$d_{\min}$ and other precoders in the case of QPSK modulation. The average transmit power E_s for diagonal precoders is choosen large enough such that the power is always allocated on both virtual subchannels. It is observed that the Neighbor-$d_{\min}$ solution is better than WaterFiling [12], max-$\lambda_{\min}$ [33] and MMSE [32] precoders in terms of $d_{\min}$. The new precoder has a small difference of $d_{\min}$ in comparison with max-$d_{\min}$ precoder [37]. Furthermore, the difference remains constant for a small channel angle ($\gamma < 17.28^o$).

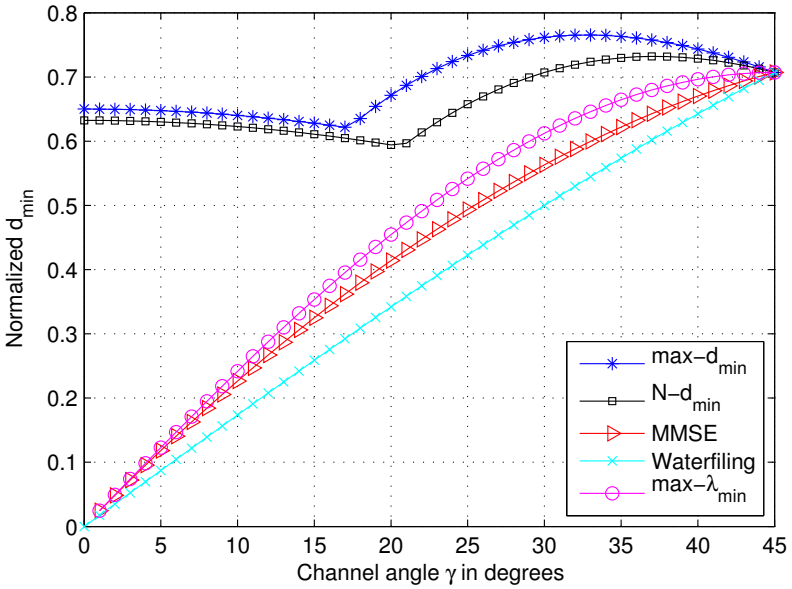

FIGURE 5.4: Normalized minimum Euclidean distance for QPSK.

According to the improvement of not only the minimum Euclidean distance (except for max-$d_{\min}$, of course) but also the average number of $d_{\min}$, an increase of BER performance for Neighbor-$d_{\min}$ precoder is expected for QPSK modulation. We consider herein a MIMO-OFDM system with $n_T = 3$ transmit and $n_R = 2$ receive antennas. The channel matrix $\mathbf{H}$ is complex Gaussian and the noise element are additive white Gaussian.

Firstly, we compare the BER performances obtained by the new precoder Neighbor-$d_{\min}$ and the max-$d_{\min}$ solution. Fig. 5.5 shows a BER improvement of the precoder $\mathbf{F}_{snr}$ and $\mathbf{F}_{rec}$ in comparison with $\mathbf{F}_{r1}$ and $\mathbf{F}_{octa}$ for small and large channel angle γ, respectively. We observe a large BER improvement of the precoder $\mathbf{F}_{rec}$ compared to $\mathbf{F}_{octa}$, and a slight superiority of $\mathbf{F}_{snr}$ in comparison with $\mathbf{F}_{r1}$, although both new precoders are inferior in terms of $d_{\min}$. This result clearly demonstrates that the number of minimum Euclidean distances has an important role in reducing the error probability when an ML detection is considered at the receiver.

The BER performance in comparison with other precoders for QPSK modulation is illustrated in Fig. 5.6. As expected, the Neighbor-$d_{\min}$ precoder provides a significant improvement in term of BER compared to diagonal precoders. Furthermore, it has a slight improvement in comparison with max-$d_{\min}$ precoder. This can be explained by the distribution of the channel angles γ: the MIMO system (3,2) uses more often the precoder $\mathbf{F}_{snr}$ than $\mathbf{F}_{rec}$.

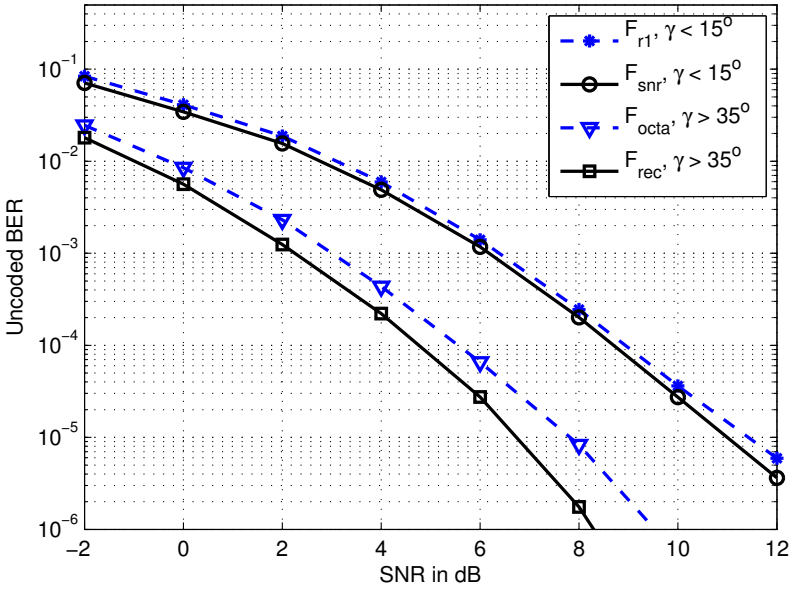

FIGURE 5.5: BER comparison of max-$d_{\min}$ and Neighbor-$d_{\min}$ precoders.

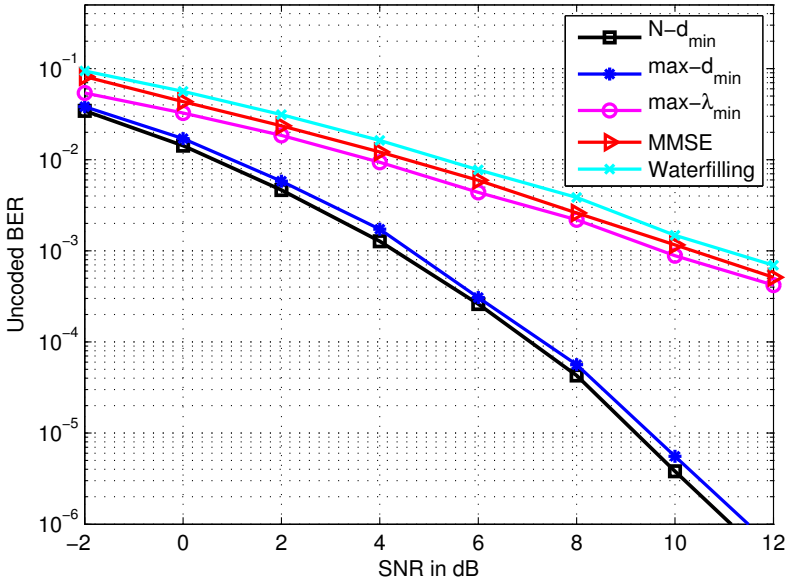

FIGURE 5.6: Uncoded BER performance for QPSK modulation.

For high-order QAM modulations

Fig. 5.7 shows the normalized minimum distance of the new precoder Neighbor-$d_{\min}$ precoder and others precoder in the case of 16-QAM modulation. The average power transmission E_s for diagonal precoder is chosen large enough such that the power is poured on all virtual subchannels. We observe that the minimum Euclidean distance provided by the Neighbor-$d_{\min}$ is greater than that of other literature precoders, for example Waterfilling, MMSE, and max-$\lambda_{\min}$.

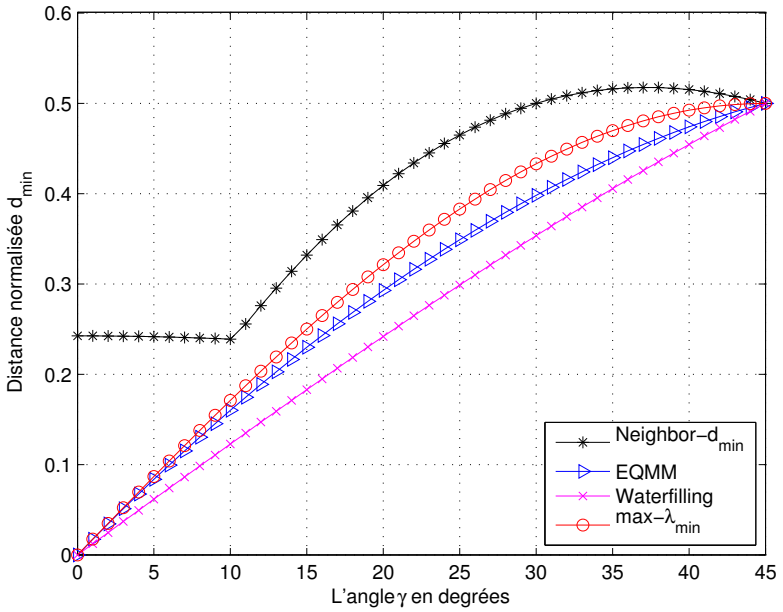

FIGURE 5.7: Comparaison $d_{\min}$ pour MAQ-16.

In addition, a large performance improvement in terms of BER is confirmed by the Fig 5.8, which represents the BER as a function of SNR for a MIMO system using 16-QAM modulation, $n_T = 3$ transmitter, $n_R = 2$ receiver through a channel Rayleigh fading. The precoder Neighbor-$d_{\min}$ provides a gain of about 6 dB for a BER = 10^{-5} in comparison with diagonal precoders.

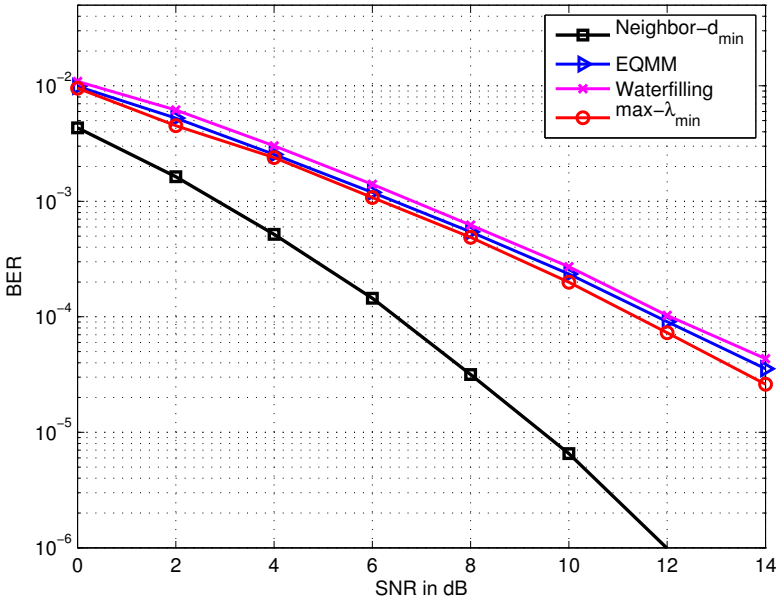

FIGURE 5.8: Comparaison des précodeurs pour MIMO(3,2).

5.4 Neighbor-$d_{\min}$ precoder for three parallel datastreams

Thanks to the representation of $\mathbf{B}^*$ in (5.17), we can find $(b-1)$ angles ψ_i and $b(b-1)/2$ angles θ_i which optimize the minimum distance criterion. When b increases, not only the number of parameters but also the received constellation size augments dramatically. In the previous section, we present the optimal solution for only small b virtual channels ($b = 2$). We point out herein the Neighbor-$d_{\min}$ precoder for three-dimensional virtual systems using rectangular QAM-modulations. As presented in section 5.2, a three-dimensional virtual channel can be parameterized as

$$\mathbf{H}_v = \rho \begin{pmatrix} \cos\gamma_1 & 0 & 0 \\ 0 & \sin\gamma_1 \cos\gamma_2 & 0 \\ 0 & 0 & \sin\gamma_1 \sin\gamma_2 \end{pmatrix}, \tag{5.35}$$

where ρ, γ_1 and γ_2 stand respectively for the channel gain and channel angles. It is noted that the diagonal elements of $\mathbf{H}_v$ are sorted in decreasing order, so $0 \le \gamma_2 \le \pi/4$ and $\cos\gamma_2 \le \operatorname{cotan}\gamma_1$.

The unitary matrix $\mathbf{B}^*$ in (5.17) can be now simplified as

$$\mathbf{B}^* = \begin{pmatrix} c_1 & s_1 c_2 & s_1 s_2 \\ -s_1 c_3 & c_1 c_2 c_3 - s_2 s_3 & c_1 s_2 c_3 + c_2 s_3 \\ s_1 s_3 & -c_1 c_2 s_3 - s_2 c_3 & -c_1 s_2 s_3 + c_2 c_3 \end{pmatrix}, \tag{5.36}$$

where $c_i = \cos\theta_i$ and $s_i = \sin\theta_i$ for $i = 1, .., 3$. The angle θ_i corresponds to the scaling of the received constellation while the parameter ψ_i of $\mathbf{\Sigma}$ controls the power allocation on each virtual subchannel.

For a rectangular 4^k-QAM modulation, the transmitted symbols belong to the complex set

$$S = \frac{1}{\sqrt{M}} \{a + b\,i\,;\, a - b\,i\,;\, -a + b\,i\,;\, -a - b\,i\}, \tag{5.37}$$

where $M = \frac{2}{3}(4^k - 1)$ and $a, b \in (1, 3, \ldots, 2^k - 1)$.

The expression of the precoding matrix which optimizes $d_{\min}$ for three independent datastreams can be classified into three types which enable power on one, two, or three virtual subchannels.

5.4.1 Precoder $\mathbf{F}_1$

The precoder is available for high dispersive channels, and can be seen as a max-SNR design that pours power only on the strongest virtual subchannel. In fact, this precoder transforms the rectangular 4^k-QAM signals on three virtual subchannels into a rectangular 4^{3k}-QAM on the first subchannel. The optimized precoding matrix is given by

$$\mathbf{F}_1 = \sqrt{\frac{E_s}{M_1}} \begin{pmatrix} 4^k & 2^k & 1 \\ 0 & 0 & 0 \\ 0 & 0 & 0 \end{pmatrix}, \tag{5.38}$$

where $M_1 = 16^k + 4^k + 1$. The optimized $d_{\min}$ is provided by the difference vector $\frac{1}{\sqrt{M}}[0\,0\,2]^T$, and defined by

$$d^2_{\mathbf{F}_1} = \frac{4}{MM_1} E_s \rho^2 \cos^2 \gamma_1. \tag{5.39}$$

Although the distance is inferior to the minimum distance obtained by SNR-like max-$d_{\min}$ precoder [65], it has less neighbors providing the distance $d_{\min}$.

5.4.2 Precoder $\mathbf{F}_2$

The optimized precoder which enables power on first and second virtual subchannels ($\psi_2 = 0$) may have many expressions. To simplify the form of $\mathbf{F}_2$, we present, herein, the most important expression of $\mathbf{F}_2$. The expression is available when there is a large dispersion between the two first subchannels and the third subchannel. For rectangular QAM modulations, a numerical approach shows that the minimum distance is provided by five difference vectors: $\breve{\mathbf{x}}_1 = \frac{1}{\sqrt{M}}[0, 2, 0]^T$, $\breve{\mathbf{x}}_2 = \frac{1}{\sqrt{M}}[0, 2(k\text{-}1), \text{-}2]^T$, $\breve{\mathbf{x}}_3 = \frac{1}{\sqrt{M}}[0, 2k, \text{-}2]^T$, $\breve{\mathbf{x}}_4 = \frac{1}{\sqrt{M}}[2, \text{-}2(M_2\text{-}k\text{+}1), 2(k\text{-}1)]^T$, and $\breve{\mathbf{x}}_5 = \frac{1}{\sqrt{M}}[2, \text{-}2M_2, 2k]^T$, where $M_2 = 2^k - 1$.

Let us note $d^2_{\breve{x}_i}$ as the corresponding distance of $\breve{\mathbf{x}}_i$ with $i = 1, .., 5$. By solving the system of equations $d^2_{\breve{x}_1} = d^2_{\breve{x}_2} = d^2_{\breve{x}_3} = d^2_{\breve{x}_4} = d^2_{\breve{x}_5}$, we obtain all constant angles of the matrix $\mathbf{B}^*$ (confirmed by Proposition 1). The optimized angles (in radians) of $\mathbf{B}^*$ are described in Tab. 5.1, while the angle ψ_1 which depends on the channel angles γ_1 and γ_2 is defined by

$$\psi_{1|(\gamma_1,\gamma_2)} = \operatorname{atan} \frac{\tan(\psi_{1|(\pi/4,0)})}{\tan \gamma_1 \cos \gamma_2}. \tag{5.40}$$

Modulation	θ_1	θ_2	θ_3	$\psi_{1\|(\pi/4,0)}$
4-QAM	0.5083	0.1753	0.9951	0.5066
16-QAM	0.6155	0.7854	0.3876	0.7227
64-QAM	0.5538	1.0216	0.2229	0.8433
256-QAM	0.6690	1.2490	0.0977	0.6331

TABLE 5.1: Optimized angles for the precoder $\mathbf{F}_2$

The minimum distance is provided by the difference vector $\frac{1}{\sqrt{M}}[0\,2\,0]^T$, and given by

$$d^2_{\mathbf{F}_2} = \kappa \frac{2E_s\rho^2}{M(2M_2+4-k)}, \tag{5.41}$$

where κ depends on γ_1 and γ_2 and is defined in (5.55).

5.4.3 Precoder $\mathbf{F}_3$

The Neighbor-$d_{\min}$ precoder which pours power on all subchannels also has many expressions. Each expression is available for different variations of the transmit channel. We present, herein, a general precoding matrix for all rectangular QAM-modulations. For every precoder has the form like (5.10), this precoder provides the highest minimum distance when the channel is small dispersive. The matrix $\mathbf{B}^*$ is then defined by

$$\mathbf{B}^* = \frac{1}{\sqrt{3}} \begin{pmatrix} 1 & 1 & 1 \\ -1 & \frac{1-\sqrt{3}}{2} & \frac{1+\sqrt{3}}{2} \\ 1 & \frac{-1-\sqrt{3}}{2} & \frac{-1+\sqrt{3}}{2} \end{pmatrix}. \tag{5.42}$$

By equalizing three difference distances provided by $\breve{\mathbf{x}}_1 = \frac{1}{\sqrt{M}}[0,2,0]^T$, $\breve{\mathbf{x}}_2 = \frac{1}{\sqrt{M}}[0,0,2]^T$, and $\breve{\mathbf{x}}_3 = \frac{1}{\sqrt{M}}[0,2,-2]^T$, we obtain

$$\begin{cases} \psi_2 = \operatorname{atan} \frac{1}{\tan\gamma_2} \\ \psi_1 = \operatorname{atan} \frac{1}{2\tan\gamma_1 \cos\gamma_2 \cos\psi_2} \end{cases} \tag{5.43}$$

The distance $d_{\min}$ obtained by $\mathbf{F}_3$ is then

$$d^2_{\mathbf{F}_3} = \frac{8E_s\rho^2 \cos^2\gamma_1 \sin^2\gamma_1 \cos^2\gamma_2 \sin^2\gamma_2}{4\sin^2\gamma_1 \cos^2\gamma_2 \sin^2\gamma_2 + \cos^2\gamma_1 \sin^2\gamma_2 + \cos^2\gamma_1 \cos^2\gamma_2}. \tag{5.44}$$

Fig. 5.9 plots the received constellation provided by the precoder $\mathbf{F}_3$ in the case of 4-QAM. One should note that whenever two received vectors are close on one virtual subchannel, they are distant on the others (e.g. A and B).

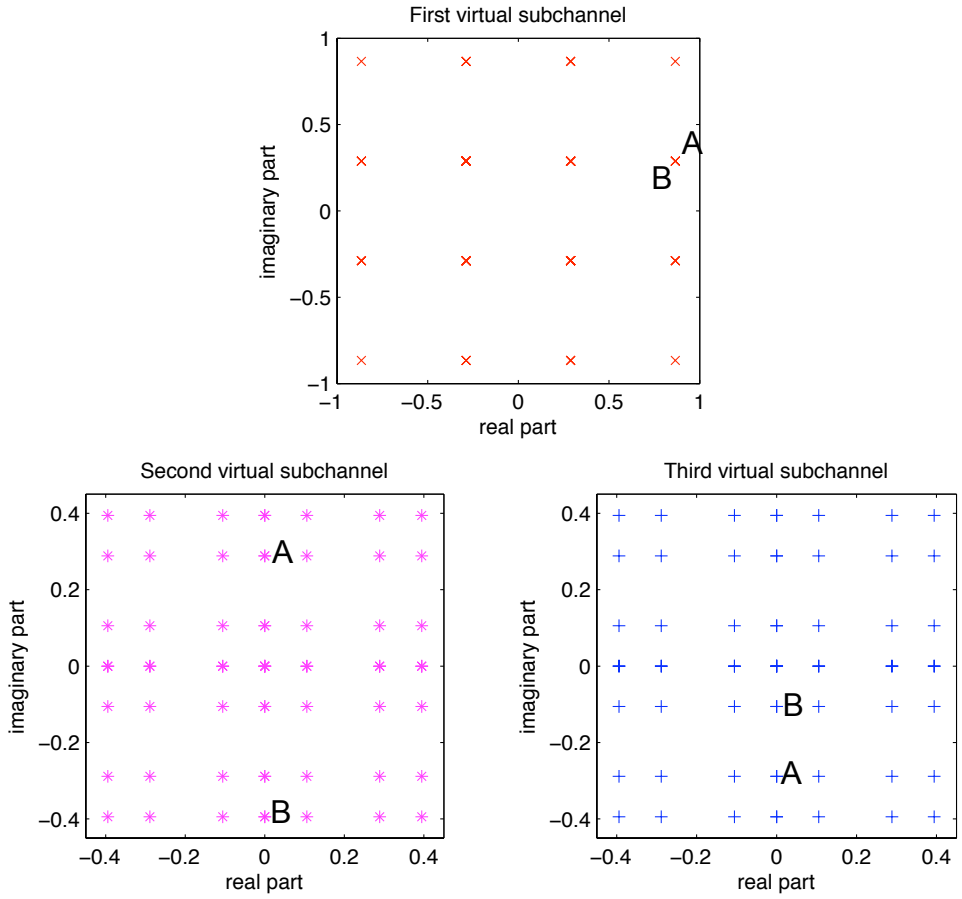

FIGURE 5.9: Received constellations provided by precoder $\mathbf{F}_3$ for QPSK modulation.

5.4.4 Simulation results

Range of definition

To improve the BER performance of a MIMO system, we can choose from the three precoding matrices above the precoder which provides the highest minimum Euclidean distance. For a given modulation order, by comparing the three minimum distances in (5.39), (5.41), and (5.44), we obtain the range of definition for each precoder.

The range of definition for QPSK is shown in Fig. 5.10. It is observed that when the modulation order increases, the normalized minimum distances ($d_{\min}/\sqrt{4E_s\rho^2/M}$) provided by $\mathbf{F}_1$ and $\mathbf{F}_2$ are decreased. In other words, two precoder $\mathbf{F}_1$ and $\mathbf{F}_2$ are less

used for higher order modulations (the range of definition changes following the arrows in Fig. 5.10).

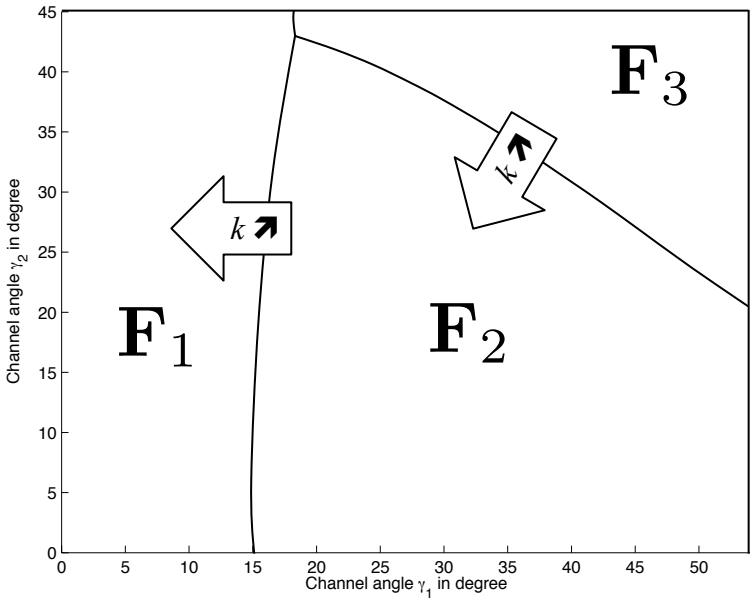

FIGURE 5.10: Range of definition for the three precoders $\mathbf{F}_1$, $\mathbf{F}_2$, and $\mathbf{F}_3$ using a QPSK modulation. The arrows represent the evolution of the borders when the modulation order increases.

Performance of Neighbor-$d_{\min}$ precoder

Thanks to the rectangular constellation (see Fig. 5.9), our new precoder not only optimizes the minimum Euclidean distance but also has less neighbors which provide the distance $d_{\min}$. The normalized minimum distance of the Neighbor-$d_{\min}$ and other precoders are illustrated in Fig. 5.11. For diagonal precoders, the transmit power is large enough to be allocated on all virtual subchannels. It is observed that the minimum distance provided by the Neighbor-$d_{\min}$ precoder is better than those of WaterFilling, max-$\lambda_{\min}$ [33] and MMSE [32]. Furthermore, unlike diagonal precoders, the minimum distance of Neighbor-$d_{\min}$ precoder is much superior to zero if the virtual channels are large dispersive. When the channels are small dispersive, the minimum distance provided by max-$\lambda_{\min}$ is better than MMSE and Waterfilling but is really outperformed by our new precoder.

Let us consider a MIMO-OFDM system with $n_T = 4$ transmit antennas and $n_R = 3$ receive antennas. The transmit channel is Rayleigh fading and the noise is additive

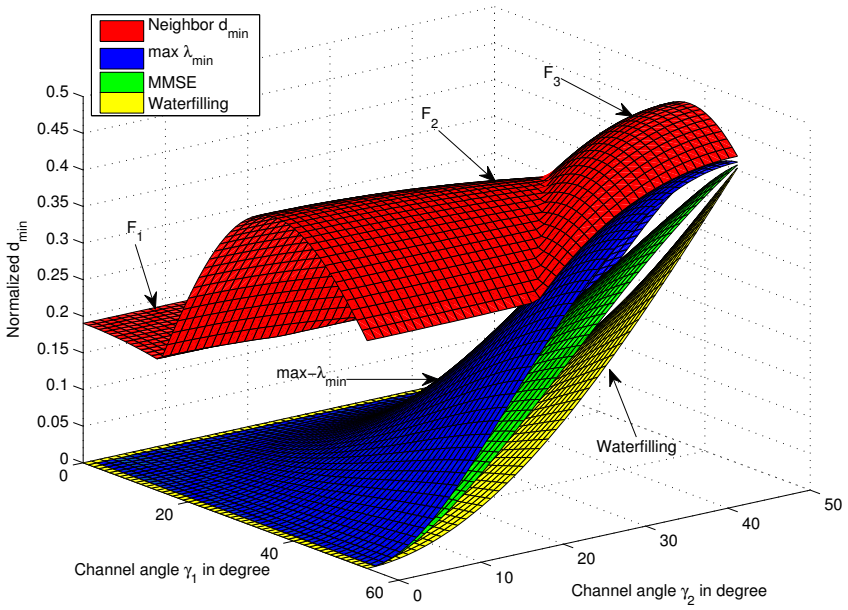

FIGURE 5.11: Normalized minimum distance for QPSK.

white Gaussian. Due to the improvement of the minimum distance and the number of neighbors providing $d_{\min}$, a large enhancement of BER performance is expected. Fig. 5.12 illustrates the BER performance with respect to SNR for QPSK modulation. It is obvious that the Neighbor-$d_{\min}$ precoder has a significant BER enhancement compared to diagonal precoders. A gain of about 5 dB is observed (at high SNR) in comparison with the beamforming design. Furthermore, we also observe a slight BER improvement of the Neighbor-$d_{\min}$ precoder compared to the optimal max-$d_{\min}$ precoder. This can be explained in the way that the number of neighbors is really important due to the maximization the error probability.

5.5 Neighbor-$d_{\min}$ precoder for large MIMO systems

5.5.1 Principles

As presented in Chapter 4, we can extend a sub-optimal solution of Neighbor-$d_{\min}$ precoder for large MIMO systems with an odd or even number of data-streams. This solution is split into four steps

1. Obtain the virtual diagonal matrix $\mathbf{H_v}$ by using a virtual transformation.

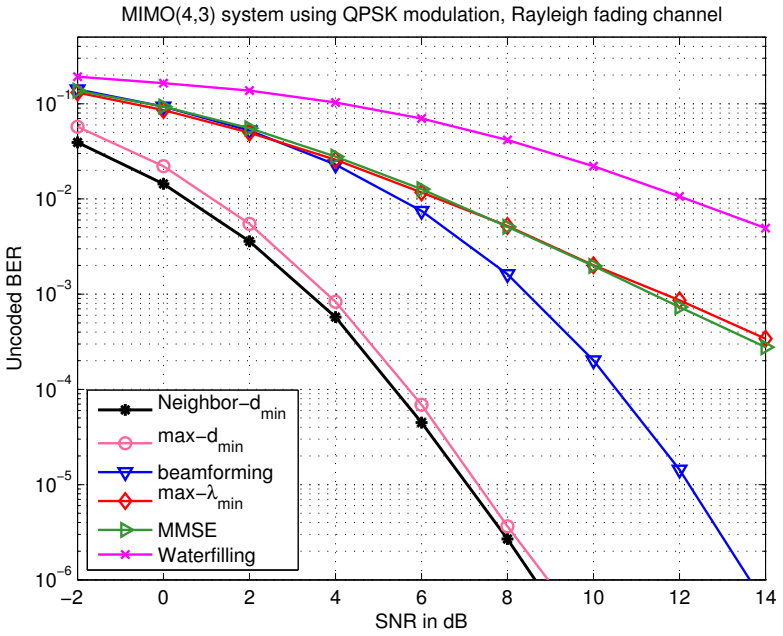

FIGURE 5.12: Uncoded BER for MIMO(4,3) system using QPSK modulation.

2. Associate the $2b$ singular values by the following combination (σ_1, σ_{2b}), $(\sigma_2, \sigma_{2b-1})$, ..., (σ_b, σ_{b+1}), or $2b+1$ singular values by the following combination $(\rho_1, \rho_{b+1}, \rho_{2b+1})$, (ρ_2, ρ_{2b}), (ρ_3, ρ_{2b-1}), $\cdots$, (ρ_b, ρ_{b+2}) to obtain b virtual subsystems.

3. Apply the 3-D Neighbor-$d_{\min}$ or 2-D Neighbor-$d_{\min}$ precoders on each subsystem under a unity power-constraint.

4. Allocate the power to each subsystem $\#i$ by computing the coefficient Υ_i such that

$$\Upsilon_i^2 = p_0 \left(\delta_i^2 \sum_{j=1}^{b} \frac{1}{\delta_j^2} \right)^{-1} \qquad \forall i = 1..b$$

where δ_i is the minimum Euclidean distance of the subsystem $\#i$ given in the step 3.

5.5.2 Simulation results

In the section, we compare the BER performance of the Neighbor-$d_{\min}$ precoder with other sophisticated transceivers such as beamforming (max-SNR), waterfilling (WF), minimum mean square error (MMSE), or maximization of the minimum eigenvalue (max-$\lambda_{\min}$). For each SNR, a numerical survey with 30000 uncorrelated Rayleigh fading channels $\mathbf{H}$ is implemented. We consider a MIMO system with $n_T = 6$ transmit and $n_R = 5$ receive antennas over which we send $b = 5$ independent QPSK datastreams. The

BER performance with respect to SNR of the proposed precoder in comparison with other precoders is shown in Fig. 5.13. It is clear that our new precoder obtains a significant improvement in terms of BER compared to other precoders. In comparison with the max-$d_{\min}$ design, although the Neighbor-$d_{\min}$ precoder has a simpler form, it provides a same BER performance due to the reduction of the neighbors providing the minimum distance.

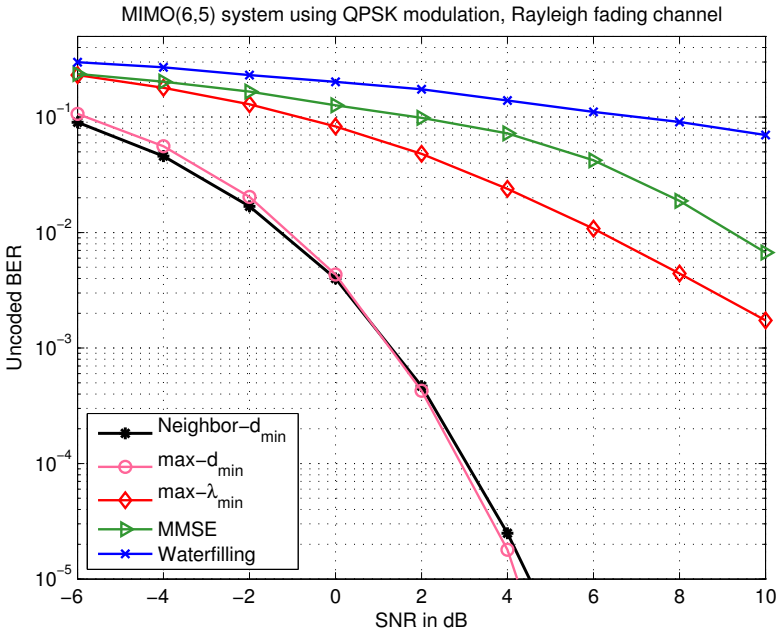

FIGURE 5.13: Uncoded BER for large MIMO system using QPSK modulation.

5.6 Conclusion

In the first part of this section, we investigated the impact of the minimum Euclidean distance on the performance of bit-error-rate when an ML detection is considered at receive side. It is realized that the number neighbors providing $d_{\min}$ has an important role in reducing the error probability. Therefore, a new precoder for MIMO transmission, which is based on the maximization of $d_{\min}$ associated with the minimization of the neighbors providing it, has been introduced.

In the new precoding strategy, the rotation parameter φ is not considered. Hence, the degree of freedom in precoding matrix $\mathbf{F}_d$ is decreased and the space of the solution is smaller. Not only reducing the complexity, the Neighbor-$d_{\min}$ precoder presents also a

significant improvement of BER compared to diagonal precoders such as MMSE, Water-filing and max-$\lambda_{\min}$. In comparison with max-$d_{\min}$ precoder, the new precoder provides a slight improvement. The BER enhancement depends on channel characteristics and is more significant if the virtual subchannels are far from dispersive.

Appendices of chapter 5

A Proof of Lemma 5.1

For all $d_\beta < d_\chi$, it is obvious that we can find a high value of $R > 0$ such that

$$d_\chi^2 - d_\beta^2 + \frac{2}{R^2} \log \frac{d_\beta - d_\alpha}{d_\delta - d_\chi} > 0 \tag{5.45}$$

with $d_\beta > d_\alpha$ and $d_\delta > d_\chi$. The inequality (5.45) can be rewritten as

$$\begin{aligned} & \log \frac{d_\beta - d_\alpha}{d_\delta - d_\chi} > -(d_\chi^2 - d_\beta^2).R^2/2 \\ \Leftrightarrow & \frac{d_\beta - d_\alpha}{d_\delta - d_\chi} > e^{-(d_\chi^2 - d_\beta^2).R^2/2} \\ \Leftrightarrow & R(d_\beta - d_\alpha).e^{-d_\beta^2.R^2/2} > R(d_\delta - d_\chi).e^{-d_\chi^2.R^2/2} \end{aligned} \tag{5.46}$$

Using the monotonic decreasing property of the function $e^{-x^2/2}$, we obtain

$$\int_{d_\alpha.R}^{d_\beta.R} e^{-x^2/2}\, dx > (d_\beta.R - d_\alpha.R).e^{-(d_\beta.R)^2/2} \tag{5.47}$$

$$(d_\delta.R - d_\chi.R).e^{-(d_\chi.R)^2/2} > \int_{d_\chi.R}^{d_\delta.R} e^{-x^2/2}\, dx \tag{5.48}$$

From (5.46), (5.47), and (5.48) we have

$$\int_{d_\alpha.R}^{d_\beta.R} e^{-x^2/2}\, dx > \int_{d_\chi.R}^{d_\delta.R} e^{-x^2/2}\, dx$$

$$\Leftrightarrow Q(d_\alpha.R) - Q(d_\beta.R) > Q(d_\chi.R) - Q(d_\delta.R)$$

$$\Leftrightarrow Q(d_\alpha.R) + Q(d_\delta.R) > Q(d_\beta.R) + Q(d_\chi.R)$$

B Proof of Lemma 5.2

The mathematical induction can be used to prove this lemma. One should note that $Q(x)$ is a monotonic decreasing function. First we show that our statement holds for $k = 2$. Indeed, there are two cases:

1. $d_{\alpha_2} \leq d_{\beta_2}$: it is obvious that $Q(d_{\alpha_1}.R) > Q(d_{\beta_1}.R)$ and $Q(d_{\alpha_2}.R) \geq Q(d_{\beta_2}.R)$ with $\forall R > 0$, so we have

$$Q(d_{\alpha_1}.R) + Q(d_{\alpha_2}.R) > Q(d_{\beta_1}.R) + Q(d_{\beta_2}.R)$$

2. $d_{\alpha_2} > d_{\beta_2}$: obviously, this is the case of the *Lemma 5.1*.

Thus it has been shown that the lemma holds for $k = 2$. We assume that our statement is true for k. It must then be shown that our statement is true for $k + 1$. Let us define $d_{\gamma_1} = \frac{1}{3}(d_{\alpha_1} + d_{\beta_1})$, and $d_{\gamma_2} = \frac{2}{3}(d_{\alpha_1} + d_{\beta_1})$. It is clear that $d_{\alpha_1} < d_{\gamma_1} < d_{\gamma_2}$, so we can find value R_1 such that $\forall R \geq R_1$

$$Q(d_{\alpha_1}.R) + Q(d_{\alpha_2}.R) > Q(d_{\gamma_1}.R) + Q(d_{\gamma_2}.R) \tag{5.49}$$

Since $d_{\gamma_2} < d_{\beta_1} \leq d_{\beta_2}$, so we get

$$Q(d_{\gamma_2}.R) > Q(d_{\beta_2}.R) \tag{5.50}$$

Furthermore, we have $d_{\gamma_1} < d_{\beta_1}$. According to the statement in the case of k, there exist values R_2 which satisfy $\forall R \geq R_2$

$$Q(d_{\gamma_1}.R) + \sum_{i=3}^{k+1} Q(d_{\alpha_i}.R) > Q(d_{\beta_1}.R) + \sum_{i=3}^{k+1} Q(d_{\beta_i}.R) \tag{5.51}$$

From (5.49), (5.50) and (5.51), it can be concluded that $\forall R \geq \max(R_1, R_2)$, we have

$$\sum_{i=1}^{k+1} Q(d_{\alpha_i}.R) > \sum_{i=1}^{k+1} Q(d_{\beta_i}.R)$$

C Proof of Proposition 5.3

Let us denote $\breve{\mathbf{a}}_1$, $\breve{\mathbf{a}}_2$, as two difference vectors which have the same Euclidean distances. These Euclidean distances are given by

$$\begin{cases} d^2_{\breve{\mathbf{a}}_1|\mathbf{H}_v} = \|\mathbf{H}_v \mathbf{\Sigma} \mathbf{B} \breve{\mathbf{a}}_1\|^2 \\ d^2_{\breve{\mathbf{a}}_2|\mathbf{H}_v} = \|\mathbf{H}_v \mathbf{\Sigma} \mathbf{B} \breve{\mathbf{a}}_2\|^2 \end{cases} \tag{5.52}$$

One should note that $\mathbf{\Sigma}$ is a diagonal matrix with real nonnegative elements, i.e. $\mathbf{\Sigma} = \text{diag}(\phi_1, ..., \phi_b)$. When the channel varies from $\mathbf{H}_v = \text{diag}(\sigma_1, ..., \sigma_b)$ to $\hat{\mathbf{H}}_v = \text{diag}(\hat{\sigma}_1, ..., \hat{\sigma}_b)$, the two distances above can be kept equal by changing only the values of ϕ_i, $i = 1, .., b$. Indeed, we define the diagonal matrix $\hat{\mathbf{\Sigma}}$ with real nonnegative elements such that

$$\hat{\phi}_i \hat{\sigma}_i = \kappa \, \phi_i \sigma_i, \tag{5.53}$$

where κ is a constant. By substituting ϕ_i into the power constraint in (5.12), we get

$$\sum_{i=1}^{n} \hat{\phi}_i^2 = \kappa^2 \sum_{i=1}^{n} \phi_i^2 \left(\frac{\sigma_i}{\hat{\sigma}_i}\right)^2 = E_s \tag{5.54}$$

or

$$\kappa = \sqrt{\frac{E_s}{\sum_{i=1}^{n} \phi_i^2 \sigma_i^2 / \hat{\sigma}_i^2}}. \tag{5.55}$$

The Euclidean distance provided by $\breve{\mathbf{a}}_1$ is then

$$\begin{aligned} d^2_{\breve{\mathbf{a}}_1|\hat{\mathbf{H}}_v} &= \|\hat{\mathbf{H}}_v \hat{\mathbf{\Sigma}} \mathbf{B} \breve{\mathbf{a}}_1\|^2 \\ &= \|\kappa \, \mathbf{H}_v \mathbf{\Sigma} \mathbf{B} \breve{\mathbf{a}}_1\|^2 \\ &= \kappa^2 \, d^2_{\breve{\mathbf{a}}_1|\mathbf{H}_v}. \end{aligned}$$

Similarly, we get

$$d^2_{\breve{\mathbf{a}}_2|\hat{\mathbf{H}}_v} = \kappa^2 \, d^2_{\breve{\mathbf{a}}_2|\mathbf{H}_v}.$$

Since $d^2_{\breve{\mathbf{a}}_1|\mathbf{H}_v} = d^2_{\breve{\mathbf{a}}_2|\mathbf{H}_v}$, we have $d^2_{\breve{\mathbf{a}}_1|\hat{\mathbf{H}}_v} = d^2_{\breve{\mathbf{a}}_2|\hat{\mathbf{H}}_v}$. Consequently, two any difference distances can be kept equal by changing only the matrix $\mathbf{\Sigma}$.

Chapter 6

Generalized precoding designs using Discrete Fourier Transform matrix

The optimal solution of max-$d_{\min}$ precoder is proposed in [37, 69] for two transmit datastreams and for 4-QAM and 16-QAM modulations. By decomposing the channel into 2×2 eigen-channel matrices and optimizing the distance $d_{\min}$ for each sub-system, the authors in [59] proposed a sub-optimal precoder for large MIMO channels. However this solution is only available for low-order QAM modulations. It is because the optimized solution depends on many parameters such as the symbol alphabet, the detection rule, or the characteristics of the virtual channel. Another sub-optimal design of the max-$d_{\min}$ precoder, which allows transmitting more than two independent datastreams and increasing the order of the modulations, is presented in [55]. But the precoding scheme considers only a block-Toeplitz form of the channel matrix and, therefore, is only suitable for quasi-stationary MIMO channels.

The problem of high-order QAM modulations and the number of datastreams is settled in this chapter. We present herein a simple form of the minimum Euclidean distance based precoder. The precoding matrix is then factorized as the product of a diagonal power allocation matrix and an input-shaping matrix. In order to minimize the minimum distance, the input-shaping matrix is chosen to be a Discrete Fourier Transform (DFT) matrix, and only the power allocation matrix depends on the channel characteristics. The expression of the precoding matrix is therefore less complex with only b variables corresponding to the b diagonal entries of the power allocation matrix. A numerical

approach shows which difference vectors provide the minimum distances, and then we can obtain the optimized precoding matrix by equalizing these distances. For any number of available datastreams, we will present a general form of the precoding matrix.

The chapter is organized as follows. A new parameterized form of the precoding matrix is described in section 6.1. Section 6.2 is devoted to the description of the new precoder which is based on the observation of the SNR-like matrix. In section 6.3, we propose general extensions of the precoder for large MIMO channels and rectangular QAM modulations. Finally, the simulation results in comparison with other traditional precoders are presented in section 6.4. The conclusion is given in section 6.5.

6.1 Parameterization of the precoding matrix

We now intend to design a precoder to minimize the probability of error subject to the constraint of transmission powers. This design is difficult because it is rarely solvable in closed form: the solution depends on the symbol alphabet and the detection rule. The average error probability can be approximated by [70]

$$P_e \simeq \frac{1}{M_s} \sum_{i=1}^{M_s} \sum_{\substack{j=1 \\ j \neq i}}^{M_s} Q\left(\frac{\bar{d}_{ij}}{2\sqrt{N_0}} \times \sqrt{E_s} \right), \tag{6.1}$$

where N_0 is the variance of the white Gaussian noise η_v, and $\bar{d}_{ij}$ is the normalized Euclidean distance between two vector $\mathbf{s}_i$ and $\mathbf{s}_j$. Let us note N_i the number of distances $\bar{d}_{ij}$ such that $\bar{d}_{ij} = d_{\min}$, where $d_{\min}$ denotes the minimum Euclidean distance and is defined by

$$d^2_{\min} = \min_{\mathbf{s}_k, \mathbf{s}_l \in S, \mathbf{s}_k \neq \mathbf{s}_l} \|\mathbf{H}_v \mathbf{F}_d (\mathbf{s}_k - \mathbf{s}_l)\|^2.$$

The probability of error in (6.1) can be now simplified as

$$\begin{aligned} P_e &\approx \frac{1}{M_s} \sum_{i=1}^{M_s} \mathrm{N}_i \, Q\left(\frac{\bar{d}_{\min}}{2\sqrt{N_0}} \times \sqrt{E_s} \right) \\ &\approx \mathrm{N}_{d_{\min}} \, Q\left(\frac{\bar{d}_{\min}}{2\sqrt{N_0}} \times \sqrt{E_s} \right), \end{aligned} \tag{6.2}$$

where M_s is the number of all possible transmitted vectors $\mathbf{s}$, and $\mathrm{N}_{d_{\min}} = \frac{1}{M_s} \sum_{i=1}^{M_s} \mathrm{N}_i$. It is observed that when an ML detection is considered at the receiver, a key to reduce

the probability of error is maximizing the minimum Euclidean distance between received symbols. We can now formulate the design problem as follows

$$\begin{aligned} &\arg\max_{\mathbf{F}_d} d^2_{\min} \\ &\text{subject to:} \quad \text{trace}\{\mathbf{F}_d\mathbf{F}_d^*\} = E_s. \end{aligned} \tag{6.3}$$

In general, by using a singular value decomposition (SVD), a linear precoder can be considered as a combination of an input shaper and a multimode beamformer with per-beam power allocation [10]

$$\mathbf{F}_d = \mathbf{A}\mathbf{\Sigma}\mathbf{B}^*, \tag{6.4}$$

where $\mathbf{A}$ and $\mathbf{B}^*$ are $b \times b$ unitary matrices, and $\mathbf{\Sigma}$ is a diagonal matrix. The orthogonal beam directions are the left singular matrix $\mathbf{A}$, of which each column represents a beam direction (pattern). It is noted that the matrix $\mathbf{A}$ contains all eigenvectors of the matrix $\mathbf{F}_d\mathbf{F}_d^*$, thus it is often referred to as eigen-beamforming. The matrix $\mathbf{\Sigma}$ controls the power allocation on each beam. These powers correspond to the squared singular values of $\mathbf{\Sigma}^2$. The right singular matrix $\mathbf{B}^*$ concerns with the rotation and scaling of the input symbols on each beam and hence is referred to as the input-shaping matrix.

Let us define $\breve{\mathbf{x}}$ a difference vector as $\breve{\mathbf{x}} = \mathbf{s}_k - \mathbf{s}_l$, with $\mathbf{s}_k \neq \mathbf{s}_l$, and the set which contains all possible difference vectors as $\breve{X}$. The optimized criterion is then

$$\begin{aligned} d^2_{\min} &= \min_{\breve{\mathbf{x}}\in\breve{X}} \|\mathbf{H}_v\mathbf{F}_d\breve{\mathbf{x}}\|^2 \\ &= \min_{\breve{\mathbf{x}}\in\breve{X}} \breve{\mathbf{x}}^*\mathbf{F}_d^*\mathbf{H}_v^*\mathbf{H}_v\mathbf{F}_d\breve{\mathbf{x}} \\ &= \min_{\breve{\mathbf{x}}\in\breve{X}} \breve{\mathbf{x}}^*\mathbf{B}\mathbf{\Sigma}^*\mathbf{A}^*\mathbf{R}_H\mathbf{A}\mathbf{\Sigma}\mathbf{B}^*\breve{\mathbf{x}}, \end{aligned} \tag{6.5}$$

where $\mathbf{R}_H$ denotes the channel covariance matrix, i.e. $\mathbf{R}_H = \mathbf{H}_v^*\mathbf{H}_v = \text{diag}(\rho_1, ..., \rho_b)$. One should note that $\mathbf{R}_H$ is a diagonal matrix because the virtual channel $\mathbf{H}_v$ is already diagonalized.

Lemma 6.1. *Without loss of optimality, the left singular matrix* $\mathbf{A}$ *of the optimal precoder* $\mathbf{F}_d$ *can always be chosen to coincide with an identity matrix.*

Proof: We first consider the eigen-decomposition of the matrix

$$\mathbf{\Sigma}^*\mathbf{A}^*\mathbf{R}_H\mathbf{A}\mathbf{\Sigma} = \mathbf{Q}\mathbf{\Lambda}\mathbf{Q}^*, \tag{6.6}$$

where $\mathbf{Q}$ is an orthonormal matrix and $\mathbf{\Lambda}$ is a diagonal matrix. The minimum distance in (6.5) can be now rewritten as

$$d_{\min}^2 = \min_{\breve{\mathbf{x}} \in \breve{X}} \breve{\mathbf{x}}^* \mathbf{B}\mathbf{Q}\mathbf{\Lambda}\mathbf{Q}^*\mathbf{B}^*\breve{\mathbf{x}}. \tag{6.7}$$

Let us denote λ_k as the diagonal elements of the matrix $\mathbf{\Lambda}$. Note that the number of non-null diagonal elements of $\mathbf{\Lambda}$ is less than the number of datastreams b. Therefore, it is always possible to find a diagonal matrix of the form $\tilde{\mathbf{\Sigma}} = \text{diag}(\sqrt{\tilde{\sigma}_1}, ..., \sqrt{\tilde{\sigma}_k})$ that satisfies

$$\tilde{\mathbf{\Sigma}}^* \mathbf{R}_H \tilde{\mathbf{\Sigma}} = \mathbf{\Lambda}, \tag{6.8}$$

where the diagonal elements of $\tilde{\mathbf{\Sigma}}$ are defined by $\tilde{\sigma}_k = \lambda_k / \rho_k$. The distance $d_{\min}$ in (6.7) can be now simplified to

$$\begin{aligned} d_{\min}^2 &= \min_{\breve{\mathbf{x}} \in \breve{X}} \breve{\mathbf{x}}^* \mathbf{B}\mathbf{Q}\tilde{\mathbf{\Sigma}}^* \mathbf{R}_H \tilde{\mathbf{\Sigma}}\mathbf{Q}^*\mathbf{B}^*\breve{\mathbf{x}} \\ &= \min_{\breve{\mathbf{x}} \in \breve{X}} \breve{\mathbf{x}}^* \tilde{\mathbf{B}}\tilde{\mathbf{\Sigma}}^* \mathbf{R}_H \tilde{\mathbf{\Sigma}}\tilde{\mathbf{B}}^*\breve{\mathbf{x}}, \end{aligned} \tag{6.9}$$

with $\tilde{\mathbf{B}}$ is defined by $\tilde{\mathbf{B}} = \mathbf{B}\mathbf{Q}$. By comparing (6.5) and (6.9), we can conclude that there exists a precoding matrix $\tilde{\mathbf{F}}_\mathbf{d} = \tilde{\mathbf{\Sigma}}\tilde{\mathbf{B}}^*$ such that its minimum Euclidean distance is the same with the one provided by $\mathbf{F}_d$.

■

From the result in Lemma 1, it follows that the max-$d_{\min}$ precoder can be parameterized as

$$\mathbf{F}_d = \mathbf{\Sigma}\mathbf{B}^*, \tag{6.10}$$

where $\mathbf{B}^*$ is a $b \times b$ unitary matrix, and $\mathbf{\Sigma} = \text{diag}(\sqrt{\sigma_1}, ..., \sqrt{\sigma_b})$ is a $b \times b$ diagonal matrix with nonnegative real numbers on the diagonal. The power constraint can be then rewritten as

$$\text{trace}\{\mathbf{F}_d\mathbf{F}_d^*\} = \text{trace}\{\mathbf{\Sigma}\mathbf{\Sigma}^*\} = E_s. \tag{6.11}$$

6.2 Design of the precoding matrix

6.2.1 Principle of the approach

Design optimizing the minimum Euclidean distance is difficult to deal with because of two reasons. Firstly, the space of solution is large and exponentially proportional to the number of datastreams b. Secondly, the exact expression of max-$d_{\min}$ precoder depends on many parameters such as the symbol alphabet or the characteristic of the virtual channel. Here, we propose a design that can come close to the desired goal. Based on (6.3), the formulation of the problem can be rewritten as

$$\max_{\mathbf{F}_d} \min_{\breve{\mathbf{x}} \in \breve{X}} d^2_{\breve{\mathbf{x}}} = \breve{\mathbf{x}}^* \mathbf{F}_d^* \mathbf{H}_v^* \mathbf{H}_v \mathbf{F}_d \breve{\mathbf{x}}. \tag{6.12}$$

Let us define a SNR-like matrix of $\mathbf{F}_d$ as $\mathrm{SNR}(\mathbf{F}_d) = \mathbf{F}_d^* \mathbf{H}_v^* \mathbf{H}_v \mathbf{F}_d$. Instead of optimizing (6.12), we can obtain a suboptimal but more general solution by realizing some properties of $\mathrm{SNR}(\mathbf{F}_d)$. The authors in [33] proposed a suboptimal precoder which is based on the observation of the minimum eigenvalue of $\mathrm{SNR}(\mathbf{F}_d)$. We present, herein, another suboptimal solution that considers the minimum diagonal element of the SNR-like matrix. Let us denote the diagonal elements of $\mathrm{SNR}(\mathbf{F}_d)$ as δ_k, we have

$$d^2_{\breve{\mathbf{x}}} = \breve{\mathbf{x}}^* \mathrm{SNR}(\mathbf{F}_d) \breve{\mathbf{x}} = \sum_{i=1}^{b} \delta_i x_i^2 + \mathcal{O}(x_i x_j)_{x_i \neq x_j}, \tag{6.13}$$

with $\breve{\mathbf{x}} = [x_1, .., x_b]^T$. For a random difference vector $\breve{\mathbf{x}}$, we can assume that the function $\mathcal{O}(x_i x_j)$ has little influence on the minimum distance in comparison with the sum of $\delta_i x_i^2$. The design problem can be, therefore, simplified by

$$\max_{\mathbf{F}_d} \min_{\breve{\mathbf{x}} \in \breve{X}} \sum_{i=1}^{b} \delta_i x_i^2. \tag{6.14}$$

The criterion on the right-hand side of (6.14) has a lower bound

$$\min_{\breve{\mathbf{x}} \in \breve{X}} \sum_{i=1}^{b} \delta_i x_i^2 \geq \delta_{\min} \min_{\breve{\mathbf{x}} \in \breve{X}} \sum_{i=1}^{b} x_i^2 = \delta_{\min} \min_{\breve{\mathbf{x}} \in \breve{X}} \|\breve{\mathbf{x}}\|^2, \tag{6.15}$$

where $\delta_{\min}$ denotes the minimum diagonal element of $\mathrm{SNR}(\mathbf{F}_d)$. It is observed that maximizing the minimum diagonal element $\delta_{\min}(\mathrm{SNR}(\mathbf{F}_d))$ will possibly force the minimum

distance to higher value. Therefore, we can solve the problem in (6.12) by first dealing with $\delta_{\min}(\mathrm{SNR}(\mathbf{F}_d))$ and then maximizing its value. By substituting (6.10) into the form of $\mathrm{SNR}(\mathbf{F}_d)$, we obtain

$$\mathrm{SNR}(\mathbf{F}_d) = \mathbf{B}\boldsymbol{\Sigma}^*\mathbf{H}_v^*\mathbf{H}_v\boldsymbol{\Sigma}\mathbf{B}^* = \mathbf{B}\boldsymbol{\Upsilon}\mathbf{B}^*, \tag{6.16}$$

where $\boldsymbol{\Upsilon} = \mathrm{diag}(\rho_1\sigma_1, ..., \rho_b\sigma_b) = \mathrm{diag}(\lambda_1, ..., \lambda_b)$ is a diagonal matrix with non-negative real numbers on the diagonal. For any given $\boldsymbol{\Upsilon}$, an optimal choice for $\mathbf{B}$ is one that maximizes the minimum diagonal element of $\mathrm{SNR}(\mathbf{F}_d)$. Such $\mathbf{B}$ is provided by the following lemma.

Lemma 6.2. *Given a $b \times b$ diagonal matrix $\boldsymbol{\Upsilon}$ whose diagonal elements are non-negative and a unitary matrix $\mathbf{B}$ of size b, then we have the following properties*

i)

$$\max_{\mathbf{B}\mathbf{B}^*=\mathbf{I}_b} \min_i [\mathbf{B}\boldsymbol{\Upsilon}\mathbf{B}^*]_{i,i} = \frac{\mathrm{trace}(\boldsymbol{\Upsilon})}{b}. \tag{6.17}$$

ii) The optimized value in (6.17) is provided by a normalized DFT-matrix

$$\mathbf{B}^* = \mathbf{D}_b = \frac{1}{\sqrt{b}} \begin{pmatrix} 1 & 1 & 1 & \cdots & 1 \\ 1 & \omega & \omega^2 & \cdots & \omega^{b-1} \\ 1 & \omega^2 & \omega^4 & \cdots & \omega^{2(b-1)} \\ \vdots & \vdots & \vdots & & \vdots \\ 1 & \omega^{b-1} & \omega^{2(b-1)} & \cdots & \omega^{(b-1)(b-1)} \end{pmatrix}, \tag{6.18}$$

where ω is a primitive b^{th} root of unity, i.e. $\omega = e^{-\frac{2\pi i}{b}}$.

Proof: Firstly, we prove that the right-hand side of (6.17) is the upper-bound for the left-hand side. Then, we show that the DFT-matrix $\mathbf{D}_b$ provides this upper bound.

i) Since $\mathbf{B}$ is a unitary matrix and $\boldsymbol{\Upsilon}$ is a diagonal matrix, we have

$$\sum_{i=1}^{b} \delta_i = \mathrm{trace}(\mathbf{B}\boldsymbol{\Upsilon}\mathbf{B}^*) = \mathrm{trace}(\boldsymbol{\Upsilon}). \tag{6.19}$$

Furthermore, since diagonal elements of $\boldsymbol{\Upsilon}$ are non-negative, the diagonal elements of $\mathbf{B}\boldsymbol{\Upsilon}\mathbf{B}^*$ are non-negative, too. Given the set of b non-negative numbers $\{\alpha_i\}_{i=1}^{b}$

that sum to $\mathcal{M}$, the minimum number is obviously less than $\mathcal{M}/b$. The left-hand side of (6.17) is, therefore, upper-bounded by

$$\min_i [\mathbf{B}\boldsymbol{\Upsilon}\mathbf{B}^*]_{i,i} \leq \frac{\sum_{i=1}^{b} \delta_i}{b} = \frac{\text{trace}(\boldsymbol{\Upsilon})}{b}. \tag{6.20}$$

ii) Let us define $\beta_{i,j}$ is the (i,j) element of the matrix $\mathbf{B}^*$, we have

$$[\mathbf{B}\boldsymbol{\Upsilon}\mathbf{B}^*]_{i,i} = \sum_{j=1}^{b} \lambda_j \|\beta_{i,j}\|^2. \tag{6.21}$$

If $\mathbf{B}^*$ is chosen to be a DFT-matrix, i.e. the magnitude of each element of the DFT-matrix $\mathbf{D}_b$ is equal to $|\beta_{i,j}|^2 = 1/b$, we obtain that

$$[\mathbf{B}\boldsymbol{\Upsilon}\mathbf{B}^*]_{i,i} = \sum_{j=1}^{b} \lambda_j \frac{1}{b} = \frac{\text{trace}(\boldsymbol{\Upsilon})}{b}, \tag{6.22}$$

for all $1 \leq i \leq b$.

■

Now, from the parameterized form of the precoder, we have to search the matrix $\boldsymbol{\Sigma}$ in order to optimize the minimum distance. A numerical approach shows that the minimum Euclidean distances on the received constellation are always provided by some difference vectors.

Proposition 6.3. *With the precoding matrix given by (6.10), two any Euclidean distances can be kept equal by changing only the power allocation matrix* $\boldsymbol{\Sigma}$ *but retaining the input-shaping matrix* $\mathbf{B}^*$.

Proof: We assume that, for $\hat{\mathbf{H}}_v = \text{diag}(\sqrt{\hat{\rho}_1}, ..., \sqrt{\hat{\rho}_b})$ and $\hat{\boldsymbol{\Sigma}} = \text{diag}(\sqrt{\hat{\sigma}_1}, ..., \sqrt{\hat{\sigma}_b})$, two difference vectors $\breve{\mathbf{x}}_1$, $\breve{\mathbf{x}}_2$ have the same Euclidean distances

$$\begin{cases} d^2_{\breve{\mathbf{x}}_1|\hat{\mathbf{H}}_v} = \|\hat{\mathbf{H}}_v\hat{\boldsymbol{\Sigma}}\mathbf{B}\breve{\mathbf{x}}_1\|^2 \\ d^2_{\breve{\mathbf{x}}_2|\hat{\mathbf{H}}_v} = \|\hat{\mathbf{H}}_v\hat{\boldsymbol{\Sigma}}\mathbf{B}\breve{\mathbf{x}}_2\|^2 \end{cases} \tag{6.23}$$

When the channel varies from $\hat{\mathbf{H}}_v$ to $\mathbf{H}_v = \text{diag}(\sqrt{\rho_1}, ..., \sqrt{\rho_b})$, let us define a diagonal matrix $\boldsymbol{\Sigma}$ with real nonnegative elements such that

$$\sigma_i\rho_i = \kappa\,\hat{\sigma}_i\hat{\rho}_i, \tag{6.24}$$

where κ is a constant. By substituting $\hat{\sigma}_i$ into the power constraint in (6.11), we obtain

$$\text{trace}\{\mathbf{\Sigma}\mathbf{\Sigma}^*\} = \sum_{i=1}^{b} \sigma_i = \kappa \sum_{i=1}^{b} \hat{\sigma}_i \left(\frac{\hat{\rho}_i}{\rho_i}\right) = E_s \tag{6.25}$$

or

$$\kappa = \frac{E_s}{\sum_{i=1}^{b} \hat{\sigma}_i \hat{\rho}_i / \rho_i}. \tag{6.26}$$

The Euclidean distance provided by $\breve{\mathbf{x}}_1$ is then

$$\begin{aligned} d^2_{\breve{\mathbf{x}}_1|\mathbf{H}_v} &= \|\mathbf{H}_v \mathbf{\Sigma} \mathbf{B} \breve{\mathbf{x}}_1\|^2 \\ &= \|\sqrt{\kappa}\, \hat{\mathbf{H}}_v \hat{\mathbf{\Sigma}} \mathbf{B} \breve{\mathbf{x}}_1\|^2 \\ &= \kappa\, d^2_{\breve{\mathbf{x}}_1|\hat{\mathbf{H}}_v}. \end{aligned}$$

Similarly, we get

$$d^2_{\breve{\mathbf{x}}_2|\mathbf{H}_v} = \kappa\, d^2_{\breve{\mathbf{x}}_2|\hat{\mathbf{H}}_v}.$$

Since $d^2_{\breve{\mathbf{x}}_1|\hat{\mathbf{H}}_v} = d^2_{\breve{\mathbf{x}}_2|\hat{\mathbf{H}}_v}$, we obtain $d^2_{\breve{\mathbf{x}}_1|\mathbf{H}_v} = d^2_{\breve{\mathbf{x}}_2|\mathbf{H}_v}$. Consequently, two any difference distances can be kept equal by changing only the power allocation matrix $\mathbf{\Sigma}$.

■

6.2.2 Design model

Lemma 2 provides an interesting key to design a new linear precoder. The precoding matrix $\mathbf{F}_d$ is then factorized as the product of the power allocation matrix $\mathbf{\Sigma}$ and the scaling matrix $\mathbf{B}^*$. As its name implies, the matrix $\mathbf{\Sigma}$ determines how many virtual channels are used to transmit signal and controls the power allocation on each beam. The maximum number of activated virtual channels is upper-bounded by the rank of matrix $\mathbf{H}$. We assume that the signal is transmitted on k subchannels, with $k \leq b = \text{rank}(\mathbf{H})$. The matrix $\mathbf{B}^*$ is then chosen to be a normalized DFT-matrix of size k. According to the proposition 1, the diagonal matrix $\mathbf{\Sigma}$ depends on the channel characteristics, and has k positive real elements on the diagonal ($1 \leq k \leq b$). Therefore, we have b different expressions of $\mathbf{F}_d$ corresponding to b precoders which pour powers on 1, 2,.., and b virtual subchannels, respectively.

The precoding system structure, which contains an input-shaping matrix and a power allocation matrix, is shown in the Fig. 6.1. Due to different forms of CSIT, the precoder first decides the number of virtual subchannels used for transmission, and then maps the data-bits into k symbols. The method used for selecting the modulation will be discussed in section 6.3.2. After that these symbols are pre-processed by a DFT block of size k. At the end of the precoder, the transmit signal is directly operated by a power distribution block, i.e. multiplied to a diagonal matrix $\mathbf{\Sigma}$.

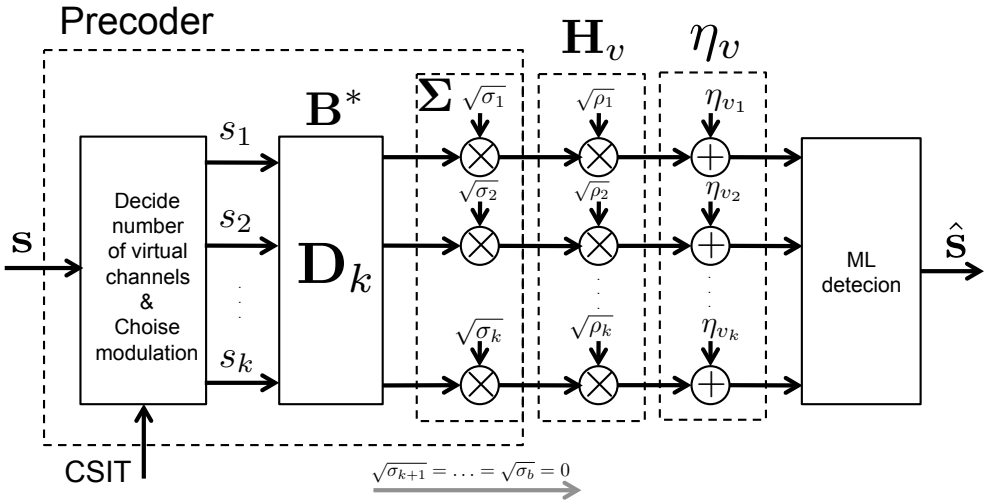

FIGURE 6.1: Design model of the precoding matrix

The determination of the power allocation matrix $\mathbf{\Sigma}$ depends on the symbol alphabet or the modulation used at the transmitter. Our objective is to determine the matrix $\mathbf{\Sigma}$ that maximizes the minimum distance for all possible transmit vectors. In next section, we propose the optimized solution for one of the most common schemes: rectangular Quadrature Amplitude Modulation (QAM).

6.3 Optimized precoder for rectangular QAM modulations

For a rectangular 4^m-QAM modulation, the transmit symbols belong to the set

$$S = \frac{1}{\sqrt{M}} \{a + b\,i\,;\, a - b\,i\,;\, -a + b\,i\,;\, -a - b\,i\}\,, \tag{6.27}$$

where $M = \frac{2}{3}(4^m - 1)$ and $a, b \in \{1, 3, \ldots, 2^m - 1\}$.

Our main purpose is to derive a matrix $\mathbf{\Sigma}$ subject to the power constraint (6.11) in order to optimize the minimum distance. The number of non-null diagonal elements in (6.11) presents the number of virtual-subchannels used for transmission. Let us denote the precoder which enables powers on k subchannels as $\mathbf{F}_k$ with $k = 1, \cdots, b$. These precoders are presented as follows.

6.3.1 Expressions of the precoder

According to (6.24) and (6.26), the diagonal entries of the optimization matrix $\mathbf{\Sigma}$ are given by

$$\sigma_i = \frac{E_s}{\sum_{j=1}^{k} \phi_j \rho_j^{-1}} \phi_i \rho_i^{-1}, \tag{6.28}$$

where ϕ_j denotes the power coefficient of the j^{th} virtual subchannel. It is obvious that the diagonal elements of $\mathbf{\Sigma}$ are linearly proportional with ϕ_j. A numerical approach is implemented in order to find which difference vectors provide the minimum distance. By equalizing the difference distances obtained by these vectors, we can derive the power coefficient ϕ_j of the optimization problem. The normalized coefficients ϕ_j are described in Tab. 6.1.

Expression	ϕ_1	ϕ_2	ϕ_3	ϕ_4	ϕ_k
$\mathbf{\Sigma}_1$	1				
$\mathbf{\Sigma}_2$	3	1			
$\mathbf{\Sigma}_3$	$6+2\sqrt{3}$	$2+\sqrt{3}$	1		
$\mathbf{\Sigma}_4$	9	5	1	1	
$\mathbf{\Sigma}_k$	...	...	...	...	...

TABLE 6.1: Optimized coefficients of the power allocation matrix $\mathbf{\Sigma}$.

Precoder $\mathbf{F}_1$

This precoder is actually the max-SNR design which pours power on only the strongest virtual subchannel, i.e. $\mathbf{\Sigma} = \text{diag}\{\sqrt{E_s}, 0, \cdots, 0\}$. In order to retain the data-rate, the precoder $\mathbf{F}_1$ can use a higher-order QAM modulation. In other words, it can transforms 4^m-QAM signals on b virtual subchannels into a rectangular $4^{b.m}$-QAM signal on the first subchannel (detailed in section 6.3.2). The minimum distance provided by $\mathbf{F}_1$ is defined by

$$d^2_{\mathbf{F}_1} = \frac{4}{M} E_s \rho_1. \tag{6.29}$$

Precoder $\mathbf{F}_2$

This precoder is the second expression of the N-$d_{\min}$ precoder which is presented in our previous work [70]. A numerical search shows that the optimized solution is obtained by two difference vectors $\breve{\mathbf{x}}_1 = \frac{1}{\sqrt{M}}[0\,2]^T$, and $\breve{\mathbf{x}}_2 = \frac{1}{\sqrt{M}}[2\text{-}2]^T$. By equalizing two normalized distances $\bar{d}^2_{\breve{x}_1} = \bar{d}^2_{\breve{x}_2}$, we obtain

$$\mathbf{F}_2 = \sqrt{\frac{E_s}{2}} \begin{pmatrix} \cos\psi & 0 \\ 0 & \sin\psi \end{pmatrix} \begin{pmatrix} 1 & 1 \\ \text{-}1 & 1 \end{pmatrix}, \tag{6.30}$$

where $\psi = \text{atan}(\sqrt{\rho_1/3\rho_2})$. The distance $d_{\min}$ provided by $\mathbf{F}_2$ is

$$d^2_{\mathbf{F}_2} = \frac{4}{M} E_s \frac{2\rho_1\rho_2}{\rho_1 + 3\rho_2}\,. \tag{6.31}$$

The received constellation provided by the precoder $\mathbf{F}_2$ is shown in Fig. 6.2. One should note that whenever two received vectors are close on one virtual subchannel, they are distant on the other (e.g. points A and B). Furthermore, it is observed that the average number of neighbors providing $d_{\min}$ of $\mathbf{F}_2$ is less than that of the max-$d_{\min}$ precoder presented in [37]. The property confirms an improvement of BER performance for our proposed precoder.

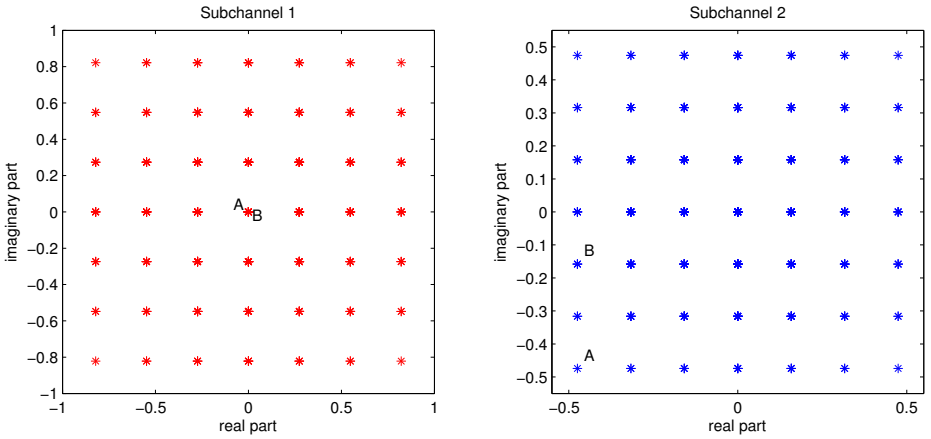

FIGURE 6.2: Received constellation for the precoder $\mathbf{F}_2$.

Precoder $\mathbf{F}_3$

This precoder pours power on three virtual subchannels, and has the input-shaping matrix $\mathbf{B}^*$ which is defined by

$$\mathbf{B}^* = \frac{1}{\sqrt{3}} \begin{pmatrix} 1 & 1 & 1 \\ 1 & \frac{-1-\sqrt{3}i}{2} & \frac{-1+\sqrt{3}i}{2} \\ 1 & \frac{-1+\sqrt{3}i}{2} & \frac{-1-\sqrt{3}i}{2} \end{pmatrix}. \tag{6.32}$$

A numerical approach shows that the optimized solution is obtained by three difference vectors

$$\begin{cases} \breve{\mathbf{x}}_1 = \frac{1}{\sqrt{M}}[0,0,2]^T \\ \breve{\mathbf{x}}_2 = \frac{1}{\sqrt{M}}[0,2,-2]^T \\ \breve{\mathbf{x}}_3 = \frac{1}{\sqrt{M}}[2,-2-2i,2i]^T \end{cases}$$

By equalizing three difference distances provided by these vectors, we obtain

$$\begin{cases} \sigma_2/\sigma_3 = \frac{2+\sqrt{3}}{\rho_2/\rho_3} \\ \sigma_1/\sigma_3 = \frac{6+2\sqrt{3}}{\rho_1/\rho_3} \end{cases} \tag{6.33}$$

The distance $d_{\min}$ obtained by $\mathbf{F}_3$ is then

$$d^2_{\mathbf{F}_3} = \frac{4}{M} E_s \frac{(3+\sqrt{3})\rho_1\rho_2\rho_3}{\rho_1\rho_2 + (2+\sqrt{3})\rho_1\rho_3 + (6+2\sqrt{3})\rho_2\rho_3}. \tag{6.34}$$

Fig. 6.3 plots the received constellation provided by the precoder $\mathbf{F}_3$ in the case of 4-QAM. Like the case of the precoder $\mathbf{F}_2$, two received vectors processed by $\mathbf{F}_3$ are close on one virtual subchannel but can be distant on the others (for example points B and C).

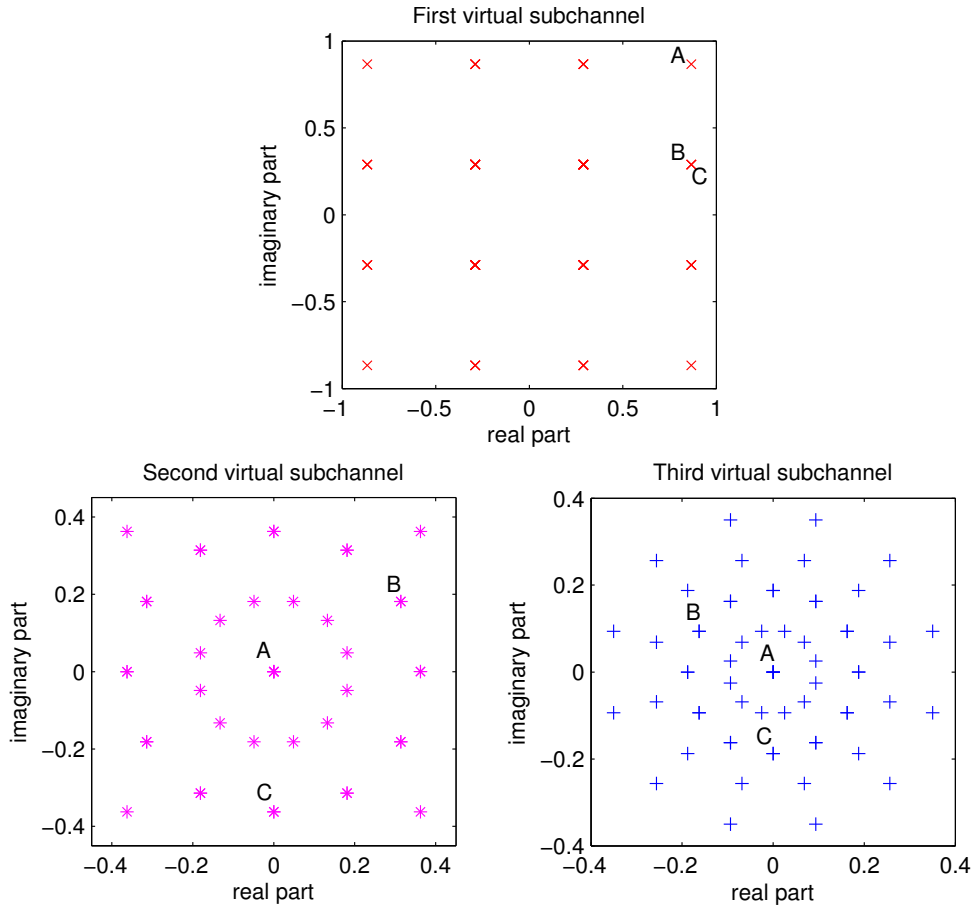

FIGURE 6.3: Received constellations provided by precoder $\mathbf{F}_3$.

Precoder $\mathbf{F}_4$

The input-shaping matrix $\mathbf{B}^*$ of the precoder $\mathbf{F}_4$ is defined by

$$\mathbf{B}^* = \frac{1}{2}\begin{pmatrix} 1 & 1 & 1 & 1 \\ 1 & -i & -1 & i \\ 1 & -1 & 1 & -1 \\ 1 & i & -1 & -i \end{pmatrix}. \tag{6.35}$$

A numerical search shows that the minimum distance is provided by four difference vectors

$$\begin{cases} \breve{\mathbf{x}}_1 = \frac{1}{\sqrt{M}}[0,0,0,2]^T \\ \breve{\mathbf{x}}_2 = \frac{1}{\sqrt{M}}[0,0,2,-2]^T \\ \breve{\mathbf{x}}_3 = \frac{1}{\sqrt{M}}[0,2,-2-2i,2i]^T \\ \breve{\mathbf{x}}_4 = \frac{1}{\sqrt{M}}[2,-2,2,-2]^T \end{cases}$$

By equalizing their difference distances, we obtain

$$\begin{cases} \sigma_3/\sigma_4 = \frac{1}{\rho_3/\rho_4} \\ \sigma_2/\sigma_4 = \frac{5}{\rho_2/\rho_4} \\ \sigma_1/\sigma_4 = \frac{9}{\rho_1/\rho_4} \end{cases} \tag{6.36}$$

The distance $d_{\min}$ obtained by $\mathbf{F}_4$ is given by

$$d^2_{\mathbf{F}_4} = \frac{4}{M} E_s \frac{4}{9/\rho_1 + 5/\rho_2 + 1/\rho_3 + 1/\rho_4}. \tag{6.37}$$

The general case $\mathbf{F}_k$

Let us denote $\breve{\mathbf{x}}_1, \breve{\mathbf{x}}_2, \cdots, \breve{\mathbf{x}}_k$ as k difference vectors providing the minimum distance. The distance $d_{\breve{\mathbf{x}}_i}$ is given by

$$\begin{aligned} d^2_{\breve{\mathbf{x}}_i} &= \breve{\mathbf{x}}_i^* \mathbf{B} \boldsymbol{\Upsilon} \mathbf{B}^* \breve{\mathbf{x}}_i \\ &= \sum_{j=1}^{k} \lambda_j |u_{i(j)}|^2 \end{aligned} \tag{6.38}$$

where $\boldsymbol{\Upsilon} = \boldsymbol{\Sigma}^* \mathbf{H}_v^* \mathbf{H}_v \boldsymbol{\Sigma} = \text{diag}(\lambda_1, ..., \lambda_k)$, and vector $\mathbf{u}_i$ is given by

$$\mathbf{u}_i = \mathbf{B}^* \breve{\mathbf{x}}_i = \left[u_{i(1)}, u_{i(2)}, \cdots, u_{i(k)}\right]^T. \tag{6.39}$$

By equalizing k difference distances, we have $(k-1)$ equations below

$$\sum_{j=1}^{k} \lambda_j \left(|u_{1(j)}|^2 - |u_{i(j)}|^2\right) = \sum_{j=1}^{k} \lambda_j v_{i,j} = 0, \tag{6.40}$$

where $v_{i,j} = |u_{1(j)}|^2 - |u_{i(j)}|^2$ with $i = 2, \cdots, k$. For a 4^m-QAM modulation, it is noted that the difference vector $\breve{\mathbf{x}}_1$ is often defined by $\breve{\mathbf{x}}_1 = [0, \cdots, 0, 2]^T$, i.e. $|u_{1(j)}|^2 = 4$ with $j = 1 \cdots k$. The power constrain in (6.11) can be now rewritten as

$$\sum_{j=1}^{k} \lambda_j/\rho_j = \sum_{j=1}^{k} \sigma_j = E_s. \tag{6.41}$$

Let us define $\lambda = [\lambda_1, \cdots, \lambda_k]^T$, and $v_{1,j} = 1/\rho_j$ with $j = 1, \cdots, k$, we have

$$\begin{pmatrix} v_{1,1} & v_{1,2} & \cdots & v_{1,k} \\ v_{2,1} & v_{2,2} & \cdots & v_{2,k} \\ \vdots & \vdots & & \vdots \\ v_{k,1} & v_{k,2} & \cdots & v_{k,k} \end{pmatrix} \begin{pmatrix} \lambda_1 \\ \lambda_2 \\ \vdots \\ \lambda_k \end{pmatrix} = \begin{pmatrix} E_s \\ 0 \\ \vdots \\ 0 \end{pmatrix} \tag{6.42}$$

or

$$\mathbf{V}\lambda = \epsilon. \tag{6.43}$$

In conclusion, the power coefficients ϕ_i are proportional to the entries of the vector λ which can be defined by $\lambda = \mathbf{V}^{-1}\epsilon$. The condition of the existence of the vector λ is that the matrix $\mathbf{V}$ is invertible. When $\breve{\mathbf{x}}_1 = [0, \cdots, 0, 2]^T$ is one of the difference vectors providing the minimum distance, the distance $d_{\min}$ is then defined by

$$d^2_{\mathbf{F}_k} = 4 \sum_{j=1}^{k} \lambda_j. \tag{6.44}$$

6.3.2 Range of definition

To improve the BER performance of a MIMO system, we choose from these precoding matrices above the precoder that provides the highest minimum Euclidean distance. One should note that the data-rate of a precoder $\mathbf{F}_i$ is different to each other's. For example, if we both use 4-QAM modulation for the precoders $\mathbf{F}_1$ and $\mathbf{F}_2$, the bit-rate of $\mathbf{F}_2$ is twice as that of $\mathbf{F}_1$. Therefore, we have to consider the data-rate of the b precoders when comparing their distances $d_{\min}$. The error probability in (6.2) can be re-expressed as

$$P_e \approx \mathrm{N}_{d_{\min}} Q\left(\frac{\bar{d}_{\min}}{2} \times \sqrt{\mathrm{SNR} \frac{B}{f_s} \frac{1}{\log_2 M}} \right), \tag{6.45}$$

where M is the number of alternative modulation symbols, B is the bandwidth, and f_s is the symbol rate. For a given modulation order, by comparing the right-hand side of (6.45) corresponding to b precoders, we can obtain the range of definition for each precoding scheme.

Another simple method to retain the data-rate is using different modulation for each precoder. Lets us come back to the example of the precoders $\mathbf{F}_1$ and $\mathbf{F}_2$. If the 4-QAM modulation is used for the precoder $\mathbf{F}_2$, it means that two 2-bits symbols are

transferred on two subchannels. Instead of transmitting like this, we can transfer one 4-bits symbols (16-QAM) on the first virtual subchannels. Then, two minimum distances that correspond to $\mathbf{F}_1$ using 16-QAM and $\mathbf{F}_2$ using 4-QAM are compared in order to determine the range of definition for two precoders $\mathbf{F}_1$ and $\mathbf{F}_2$.

$$\begin{cases} d^2_{\mathbf{F}_1} = \frac{2}{5} E_s \rho_1 \\ d^2_{\mathbf{F}_2} = 2\, E_s \frac{2\rho_1\rho_2}{\rho_1+3\rho_2} \end{cases} \tag{6.46}$$

In other words, if $d^2_{\mathbf{F}_1} > d^2_{\mathbf{F}_2}$ or $\rho_1/\rho_2 > 7$: the precoder $\mathbf{F}_1$ is chosen, and for $\rho_1/\rho_2 < 7$: the precoder $\mathbf{F}_2$ is selected. Other precoders can be implemented in a similar way.

6.4 Simulation results

6.4.1 Comparison of minimum Euclidean distance

In this section, we indicate the improvement of the proposed precoder in terms of the minimum Euclidean distance compared to diagonal precoders. Indeed, the minimum Euclidean distance provided by a diagonal precoder is

$$\begin{aligned} d^2_{\min} &= \min_{\mathbf{s},\mathbf{r}\in S, \mathbf{s}\neq\mathbf{r}} \|\mathbf{H}_v \mathbf{F}_d(\mathbf{s}-\mathbf{r})\|^2 \\ &= \min_{\mathbf{s},\mathbf{r}\in S, \mathbf{s}\neq\mathbf{r}} \sum_i^b \rho_i f_i^2 |s_i - r_i|^2 \end{aligned} \tag{6.47}$$

where $\mathbf{s} = [s_1, s_2, .., s_b]^T$, $\mathbf{r} = [r_1, r_2, .., r_b]^T$, and $\mathbf{F}_d = \mathrm{diag}(f_1, .., f_b)$. One should note that the minimum Euclidean distance is obtained when the two vectors $\mathbf{s}$ and $\mathbf{r}$ are different from only a symbol. The minimum Euclidean distance of $\mathbf{F}_d$ is then given by

$$\begin{aligned} d^2_{\min} &= \min_{\mathbf{s},\mathbf{r}\in S, \mathbf{s}\neq\mathbf{r}} \min_{i=1..b} \rho_i f_i^2 |s_i - r_i|^2 \\ &= \min_{i=1..b} \rho_i f_i^2 \min_{\mathbf{s},\mathbf{r}\in S, \mathbf{s}\neq\mathbf{r}} |s_i - r_i|^2 \\ &= \frac{4}{M} \min_{i=1..b} \rho_i f_i^2. \end{aligned} \tag{6.48}$$

It is noted that the diagonal entries of $\mathbf{H}_v = \text{diag}(\sqrt{\rho_1}, ..., \sqrt{\rho_b})$ are sorted in decreasing order, i.e. $\rho_1 \geq \rho_2 \geq \cdots \geq \rho_b$. By comparing the right-hand side of (6.48), the minimum distances corresponding to some traditional precoders, for example: beamforming, max-$\lambda_{\min}$ [33], WaterFiling [12], and MMSE [32], are determined. Tab. 6.2 illutrates the distance $d_{\min}$ obtained by these diagonal precoders in comparison with our proposed precoder, where $(x)^+ \overset{\text{def}}{=} \max(x, 0)$.

The normalized minimum distances for $b = 2$ virtual subchannels and 4-QAM modulation are illustrated in Fig. 6.4. It is observed that our precoder provides a large improvement in terms of $d_{\min}$ compared to the diagonal precoders. In comparison with the max-$d_{\min}$ precoder presented in [37], the proposed precoder has a small difference in the minimum distance. However, its average number of neighbors providing $d_{\min}$ is less than that of the max-$d_{\min}$ precoder [70]. According to the improvement of the minimum distance and the number of neighbors $\text{N}_{d_{\min}}$, an improvement of BER performance is expected for the new precoder.

Precoder	Minimum Euclidean distance $d^2_{\min}$
Beamforming	$\frac{4}{M} E_s \rho_1$
Water-filling	$\frac{4}{M}\left(\rho_b \frac{E_s + \sum_{j=1}^{b} 1/\rho_j}{b} - 1\right)^+$
MMSE	$\frac{4}{M}\left(\sqrt{\rho_b}\frac{E_s + \sum_{j=1}^{b} 1/\rho_j}{\sum_{j=1}^{b} 1/\sqrt{\rho_j}} - 1\right)^+$
max-$\lambda_{\min}$	$\frac{4}{M}\frac{E_s}{\sum_{j=1}^{b} 1/\rho_j}$
Our proposed scheme	$\begin{cases} \frac{4}{M} E_s \rho_1 & \text{for } \mathbf{F}_1 \\ \frac{4}{M} E_s \frac{2\rho_1\rho_2}{\rho_1 + 3\rho_2} & \text{for } \mathbf{F}_2 \\ \cdots\cdots & \end{cases}$

TABLE 6.2: Comparison of the minimum Euclidean distances.

6.4.2 Bit-Error-Rate performance

In this section, the BER performance of the proposed precoder is illustrated in comparison with other traditional precoding strategies. The proposed precoder obtains a significant improvement of BER performance in comparison with the diagonal precoders: WaterFiling, MMSE, and max-$\lambda_{\min}$. A gain about 6 dB can be observed at high SNR. Furthermore, as discussed above, our precoder has the number of neighbors providing

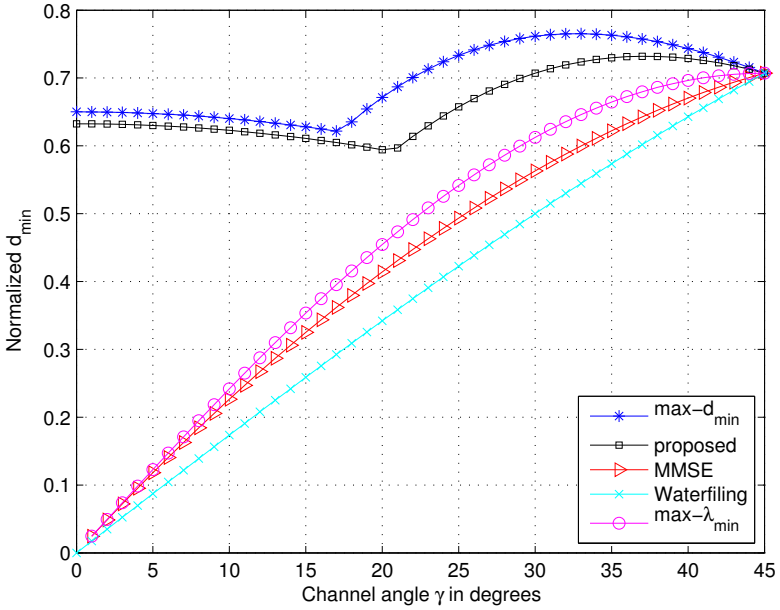

FIGURE 6.4: Normalized minimum Euclidean distance for two datastreams and 4-QAM modulation, with the channel angle $\gamma = \text{atan}\sqrt{\rho_2/\rho_1}$.

$d_{\min}$ less than that of the optimal solution max-$d_{\min}$ in [37], although it has a small difference in terms of $d_{\min}$. Therefore, the new precoder provides a slight BER improvement compared to the max-$d_{\min}$ solution. The BER performance with respect to SNR for two transmit datastreams and 4-QAM modulation is plotted in Fig. 6.5.

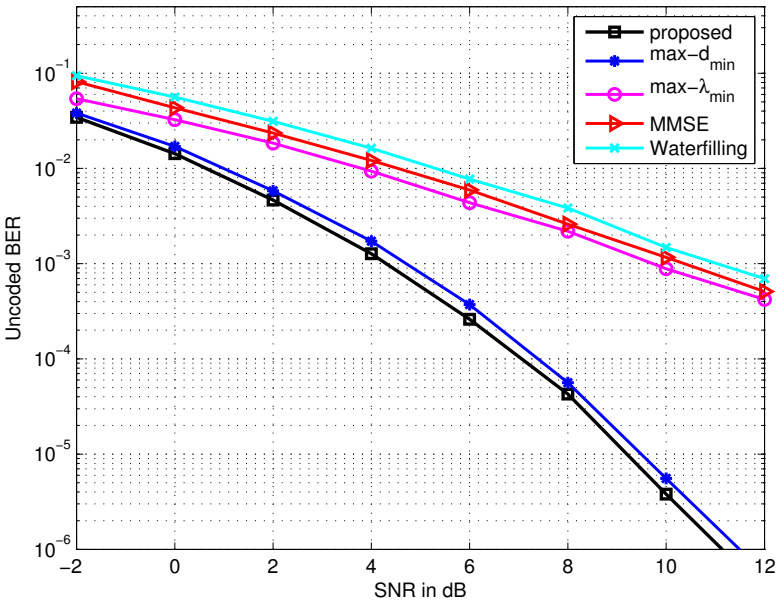

FIGURE 6.5: Uncoded BER performance for $b = 2$ datastreams.

The optimal solution for max-$d_{\min}$ precoder is presented in [37, 69], but it is only available

for two transmit datastreams with 4-QAM and 16-QAM modulations. By decomposing the channel into 2×2 eigen-channel matrices and optimize the distance $d_{\min}$ for each pair of datastreams, the authors in [59] proposed a sub-optimal precoder for large MIMO channels. This extension is split into four steps: virtual diagonalization of the channel, combination in pairs of sub-channels, application of the optimal 2D max-$d_{\min}$ solution, and power allocation on each sub-system. However, this solution is also suitable for low-order QAM modulations. A main advantage of our new precoder is that the solution is available for all rectangular QAM-modulations and for any number of datastreams.

For large MIMO simulations, we consider a system with $n_T = 5$ transmit and $n_R = 4$ receive antennas. The bit-streams are separated into $b = 4$ independent virtual subchannels, and the channel matrix $\mathbf{H}$ is i.i.d zero-mean complex Gaussian. For each SNR, the precoders are optimized for about 30,000 random matrices $\mathbf{H}$. It is observed in Fig. 6.6 that the BER performance of the max-$\lambda_{\min}$ solution is better than those of MMSE and WaterFiling. Therefore, the max-$\lambda_{\min}$ precoder is chosen to compare with our proposed precoder. Beside that some sophisticated transceivers such as: the Schur-convex ARITH-BER design [71], the linear precoder using Decision Feedback Equalization (DFE) [50], and the linear transceiver with bit allocation [72] are also mentioned in the comparison with our precoder. The comparison of the proposed precoder and other schemes for $b = 4$ transmit datastreams shows that the performance is significantly enhanced in terms of BER. We observe that the new precoder also presents a significant improvement of BER compared to the DFE, the Schur-convex ARITH-BER, and the maximum bit-rate solutions, especially when the SNR is high. The new precoder was found to be better than E-$d_{\min}$ schemes and this is due to the fact that not only the minimum distance but also the number of neighbors providing $d_{\min}$ is taken into consideration.

We also consider, in this section, the impact of imperfect CSI estimation on the BER performance of the proposed precoder. Fig. 6.7 illustrates the BER performance with respect to SNR in the case of perfect CSI and imperfect CSI estimation. The estimated channel matrix of imperfect CSI system can be modeled as $\mathbf{H}_{\text{est}} = \mathbf{H} + \mathbf{H}_{\text{err}}$, where $\mathbf{H}_{\text{err}}$ represents the channel estimation error. The optimal training signals for the MIMO-OFDM channel estimation can be found in [64]. In this simulation, we assume that the entries of $\mathbf{H}_{\text{err}}$ are complex Gaussian i.i.d random with mean zero and variance $\sigma_{\text{err}} = 0.3\,\sigma$, where σ is the variance of the complex Gaussian entries of $\mathbf{H}$. It is observed that the BER performance of our precoder decreases at high SNR, but it still remains

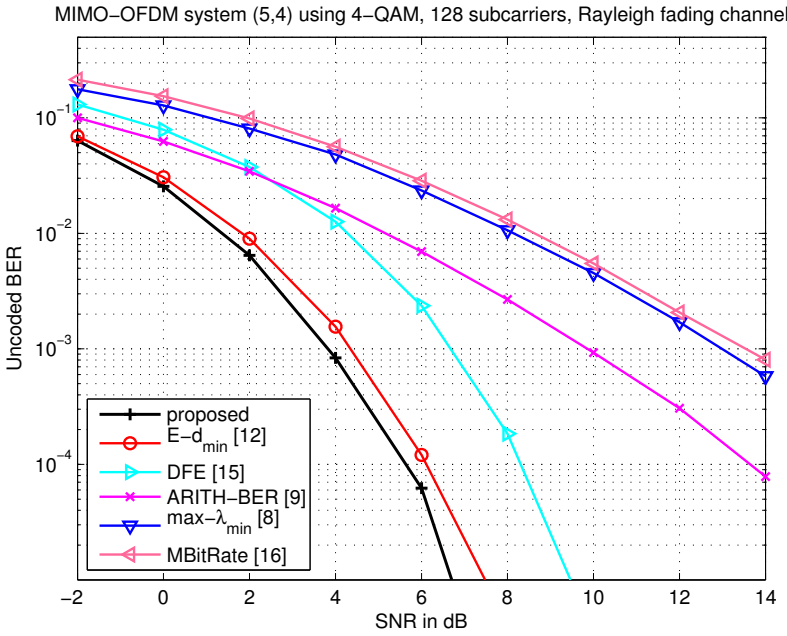

FIGURE 6.6: Comparison of BER performance for large MIMO(5,4) systems.

better than the other precoding strategies. Furthermore, the BER reduction obtained by the proposed precoder is much better than for the case of full CSI in comparison with the E-$d_{\min}$ solution: a gain of 2 dB can be observed at SNR = 10^{-5}.

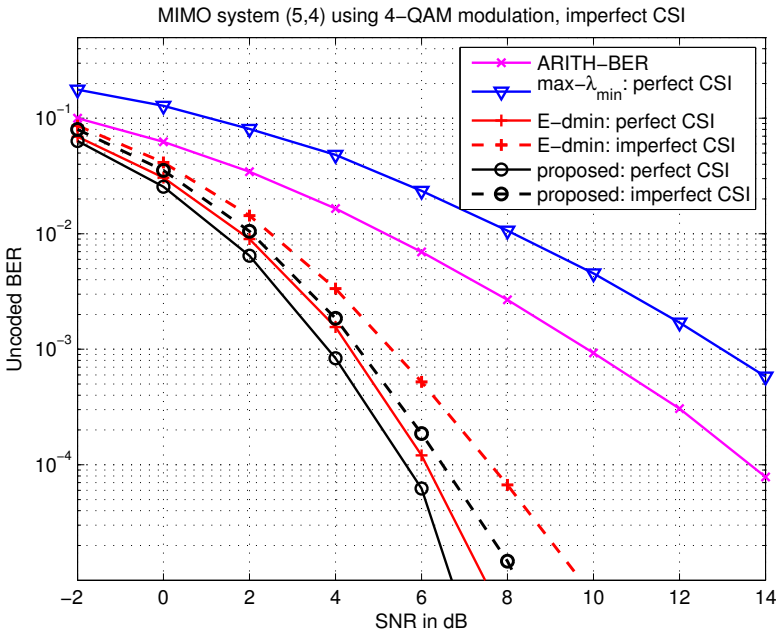

FIGURE 6.7: BER performance for perfect CSI and imperfect CSI estimations.

6.5 Conclusion

The optimized design of this new linear precoder was obtained by observing the SNR-like matrix of the precoding matrix. An approximation of the minimum distance was derived, and its maximum value was obtained by maximizing the minimum diagonal element of the SNR-like matrix. We then showed that the maximum value of minimum diagonal elements can be attained by a specific set of precoders. The precoding matrix is then parameterized as the product of a diagonal power allocation matrix and an input-shaping matrix. The input-shaping matrix concerns with the rotation and scaling of the input symbols on each virtual subchannel. One should note that it is a unitary matrix, and the minimum diagonal entry of the SNR-like matrix is obtained from a special choice of this unitary matrix. The input-shaping matrix is chosen to be a DFT-matrix, and the optimization becomes determining the power allocation matrix $\mathbf{\Sigma}$. As its name implies, the matrix $\mathbf{\Sigma}$ decides how many subchannels are used by the precoder for data transmission. For each number of available datastreams, we propose a general expression of the precoder.

We have also provided performance comparisons to demonstrate that the proposed precoder obtains a significant improvement in terms of BER compared to other designs. The improvement may be more than several dB at reasonable BER levels. In comparison with the optimal max-$d_{\min}$ solution, our proposed precoder also provides a slight improvement in BER performance. Another advantage of our design is that the solution can be available for all rectangular QAM-modulations and for any number of datastreams. It is because the precoder has a simpler analytic form, and the space of the solutions is smaller than the full design of minimum distance based precoders.

Conclusion and perspectives

The use of multiple transmit and receive antennas, popularly known as multiple-input multiple-output (MIMO) system, is an emerging cost-effective technique that offers higher data rate, increases the robustness and user capacity for wireless communications. Through a feedback link, the channel state information is available at the transmitter, and a linear precoding technique can be used to improve the performance of MIMO systems. In this thesis the precoder which maximizes the minimum Euclidean distance ($d_{\min}$) between two received symbols is derived. We have studied the performance in terms of $d_{\min}$ and bit-error-rate for different channel configurations and proposed some non-optimal extensions for the max-$d_{\min}$ based precoder.

After a brief introduction about MIMO systems, the principles and different techniques which permit to exploit the spatial diversity at the transmitter and the receiver are presented. These techniques can be divided into two categories depending on the possibility for the transmitter to know the propagation channel. Diversity Coding technique is used when there is no channel state information (CSI) at the transmitter. In this method, the signal is emitted from each of the transmit antennas using techniques called space-time coding. The inconvenient of space time codes is the appearance of the transmission rate $1/2 \leq \mathcal{R} \leq 1$ (only the Alamouti code for two transmit antennas provides $\mathcal{R} = 1$).

On the other hand, precoding is a processing technique that exploits CSI at transmitter by operating on the signal before transmission. This design depends not only on the type of CSIT but also on the optimization criteria. By using a singular value decomposition to decouple a MIMO channel into independent and parallel data-streams, an important family of precoding, denoted as diagonal precoders, performs a power allocation strategy on these MIMO eigen-subchannels. There exist lots of diagonal precoding structures such as Beamforming, Water-Filling, Minimum Mean Square Error , Quality of Service,

and Equal Error. The alternative set of linear precoders is obviously the non-diagonal schemes. It is shown that the precoder which maximizes the minimum Euclidean distance provides a significant BER reduction in comparison with diagonal precoders. Unfortunately, this solution is only available for two independent data-streams with a low-order QAM modulation. That is due to the expression of the minimum distance that depends on the number of data-streams, the channel characteristics, and the modulation used at the transmitter.

We firstly presented an extension of the max-$d_{\min}$ precoder for high order QAM modulations. The optimal solution for 16-QAM modulation has five different expressions, which vary depending on the channel angle γ. In order to reduce the complexity of this precoder, we proposed a general expression of minimum Euclidean distance based precoders for all rectangular QAM modulations. For a two independent data-streams transmission, the precoding matrix is obtained by optimizing the minimum distance on both virtual subchannels. Hence, the optimized expressions can be simplified by two forms: the precoder $\mathbf{F}_1$ pours power only on the first virtual subchannel, and the precoder $\mathbf{F}_2$ uses both virtual subchannels to transmit data symbols. These precoding matrices are designed to optimize the distance $d_{\min}$ whatever the dispersive characteristics of the channels are. The expression of $\mathbf{F}_1$ depends on the order of the rectangular QAM modulation, while that of $\mathbf{F}_2$ does not change for all of the modulations. The two general forms obtain the optimized minimum distance for small and large dispersive channels.

By decomposing the propagation channel into 2×2 eigen-channel matrices, and applying the new max-$d_{\min}$ precoder for independent pairs of data-streams, a suboptimal solution, denoted as Equal-$d_{\min}$(E-$d_{\min}$), was proposed for large MIMO systems. This sub-optimal solution can only achieve an even number of data-streams. Therefore, we extended a new design of max-$d_{\min}$ precoders for a three parallel data-stream scheme. Thanks to this 3-D max-$d_{\min}$ precoder, an extension for an odd number of data-streams is obtained by decomposing the virtual channel into (2×2) and (3×3) eigen-channel matrices. For a given number of data-streams, this extension exhibits a higher diversity order in comparison with diagonal precoder. In addition, the robustness of the proposed precoder is also better when an imperfect CSI estimation is considered at the transmitter.

One should note that not only the minimum Euclidean distance but also the number of neighbors providing it has an important role in reducing the error probability when

a ML detection is used at the receiver. In order to reduce the number of neighbors, a new precoder in which the rotation parameter has no influence was proposed. The expression of the new precoding strategy is, therefore, less complex and the space of solution is smaller. The simulation results for two and three independent data-streams confirm a slight bit-error-rate improvement of the new precoder in comparison with the optimal max-$d_{\min}$ solution. Furthermore, an extension for large MIMO systems can also be obtained by decomposing the virtual channel into (2×2) or (3×3) eigen-channel matrices.

Still observing the SNR-like precoding matrix, an approximation of the minimum distance was derived by maximizing the minimum diagonal element of the SNR-like matrix. The precoding matrix is then parameterized as the product of a power allocation matrix and an input-shaping matrix acting on rotation and scaling of the input symbols. It was demonstrated that the minimum diagonal entry of the SNR-like matrix is obtained when the input-shaping matrix is a Discrete Fourier Transform matrix. The power allocation matrix is diagonal and depends on the channel characteristics. In comparison with the traditional max-$d_{\min}$ solution, the new precoder provides a slight improvement in BER performance. But the major advantage of this design is that the solution can be available for all rectangular QAM-modulations and for any number of datastreams.

Several future works can be considered to enhance our proposed precoders. They can be divided into three parts.

We proposed a precoding strategy for the MIMO transmission that increases the minimum Euclidean distance between the received signals, and compared the uncoded BER performances of proposed precoder with several solutions. We can expect that the proposed precoding will outperform other solutions in terms of capacity (due to larger $d_{\min}$) but it is depends also on the mapping. Such an observation is presented in [73], and called as symbol mapping diversity. The mapping design depends on the targeted spectral efficiency, and the de-mapping can be used to improve our coded modulations capacities [74]. Therefore, we can think on the association of the minimum distance based precoder and the mapping diversity design. Some simulation results confirm that this idea is really promising.

Although the performance in terms of BER of our proposed precoder is better than other sophisticated transceivers, its ML complexity is really outperformed by the diagonal

precoders. In order to reduce the complexity of the ML detection, we can use a sphere decoder (SD) at the receiver. For the sphere-decoding algorithm, the authors in [25, 75] presented a closed form expression for the expected complexity. They demonstrated that, for a wide range of SNRs, this expected complexity is polynomial, and often roughly cubic. One of the most promising approaches of SD algorithm is the fixed-complexity sphere-decoding scheme (FSD). The new scheme of FSD can be found in the paper [27]. It is shown that the new scheme, named as real-valued fixed-complexity sphere decoder (RFSD), not only maintains quasi-ML decoding accuracy but also is less complex than FSD. We can also consider another algorithm, which excludes unreliable candidate symbols in data streams and is based on the MMSE criterion to reduce significantly the ML complexity [21].

The third part deals with the channel state information at the transmitter, in particular with the feedback of the knowledge of the channel. It would be interesting to combine our proposed precoder with several methods of estimation. One should note that we can not obtain the perfect CSI at the transmitter due to the estimation error of the channel. In addition, the data rate of feedback link to the transmitter is limited, and, therefore, it is difficult to recreate the form of CSI. Our objective becomes to take the rotation and permutation invariance properties into the definition of distortion function, quantify the information returned, and design a new codebook associated with the minimum Euclidean distance criterion. Several designs of limited feedback communication can be found in [76, 77]. Our proposed solutions can work properly with the precoding codebook, and can obtain excellent performance under spatial multiplexing environments.

Personal Publications

International peer-reviewed conferences

- **Q-T. NGO**, O. Berder, B. Vrigneau, and O. Sentieys, Minimum distance based precoder for MIMO-OFDM systems using a 16-QAM modulation, *Proceedings of IEEE International Conference on Communications (ICC)*, Dresden, Germany, June 2009.

- **Q-T. NGO**, O. Berder, and P. Scalart, 3-D minimum Euclidean distance based sub-optimal precoder for MIMO spatial multiplexing systems, *Proceedings of IEEE International Conference on Communications (ICC)*, Cape Town, South Africa, June 2010.

- **Q-T. NGO**, O. Berder, and P. Scalart, Reducing the number of neighbors in the received constellation of dmin precoded MIMO systems, *Proceedings of IEEE Wireless Communications and Networking (WCNC)*, Cancun, Mexico, March 2011.

- **Q-T. NGO**, O. Berder, and P. Scalart, Neighbor-dmin precoder for three data-stream MIMO systems, *Proceedings of 19th European Signal Processing Conference (EUSIPCO)*, Barcelona, Spain, September 2011.

- **Q-T. NGO**, O. Berder, and P. Scalart, Influence du nombre de symboles voisins sur les performances des systèmes MIMO précodés par le critère de la distance minimale, *Actes du 23ème colloque GRETSI*, Bordeaux, France, September 2011.

International peer-reviewed journals

- **Q-T. NGO**, O. Berder, and P. Scalart, Minimum Euclidean distance based precoders for MIMO systems using rectangular QAM modulations, *IEEE transactions on Signal Processing*, 60(3): 1527 - 1533, 2012.

- **Q-T. NGO**, O. Berder, and P. Scalart, Minimum Euclidean distance based precoding for three-dimensional Multiple-Input Multiple-Output spatial multiplexing systems, *IEEE transactions on Wireless Communications*, 11(7): 2486 - 2495, 2012.

- **Q-T. NGO**, O. Berder, and P. Scalart, General minimum Euclidean distance based precoder for MIMO wireless systems, appear soon in *EURASIP Journal on Advances in Signal Processing, Special Issue on Signal Processing Methods for Diversity and its Applications.*

Bibliography

[1] J.C. Guey, M.P. Fitz, M.R. Bell, and W.Y. Kuo. Signal design for transmitter diversity wireless communication systems over rayleigh fading channels. *IEEE Transactions on Communications*, 47(4):527–537, 1999.

[2] R. Burrows and S.S. Attwood. *Radio wave propagation*. Academic Press, 1949.

[3] J.P. Linnartz. *Narrowband land-mobile radio networks*. Artech House, Inc., 1993.

[4] M.K. Simon and M.S. Alouini. *Digital communication over fading channels*, volume 86. Wiley-IEEE Press, 2005.

[5] M. Nakagami. The m-distribution-a general formula of intensity distribution of rapid fading. *Statistical Method of Radio Propagation*, 1960.

[6] J.H. Winters, J. Salz, and R.D. Gitlin. The impact of antenna diversity on the capacity of wireless communication systems. *IEEE Transactions on Communications*, 42(234):1740–1751, 1994.

[7] G.J. Foschini. Layered space-time architecture for wireless communication in a fading environment when using multi-element antennas. *Bell labs technical journal*, 1(2):41–59, 1996.

[8] AJ Paulraj, DA Gore, RU Nabar, and H. Bolcskei. An overview of MIMO communications-a key to gigabit wireless. *Proceedings of the IEEE*, 92(2):198–218, february 2004.

[9] G.J. Foschini and M.J. Gans. On limits of wireless communications in a fading environment when using multiple antennas. *Wireless personal communications*, 6 (3):311–335, 1998.

[10] M. Vu and A. Paulraj. MIMO wireless linear precoding. *IEEE Signal Processing Magazine*, 24(5):86–105, 2007.

[11] C.E. Shannon. A mathematical theory of communication. *Bell Syst. Tech. J.*, 27: 379–423, 1948.

[12] E. Telatar. Capacity of multi-antenna Gaussian channels. *European transactions on telecommunications*, 10(6):585–595, 1999.

[13] S.M. Alamouti. A simple transmitter diversity scheme for wireless communications. *IEEE Journal on Selected Areas in Communications*, 16(8):1451–1458, 1998.

[14] V. Tarokh, N. Seshadri, and AR Calderbank. Space-time codes for high data rate wireless communication: Performance criterion and code construction. *IEEE transactions on information theory*, 44(2):744–765, 1998.

[15] G. Ganesan and P. Stoica. Space-time diversity using orthogonal and amicable orthogonal designs. *Wireless Personal Communications*, 18(2):165–178, 2001.

[16] H. Jafarkhani. A quasi-orthogonal space-time block code. *IEEE Transactions on Communications*, 49(1):1–4, 2001.

[17] V. Tarokh, H. Jafarkhani, and A.R. Calderbank. Space-time block codes from orthogonal designs. *IEEE Transactions on Information Theory*, 45(5):1456–1467, 1999.

[18] G. Ungerboeck. Channel coding with multilevel/phase signals. *IEEE Transactions on Information Theory*, 28(1):55–67, 1982.

[19] GG Raleigh, JM Cioffi, C.W. Inc, and CA Belmont. Spatio-temporal coding for wireless communication. *IEEE Transactions on Communications*, 46(3):357–366, 1998.

[20] R.A. Horn and C.R. Johnson. *Matrix analysis*. Cambridge university press, 2005.

[21] Jin-Sung Kim, Sung-Hyun Moon, and Inkyu Lee. A new reduced complexity ml detection scheme for mimo systems. *IEEE Transactions on Communications*, 58(4): 1302 –1310, april 2010.

[22] O. Damen, K. Abed-Meraim, and J.C. Belfiore. Generalised sphere decoder for asymmetrical space-time communication architecture. *Electronics Letters*, 36(2): 166–167, 2000.

[23] O. Damen, A. Chkeif, and J.C. Belfiore. Lattice code decoder for space-time codes. *IEEE Communications Letters*, 4(5):161–163, 2000.

[24] E. Viterbo and J. Boutros. A universal lattice code decoder for fading channels. *IEEE Transactions on Information Theory*, 45(5):1639–1642, 1999.

[25] B. Hassibi and H. Vikalo. On the sphere-decoding algorithm i. expected complexity. *IEEE Transactions on Signal Processing*, 53(8):2806 – 2818, aug. 2005.

[26] J. Jaldén and B. Ottersten. On the complexity of sphere decoding in digital communications. *IEEE Transactions on Signal Processing*, 53(4):1474–1484, 2005.

[27] Chengwei Zheng, Xuezheng Chu, J. McAllister, and R. Woods. Real-valued fixed-complexity sphere decoder for high dimensional qam-mimo systems. *IEEE Transactions on Signal Processing*, 59(9):4493 –4499, sept. 2011.

[28] E. Agrell, T. Eriksson, A. Vardy, and K. Zeger. Closest point search in lattices. *IEEE Transactions on Information Theory*, 48(8):2201–2214, 2002.

[29] H. Meyr, M. Moeneclaey, and S. Fechtel. *Digital communication receivers: synchronization, channel estimation, and signal processing.* John Wiley & Sons, Inc. New York, NY, USA, 1997.

[30] V. Lottici, A. D'Andrea, and U. Mengali. Channel estimation for ultra-wideband communications. *IEEE Journal on Selected Areas in Communications*, 20(9):1638–1645, 2002.

[31] P. Stoica and G. Ganesan. Maximum-SNR spatial-temporal formatting designs for MIMO channels. *IEEE Transactions on Signal Processing*, 50(12):3036–3042, 2002.

[32] H. Sampath, P. Stoica, and A. Paulraj. Generalized linear precoder and decoder design for MIMO channels using the weighted MMSE criterion. *IEEE Transactions on Communications*, 49(12):2198–2206, 2001.

[33] A. Scaglione, P. Stoica, S. Barbarossa, GB Giannakis, and H. Sampath. Optimal designs for space-time linear precoders and decoders. *IEEE Transactions on Signal Processing*, 50(5):1051–1064, 2002.

[34] M. Tomlinson. New automatic equaliser employing modulo arithmetic. *Electronics Letters*, 7(5):138–139, 1971.

[35] H. Harashima and H. Miyakawa. Matched-transmission technique for channels with intersymbol interference. *IEEE Transactions on Communications*, 20(4):774–780, 1972.

[36] D.P. Palomar and Y. Jiang. *MIMO transceiver design via majorization theory*, volume 3. Now Publishers Inc., 2006.

[37] L. Collin, O. Berder, P. Rostaing, and G. Burel. Optimal minimum distance-based precoder for MIMO spatial multiplexing systems. *IEEE Transactions on Signal Processing*, 52(3):617–627, 2004.

[38] M. Kang and M.S. Alouini. Largest eigenvalue of complex wishart matrices and performance analysis of mimo mrc systems. *IEEE Journal on Selected Areas in Communications*, 21(3):418–426, 2003.

[39] P.A. Dighe, R.K. Mallik, and S.S. Jamuar. Analysis of transmit-receive diversity in rayleigh fading. *IEEE Transactions on Communications*, 51(4):694–703, 2003.

[40] P. Rostaing, O. Berder, G. Burel, and L. Collin. Minimum BER diagonal precoder for MIMO digital transmissions. *Signal Processing*, 82(10):1477–1480, 2002.

[41] J.G. Proakis. *Digital communications, 4th edition.* McGraw-Hill, 2000.

[42] R.M. Corless, G.H. Gonnet, D.E.G. Hare, D.J. Jeffrey, and D.E. Knuth. On the lambertw function. *Advances in Computational mathematics*, 5(1):329–359, 1996.

[43] S.K. Mohammed, E. Viterbo, Y. Hong, and A. Chockalingam. X-and Y-Codes for MIMO precoding. *IEEE International Symposium on Information Theory Proceedings (ISIT)*, pages 2143–2147, 2010.

[44] S.K. Mohammed, E. Viterbo, Yi Hong, and A. Chockalingam. Mimo precoding with x- and y-codes. *IEEE Transactions on Information Theory*, 57(6):3542 –3566, june 2011.

[45] Y. Jiang, J. Li, and W.W. Hager. Joint transceiver design for mimo communications using geometric mean decomposition. *IEEE Transactions on Signal Processing*, 53 (10):3791–3803, 2005.

[46] J.K. Zhang, A. Kavcic, and K.M. Wong. Equal-diagonal qr decomposition and its application to precoder design for successive-cancellation detection. *IEEE Transactions on Information Theory*, 51(1):154–172, 2005.

[47] C.C. Weng, C.Y. Chen, and PP Vaidyanathan. Mimo transceivers with decision feedback and bit loading: Theory and optimization. *IEEE Transactions on Signal Processing*, 58(3):1334–1346, 2010.

[48] O. Simeone, Y. Bar-Ness, and U. Spagnolini. Linear and nonlinear preequalization/equalization for mimo systems with long-term channel state information at the transmitter. *IEEE Transactions on Wireless Communications*, 3(2):373–378, 2004.

[49] F. Xu, T.N. Davidson, J.K. Zhang, and K.M. Wong. Design of block transceivers with decision feedback detection. *IEEE Transactions on Signal Processing*, 54(3): 965–978, 2006.

[50] M.B. Shenouda and T.N. Davidson. A framework for designing mimo systems with decision feedback equalization or tomlinson-harashima precoding. *IEEE Journal on Selected Areas in Communications*, 26(2):401–411, 2008.

[51] X. Zhu and RD Murch. Performance analysis of maximum likelihood detection in a MIMO antenna system. *IEEE Transactions on Communications*, 50(2):187–191, 2002.

[52] C. Lamy and J. Boutros. On random rotations diversity and minimum mse decoding of lattices. *IEEE Transactions on Information Theory*, 46(4):1584 –1589, jul 2000.

[53] R. van Nee, A. van Zelst, and G. Awater. Maximum likelihood decoding in a space division multiplexing system. In *IEEE 51st Vehicular Technology Conference Proceedings (VTC 2000-Spring), Tokyo*, volume 1, pages 6 –10 vol.1, 2000.

[54] M.R. Bhatnagar and A. Hjorungnes. Linear precoding of stbc over correlated ricean mimo channels. *IEEE Transactions on Wireless Communications*, 9(6):1832 –1836, june 2010.

[55] D. Kapetanović and and F. Rusek. On precoder design under maximum-likelihood detection for quasi-stationary mimo channels. *IEEE International Conference on Communications (ICC), Cape Town, South Africa*, May 2010.

[56] A. Goldsmith. *Wireless communications*. Cambridge Univ Press, 2005.

[57] A. Paulraj, R. Nabar, and D. Gore. *Introduction to space-time wireless communications*. Cambridge University Press, 2003.

[58] A. Edelman. *Eigenvalues and condition numbers of random matrices*. PhD thesis, Massachusetts Institute of Technology, 1989.

[59] B. Vrigneau, J. Letessier, P. Rostaing, L. Collin, and G. Burel. Extension of the MIMO precoder based on the minimum Euclidean distance: a cross-form matrix. *IEEE Journal on Selected Topics in Signal Processing*, 2(2):135–146, 2008.

[60] M.B. Shenouda and T.N. Davidson. A framework for designing mimo systems with decision feedback equalization or tomlinson-harashima precoding. *IEEE Journal on Selected Areas in Communications*, 26(2):401 –411, february 2008.

[61] Chien-Chang Li, Yuan-Pei Lin, Shang-Ho Tsai, and P.P. Vaidyanathan. Optimization of transceivers with bit allocation to maximize bit rate for mimo transmission. *IEEE Transactions on Communications*, 57(12):3556 –3560, december 2009.

[62] C.B. Peel, B.M. Hochwald, and A.L. Swindlehurst. A vector-perturbation technique for near-capacity multiantenna multiuser communication-part i: channel inversion and regularization. *IEEE Transactions on Communications*, 53(1):195 – 202, jan. 2005.

[63] Y. Ding, T.N. Davidson, Z.Q. Luo, and K.M. Wong. Minimum ber block precoders for zero-forcing equalization. *IEEE Transactions on Signal Processing*, 51(9):2410–2423, sept. 2003.

[64] H. Minn and N. Al-Dhahir. Optimal training signals for MIMO OFDM channel estimation. *IEEE transactions on wireless communications*, 5(5):1158–1168, 2006.

[65] Quoc-Tuong Ngo, O. Berder, and P. Scalart. 3-d minimum euclidean distance based sub-optimal precoder for mimo spatial multiplexing systems. *IEEE International Conference on Communications (ICC), Cape Town, South Africa*, May 2010.

[66] P. Dita. Separation of unistochastic matrices from the double stochastic ones: Recovery of a 3× 3 unitary matrix from experimental data. *Journal of mathematical physics*, 47(8):3510–3537, 2006.

[67] M. Payaro and D.P. Palomar. On optimal precoding in linear vector gaussian channels with arbitrary input distribution. In *IEEE International Symposium on Information Theory (ISIT)*, pages 1085 –1089, June 28 2009-July 3 2009.

[68] P. Dita. Factorization of unitary matrices. *Journal of Physics A: Mathematical and General*, 36:2781, 2003.

[69] Quoc-Tuong Ngo, O. Berder, B. Vrigneau, and O. Sentieys. Minimum distance based precoder for mimo-ofdm systems using 16-qam modulation. *IEEE International Conference on Communications (ICC), Dresden, Germany*, June 2009.

[70] Quoc-Tuong Ngo, O. Berder, and P. Scalart. Reducing the number of neighbors in the received constellation of dmin precoded mimo systems. *IEEE Wireless Communications and Networking Conference (WCNC), Cancun, Mexico*, March 2011.

[71] D.P. Palomar, J.M. Cioffi, and M.A. Lagunas. Joint tx-rx beamforming design for multicarrier mimo channels: A unified framework for convex optimization. *IEEE Transactions on Signal Processing*, 51(9):2381–2401, 2003.

[72] C.C. Li, Y.P. Lin, S.H. Tsai, and PP Vaidyanathan. Optimization of transceivers with bit allocation to maximize bit rate for mimo transmission. *IEEE Transactions on Communications*, 57(12):3556–3560, 2009.

[73] H. Samra, Z. Ding, and P.M. Hahn. Symbol mapping diversity design for multiple packet transmissions. *Communications, IEEE Transactions on*, 53(5):810–817, 2005.

[74] L. Szczecinski, F.K. Diop, and M. Benjillali. On the performance of bicm with mapping diversity in hybrid arq. *Wireless Communications and Mobile Computing*, 8(7):963–972, 2008.

[75] H. Vikalo and B. Hassibi. On the sphere-decoding algorithm ii. generalizations, second-order statistics, and applications to communications. *IEEE Transactions on Signal Processing*, 53(8):2819–2834, 2005.

[76] D.J. Love. Duplex distortion models for limited feedback mimo communication. *IEEE Transactions on Signal Processing*, 54(2):766–774, 2006.

[77] D.J. Love and RW Heath. Limited feedback unitary precoding for spatial multiplexing systems. *IEEE Transactions on Information Theory*, 51(8):2967–2976, 2005.